The University of Nottingham

UNITED KINGDOM · CHINA · MALAYSIA

Department of Civil Engineering

Properties and Microstructure of Pre-formed Foamed Concretes

By

Ameer A. Hilal, BSc Eng., MSc Eng.

Thesis submitted to the University of Nottingham for the degree of **Doctor of Philosophy**

February 2015

To my family

Abstract

In construction buildings, use of thermal insulating materials is essential and beneficial not only by reducing the cooling/heating cost and the structural element sizes but also reducing the pollution of the environment which results from heavy use of fuel.

Foamed concrete is a lightweight material. In this research, by using the preformed foam method, foamed concrete mixes with/without lightweight aggregate (LWA), which are suitable for semi-structural or structural purposes with good insulation and durability properties, were designed and produced. Then, their behaviour and the effect of microstructure on their macro properties were established. As a result, the mechanical, thermal and permeation performance as well as damage behaviour of foamed concrete, associated with changes in its microstructure that result from inclusion of superplasticizer, additives (silica fume and fly ash) and LWA, were investigated.

The results showed that, for a given density, although the additives in combination led to increased void numbers, both void size and connectivity were reduced by preventing their merging and this resulted in a narrow void size distribution. As a result, the mineral admixtures (silica fume and fly ash) and superplasticizer combination provides improvement in the strength properties of foamed concrete. In addition, due to their making the cement paste denser and less porous, addition of additives and superplasticizer in combination led to slightly increased thermal conductivity in the dry state. However, owing to reduced water absorption, the thermal conductivity in the saturated state was slightly lower for mixes with additives than conventional mixes. Adding additives (individually or in combination) helped in reducing the water absorption, sorptivity and permeability of foamed concrete. However, inclusion of LWA resulted in increased sorptivity and permeability compared to the same density mixes, conventional or with additives in

combination. From elasticity, fracture and fractal points of view, it was found that brittleness increases with additives while it reduces with inclusion of LWA. However, at a micro level, less damage occurred in mixes with LWA and the bond microcracks percentage increased with inclusion of additives.

Finally, although the findings of this study are encouraging for the potential of using modified foamed concrete with additives in semi-structural and structural applications, it was recommended that using it in reinforced structural elements such as beams, columns, slabs and reinforced walls or load bearing masonry walls needs to be experimentally examined and evaluated.

Publication

From the results of this study, four journal papers have been published and two conference papers have been presented, as follows:

1. Hilal, A.A., Thom, N.H., and Dawson, A.R. 2015. *The Use of Additives to Enhance Properties of Pre- formed Foamed Concrete.* International Journal of Engineering and Technology, **7**(4): p. 286-293.

2. Hilal, A.A., Thom, N.H., and Dawson, A.R. 2014. *Pore Structure and Permeation Characteristics of Foamed Concrete* Journal of Advanced Concrete Technology, 12. p: 535-544.

3. Hilal, A.A., Thom, N.H., and Dawson, A.R. 2015. *On entrained pore size distribution of foamed concrete.* Construction and Building Materials, 75, 227-233.

4. Hilal, A.A., Thom, N.H., and Dawson, A.R. 2014. *Effect of additives on void structure of foamed concrete*, in *34th Annual Cement and Concrete Science Conference*, S.A. Bernal and J.L. Provis, Editors: University of Sheffield, UK. p. 63-66.

5. Hilal, A.A., Thom, N.H., and Dawson, A.R. 2014. *Foamed Concrete: From Weakness to Strength* in *34th Annual Cement and Concrete Science Conference*, S.A. Bernal and J.L. Provis, Editors: University of Sheffield, UK p. 231-234.

6. Hilal, A. A., Thom, N. H. & Dawson, A. R. 2015. On void structure and strength of foamed concrete made without/with additives. Construction and Building Materials, 85, 157-164.

Prize:

1. Acknowledgment from Iraqi Cultural Attaché- London (Representative of the Iraqi Ministry of Higher Education and Scientific Research in the UK and Ireland) for a presentation about this project on Iraqi Day which was held at the University of Nottingham, 28 February 2014.

2. Acknowledgment and prize from the Minister of Higher Education and Scientific Research/ Iraq, for publications and contributions during the period of PhD study. Iraqi Cultural Centre, London, 17 January 2015.

Acknowledgment

The author would like to express his sincere thanks and gratitude to his supervisors, Dr Nick Thom and Assoc. Prof Andrew Dawson, for their invaluable guidance, advice and encouragement throughout this study and to record that he will never forget their kindness and good manners.

The author would like also to acknowledge the support provided by the Higher Committee for Education Development in Iraq (HCED) during a full scholarship. In addition, gratitude must be conveyed to the Civil Engineering Laboratory technical staff: Mr Mike Langford, Mr Nigel Rook, Mr Gary Davies and Mr Balbir Loyla. Moreover, the valuable help and comments of Dr Nigel Neate, Mr Martin Roe, Mrs Julie Thompson, Mr Keith Dinsdale and Mr Thomas Buss in optical microscopy, SEM, MIP, Micro CT, DIC tests are gratefully acknowledged. My thanks are also extended to the laboratory staff at Nottingham Transportation Engineering Centre (NTEC) for all their valuable assistance regarding laboratory experimental works.

My appreciation needs to be expressed to a long list of colleagues: Dr Khalid, Dr Abdulkader, Dr Savas, Dr Pejman, Dr Usama, Mahmoud, Mohamed, Maher, Hasan, Younis, Venon, Chibuzor, Ahmed Nassar, Abdulshafi, Rami, Waleed, Said Bilal, Jwan, Haneen, Tariq, Ahmed, Giacomo, Ana, Helena, Diana, Laura and Yasameen for their time in discussion and their supporting. Special thanks are due to Mahmoud Elnasri, Ayad Subhy, Hamid and Ahmed Hilal for their efforts and advices.

I am particularly indebted to my parents for inspiring me during this work; Mum, thank you for patience while I was away and Dad, I really wanted you to be with us during this journey although your memory never left me, may God bless your soul. Finally, the author expresses his deepest appreciation for the patience, understanding and unwavering support of his lovely wife and kids; without them it would have been so difficult to reach this stage.

Ameer (2015)

Declaration

The work described in this thesis was conducted at the Department of Civil Engineering, University of Nottingham between October 2011 and February 2015. I declare that, unless otherwise cited in the text, the work is my own and has not been submitted for a degree at another university.

Ameer Abdulrahman Hilal
February 2015

Abbreviations and notations

ACI	American Concrete Institute
ASTM	The American Society for Testing and Materials
BS	British Standard
BS EN	British European Standard
ITZ	Interfacial transition zone
LWC	Structural concrete
SLWC	Structural lightweight concrete
LWAC	Lightweight aggregate concrete
LWA	Lightweight aggregate
Υ_{dry}	Dry density
W_{da}	Weight of dry aggregate in the batch
W_{ct}	Weight of cement in the batch
w/c	Water-cement ratio
w/b	Water-binder ratio
a/c	Air-cement ratio
E_s	Static modulus of elasticity
E_d	Dynamic modulus of elasticity
ν	Poisons ratio
C-S-H	Calcium silicate hydrate
CH	Calcium hydroxide
UH	unhydrated particles
AAC	Autoclaved aerated concrete
NAAC	Non-autoclaved aerated concrete
Å	Angstrom
SEM	Scanning electron microscopy
MIP	Mercury intrusion porosimetry
LEFM	Linear elastic fracture mechanics
NLFM	Nonlinear fracture mechanics
FPZ	Fracture process zone
G_f	Fracture energy and effective
RHA	Rice-husk ash
S.G.	Specific gravity
SF	Silica fume
FA	Fly ash
FC	Conventional foamed concrete (without additives)
FCa	Foamed concrete with additives
FCs	Foamed concrete with silica fume
FCf	Foamed concrete with fly ash
FCp	Foamed concrete with superplasticizer
FCsp	Foamed concrete with silica fume and superplasticizer
FCL	Foamed concrete with lightweight aggregate
FCLa	Foamed concrete with lightweight aggregate and additives
Υ_{wet}	Wet density (after cling film curing)
W_a	Weight of specimen in air
W_w	Weight of specimen in water
P_c	Capillary pressure,
ρ	Surface tension,
θ	Contact angle
d	Diameter of the void

l_c	Characteristic length
OM	Optical microscopy
CCD	charge-coupled device
SEM	Scanning electron microscope
SE	Secondary electrons
BSE	Backscattered electrons
μCT	Micro computed tomography
$I_\circ$	intensity
L_{att}	linear attenuation coefficient
ϕ_{th}	Theoretical porosity
Υ_c	Concrete density
G_c	Specific gravity of the cement
Υ_w	Water unit weight
Υ_{th}	Theoretical density
R_{ca}	Cement to aggregate ratio by weight
G_a	Specific gravity of aggregate
ϕ_T	Total porosity
Υ_b	Bulk density
F_v	Foam volume
ϕ_{app}	Apparent porosity (%)
$W_{s,a}$	Weight of a saturated sample in air
$W_{s,w}$	Weight of the saturated sample in water
W_{dry}	Weight of the oven-dried sample
D_{50}	Median opening pore size for pre-formed foam
D_{90}	90th percentile for pre-formed foam
O_{50}	Median opening pore size for foamed concrete mixes
O_{90}	90th percentile for foamed concrete mixes
F_{circ}	Circularity factor
F_{circ50}	Median circularity factor
F_{circ10}	Circularity factor at which 10% are less
Conn. D.	Connectivity density
χ	Euler characteristic
β_0	Number of separate particles of the structure
β_1	Connectivity
β_2	Number of cavities enclosed within the structure
f_r	modulus of rupture
f_{sp}	Splitting tensile strength
f_{cu}	Cube compressive strength
σ_a	Upper loading stress (MPa), ($\sigma a=f'c/3$)
σ_b	Basic stress, (0.5 MPa)
ε_a	Strain under σa
ε_b	Strain under σb
agg/b	Aggregate-binder ratio
ΔT	Temperature difference
λ	Thermal conductivity
λ_d	Thermal conductivity at dry state
λ_s	Thermal conductivity at saturated state
W/mK	Watts per square meter of area of body when the temperature difference is $1°K$ per metre
HFM	Heat flow meter
C_p	Specific heat capacity

β	Thermal effusivity
fc/λ	Structural efficiency
A_{bw}	Water absorption
V_w	Volume of water absorbed
V_c	Specimen volume,
i	Cumulative volume of absorbed water
t	Time
B	Constant term representing the y-intercept at t=0
S	Sorptivity
k_{air}	Air permeability coefficient
Q	Air flow rate
μ	Air dynamic viscosity
P	Absolute inlet pressure
P_a	Outlet pressure
P_o	Measuring pressure
A	Cross-section area
Z	Specimen thickness
V_{ch}	Air chamber volume
P_{atm}	Atmospheric pressure
m	Slope of the $\ln[c(P_{(t)}-P_{atm})/(P_{(t)}+P_{atm})]$ versus t straight line
$P_{(t)}$	Pressure at any time
n_a	Air-filled porosity
P_m	Main air pressure
σ	Electrical conductivity of the saturated porous material
σ_o	Conductivity of the solution in the pores
σ/σ_o	Conductivity factor
DIC	Digital image correlation
l_{ch}	Parameter used to describe the brittleness
W_f	Area under the load-displacement curve
LVDTs	Linear variable differential transformers
ε_v	Volumetric strain
ε_A	Axial strain
ε_L	Lateral strain
D	Fractal dimension
θ_{crack}	Angle of inclination of cracks

Table of Contents

List of Figures

List of Tables

Chapter 1: Introduction

1.1 Theoretical Background

Concrete is a construction material which is extensively used because of its excellent properties such as durability, workability, satisfactory strength and the easy availability of raw materials (cement, aggregates and water) which are used to produce it (Mehta and Monteiro, 2006).

By definition, concrete is a composite material which consists of a binding medium and aggregate particles and can be formed in several types (Kosmatka et al., 2002). It may be considered to consist of three phases: a cement paste, aggregate and the interfacial transition zone (ITZ) between them (Akçaoğlu et al., 2004). Concrete is a heterogeneous substance. On a macroscopic scale, it is a mixture of cement paste and aggregates while on a microscopic scale, the cement paste itself consists of unreacted cement grains, amorphous hydration products (crystals of calcium hydroxide, needles of ettringite and fibrous crystals of calcium silicate hydrate) and pores (Nemati et al., 1998), see **Figure 1-1**.

In terms of density, concrete can be classified into several types such as lightweight, normal weight and heavy concrete. Neville (2011), mentioned that a reduction in concrete density can be achieved by replacing some of the solid materials by air voids locating in three possible locations which are: in the aggregate particles (lightweight aggregate concrete), in the cement paste (cellular concrete) and between the coarse aggregate particles by omitting fine aggregate (no-fines concrete). The practical density range of lightweight concrete is from about 300 kg/m^3 to 1850 kg/m^3. Moreover, ACI 213R-87 uses density in order to categorize lightweight concrete depending on its application. The three categories are: low-density concrete with a density between 300 and 800 kg/m^3 used for

thermal insulation (non-structural purposes). Secondly, structural lightweight concrete which has a density from 1350 to 1900 kg/m^3 with a minimum compressive strength of 17 MPa and used for structural purposes. Finally, moderate strength concrete lies between the above two categories with a compressive strength between 7 and 17 MPa (Neville, 2011).

Cellular (aerated) concrete is a lightweight material composed of cementitious mortar surrounding disconnected bubbles (more than 50% by volume) which are a result of either physical or chemical processes during which either air is introduced into the mortar (unfoamed) mixture or gas is formed within it (Tikalsky et al., 2004). Since there are two basic methods of producing aeration in concrete, an appropriate name for the end product, gas or foamed concrete, is given according to these methods.

Foamed concrete is manufactured either by adding to the mix an air-entraining agent (usually some form of hydrolyzed protein or resin soap) which introduces air bubbles during mixing at high speed (mix-foam method) or, in some processes, by adding a stable pre-formed foam to the unfoamed mixture during mixing in an ordinary mixer (pre-formed foam method) (Neville, 2011).

Pre-formed foamed concrete is made by adding preformed stable foam, prepared by aerating a foaming agent solution, to cement paste or cement mortar. Thereby, this action makes the concrete lighter by incorporating small enclosed air bubbles within the unfoamed mixture (Nambiar and Ramamurthy, 2006).

The future need for construction materials which are light, durable, economic and more environmentally sustainable has been identified by many groups around the world (Jones and McCarthy, 2005). Because of the possibility of producing a wide range of densities (400-1600) kg/m^3 and also of achieving a strength of at least 25 MPa (both economically and in an environmentally sustainable manner), foamed concrete has the potential to fulfil these requirements and has now become widely

used in the construction industry (Jones and McCarthy, 2005, Tarasov et al., 2010). With foamed concrete, sustainability is enhanced because no coarse aggregate is required in its manufacturing and there is the possibility of partially or fully replacing fine aggregate with recycled or secondary materials (Jones and McCarthy, 2006).

It should be noted that this research is concerned with aerated concrete, in particular foamed concrete, which is manufactured by using the preformed foam method to introduce large voids with size from 0.02 mm to 1.0 mm into the cement paste.
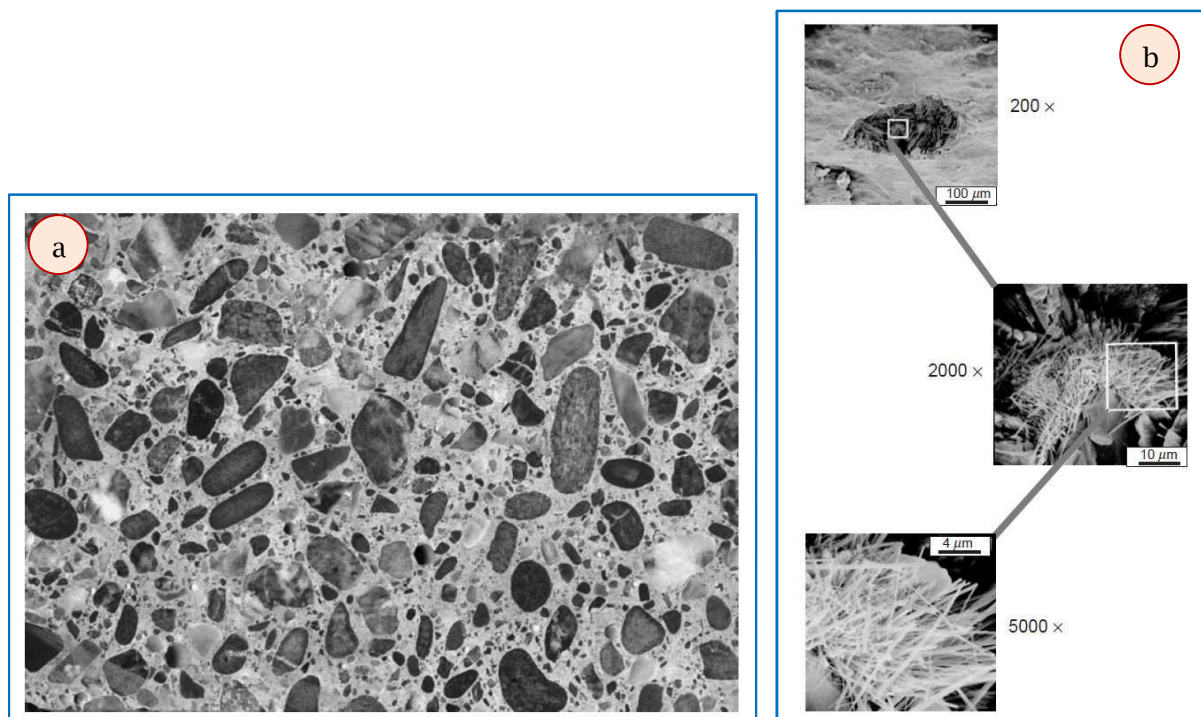
Figure 1-1 (a) polished section of concrete specimen (b) microstructure of a hydrated cement paste (Mehta and Monteiro, 2006).

1.2 Why Use Structural Lightweight Concrete (SLWC)?

In construction projects, the main use of structural lightweight concrete (SLWC) is to reduce the dead load of concrete structures resulting in reducing the size of columns, beams, foundations and other load bearing elements (Kosmatka et al., 2002). SLWC can be produced to achieve similar strengths to normal weight

concrete as well as meeting other mechanical and durability requirements. However, the former provides a good strength/weight ratio in structural elements.

Structurally, SLWC leads to reduced structural element size, less reinforcing steel and reduced concrete volume resulting in lower overall cost. Another cost saving by reducing weight comes from handling, transport costs and manpower.

Functionally, SLWC provides good thermal insulation properties giving energy conservation benefits, and thereby reducing costs of operation such as heating and air-conditioning. In addition, it has good acoustic properties whereby sound is absorbed, not reflected as in the case of dense concrete. Moreover, it is non-combustible and resistant to fire. As such, with good planning, using structural lightweight concrete may achieve an economic benefit to many engineering applications (NRMCA, 2003).

Mackie (1985), mentioned that use of lightweight concrete may cause a reduction in dead weight which makes it well suited for seismic design because the lateral forces on a structure during an earthquake, which are directly proportional to the structure's weight, will be smaller. According to the above author, a 1982 study by the National Science Foundation showed that columns made of lightweight concrete performed under seismic conditions in much the same way as similar strength columns made of normal weight concrete.

Because lightweight concrete cannot only reduce the total load on the structure but also provides a very good thermal insulation and achieves energy conservation advantages, one type of it, foamed concrete, was investigated in this project.

1.3 Applications of Lightweight Aggregate Concrete

Mehta and Monteiro (2006), cited many examples showing that use of lightweight aggregate concrete (LWAC) reduces costs for foundations and reinforcing steel as follows: In 1936, about $3 million saving in steel reinforcing resulted from the use

of a lightweight concrete bridge deck for the San Francisco-Oakland Bay bridge, **Figure 1-2a**. Another example of use of LWAC in floors of high-rise buildings is the 71-story Lake Point Tower in Chicago, Illinois, which was built in 1968 by using LWAC with 1730 kg/m^3 unit weight and 20 to 22 MPa 7-day compressive strength, see **Figure 1-2b**. Similarly, for the construction of a 50-story circular tower, the Australian square building in Sydney, through use of 31000 m^3 of LWAC beams, columns and floors, 28-day compressive strength of 34.3 MPa and 1792 kg/m^3 density, a 13% saving in the construction cost was achieved, see **Figure 1-2c**. An example for an all lightweight concrete structure is One Shell Plaza, Houston, Texas, of 52 stories containing LWAC of 1840 kg/m^3 density and compressive strength of 41.2 MPa. In this building, owing to the limited bearing capacity of the soil, only a 35-story structure could have been safely constructed if normal weight concrete had been used, see **Figure 1-2d**. Mackie (1985), mentioned that, according to a study by the Expanded Shale, Clay and Slate Institute (ESCSI), there will be a saving of an average of over \$32.00 and in some cases over \$90.00 per cubic yard (0.7645 m^3) by using structural lightweight concrete in floor slabs of steel frame mid-rise buildings. However, the ESCSI study only considered material savings in floor slabs, beams and girders and it would be greater if the material saving in columns and foundations had been considered. Furthermore, in the 640-foot (195 m) centre span of California Parrotts Ferry Bridge (**Figure 1-2e**), use of structural lightweight concrete reduced the dead load by 20% and construction costs by 10%. Another example is the Calgary Saddledome Stadium which was built for the 1988 Winter Olympics in Canada which was constructed almost entirely of precast concrete, see **Figure 1-2f**. It should be noted that using precast lightweight concrete may also save cost by reducing transportation and erection costs.
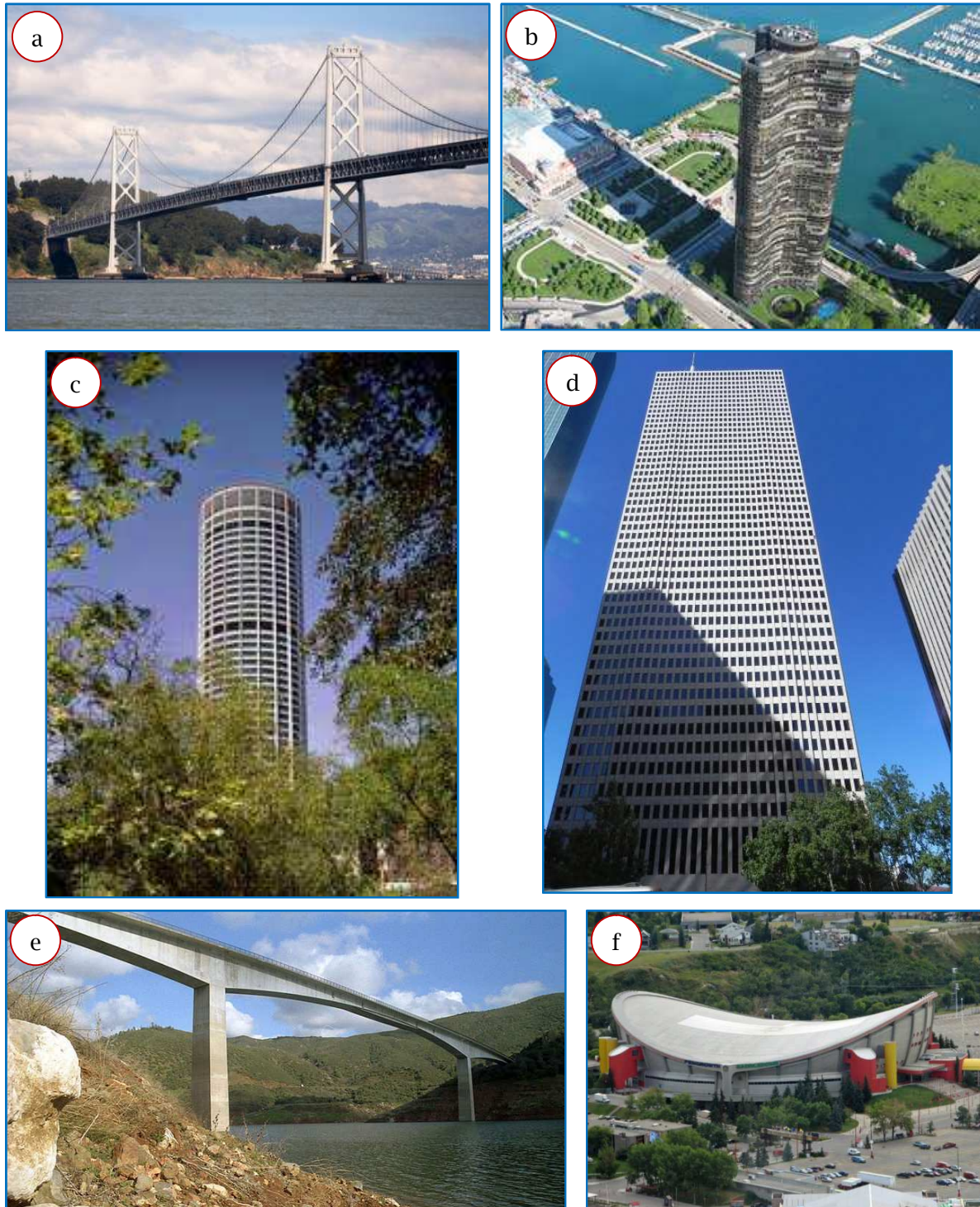
Figure 1-2 Some applications of structural lightweight concrete (a) San Francisco-Oakland Bay bridge (http://www.planetware.com/picture/san-francisco-oakland-bay-bridge-us-casfvw7.htm) (b) Lake Point Tower in Chicago (http://www.elixirwellnesscentre.com/locations) (c) Circular Tower, the Australian square building in Sydney(http://seidler.net.au/?id=18)(d) One Shell Plaza, Houston, Texas (http://khan.princeton.edu/khanOneShell.html) (e) California Parrotts Ferry Bridge (http://www.highestbridges.hk/wiki/index.php/Parrotts_Ferry_Bridge) (f) Calgary Saddledome Stadium in Canada(http://blog.travelpod.com/travel-photo/travelingdiva/10/1220633580/saddledome.jpg/tpod.html)

1.4 Applications of Foamed Concrete

The most obvious advantage of foamed concrete is its lower density which results in reduction of dead load (additional substantial savings are achieved), reduction of handling and transport costs, faster construction rates (reduction in manpower), good thermal insulation properties (giving energy conservation advantages, and thereby reducing operating costs, heating/air conditioning) and good acoustic properties.

The application of foamed concrete can be divided in three main fields: Pre cast elements (wall and ceiling panels), block production (sawed from big blocks or cast in specified moulds) and cast in situ (flooring system, roof insulation and wall filling), **Figure 1-3**.

Figure 1-3 Some applications of foamed concrete (www.dr-luca.com, 2009)

Other applications of foamed concrete are shown in **Table 1-1**. It can be seen that the use of foamed concrete has been limited to non-structural purposes such as void and cavities filling, backfill, bottom layer and settlement free construction; however, its structural features are also of considerable interest.

Table 1-1 Some applications of foamed concrete

Application	Density (kg/m³)	Volume used (m³)	Advantages	Images
Bridge Abutment/Approach backfill (1997) (www.provoton.com, 2006)	480-640	6117	-Less overburden on the structure and underlying soils -No lateral pressure on the structure	
Load Reduction Fill/Void Fill (2001) (www.provoton.com, 2006)	430-480	22937	-Greatly reduced loading on the basement floor and roof column piers -No need for additional piling in the basement	
Oil Platform (1992) (www.provoton.com, 2006)	800	2294	-Used as impact layer due to its energy absorbing properties	
Cycle Path (1997) (www.provoton.com, 2006)	640	917	-Minimise settlement of an asphalt cycle path due to soft compressible soils	
Running Track (1988) (www.provoton.com, 2006)	640-913	2905	-Minimise settlement of an asphalt bike path due to soft compressible soils	

Road sub Base (1998) (www.provoton.com, 2006)	480-640	9557	-Reduce the loads on very poor underlying soils	
Tunnel and Underground Construction (1998-1999) (www.provoton.com, 2006)	640	10245	-Backfilling due to its excellent fluidity	
Retaining Wall Backfill (1988-1997) (www.provoton.com, 2006)	500	50000	-No compaction and no too much added weight -High performance void-filling -Allowed for minimal use of skin friction piles -Reduced foundation costs	
Foam Concrete being Poured (www.foamconcrete.co.uk , 2013)	350-1600	-	-Imposes a little vertical stress on the substructure -Reducing loading on burden soil	
Settlement Free Construction (www.foamconcrete.co.uk , 2013)	-	-	-Forming a well-bonded body -Preventing settlement -Imposing no lateral loads on adjacent structures	
Filling (www.foamconcrete.co.uk , 2013)	-	-	-Naturally self-levelling -Filling the smallest cavities -Pump easily with low pressure over long distances	

1.5 Scope of Study

Although aerated concrete is known as an insulation substance, there has also been interest in its structural features (Narayanan and Ramamurthy, 2000).

From a functional point of view, energy for air-conditioning purposes, which is one-third of total energy consumption in many countries, is necessary for maintaining a comfortable indoor environment. Therefore, improving building energy efficiency seems to be an effective way to reduce total energy consumption. The possible methods to enhance building energy efficiency are by using construction materials with low thermal conductivity and/or high thermal energy storage capacity (Zhang et al., 2004).

From a structural point of view, in concrete construction, a large proportion of the overall weight on a structure comes from concrete self-weight; therefore reducing its density represents a considerable benefit. One of the most effective approaches to decreasing the dead load on a structure is using lightweight concrete.

Unfortunately, the Middle East Asian region, where the author originates, is not yet dealing with structural applications of lightweight concrete. This may be attributed to a lack of understanding about not only the production technique of LWC but also its structural and serviceability performance. More specifically, in Iraq, which is one of the Arab Gulf countries, the summer is too hot and the winter is too cold. Therefore, in order to make the inside of a building comfortable, heavy use of electric power is required for cooling purposes in summer, when outdoor temperature may reach up to $50\,^{\circ}C$, and heating purposes in winter, when outdoor temperature can be about zero $^{\circ}C$, **Figure 1-4a**. Thus, use of thermal insulating materials is essential and beneficial, see **Figure 1-4b**, not only by reducing the cooling/heating cost and the structural element sizes but also reducing the pollution of the environment which results from heavy use of fuel.

When lightweight concrete is used structurally, its load-bearing function is normally the priority and its thermal benefits are not considered. Therefore, this project aims to produce foamed concrete with a satisfactory strength suitable for semi-structural or structural purposes with good insulation and durability properties. Furthermore, knowing about the fundamentals of how this concrete will behave and how to develop this material to make it capable of withstanding the mechanical, thermal and permeation loadings is essential to improve its long term durability. In other words, based on a fundamental understanding of the material behaviour, its performance in service can be assessed. Therefore, in addition to the mechanical and thermal properties, the pore structure, permeation properties and damage behaviour of foamed concrete will also be of interest.
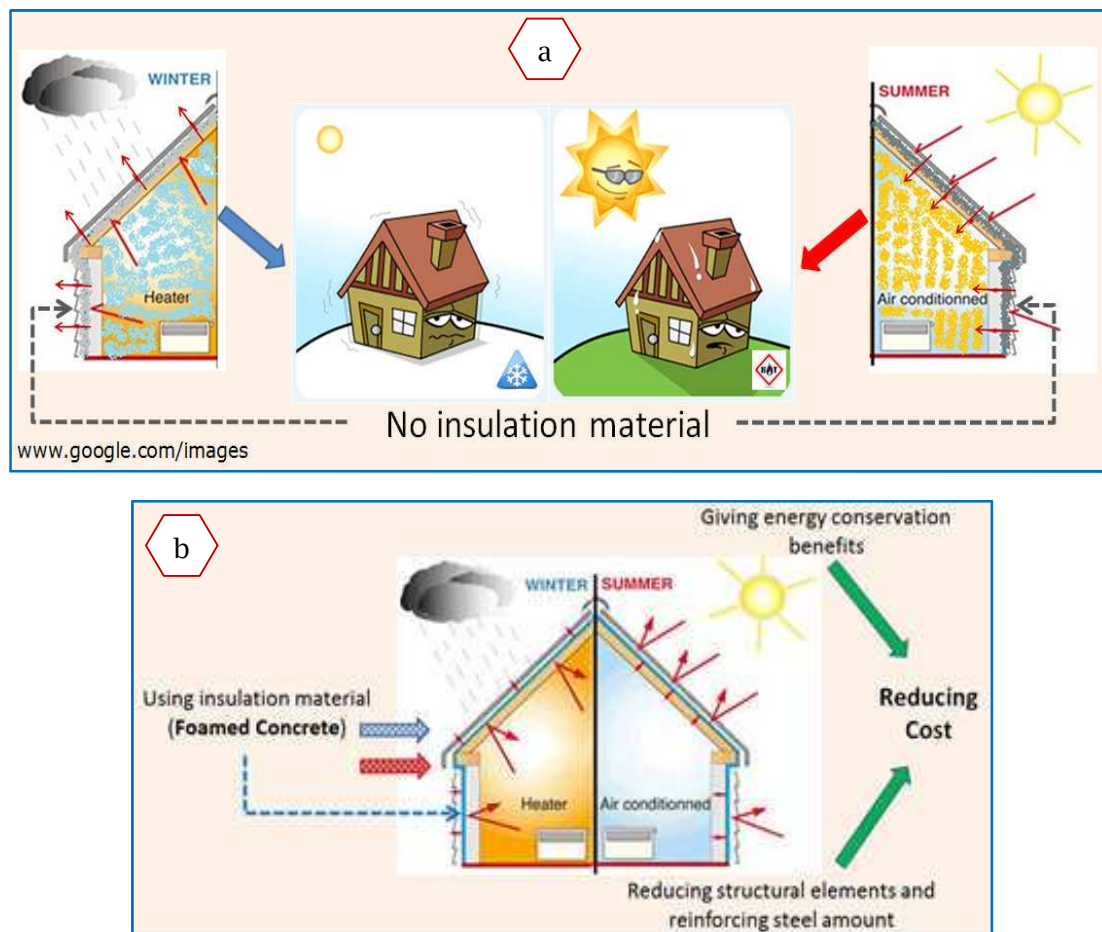
Figure 1-4 (a) Without thermal insulation material (b) with thermal insulation material

1.6 Scientific Novelty

To the author's best knowledge, there has been no specific study to evaluate the influence of microstructure changes, resulting from different added foam volumes or, for a given density, from inclusion of additives or lightweight aggregate (LWA), on the damage mechanism of foamed concrete. In addition, it is the first trial to investigate the formation of voids during mixing by determining and comparing the size distributions of air voids in the foamed concrete mixes (after hardening) to those of bubbles in the preformed foam based on both number and area of bubbles/voids and by investigating the circularity of the voids within the mixes. In addition, a study has been undertaken to investigate the effect of different additives on the strength of foamed concrete by characterising air-void size and shape parameters and identifying the influence of these parameters and changes to cement paste microstructure on strength.

The merit of this research is to understand how foamed concrete behaves with changes in its microstructure and provide a quantitative and qualitative analysis to correlate the microstructure with its mechanical, thermal and permeation properties as well as to establish, in the future, numerical models of the damage process.

1.7 Aim, Objectives and Methodology

1.7.1 Aim

The aim of this research is to produce, by using the preformed foam method, foamed concrete with/without lightweight aggregate which is suitable for semi-structural or structural purposes with good insulation and durability properties and to evaluate its damage behaviour. The idea is to make different mixes of foamed concrete with enhanced strength/weight ratio, to understand their behaviour and establish the effect of their microstructure on the macro properties. To achieve that, an attempt has been made to investigate the mechanical, thermal and permeation performance as well as damage behaviour of foamed concrete, associated with changes in its microstructure that result from inclusion of admixture, additives and lightweight aggregate (LWA).

1.7.2 Objectives

In order to achieve the aim of the research, the study includes the following specific objectives:

1- Produce a range of structural and non-structural foamed concretes with varying insulation and durability properties.

2- Study and understand how microstructure affects their mechanical, thermal and permeation properties.

3- Investigate and understand mechanisms of stress-induced damage (micro and macrocracks) for this type of lightweight concrete by using several techniques classified into surface observations, internal observations as well as fracture energy tests.

1.7.3 Methodology

The work consists of the following tasks; see **Figure 1-5**:

Task 1: **(A)** Design the mixes with or without admixtures, additives and LWA by means of the absolute volumes method, **(B)** Produce foamed concretes with a density not exceeding 2000 kg/m³ including mixes, for structural purposes, with a 28-day compressive strength in excess of 17 MPa and good thermal properties.

Task 2: Investigate the mechanical properties of the selected foamed concrete mixes such as compressive strength, tensile strength, flexural strength and modulus of elasticity as well as thermal insulation properties such as thermal conductivity and heat capacity and durability properties such as porosity, water absorption, sorptivity and permeability.

Task 3: Study the effects of microstructural characteristics in terms of the air voids system and ITZ characteristics on the behaviour of foamed concrete mixes by using Scanning Electron Microscopy (SEM), Mercury Intrusion Porosimetry (MIP), Optical Microscopy (OM) and Micro Computed Tomography (μ CT) techniques.

Task 4: **(A)** At micro level, investigate damage inside foamed concretes exposed to mechanical loading by examine the internal structure using 2D captured images from the SEM technique. In order to understand the failure mechanism, quantitative (distribution and orientation of formed microcracks) and qualitative (formation and propagation of microcracks) studies will be done, **(B)** At macro level, identify surface cracks at different stages of loading by taking pictures during loading and measuring the surface displacements and strains using the Digital Image Correlation (DIC) technique.

Task 5: Describe the fracture behaviour of foamed concrete mixes as well as characterizing them using fracture energy G_f and investigate the ductility from elasticity, fracture and fractal points of view.
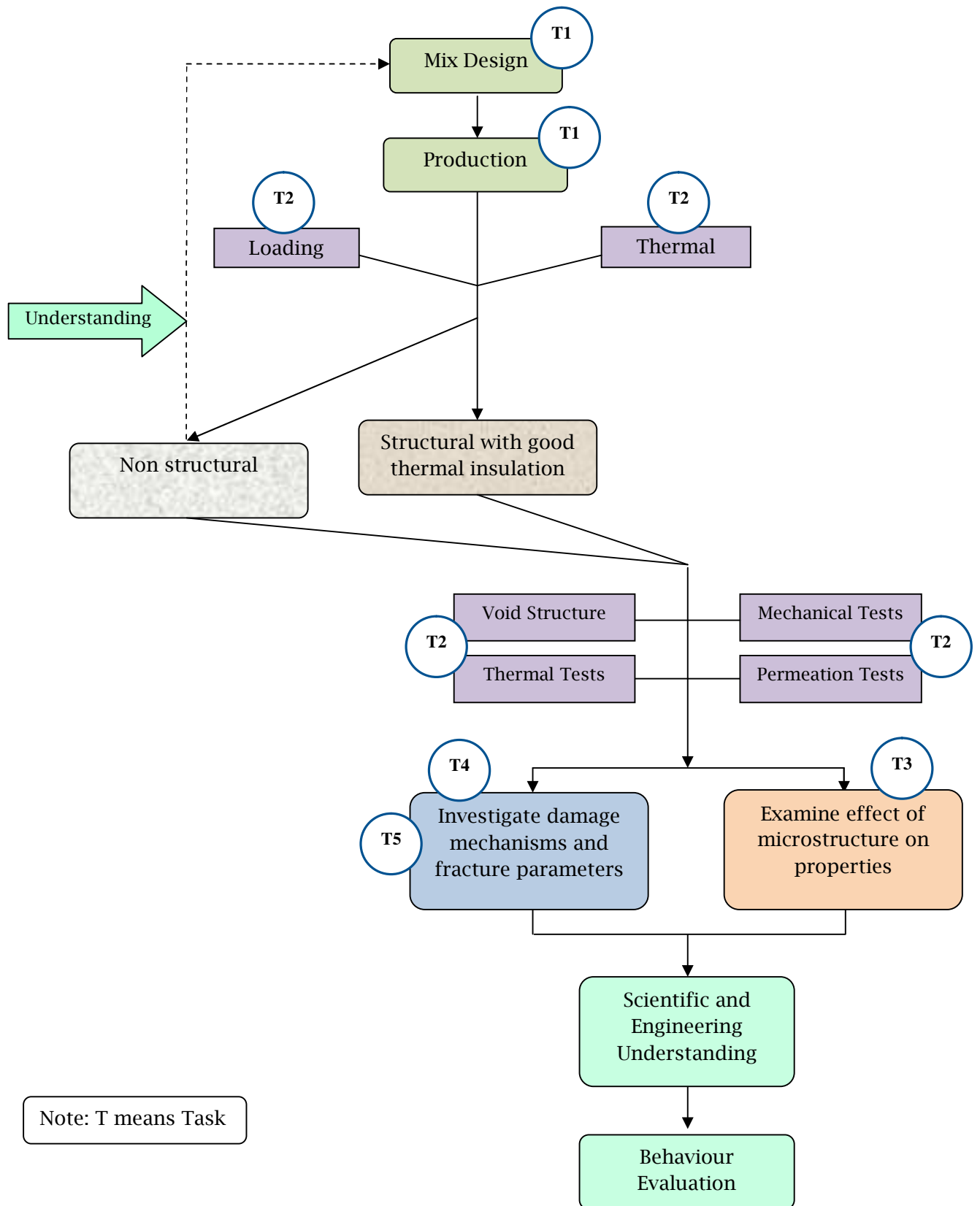
Figure 1-5 Project Flowchart

1.8 Structure of the Thesis

The organization of the thesis is as follows:

Chapter one has provided the general theoretical background in terms of definition and classification of concrete. In addition, reasons for use of structural lightweight concrete and its applications as well as some applications of foamed concrete have also been discussed. Finally, the aim, objectives and research methodology were presented.

Chapter two contains a brief review of lightweight concrete. In addition, it reviews pertinent literature on foamed concrete in terms of production and properties.

Chapter three introduces the details of the experimental programme in terms of mix design and production. Then, it presents the results of consistency and density of the investigated foamed concrete mixes. Finally, the test programme is presented.

Chapter four covers the techniques used to characterise air-void structure of foamed concrete in terms of porosity, void distribution, void shape and void connectivity. In addition, the effect of additives on air-void structure is examined and discussed.

Chapter five presents the results of mechanical and thermal properties of the investigated mixes. In addition, the effect of void characterisation on strength is discussed.

Chapter six covers the permeation properties in terms of water absorption, sorptivity and permeability. It discusses different measurement and calculation methods for permeability and the correlation between them. Finally, the effect of air-void characterisation on the permeation characteristics is examined.

Chapter seven discusses the brittleness of the foamed concrete mixes from fracture, fractal and elasticity points of view. In addition, surface cracks at different stages of loading are identified. Finally, to understand the failure mechanism, it presents quantitative (distribution and orientation of formed microcracks) and qualitative (formation and propagation of microcracks) studies.

Chapter eight summarizes the main conclusions of this study and makes recommendations for future work.

Chapter 2: Literature Review

2.1 General

Today, in various applications, concrete is the most widely used construction material worldwide. It is obvious that in concrete construction there are important advantages in reducing the weight of concrete. One of the most successful approaches to reduce the total load in a multi-storey building is to reduce its weight by using light construction materials.

Lightweight concrete is a light building material with a satisfactory strength as well as good thermal insulation. Thus, it is not only beneficial in reducing the total load from the structure, but also achieving energy conservation advantages and reducing heating/air-conditioning costs.

2.2 Lightweight Concrete

According to Bouvard et al. (2007), lightweight concrete (LWC) can be produced by replacing all or part of standard aggregate by lightweight materials. Depending on production methods, lightweight concrete can be classified into three types: no-fines concrete (leaving out the fine aggregate from the mix), lightweight aggregate concrete (using lightweight aggregates) and aerated concrete (introducing gas or bubbles) (Neville, 2011), see **Figure 2-1**.

Newman and Choo (2003), suggested that lightweight concrete can be produced with densities ranging from 300 to 2000 kg/m³ and corresponding cube strengths between 1 and 60 MPa and values of thermal conductivities from 0.2 to 1.0 W/mK compared with 2100-2500 kg/m³, 15 to greater than 100 MPa and 1.6-1.9 W/mK for normal weight concrete. By exploiting the properties of lightweight concrete, it can be used as a structural material as well as enhancing thermal insulation. Lightweight concrete has been used for structural applications and the demand for

it in modern construction has already been increasing for many years because of envisaged benefits of use such as higher strength/weight ratio and lower thermal conductivity (Tanyildizi and Coskun, 2008, Shannag, 2011). According to Kosmatka et al. (2002), except that structural lightweight concrete having a lower density, ranging from 1350 to 1850 kg/m^3, it is similar to normal weight concrete with 28-day compressive strength exceeding 17 MPa and its primary use is to reduce the dead load in concrete members.
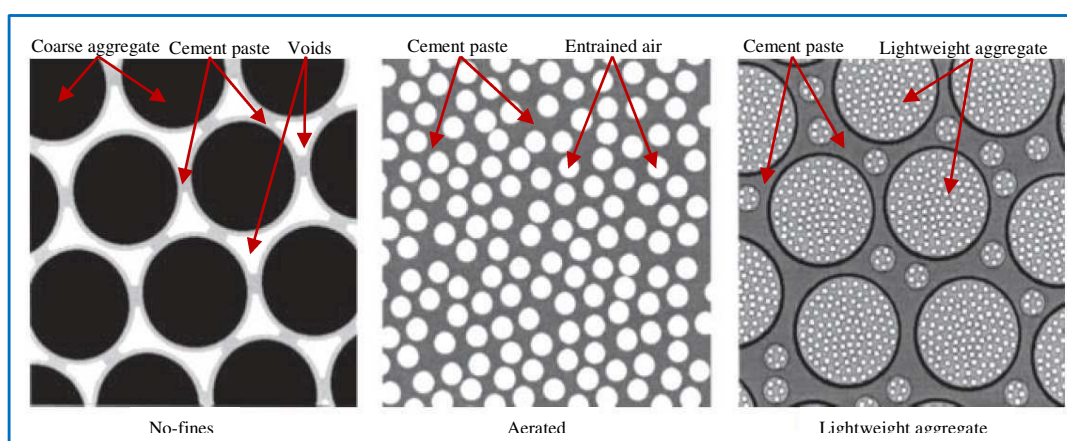
Figure 2-1 Basic forms of lightweight concrete, after (Newman and Choo, 2003)

2.3 Cellular or Aerated Concrete

ACI committee 523.2R-96 (1997), stated that "the material which is commonly referred to as cellular or aerated concrete, may be defined as: lightweight product consisting of Portland cement and/or lime with siliceous fine material, such as sand, slag, or fly ash, mixed with water to form a paste that has homogeneous void or cell structure. The cellular structure is attained essentially by the inclusion of macroscopic voids resulting from a gas-releasing chemical reaction or the mechanical incorporation of air or other gases". Neville (2011), demonstrated that the cellular structure of aerated concrete represents cells of size 0.1 to 1 mm being able to withstand mixing, moulding and compaction.

Orchard (1976), reported that aerated (cellular) concrete (depending on the pore formation method) can be produced in the following ways which are also illustrated in **Figure 2-2**.

- By mixing air entraining agents with cement or cement and sand in special high speed mixers (mix-foam method).

- By making foam (by using a foam generator) and then adding a given quantity of it to cement or cement-sand mortar in an ordinary mixer (pre-formed foam method).

- By adding hydrogen peroxide (H_2O_2) to the concrete to generate oxygen.

- By the use of calcium carbide (CaC_2) to produce acetylene gas (C_2H_2).

- By adding aluminium powder or zinc powder to cement mortar to generate hydrogen.

Depending on the curing method, aerated concrete can be non-autoclaved (NAAC) or autoclaved (AAC) (Narayanan and Ramamurthy, 2000). Narayanan and Ramamurthy (2000) added that although aerated concrete is known as an insulation substance, there has been interest in its structural features. Currently, cellular lightweight concrete can be produced for structural, insulation and filling purposes (Jitchaiyaphum et al., 2011).
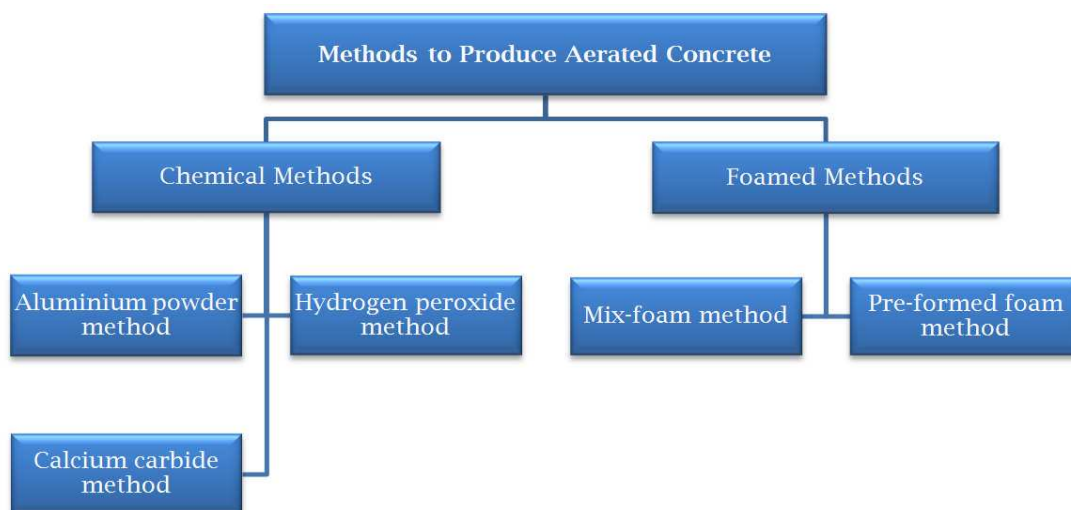
Figure 2-2 Methods to produce aerated concrete

2.4 Foamed Concrete

2.4.1 General

Pan et al. (2007), stated that research activities which relate to foamed concrete preparation and its technology date back to 1923, when a foamed concrete patent was granted to J. A. Eriksson. However, they added, due to the relationship between foamed concrete and its practical application techniques, most information about the early research activities is presented in the form of patent documents.

Foamed concrete is a versatile material consisting of either Portland cement paste or cement filler matrix (mortar) with homogeneous pore structure created by entrained air voids roughly 0.1-1.0 mm size (Nambiar and Ramamurthy, 2007a), (Ramamurthy et al., 2009), (Othuman and Wang, 2011), (Jitchaiyaphum et al., 2011). According to production method, foamed concrete can be divided into two groups: physically foamed concrete (by using foaming agents) and chemically aerated concrete (by adding aluminium powder), (Just and Middendorf, 2009). However, Esmaily and Nuranian (2012), showed that foamed concrete based on the method of pore formation can be classified into three groups: air-entraining method (chemical reaction), foamed method (pre-formed foam method) and combined method (introducing air and stabilizing it with gas). In addition, Nambiar and Ramamurthy (2007a), reported that introduction of pores inside foamed concrete can be achieved mechanically by preformed foaming (preformed foam before being added to the mix) or mix foaming (mixing foaming agent with the matrix). It should be noted that the foamed concrete investigated in this project has been manufactured using the preformed foaming method, see **Figure 2-3**. Moreover, foamed concrete can be cured either at ambient or slightly elevated temperature or in a high pressure steam environment at higher than 100 C˚ (Esmaily and Nuranian, 2012).

Owing to the presence of air bubbles, foamed concrete may possess several benefits and be widely used in construction projects as thermal, sound insulation

and void filling material (Pan et al., 2007). Where higher strength is required, foamed concrete can also be used in semi-structural applications such as bridge abutments, road sub-bases, floor and roof screeding (Jones and McCarthy, 2006). Furthermore, some applications exploit foamed concrete's ability to absorb energy such as vehicle arresters on airport aprons, ballistic range targets and roadway crash barriers (Tikalsky et al., 2004).
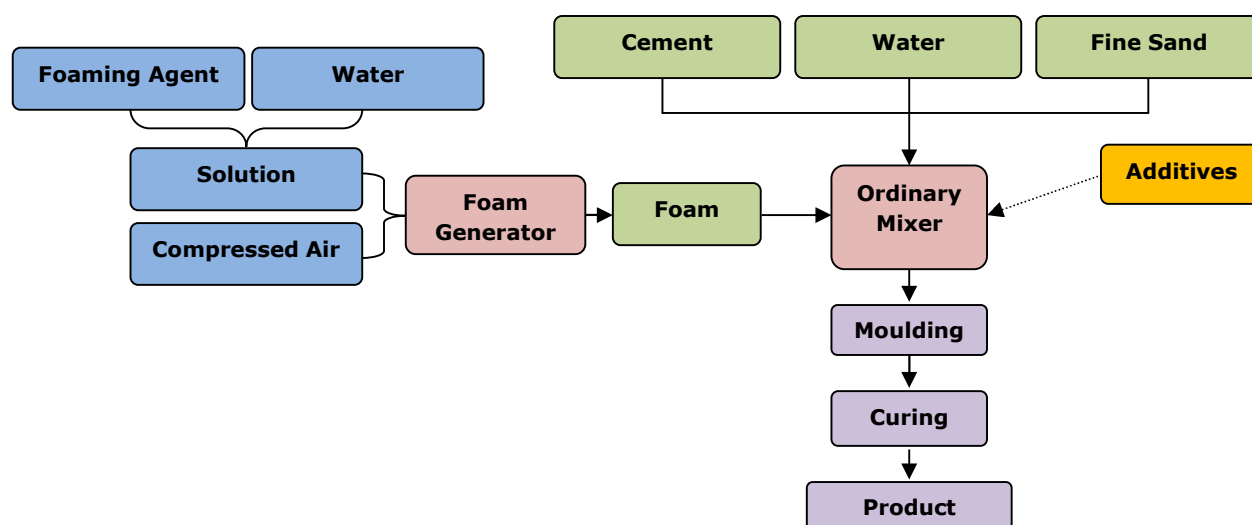
Figure 2-3 Flowchart of foamed concrete production via preformed foaming process

2.4.2 Production of Foamed Concrete

2.4.2.1 Constituent Materials

i. Constituent of Base Mix

In addition to ordinary Portland cement, the essential components of the base of foamed concrete are fine sand and water. For practical requirements, additives with various particle sizes and specific surface areas can be added to the raw materials to improve some desirable characteristics of the final product, see **Figure 2-4**.
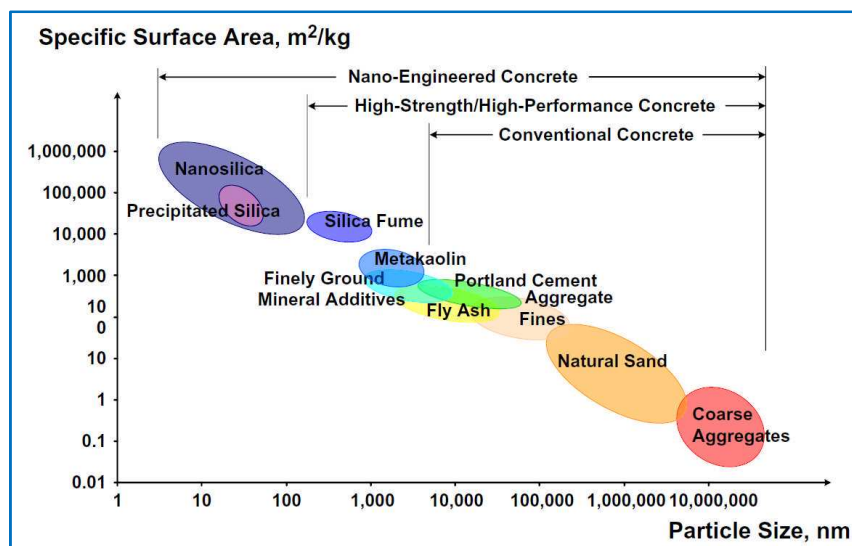
Figure 2-4 Raw materials of concrete and some supplementary additives (Sanchez and Sobolev, 2010)

Cement is the most commonly used binder; however other supplementary materials can also be used. The most available supplementary cementing materials are silica fume, a by-product of the reduction of high-purity quartz with coal in electric furnaces in the production of silicon and ferrosilicon alloys, and fly ash, a by-product of the burning of coal in thermal power stations (Tanyildizi and Coskun, 2008, Chen and Liu, 2008, Agarwal, 2006, Kayali, 2008). **Figure 2-5** shows that the particles in a typical fly ash vary from <1 μm to about 100 μm in diameter with more than 50% by mass less than 10 μm. In addition, compared to Portland cement and fly ash, silica fume shows finer particle size distribution by two orders of magnitude with a mean particle diameter of about 0.1 μm.

The use of fly ash in foamed concrete either as a cement or as a fine aggregate replacement can lead to enhancement in properties by reducing heat of hydration and giving the material good thermal insulation (Jones and McCarthy, 2005). Meanwhile, silica fume is usually added to improve cement paste/aggregate bonds (Balendran et al., 2002). In addition, fly ash and ultra- fine granulated blast-furnace slag have been used to reduce the cost, improve the mix consistency, reduce heat hydration and enhance the strength of high performance foamed concrete (Pan et

al., 2007). Fly ash has ever been used as a binder on its own, giving increased strength (Kearsley and Wainwright, 2001b), (Nambiar and Ramamurthy, 2007b), (Jitchaiyaphum et al., 2011). In addition, silica fume up to 10% of binder has been added to improve the strength of foamed concrete (Tikalsky et al., 2004), (Pan et al., 2007).
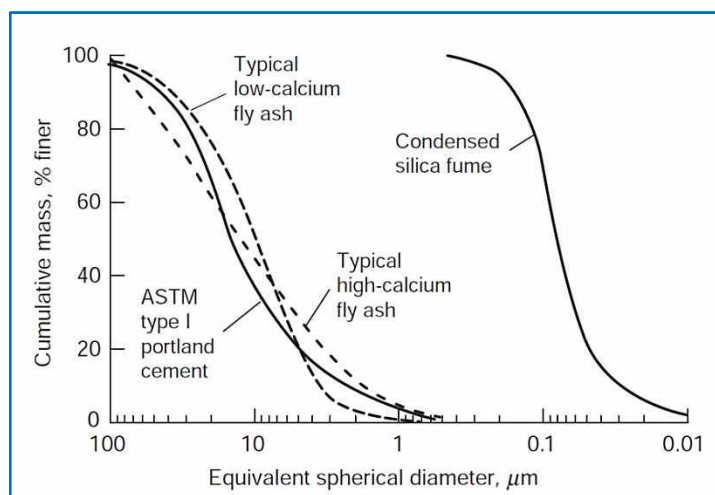
Figure 2-5 Particle size distribution of cement, fly ash and silica (Mehta and Monteiro, 2006)

The requirement of water for a mix relates to the consistency and stability of the mix and use of admixtures. According to ACI 523.3R-93 (1993), mixing water for foamed concrete should be fresh, clean and drinkable.

Sand, inorganic fine aggregate, is most commonly used for producing foamed concrete and it can be classified into natural and artificial. According to ACI 523.3R-93 (1993), sands conforming to ASTM C33 and ASTM C144 are acceptable for production of foamed concrete. Jones and McCarthy (2005) and Othuman and Wang (2011) used fine sand conforming to BS EN 12620 to produce foamed concrete with density between 800 and 1600 kg/m³. Based on several studies, Ramamurthy et al. (2009) pointed out that alternative fine aggregate materials are possible. Lime, chalk, crushed concrete, incinerator bottom ash, recycled glass, expanded

polystyrene and Lytag fines have all been used to reduce the density of foamed concrete and/or to use waste materials.

Regan and Arasteh (1990) stated that the combination of a foamed cement matrix with a lightweight aggregate (LWA) leads to a material with real saving in weight, significant thermal insulation and sufficient strength for structural purposes. These authors also reported that, though some research has been made in this area, the information available on foamed lightweight concrete is very limited.

Lightweight aggregates (LWA) can be divided into two categories: natural substances and synthetic materials made from natural materials or from industrial by-products (Neville, 2011). Their light weight is due to the cellular or highly porous microstructure which results also in a low apparent specific gravity. Natural LWA is made by crushing igneous volcanic rocks such as pumice, scoria and tuff. Synthetic or manufactured LWA is best classified on the basis of the raw materials used and the manufacturing method. They are manufactured by thermal treatment (1000-1200 °C) of a variety of materials such as clays, shale, slate, pearlite, blast furnace slag and fly ash. This treatment causes expansion due to the generation of gases which become entrapped in a viscous pyroplastic mass leading to a reduction in apparent specific gravity (Mehta and Monteiro, 2006, Neville, 2011).

Figure 2-6 illustrates the spectrum of lightweight aggregates in terms of their types and weights. It shows, at the lighter end, very porous aggregates for non-structural insulating concretes and, at the other end, relatively less porous aggregates capable of producing structural concrete (Mehta and Monteiro, 2006).
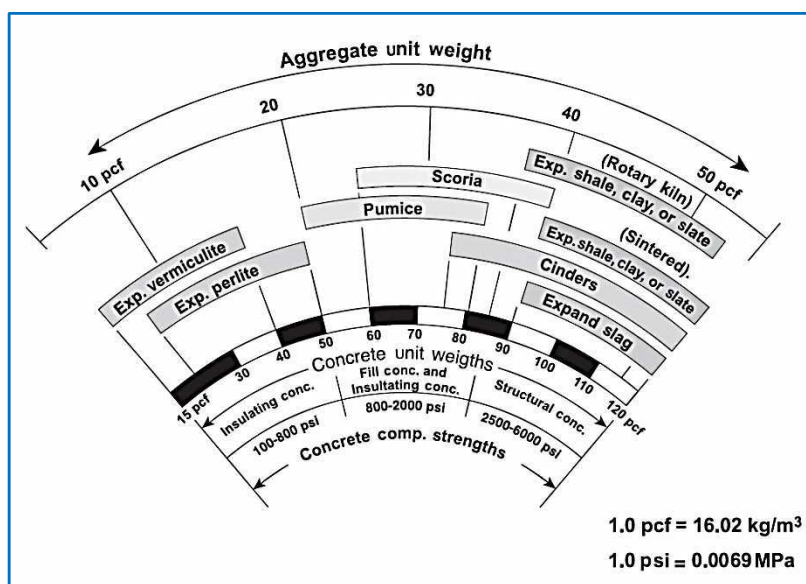
Figure 2-6 Lightweight aggregate spectrum (Mehta and Monteiro, 2006)

The use of fibres can help to reduce cracking of foamed concrete. However, they must have a high modulus of elasticity and be of sufficient strength to develop the required tensile resistance. For example, polypropylene fibres of 19.2 mm length have been used to enhance plasticity and tensile strength of foamed concrete (Jones and McCarthy, 2005). Fibres that can used for production of foamed concrete are: glass fibre, synthetic fibre and carbon fibre, however steel fibres are not suitable for foamed concrete since they may settle to the bottom of a concrete mixture (Ruiwen, 2004).

Superplasticizers, water-reducing admixtures, were developed in the 1970s and have found wide acceptance in the concrete construction industry. The surfactant imparts a strong negative charge when adsorbed on cement particles, leads to lower the surface tension of the surrounding water and greatly improves the fluidity of the system (Mehta and Monteiro, 2006). The mechanism of action is illustrated in **Figure 2-7** and can be summarised as follows: when the cement particles (which have a mixture of positive and negative charges) are mixed with water, they coalesce into flocks resulting in trapping a considerable amount of mixing water and therefore reducing the fluidity. To solve this, adding the superplasticizer

(which constitutes a negative ionic group) will form a negative charge on the cement particles after adsorbing onto them. Now, the cement particles repel each other and become more dispersed releasing the trapped water and increasing the fluidity (Domone and Illston, 2010). To ensure the successful introduction of foamed concrete, it is important to maintain a sufficient workability of the base (unfoamed) mix. To achieve this and to produce foamed concrete with good strength, the addition of water-reducing agent would be necessary (Ruiwen, 2004). Although superplasticisers are important to increase the strength, their use in foamed concrete can lead to instability of the foam; therefore compatibility of admixture with foamed concrete must be tested (Ramamurthy et al., 2009). Jones and McCarthy (2005) used superplasticiser, conforming to BS EN 934-2, to produce foamed concrete as a structural material.

(a) Adsorption on to cement particle surface

(b) Dispersion of particle flocs and realease of entrapped water to give greater fluidity
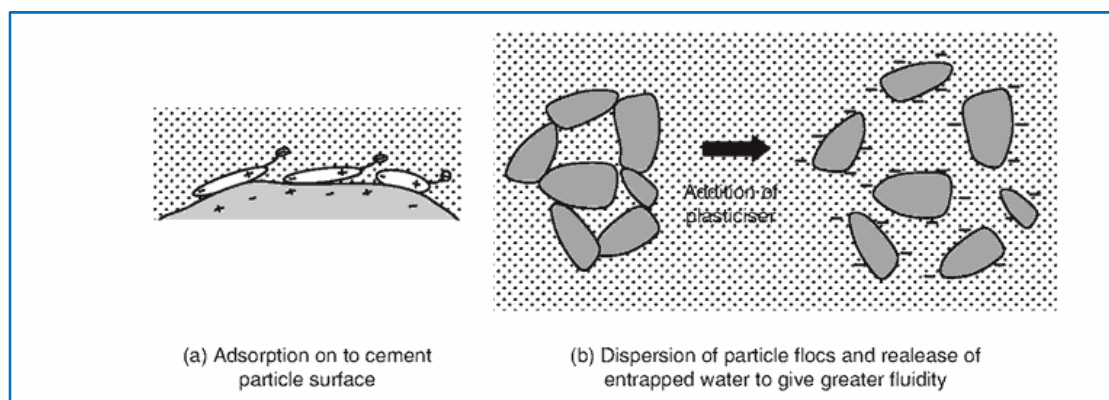
Figure 2-7 Diagrammatic representation of plasticisers' action (Domone and Illston, 2010)

ii. Foam

Foam bubbles are air voids enclosed by a foaming agent solution wall. There are many types of foaming agents; however the common ones are synthetic agents such as resin soap and protein-based foaming agents such as hydrolysed protein. As described by ACI 523.3R-93 (1993), preformed foam is produced by blending predetermined proportions of a foaming agent, water and compressed air in a foam

generator, see **Figure 2-8**. It should be noted that the quality of foam is affected by several factors such as its density, the dilution ratio of the foaming agent, the applied pressure and the blending process with the base (unfoamed) mix (Ruiwen, 2004).

Ramamurthy et al. (2009) stated that the foam must be stable in order to resist the pressure of the mortar during mixing and placing until the cement takes its initial set. In addition and depending on the method of production, preformed foam can be either wet or dry. Wet foam, 2-5 mm bubble size, can be generated by spraying a foaming agent solution over a fine mesh, while dry foam, extremely stable with size smaller than 1 mm, "is produced by forcing the solution of foaming agent through a series of high density restrictions and forcing compressed air simultaneously into the mixing chamber" (Ramamurthy et al., 2009).
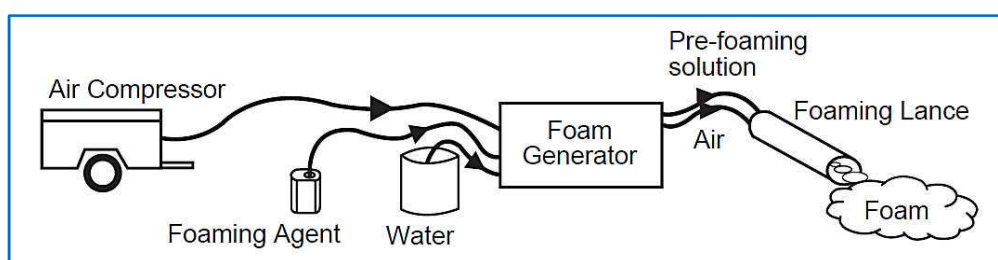
Figure 2-8 Making foam from foaming agent, water and compressed air (EAB Associates, 2001)

2.4.2.2 Mix Design and Mixing Procedure

In general, the properties of concrete depend on the proportions of its raw materials. ACI 523.3R-93 (1993) stated that the mix proportioning of foamed concrete begins with the selection of its wet density, cement content and the water to cement ratio and then the mix is designed by the absolute volumes method.

For production of foamed concrete, the mixing procedure adopted by several researchers is as follows: after the quantity of raw materials has been worked out, dry constituents will be mixed in an ordinary mixer for a few minutes. Then, mixing

water will be added in stages. After thorough mixing, preformed foam will be added to the wet slurry. Even though foam should be completely mixed with the mortar, excessive mixing should be avoided due to the possibility of changes in density and consistency. Ruiwen (2004) stated that component materials of foamed concrete can be added into a mixer by three different sequences which are as follows:

i. Dry materials ⟶ water with admixtures dissolved in ⟶ foam (Valore,1954)

ii. Water with admixtures dissolved in ⟶ dry materials ⟶ foam (American Concrete Institute, 1993).

iii. Partial water ⟶ partial dry materials ⟶ partial water ⟶ partial dry materials ⟶ foam (E-A-B Associates Bayley-Edge Limited).

2.4.3 Preparation of Foamed Concrete

In terms of moulding, ASTM C 495-99a (1999) stated that the concrete should be placed in two approximately equal layers and tapping the sides of the mould lightly with a rubber hammer during the filling operation until the layer surface has settled to a plane. Then, the top surface should be finished and covered with a plastic bag to prevent evaporation. However, if desired, a glass or metal plate should be used to obtain a suitable surface for testing without capping.

As far as removal from moulds is concerned and as for all types of concrete, foamed concrete specimens must not be removed from moulds if there is a danger of damage. However, in any event, removal of specimens from moulds within 7 days after moulding is recommended by ASTM C 495-99a (1999).

With regard to the curing, there are several ways that have been adopted to prevent the loss of specimen water. According to both of ASTM C796 (1997) and ASTM C495 (1999), for the first 24 hours after moulding, the specimens should be maintained at a temperature of 21.1±5.5°C. After that, they should be cured, for 7

days, under damp sand and wet burlap or similar materials with temperature lower than that of the surrounding atmosphere. Then, they should be stored at a temperature of 21.1±5.5°C and a relative humidity of 50±30% for 18 days. For curing foamed concrete specimens, both Han (2006) and Babu (2008) adopted the method of moist curing in a fog room at a temperature of 30±2°C until the day of testing. However, Ruiwen (2004) cured the specimens for splitting tensile strength in moist condition for 7 days and in air at a temperature of 30±2°C for the remaining time. In preliminary views on the potential of foamed concrete as a structural material expresed by Jones and McCarthy (2005), the specimens were sealed-cured (wrapped in cling film and stored at 20°C until testing). They also added that sealed-curing reflects typical industry practice for foamed concrete. For curing specimens of structural lightweight concrete, ASTM C330 (2003) stated that the unhardened specimen should be covered with a nonabsorptive or nonreactive plate, and then it should be stored in a moist room at 23±2°C with a relative humidity of not less than 95%. While, for precast cellular concrete units, ACI 523.2R-96 (1997) reported that these units are normally cured by high-pressure steam curing (autoclaving) or by atmospheric steam curing.

2.4.4 Properties of Foamed Concrete

This section is concerned with properties of foamed concrete in both the fresh and hardened state.

2.4.4.1 Fresh Properties

Foamed concrete, unlike normal weight concrete, must not be compacted or vibrated since this would affect its design density; however, both ASTM C495-99a (1999) and C796-97 (1997) stated that, in moulding, the sides of moulds should be tapped lightly with a rubber mallet after mix placing. Therefore, flowability and self-compactibility represent significant fresh state characteristics of foamed

concrete and they are evaluated in terms of consistency and stability of the mix. The consistency and stability of foamed concrete are affected by the water content in the base (unfoamed) mix and the amount of foam (Ramamurthy et al., 2009).

The stability of foamed concrete, the state of the mix at a density ratio (measured fresh density divided by design density) close to unity, relates to the consistency of the unfoamed mix and can be expressed in terms of the water-solids ratio. The consistency of foam concrete is defined by its spreadability and flowability measurement. It is reduced by adding foam to the unfoamed mix depending on the added foam volume or for a given density on filler type (Nambiar and Ramamurthy, 2008). Before that, Nambiar and Ramamurthy (2006), also stated that for a given mix: the flow reduces when foam is added and it therefore reduces steeply with a reduction in design density (increase in foam volume). They added that a possible reason for this may be that the adhesion between the bubbles and solid particles in the mixture increases the stability of the paste resulting in reduced spreadability, noting that there are more bubbles at the lower densities.

According to Nambiar and Ramamurthy (2006), by using a standard flow cone (ASTM C230), the consistency of the mix before adding foam and the flow characteristics of it after adding foam can be determined by measuring the flow %. The variation of density ratio (measured fresh density divided by design density) with water-solids ratios for different filler type mixes for densities between 1000 to 1500 kg/m³ is illustrated in **Figure 2-9**.
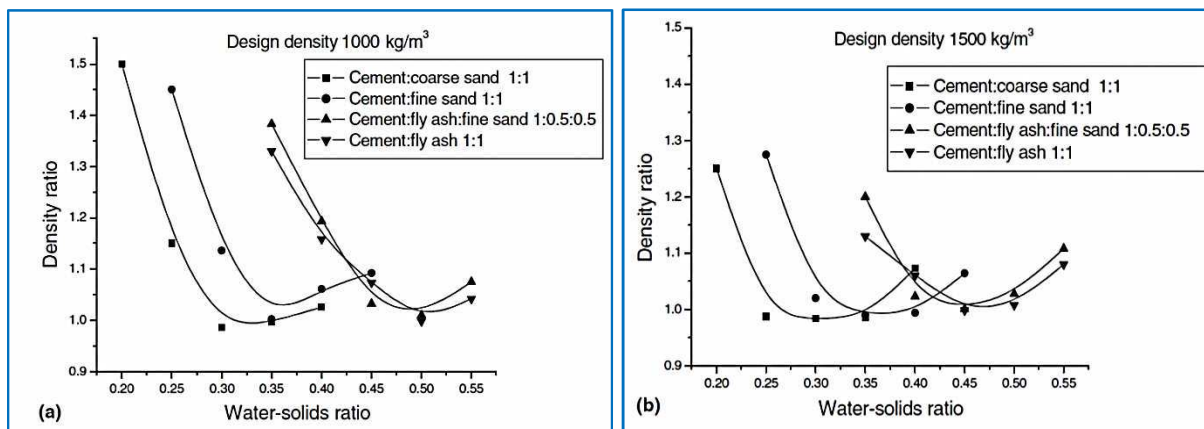
Figure 2-9 Variation of density ratio with water-solids ratio for different filler foam concrete (a) design density 1000 kg/m^3 (b) design density 1500 kg/m^3 (Nambiar and Ramamurthy, 2006)

At lower w/s ratios, with lower consistency, the density ratio is higher than unity. This is because the mix is too stiff to mix resulting in increased density owing to breaking of bubbles during mixing. On the other hand, there is also an increase in density ratio at higher water-solids ratios because higher water contents may result in foam segregation from the mix by making the slurry too thin to hold the bubbles, thus causing an increase in measured density.

Nambiar and Ramamurthy (2008), mentioned that even though superplasticizers are used to achieve a suitable workability, they may reduce the foam stability. As an alternative, in 1997, the Marsh cone was used by Marata and Suzuki to determine the flowability by measuring the time required for a paste to flow through a cone with a small opening. Then, to take account of sand particles as well as to classify the consistency of foam concrete based on flow time; this test was developed by Jones et al. (2003) by making the orifice diameter 12.5 mm instead of 8 mm and the volume of afflux 1 L instead of 200 mL. In addition, the Brewer spread test and slump flow test as per BS 4551-1 were used by Jones et al. (2003); however, Kearsley and Mostert (2005) used the ASTM hydraulic cement flow table for measuring spreadability. As described by Brewer (1996), workability of both the unfoamed mix

and foamed concrete can be quantified by the spreadability of a cylinder of material of 76.2mm diameter and 152.4mm height (Brady et al., 2001a).

From the above discussion, it is clear that the fresh properties of foamed concrete such as stability and consistency are affected by the volume of foam and water-solids ratio. By assessing the stability of foamed concrete, the water requirement for obtaining a density ratio near one is determined by trials. Moreover, the spreadability and the fluidity can be measured by using a standard flow cone (ASTM C230-1998) and the modified Marsh cone test, respectively (Nambiar and Ramamurthy, 2006).

2.4.4.2 Hardened Properties

i. Density

The properties of foamed concrete are influenced by its density and therefore, they should be qualified by the density, which is greatly affected by the moisture condition (Narayanan and Ramamurthy, 2000). Based on the previous studies, the density of foamed concrete is affected by the type of fine aggregate, aggregate gradation, sand-cement ratio and type of foam. For the same foam volume, compared to a product based on sand and cement, Ramamurthy et al. (2009) reported that replacement of sand with fly ash (lower specific gravity) led to reduced density with an increased strength. Thus, in order to achieve a specific density of foamed concrete with fly ash, a reduction in foam volume is required to gain the target density.

In the literature, empirical relationships for determination of foam concrete density are proposed. ACI Committee 523 (ACI-523.1R-92, 1992) reported the following equation as a useful method for calculating approximate oven-dry unit weight of foamed concrete:

$$Dry\ density = \frac{W_{da} + 1.2W_{ct}}{V} \qquad\qquad (2\text{-}1)$$

where: W_{da} is the weight of dry aggregate in the batch, W_{ct} is the weight of cement in the batch and V is the volume of concrete produced by the batch. It should be noted here that $1.2W_{ct}$ represents weight of cement plus water of hydration (considering water of hydration to be 20% of the cement weight).

ii. Mechanical Properties

It is obvious that, the compressive strength of foamed concrete decreases dramatically with a reduction in density. In total, it has been reported that the size and shape of the specimen, the method of pore formation, age, water content, characteristics of ingredients, method of curing and direction of loading all affect the strength of cellular concrete. In addition, cement-sand and water-cement ratios, curing regime, distribution of sand particles and type of foaming agent used have also been reported as parameters affecting the strength of foam concrete (Ramamurthy et al., 2009). Moreover, the compressive strength of foamed concrete is also influenced by the air void size and its distribution, the void/paste ratio, spacing and number of air voids. Also, Narayanan and Ramamurthy (2000), stated that the structure of air pores has a significant influence on the compressive strength of cellular concrete. In a study on the effect of replacing large volumes of cement (up to 75% by weight) with both ungraded and graded fly ash on the strength of foam concrete, it has been reported that up to 67% of the cement could be replaced without any significant reduction in strength (Kearsley and Wainwright, 2001a).

The modified form of Feret's rule (Kearsley and Wainwright, 2002) relating the strength of foamed concrete, water-cement ratio (w/c) and air-cement ratio (a/c), is given as (Narayanan and Ramamurthy, 2000):

$$Compressive\ Strength = K\left[\frac{1}{1+\frac{w}{c}+\frac{a}{c}}\right]^{n} \tag{2-2}$$

where, K and n are empirical constants.

According to Narayanan and Ramamurthy (2000), Valore reported the ratio of direct tensile to compressive strength of autoclaved aerated concrete to be 0.15 to 0.35, whereas Legatski placed it at 10-15%. Using sand may lead to improved shear capacity between its particles with the paste resulting in higher values of tensile strength (Ramamurthy et al., 2009). In addition, the ratio of flexural to compressive strength varies between 0.22 and 0.27.

The static modulus of elasticity (E_s) of foamed concrete is reported to be lower than that for normal concrete. For dry densities between 500 and 1500 kg/m³, its values vary from 1.0 to 8.0 kN/mm². Jones and McCarthy (2005), stated that use of polypropylene fibres has been observed to increase the E-value by between two and four times. They have reported relations for modulus of elasticity with density and compressive strength as follows:

$$E_s = 0.42f_c^{1.18} \qquad \text{Sand as fine aggregate} \tag{2-3}$$

$$E_s = 0.99f_c^{0.67} \qquad \text{Fly ash as fine aggregate} \tag{2-4}$$

It can easily be seen from the above equations that foamed concrete with sand as fine aggregate is reported to exhibit a higher E-value than that with fly ash.

Poisons ratio (v) is the ratio of the relative contraction strain to the relative extension strain. In a study on lightweight concretes (Babu, 2008), the Poison's ratios were found to be in the range of 0.18 to 0.24, 0.15 to 0.2 and 0.16 to 0.27 for foamed concrete, foamed lightweight concrete and lightweight aggregate concrete, respectively.

Based on both Narayanan and Ramamurthy (2000) and Ramamurthy et al. (2009), foamed concrete possesses high drying shrinkage, up to 10 times greater than that observed for normal concrete, owing to its high total porosity (40-80% by total volume) and the absence of aggregates. In addition, because the drying shrinkage of cellular concrete is dependent on the physical structure of the gel rather than on its chemical composition, additives such as superplacticiser and silica fume were found to have little effect on shrinkage. Moreover, it is reported that use of lightweight aggregate could reduce the shrinkage of foamed concrete. Furthermore, as a result of changes in mineralogical composition, autoclaving is reported to reduce the drying shrinkage dramatically by 12-50% of that of moist-cured concrete. However, Nambiar and Ramamurthy (2009) concluded that shrinkage of foamed concrete is lower than for the corresponding unfoamed mix. For example, with 50% foam volume, the shrinkage of foamed concrete was observed to be about 36% lower than that of an unfoamed mix. Furthermore, it decreases with an increase in foam content since higher foam content results in lower paste content and thereby the shrinkage will be affected by the lower content of pores in the paste.

iii. Thermal Properties

For aerated concrete, it is not really important whether the product is moist cured or autoclaved since the thermal conductivity depends on density, moisture content and the constituents of the material (Narayanan and Ramamurthy, 2000). Owing to its cellular microstructure, foamed concrete has excellent thermal insulating properties. For example, the thermal conductivity of foamed concrete of density 1000 kg/m^3 is reported to be one-sixth the value of typical cement-sand mortar and it ranges from 0.1 to 0.7 W/mK for dry density values of 600-1600 kg/m^3, reducing with decreasing density (Ramamurthy et al., 2009). According to Jones and McCarthy (2006), foamed concrete of density between 1000 and 1200 kg/m^3

exhibited typical thermal conductivity from 0.23 to 0.42 W/mK. Furthermore, use of fly ash and lightweight aggregate has been observed to be advantageous in reducing thermal conductivity. As the thermal conductivity is influenced by the moisture content (a 1% increase in moisture by mass increases thermal conductivity by about 42%), Narayanan and Ramamurthy (2000) suggested that it should not be reported in an oven dry condition.

From reviewing earlier studies, Narayanan and Ramamurthy (2000) surmised that the fire resistance of cellular concrete is more than or as good as ordinary concrete since it is relatively homogeneous and does not contain coarse aggregate which may lead to differential rates of expansion, cracking and dissolution. A study of fire resistance of foamed concrete by Othuman and Wang (2011) has concluded that foamed concrete offers a suitable alternative to gypsum as a construction material for partition walls. In summary, because the ratio of connected pores to total pores is lower, foamed concrete has lower thermal conductivity and good resistance to fire.

iv. Durability of Foamed Concrete

In general, the durability of concrete is affected by the fluid (gas or liquid) transport through its pore system resulting in deterioration of it. The transport of aggressive liquids into concrete depends on its permeation characteristics such as permeability, water absorption and sorption (Nambiar and Ramamurthy, 2007b) which represent the most important factors affecting the service life of a concrete structure (Sanjuan and Munoz-Martialay, 1996b). In consequence, an important indicator of concrete long term durability is its permeability which is the relative ease with which an aggressive substance can penetrate into concrete (Sanjuan and Munoz-Martialay, 1996b, Alshamsi and Imran, 2002, Neville, 2011). Therefore and because the durability of concrete is governed by its resistance to be penetrated by external aggressive agents, the property of permeability seems to be a reliable

estimator of its quality (Sanjuan and Munoz-Martialay, 1996a, Sanjuán and Muñoz-Martialay, 1997). Moreover, it is well known that transport properties are affected by the pore structure (Yang et al., 2006).

In terms of permeation characteristics, a relationship between porosity and water vapour permeability has been studied in foamed concrete and cement pastes by Kearsley and Wainwright (2001b). In this study, it was concluded that the water vapour permeability increases with increased porosity, or with decreased density, with similar trend lines for mixtures both with and without foam. The authors claimed that in the case of foamed concrete the air voids that are entrained can be considered as an aggregate and their inclusion might reduce the permeability not only by obstructing flow but also because of the absence of microcraking at the interface between air voids and the mortar.

Based on several studies, Ramamurthy et al. (2009) stated that the permeability coefficient of foamed concrete is proportional to pore content. In addition, the water transmission property may be better explained by sorptivity, absorbing and transmitting water by capillarity, than by permeability. Moreover, foamed concrete sorption may depend upon the filler type, pore structure and mechanisms of permeation. Nambiar and Ramamurthy (2007b), concluded that for a given mix type of foamed concrete, sorptivity and water absorption are mainly controlled by capillary porosity and decrease with a reduction in density. This is because the water absorption of foamed concrete is mainly influenced by the paste phase, which is of reduced volume, and the air voids are not involved in water absorption as their suction is much weaker than that of capillary pores (Nambiar and Ramamurthy, 2006).

With regard to resistance to aggressive environment, Ramamurthy et al. (2009) reported that foamed concrete provides good freeze-thaw resistance as well as good resistance to aggressive chemical attacks. However, according to Scheffler and

Colombo (2005), higher porosity leads to an increase in permeability resulting in an increase in susceptibility to the effects of freezing and thawing, also freeze-thaw damage increases as the density decreases. In addition, when sulphate attack is anticipated, protective precautions using bitumen-based materials should be applied (Narayanan and Ramamurthy, 2000). Jones and McCarthy (2005), reported that lower density concrete appears to carbonate at a relatively higher rate but that is not very serious unless the exposure to CO_2 is severe. Depending on the curing method, autoclaved aerated concrete is more durable than normally cured aerated concrete because the former consists of tobermorite, which is much more stable than the products formed in the latter (Narayanan and Ramamurthy, 2000).

2.4.5   Structure of Foamed Concrete

2.4.5.1 Base structure

Cement mainly consists of silica (SiO_2) or (S), alumina (Al_2O_3) or (A), lime (CaO) or (C) and iron oxide (Fe_2O_3) or (F). The main compounds of ordinary Portland cement are: Tri-calcium silicate (C_3S), Di-calcium silicate (C_2S), Tri-calcium aluminate (C_3A) and Tetra-calcium aluminoferrite (C_4AF).

The main phases present in hydrated cement paste microstructure can be listed as, (1) calcium silicate hydrate, C-S-H; (2) calcium hydroxide, CH; (3) ettringite, (4) monosulfate, (5) unhydrated cement particles, and (6) air voids (Mehta and Monteiro, 2006).

Based on the curing method, Narayanan and Ramamurthy (2000), stated that aerated concrete may be non-autoclaved (NAAC) or autoclaved (AAC). Even though the system of air voids remains comparable, there is a difference in the structure of NAAC and AAC which results from alteration in the hydration products.

Autoclaving initiates reaction between lime and silica/alumina bearing ingredients. In it, due to cement hydration, a part of the fine siliceous material

reacts chemically with lime and lime is liberated (calcareous material) forming a microcrystalline structure of lower specific surface.

For AAC, several studies have confirmed that the main reaction product belongs to the tobermorite group of calcium silicate hydrates (C-S-H) (Narayanan and Ramamurthy, 2000). In addition, the reaction product is a mixture of crystalline, semi-crystalline and near amorphous tobermorite. It should be noted that these reaction products of AAC have a much lower specific surface than that obtained by moist curing. Moreover, compared to AAC and over continued duration of moist curing, the structure of NAAC is changed from initial needle shaped hydrates to hexagonal ones and then to block shaped calcite crystals.

2.4.5.2 Pore Structure

The pore structure of cementitious material is a very significant characteristic since it affects properties such as strength and durability due to their dependence on material porosity, permeability and pore size distribution (Ramamurthy et al., 2009). The typical sizes of the voids in hydrated cement paste are illustrated in **Figure 2-10**.
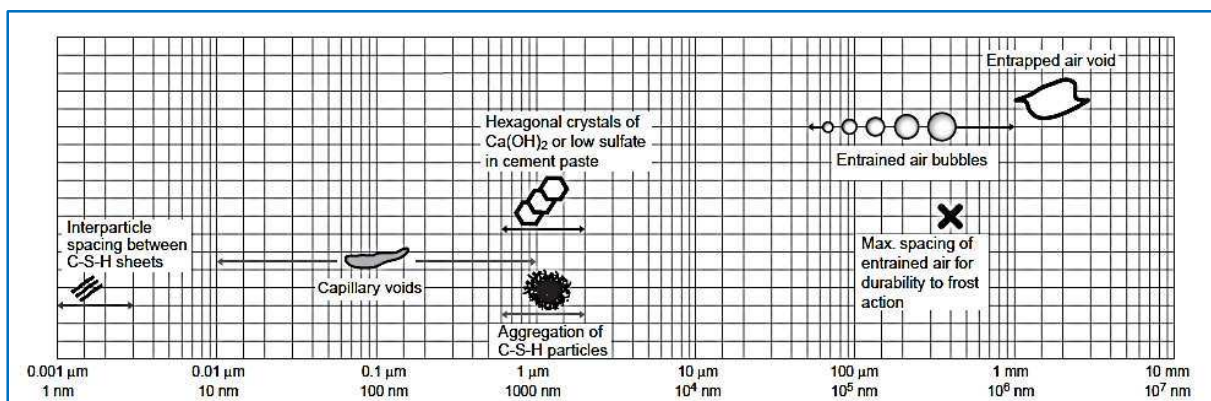
Figure 2-10 Dimensional range of pores in a hydrated cement paste (Mehta and Monteiro, 2006)

In aerated concrete, the structure is affected by the method of pore-formation (gas or foaming) and characterised into solid micro-porous matrix and macropores.

The micropores (with a diameter of more than 60 μm) appear in the walls of macrpores which are formed due to the expansion of the mass by aeration (Ramamurthy et al., 2009).

Based on pore size, the porous system of aerated concrete can be classified as artificial air pores, inter-cluster pores and inter-particle pores. Another method classifies the structure of aerated concrete in terms of pores with a radius of 50 to 500 μm as: microcapillaries of 50 nm or less (formed in the wall between the air pores), macrocapillaries of 50 nm to 50 μm and pores of more than 50 μm (introduced by aerating). Nambiar and Ramamurthy (2007a), stated that the pore system in cementitious material consists of gel pores, capillary pores and macro pores. Although the gel pores do not influence the concrete strength, they are directly related to creep and shrinkage. On the other hand, capillary and other large pores are responsible for reduction in strength and elasticity. According to both Just and Middendorf (2009) and Ramamurthy et al. (2009), the pore structure of foamed concrete is classified as gel pores, capillary pores and air-voids (air entrained and entrapped pores). In addition, the latter authors added that the air-voids in the foamed concrete may be characterized by a few parameters such as volume, size, shape, size distribution and spacing between air-voids. Compared to gas concrete (chemical reaction), the ratio of connected pores to total pores in foamed concrete is lower leading to lower air permeability (Ramamurthy et al., 2009).

Just and Middendorf (2009), stated that by using low w/c ratio and adding microsilica, density increases and the average air voids diameter decreases. Furthermore, decreasing of the diameter of the pores may lead to regularly formed air voids resulting in increasing compressive strength for the same densities.

The above discussion indicates that the air-void system of foamed concrete could be a primary factor influencing its properties. Therefore, understanding the

pore parameters is important for producing a product with a high strength to weight ratio and good properties.

Narayanan and Ramamurthy (2000), listed some methods to determine the structure of cellular materials as follow:

1- Scanning electron microscopy (SEM), which is a precise method to determine the pore sizes and their distribution in cellular materials.

2- Mercury intrusion porosimetry (MIP); it corresponds to a minimum pore diameter of 75 Å and pores larger than 400μm cannot be characterized by this method.

3- Gas permeability, in which, the pore structure of material can be characterized by measuring gas permeability because the type, size and distribution of pores are responsible for permeability.

More recently, Just and Middendorf (2009), mentioned that light optical microscopy with an associated digital image analysis, mercury intrusion porosimetry as well as scanning electron microscopy were methods suited to examining foamed concrete samples. While Nambiar and Ramamurthy (2007a) mentioned added nitrogen gas absorption-desorption and X ray computed tomography with image processing to the above methods to measure the pores of foamed concrete.

Yu et al. (2011), stated that compared to scanning electron microscopy, light microscopy combined with digital analysis is much more convenient, cheaper and appropriate for the pore structure analysis of foamed concrete. However, the former is more powerful for both pore and micro structure as well as composition analysis of foamed concrete.

In terms of the pore structure parameters, Nambiar and Ramamurthy (2007a); suggested that to explain and quantify the air-void structure of foamed concrete, in-depth study is necessary to characterise the air voids through certain parameters

such as volume, size, distribution, shape and spacing as well as to investigate the influence of these parameters on density and strength. To achieve that, image analysis software was used on images of specimens captured by using an optical microscope. Both Nambiar and Ramamurthy (2007a) and Ramamurthy et al. (2009), mentioned that the air-void distribution is one of the most significant micro-properties influencing strength of foamed concrete whereas the latter author concluded that foamed concrete with narrower air-void distribution shows higher strength.

The pore structure and microstructure of foamed concrete have important influence on its properties. In spite of this significant influence, the investigation and evaluation of pore structure are seldom reported (Yu et al., 2011).

2.4.6 Interfacial Transition Zone (ITZ) in Concrete

Concrete may be considered to consist of three phases: a cement paste, aggregates and the interfacial transition zone (ITZ) between them. In the ITZ, the structure of the cement paste is different from that of the bulk paste in terms of morphology, composition and density. Compared to the bulk paste, the ITZ has less unhydrated cement, less C-S-H, large crystals of calcium hydroxide, greater concentration of ettringite and higher porosity (lower density) (Mindess et al., 2003). As in the bulk paste, calcium, sulphate, hydroxyl and aluminate ions are produced by the dissolution of calcium sulphate and calcium aluminate compounds. These ions combine to form ettringite and calcium hydroxide which, owing to the high w/c ratio, become larger in the vicinity of the aggregate resulting in more porous framework than in the bulk cement paste or unfoamed matrix (Mehta and Monteiro, 2006). The microstrucuture of an interfacial transition zone in concrete is presented schematically in **Figure 2-11**.
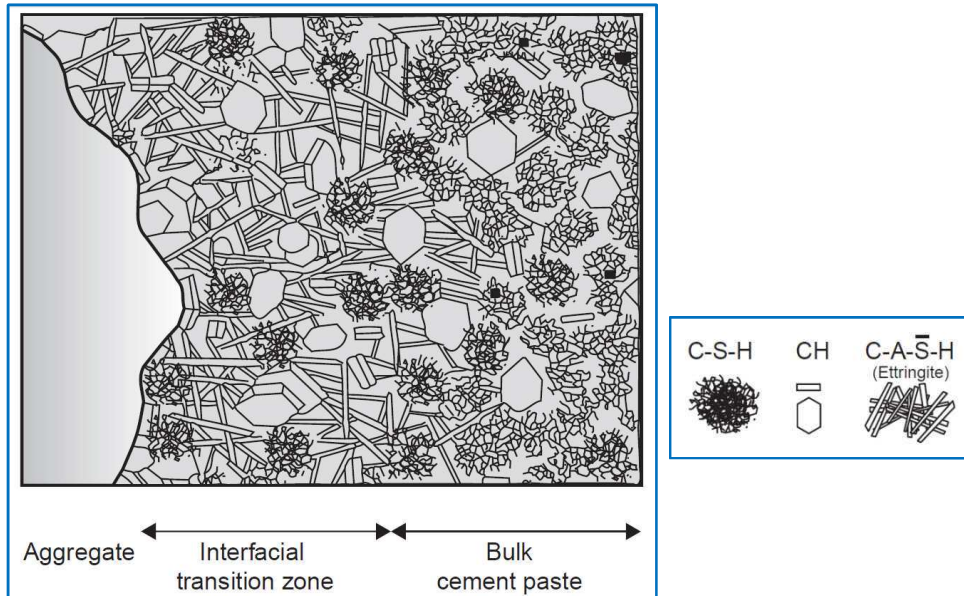
Figure 2-11 Schematic diagram of ITZ in concrete (Mehta and Monteiro, 2006)

Quantitative characterisation of the ITZ between aggregate and the cement paste in concrete confirms that it arises due to the packing of cement grains (1-100 μm) against the larger aggregate particles. In other words, this difference in size means that each aggregate particle is a mini "wall", disrupting the normal packing of the cement grains and leading to accumulation of smaller grains in the zone close to the aggregate while larger grains are found further out, see **Figure 2-12**. This packing leads to a more porous zone and the deposition of hydration products, especially calcium hydroxide, tends to fill this zone (Scrivener et al., 2004).
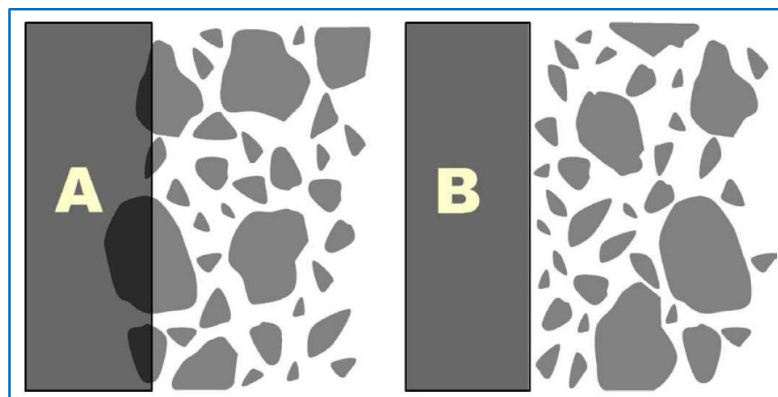
Figure 2-12 Schematic diagram showing "wall" effect of aggregate A) imaginary case B) reliable case (Scrivener et al., 2004)

The ITZ, about 50 µm thick, plays a role in the stiffness, strength and permeability of cementitious materials containing aggregate due to its generally lower density and strength compared to bulk cement paste. When the material is subjected to loads, microcracks may appear within the ITZ due to its weakness leading to the quasi-brittle nature of concrete (Mondal et al., 2007), see **Figure 2-13**. This explains the phenomenon that the components of concrete (aggregates and hydrated cement paste) usually remain elastic until failure during a uniaxial compression test, while concrete shows inelastic behaviour at levels higher than 70% of ultimate strength (Mehta and Monteiro, 2006).
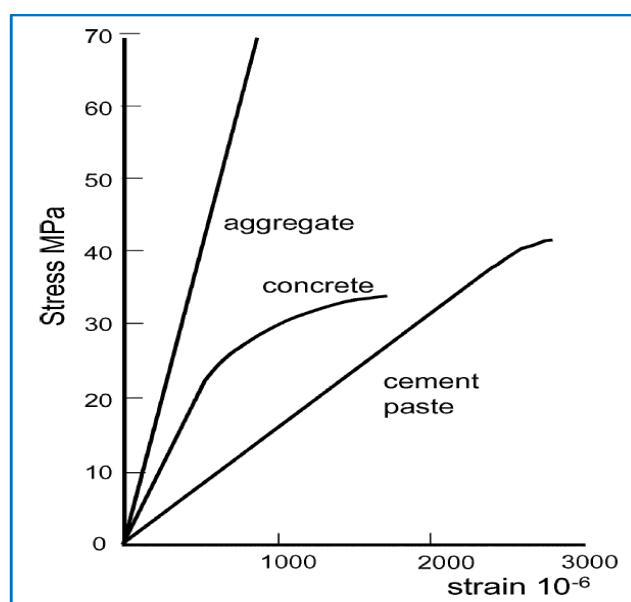
Figure 2-13 Effects of the ITZ on mechanical properties of concrete (Scrivener et al., 2004)

The quality of the bond between the paste matrix and aggregates is influenced by the shape, size, mineral composition, surface roughness, surface moisture content and porosity of aggregates as well as water to cement ratio. (Mondal et al., 2007).

In a study on the effect of water-cement ratio (w/c), aggregate size and age on the microstructure of the interfacial transition zone between normal weight aggregate and the bulk cement paste, it was concluded that the w/c plays an

important role in controlling the microstructure of the ITZ and its thickness. In addition, at the same w/c and age, reducing the aggregate size tends to reduce the porosity and increase the content of unhydrated particles (UH) in the region surrounding the aggregate. Moreover, at the same w/c (0.55), they reported the ITZ being more porous compared to the bulk paste at 180 days than at 7 days due to deficiency of UH content in the ITZ compared to bulk paste at an early age (Elsharief et al., 2003).

Zhang and Gjørv (1990) carried out an experimental work on the interfacial zone between different types of lightweight aggregates (LWA) and cement paste. They found that for LWA with a dense outer layer the nature of the ITZ is similar to that for normal weight aggregate. However, for LWA with a weaker and more porous outer layer and without any outer layer, the ITZ is more dense and homogenous with a better bond resulting from an improved mechanical interlocking between the aggregate and the cement paste. Moreover, LWA can act as an internal water reservoir (pre-wetted) and may increase the degree of hydration of cement in the ITZ by means of internal curing as schematically illustrated in **Figure 2-14**. This leads to the conclusion that the ITZ appears to depend on the microstructural characteristics of the aggregate.

In aerated concrete, the large pores may be treated as zero density aggregate and the interfacial transition zone between them and a paste is similar to that between aggregate and paste of normal concrete (Ramamurthy et al., 2009).
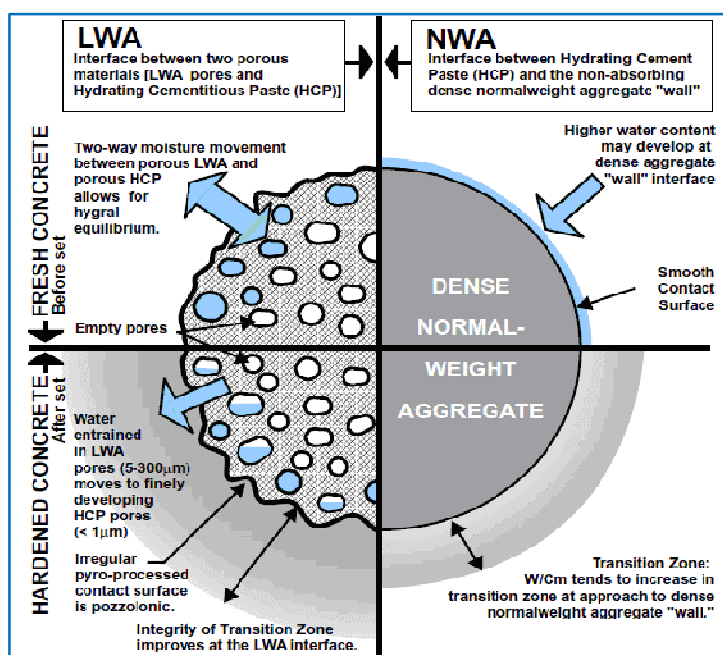
Figure 2-14 Schematic view of improving of the transition zone via internal curing process (Expanded Shale Clay and Slat Institute, 2010)

2.4.6 Fracture, Micro and Macrocracks

2.4.6.1 Fracture Mechanics of concrete

Fracture mechanics is a branch of solid mechanics which deals with the behaviour of the material in the vicinity of a crack and at the crack tip (Kumar and Barai, 2011). The theory of fracture mechanics was first applied to metals. However, during the past three decades, it has also been applied to concrete (Zhou, 1992).

Fracture mechanics of concrete, which is a branch of nonlinear fracture mechanics (NLFM) due to inelastic behaviour resulting from the presence of a fracture process zone (FPZ) ahead of a crack, was developed from the theory of linear elastic fracture mechanics (LEFM) (Shi, 2009).

Akçay (2007), stated that many attempts have been conducted over the years to make LEFM applicable to concrete and to establish the theories of nonlinear fracture mechanics. Zhou (1992) concluded that according to the stress-strain behaviour, there will be three different zones which are: linear elastic zone,

nonlinear hardening zone and fracture process zone around the crack tip, see **Figure 2-15**. It can be observed that LEFM is applied to the material in which the zone is very small **(Figure 2-15a)**, while the second case **(Figure 2-15b)** represents nonlinear behaviour for ductile material in which the fracture zone is small and the hardening plasticity zone is large. In addition, the case for concrete with a large fracture zone and small hardening plasticity is illustrated in **Figure 2-15c**.
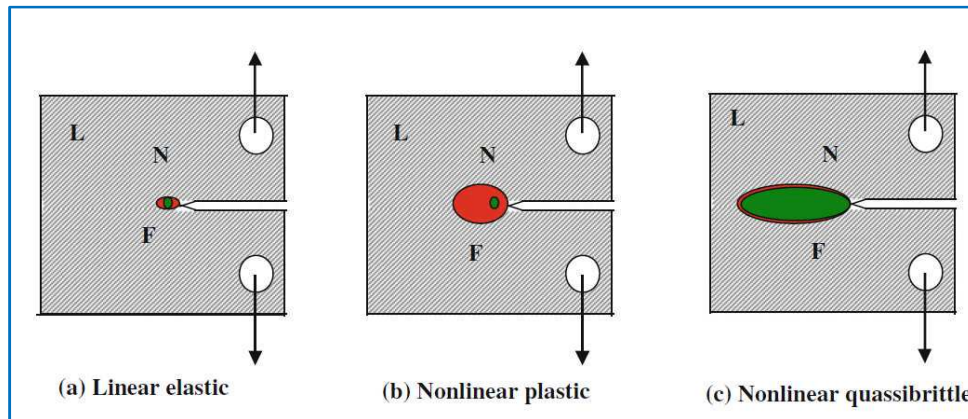
Figure 2-15 Types of nonlinear zones in different types of materials, L denotes linear elastic, N denotes the nonlinear behaviour due to plasticity, and F denotes the fracture process zone (Kumar and Barai, 2011)

Generally, there are three possible modes of deformation at the tip of a crack as below, also see **Figure 2-16** (Zhou, 1992, Akçay, 2007):

1- Opening or tensile mode (Mode I), which was examined by Griffith (1920) where the crack surfaces move directly apart.

2- Sliding or in-plane shear mode (Mode II), in which the crack surfaces slide over one another in a direction perpendicular to the major edge of the crack.

3- Tearing or antiplane shear mode (Mode III), the crack surfaces, in this type, move relative to one another and parallel to the major edge of the crack. The present investigation mainly concerns fracture in mode I.
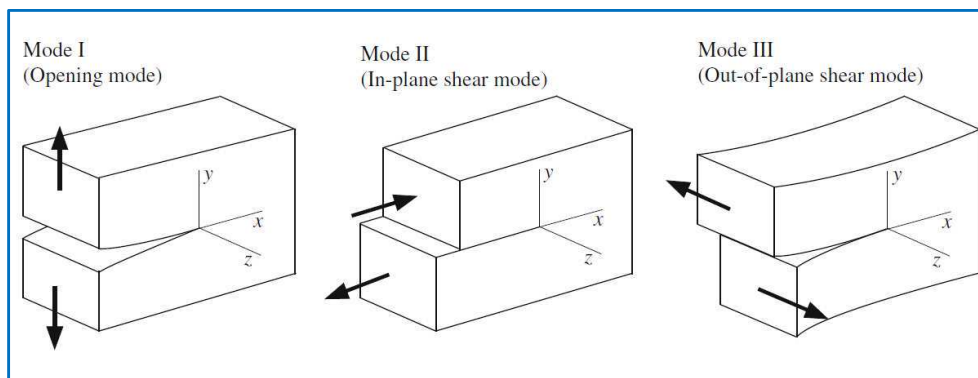
Figure 2-16 Three independent modes of deformation at the crack tip (Shi, 2009)

2.4.6.2 Fracture Mechanics of LWC

It is reasonable to suggest, the mechanical behaviour of concrete may be modelled at three levels which are: micro, meso and macro. For fracture modelling of concrete at a macro level, there is a need to know the fracture mechanics properties at the meso level. This is because of non-uniformity of the strain distribution in concrete. In addition, at a meso scale, the internal structure of concrete includes cement paste with voids, aggregates and the interfacial transition zones between them.

In concrete, the post peak tension softening of stress-strain behaviour is related to the crack propagation and the interaction between the cracks and other interfacial cracks and aggregates. There are several toughening mechanisms which are effective in the FPZ and lead to energy dissipation such as, crack shielding, aggregate bridging, crack deflection, crack trapping, distributed interfacial cracking, crack tip blunting by voids and crack trapping mechanisms; see **Figure 2-17**, (Shah et al., 1995).
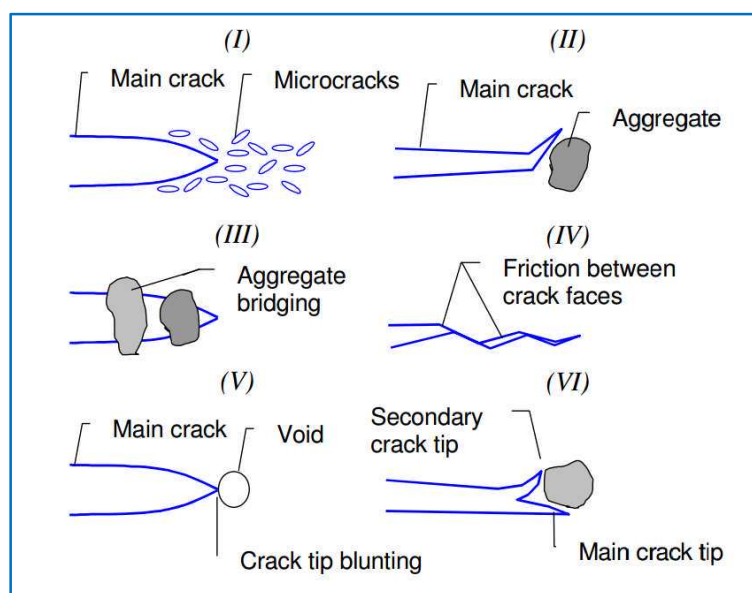
Figure 2-17 Some toughening mechanisms in FPZ (I) crack shielding (II) crack deflection (III) aggregate bridging (IV) crack surface roughness-induced closure (V) crack tip blunted by void (VI) crack branching (Shah et al., 1995)

In concrete, when the aggregate is stronger than the matrix, cracks propagate through the matrix; thus, the concrete strength is not very dependent on the aggregate strength. However, in lightweight concrete (LWC), the cracks pass through the relevant aggregate particles and their properties and volume concentration are very important (Akçay, 2007); see **Figure 2-18**. Thus, it has been suggested that the mechanism of aggregate/ligament bridging is expected to appear in LWC.

Chang and Shieh (1996) stated that the value range of energy fracture with artificial lightweight aggregates (LWAs), 34.42 to 37.20 N/m, is similar to that of normal concrete with similar strength. However, they added that, the application of fracture mechanics to LWC is still at an early stage.

According to Zhang and Ansari (2006), local intensification of stresses and propagation of micro and macro cracks result from the existence of spherical air voids in concrete. In general, damage develops in two stages. The first is the growth of cracks which emanate from the voids owing to their own stress intensity, while

the second stage involves growth of cracks related to the effect of their own stress field and the stress field of other cracks. It was assumed that for the first stage of damage a Mode I crack emanated from a single void; while during the second stage, crack extension caused interaction of stress fields among neighbouring cracks resulting in crack coalescence and final failure.
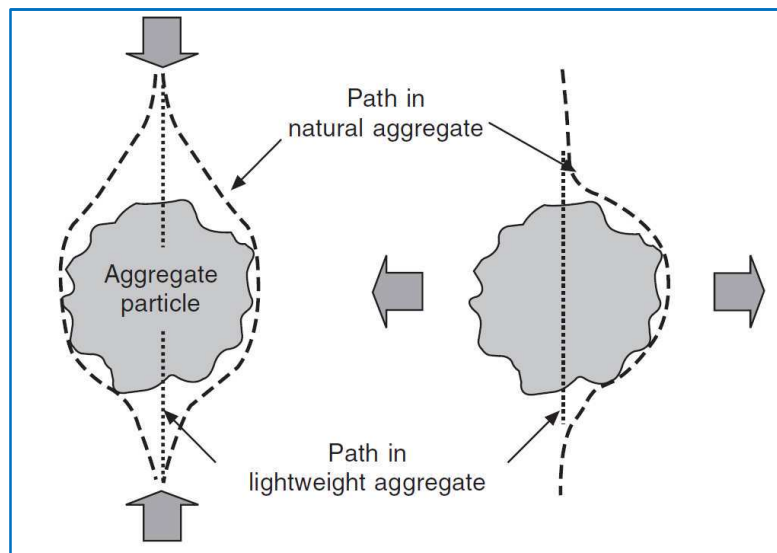
Figure 2-18 Fracture path in normal weight and lightweight concrete (Newman and Choo, 2003)

In a study of analysis of compressive fracture of three different concretes (high strength, normal strength and foamed concrete) (Caduff and Van Mier, 2010), it was found that, for all three types, cracks have a vertical orientation when specimens are loaded between Teflon inserts, while they have a certain inclination when steel loading platens are used. However, for foamed concrete, the use of Teflon seemed less useful for friction reduction and no influence on the compressive strength could be observed.

2.4.6.3 Micro and Macrocracks

Neville (2011) noted that although a crack may initiate due to one particular cause, its development may be due to another cause. In addition, in hardened concrete, cracking may be caused by drying shrinkage or by restrained thermal movement;

however, it can be also caused by applying a load greater than the actual strength of the concrete element. Cracks are initiated when the stress conditions exceed the matrix strength, the medium shear strength and the bond frictional strength between the matrix and the aggregate (Nawy, 2001).

Depending on their location, microcracks can be divided into three categories: bond cracks (within the ITZ), mortar cracks (within the mortar matrix) and aggregate cracks (through the aggregate), see **Figure 2-19**. Moreover, depending on their connectivity, cracks can be categorized into two types, namely single (isolated) and combined (connected) cracks. The simple cracks (bond or mortar cracks) are not connected to any other cracks. On the other hand, when two or more cracks become connected to each other (a combination of bond and mortar cracks), a combined crack will be generated (Erdem, 2012).
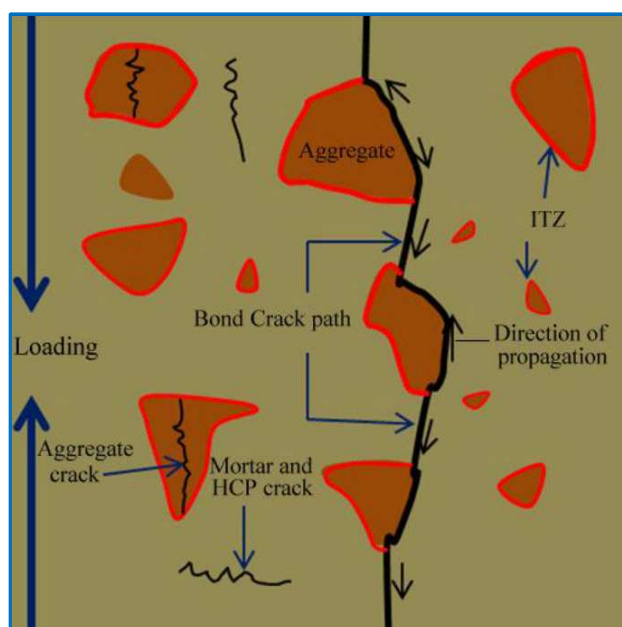
Figure 2-19 Cracking pattern in normal weight concrete (Domone and Illston, 2010)

It is generally agreed that mechanical loading causes the formation of microcracks in concrete. The mechanism of load induced microcracks can be summarised as follows: Soroushian and Elzafraney (2004) stated that before any loading, microcracks exist at interfaces between aggregates and cement paste due

to drying and thermal shrinkage. Furthermore, with additional stresses such as external structural load and environmental effects, tensile and shear stresses may be concentrated at these interfaces resulting in the growth and propagation of microcracks, which then join together causing large cracks and leading to concrete failure. Nemati (1997) reported that there are several factors leading to the existence of preload cracks such as bleeding, drying shrinkage and creep.

According to Caduff and Van Mier (2010), the fracture process in compression can be divided into four stages as follows: (1) linear elastic stage and (2) microcracking, which is associated with the rising branch of the stress-strain curve leading to maximum stress, while stages, (3) macrocrack and (4) bridging and frictional restraint, are related to the deterioration of the specimen in the post-peak softening regime.

According to Akçaoğlu et al. (2004) several researchers have investigated crack propagation in concrete under uniaxial compressive stress. It was concluded that before any applied loading, very fine cracks, microcracks, exist at the interfacial zone (ITZ) between the aggregates and the cement paste. With application of load up to 30% of the ultimate compressive strength (σ_c), these microcracks remain stable; therefore the stress-strain curve is almost linear. After that and until 50% of σ_c, they start to grow in length, width and number within the ITZ and non-linearity can be noticed. Between 50-75% of ultimate load, the cracks become unstable and propagate into the matrix body causing further non-linearity. At the final stage (beyond 75% of σ_c), bond and mortar cracks coalesce into single or multiple cracks and then rapid and continuous crack propagation is initiated through the matrix until fracture; see **Figure 2-20**.

Akçaoğlu (2005), stated that the microcracking process in the ITZ may be affected by two factors: the relative strength of the ITZ with respect to the mortar and the strength of the mortar itself. A high tendency for ITZ microcracking results

from a bigger difference between the ITZ and mortar strengths. Furthermore, cracks confined within the ITZ may be bounded by a stronger mortar matrix.

By experimental observation including scanning electron microscopy (SEM) on air-entrained concrete subjected to compression, it was shown that microcracks propagated in the direction of applied compressive stress and finally linked to form larger cracks leading to failure (Zhang and Ansari, 2006).

An experimental study on the effect of aggregate content on fracture behaviour of concrete under tension loading was done by Amparano et al. (2000). In which the fracture behaviour of concrete was characterized by two parameters: fracture energy G_f and effective fracture process zone. Later, Giaccio et al. (2007) studied the failure mechanism of normal and high strength concrete with rice-husk ash (RHA) in compression and tension by testing the stress-strain and load-deflection behaviour of specimens. From the analysis of failure mechanism, they found a tendency for more brittle failure behaviour in mixes with RHA.

Based on previous studies, Lofgren (2005) explained the uni-axial behaviour of concrete as presented in **Figure 2-21**. When a stress is applied, microcracks (pre-existing in the ITZ) will start to grow within the ITZ (A). Then, they propagate into the mortar (B); therefore non-linearity behaviour exists until the peak stress is reached (C). After that, microcraks propagate in an unstable manner and crack localisation occurs through the specimen leading to the stress drop (D). Finally, the softening tail (D-E) is observed resulting from the mechanism of crack bridging and branching.

Previous studies of foamed concrete have focused on the investigation of its properties and the factors influencing them. As a result, our knowledge of damage in foamed concrete and mechanical loading-induced cracks (macro and micro) is scarce. To improve the properties of foamed concrete it is essential to study its damage to realise how the cracks propagate under mechanical loading: through the

matrix, the voids or the interface between them; and to what extent additives are influential in determining which of these happens.
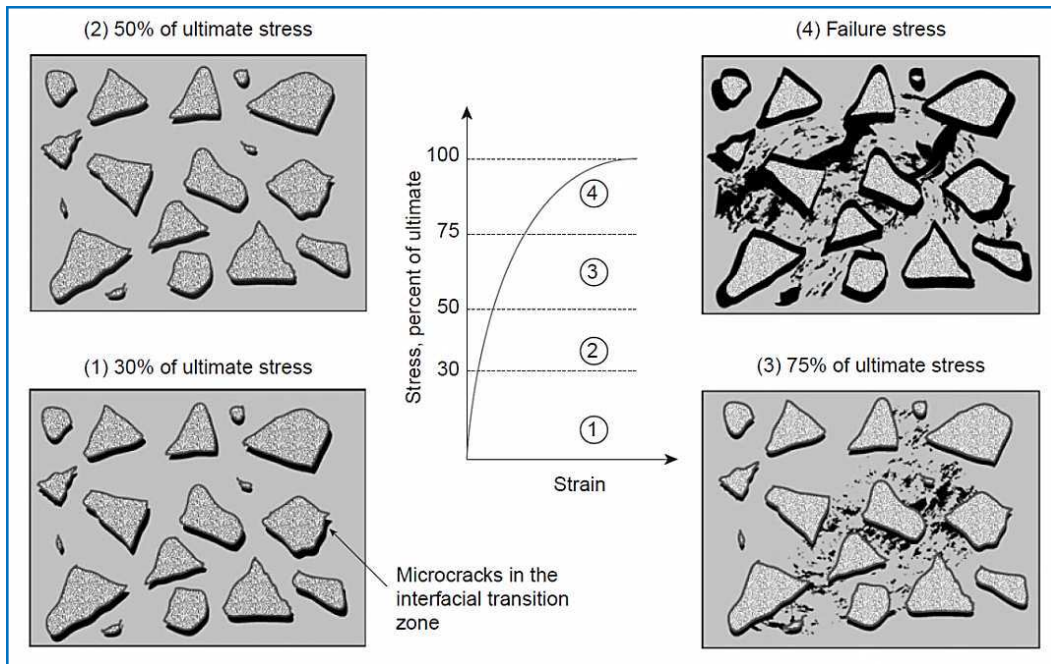
Figure 2-20 Diagrammatic representation of the stress-strain behaviour of concrete under compression (Mehta and Monteiro, 2006)
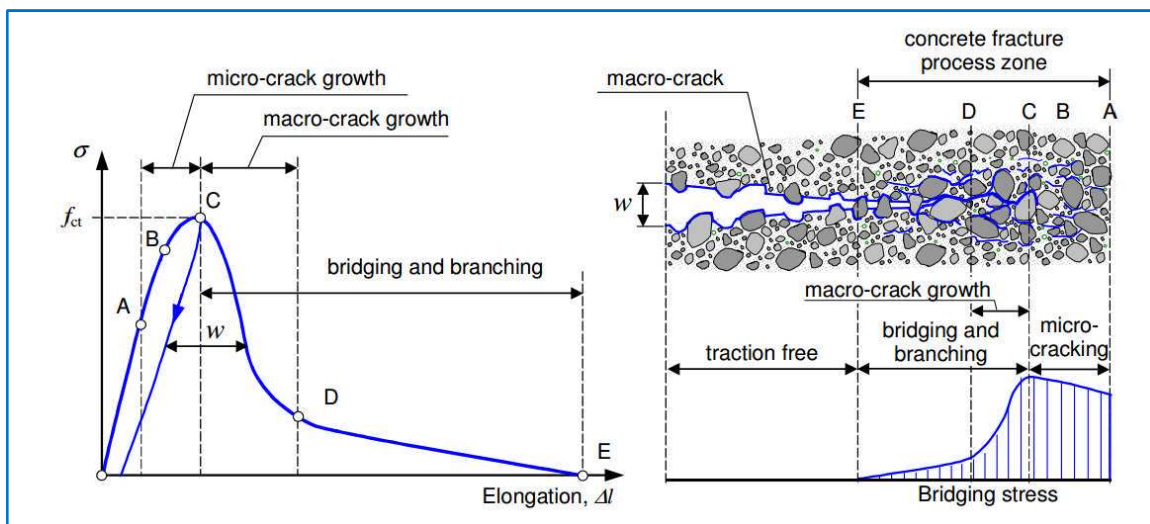
Figure 2-21 Schematic description of the fracture process in uni-axial tension and the resulting stress-crack opening relationship (Lofgren, 2005)

2.5 Summary

This chapter has aimed to provide the reader with a good background to the foamed concrete investigated in this research. To summarise and based on the literature that has been reviewed, the following points can be drawn:

- Foamed concrete is a type of lightweight concrete which is a versatile material consisting of either Portland cement paste or cement filler matrix (mortar) with homogeneous pore structure created by entrained air voids roughly 0.1-1.0 mm size.

- It can be produced physically (by using foaming agents) or chemically (by adding aluminium powder, hydrogen peroxide and calcium carbide).

- Owing to the presence of air bubbles, foamed concrete may be used in construction projects as thermal, sound insulation and void filling materials. Nevertheless, it is also used in semi-structural applications where higher strength is required.

- The properties of foamed concrete are influenced by its density, which is affected by the fine aggregate type, aggregate gradation, sand-cement ratio and foam type. Additionally, the air void system of foamed concrete could be a primary factor influencing its properties.

- Due to its cellular structure, foamed concrete has low water absorption, low thermal conductivity, high fire resistance and good resistance to freeze and thaw.

- Although studies of foamed concrete have focused on the investigation of its properties and the factors influencing them, its damage and mechanical loading-induced cracks (macro and micro) is still at an early stage.

Chapter 3: Materials and Experimental Programme

3.1 General

This chapter focuses on describing the materials used to produce a conventional foamed concrete and the additives adopted to enhance its properties, and the basis on which their proportions were chosen. Moreover, information about the equipment used, production, density, consistency and cost is provided. Finally, the test programme in terms of void structure, mechanical, thermal, permeation properties, and damage quantification, is presented.

3.2 Materials Used

As mentioned earlier, the main raw materials of foamed concrete (FC) are cement, sand, water and foam; however admixtures or additives may be used when a specific change in the properties of concrete is desired. Therefore, in order to carry out the aim of producing foamed concrete with enhanced strength (FCa); certain additives, namely superplasticizer, silica fume and fly ash as well as lightweight aggregate, were used in this project, see **Figure 3-1**. The materials used for this investigation can be explained as follows, see **Figure 3-2**:

Combinations of the following constituent materials were used to produce foamed concrete in this research.

- **Portland cement** CEM I-52,5 N, 3.15 specific gravity (S.G.), conforming to BS EN 197-1 (2011).

- **Fine aggregate (sand)**, 2.65 S.G., conforming to BS 882 (1992) with additional sieving to remove particles greater than 2.36 mm, to help improve the flow characteristics and stability of the final product (Jones and McCarthy, 2005, ASTM C144, 1987). The gradation of the used sand is illustrated in **Figure 3-3**.

- Fresh, clean and drinkable water.

- **Foam**: the quality of foam is critical to the stability of foamed concrete and will affect the strength and stiffness of the final product; therefore, good quality foam (45 kg/m^3) was produced by blending the foaming agent, EABASSOC (1.05 S.G.), water and compressed air in predetermined proportions (45 g water to 0.8 ml foaming agent) in a foam generator, STONFOAMM-4. The water for producing foam will be considered as part of the total mixing water (ASTM C796, 1997).

- **Superplasticizer**: MIGHTY 21 EG made by Kao Chemical GmbH of density 1.1 g/cm^3, was used as a water-reducing agent to maintain sufficient workability of the unfoamed mixture (without foam) and to produce a high strength foamed concrete with low water/binder ratio. In addition, this superplasticizer has been proved to be compatible with the EABASSOC foaming agent (Ruiwen, 2004).

- **Silica fume**: Elkem Microsilica (2.2 S.G., 92% SiO2, mean particle size 0.15 μm and specific surface 20 m^2/g) made by Elkem A Bluestar Company was used to fill the space between cement particles making the cement matrix denser and stronger, to gain early age strength and to improve cement/aggregate bonds.

- **Fly Ash**: to gain high strength and achieve more uniform distribution of air voids, CEMEX fly ash-class S (2.09 S.G.) conforming to BS EN 405-1 (2005), was used instead of part of the fine sand in the production of foamed concrete.

- **Light weight aggregate**: LYTAG lightweight aggregate conforming to BS EN 13055-1 (2002) with a saturated surface dry specific gravity of 1.64 in its coarse (4-10mm) size was used in some mixes, **Figure 3-4**. It is manufactured from pulverised fuel ash (provided by Lytag Ltd, UK) and sintered fly ash, a by-product from coal fired power stations (Cheeseman et al., 2005).
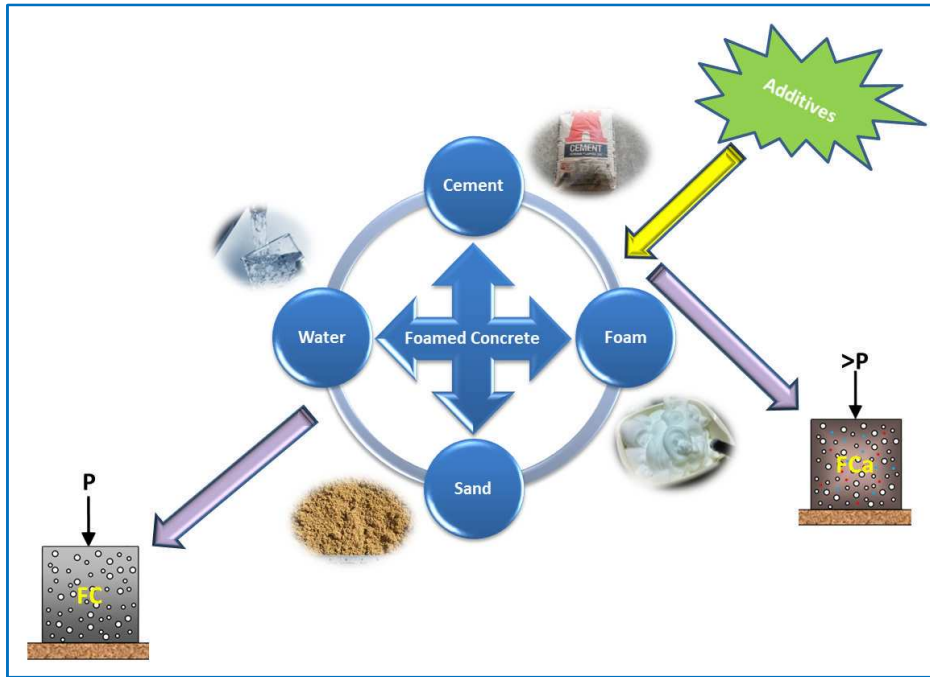
Figure 3-1 Materials used for production of foamed concrete
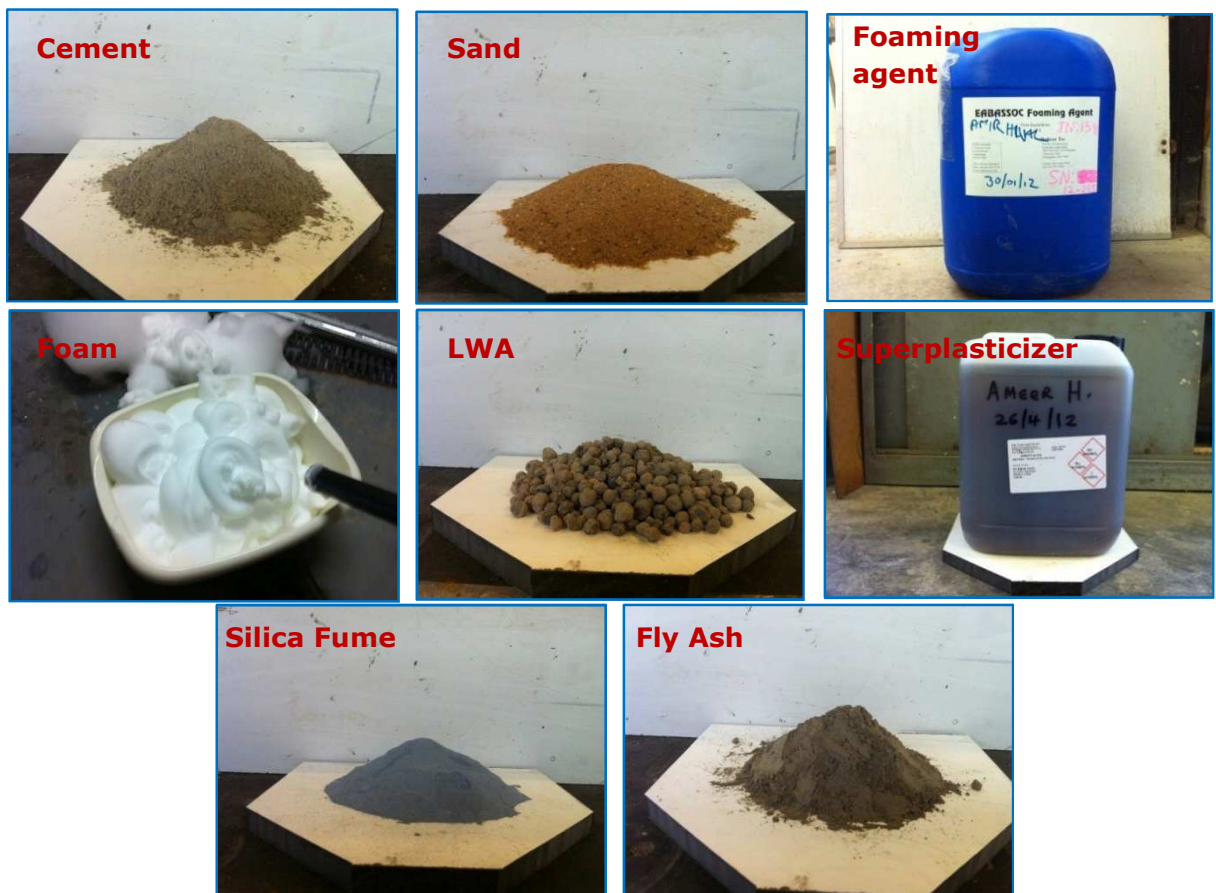
Figure 3-2 Materials used for production of foamed concrete
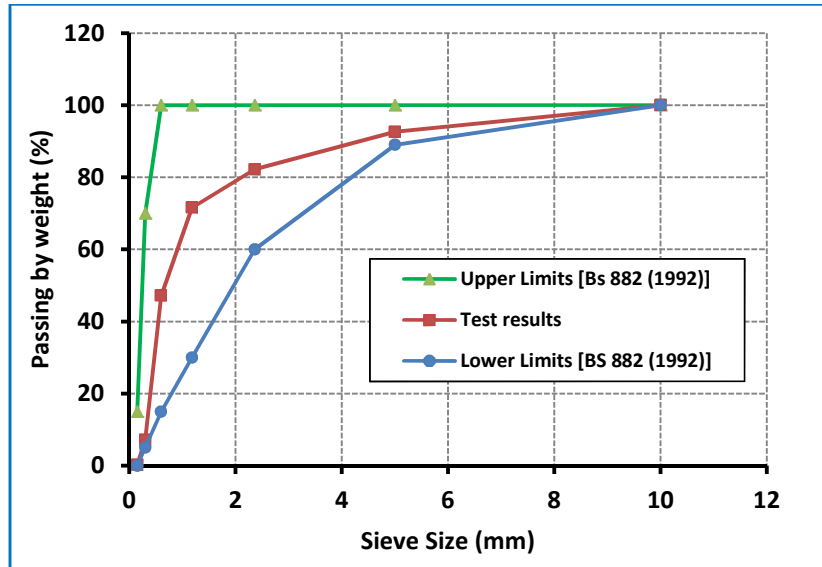
Figure 3-3 Grading curves for standard requirements and sand used
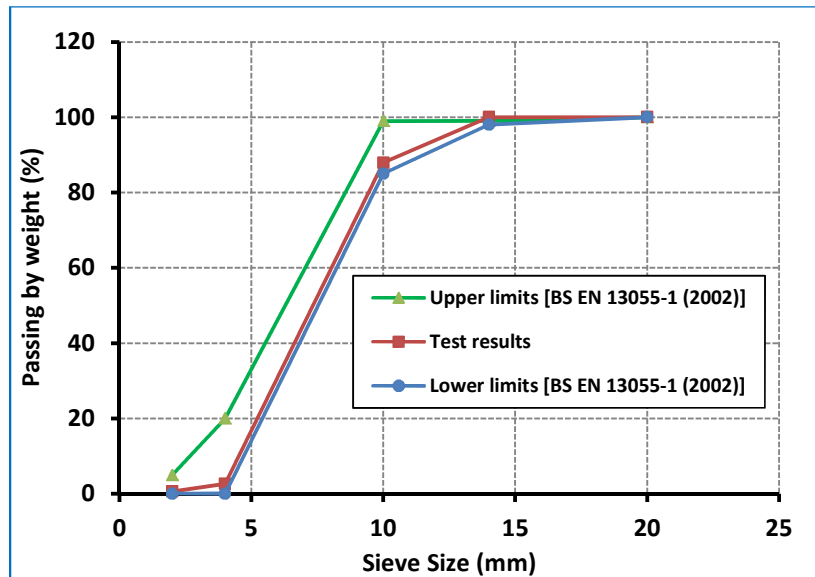
Figure 3-4 Grading curves for standard requirements and lightweight aggregate used

3.3 Equipment Used

Equipment used in the project comprises: an ordinary mixer for mixing the raw materials, a foam generator (STONEFOAM-4) running on a 12 Vdc (40-50 A) battery for generating stable foam by blending a foaming agent, EABASSOC (1.05 S.G.), water and compressed air of predetermined proportions (45 g water to 0.8 ml foaming agent) in it, **Figure 3-5**, and different types of moulds for casting the specimens.
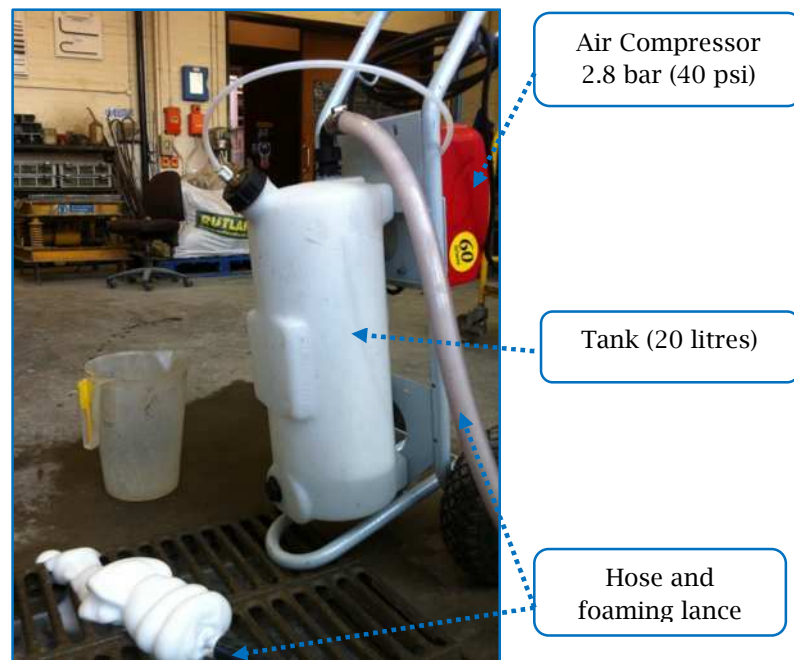
Figure 3-5 Foam generator used (STONEFOAM-4)

3.4 Mix Design

In this research, mix proportioning began with the selection of the unit weight (wet density), the cement content and the water to cement ratio. The mix was then proportioned by the method of absolute volumes (ACI-523.3R-93, 1993).

It has been reported that mix proportions of concrete should be chosen according to particular requirements such as strength, shrinkage, thermal conductivity etc. For this reason and based on the best findings from the literature, the constituent materials selected for this project have been chosen to produce foamed concrete with relatively high strength and good thermal properties.

Ruiwen (2004) stated that based on previous studies, (Indian concrete Journal, 1989; ACI, 1993; Valore, 1954), cement content in conventional foamed concrete with or without sand should be between 250 and 500 kg/m³; in this project, to produce foamed concrete with high strength it was chosen to be 500 kg/m³.

According to Ruiwen (2004), some studies have reported that in general, the optimum w/c ratio of foamed concrete lies between 0.5 and 0.6 but with superplasticizer w/c ratio may reach as little as 0.19, although he stated that water/binder ratio less than 0.2 will lead to very difficult mixing. On the other hand, if it exceeds 0.4 the mix becomes too watery. It was discussed in **Chapter two** that the stability and consistency of foamed concrete are affected by the volume of foam and water-solid ratio. In this project, for a given density, the foam volume was determined by the mix design while the water/binder ratio required to produce a stable mix (density ratio close to unity) while achieving the design density was determined by trials.

The stability of foamed concrete is affected by the quality of foam which is affected by its density. According to ASTM C796 (1997), for production of foamed concrete the weight of the foam usually ranges from 32 to 64 kg/m^3. Therefore, trials were carried out to produce foam within this range of density. From the preliminary work, 0.8 ml of chemical foaming agent has been diluted in 45 g of water to produce one litre of 45 kg/m^3 density stable foam with a volume about 22 times that of the pre-foamed solution. Note that the EABASSOC Ltd creates foam with a volume 20 to 25 times the solution.

It is accepted that to achieve the target flow value, the proper dosage of superplasticizer should be determined by trial and error. However, in this project there is no target flow value but there is a target density which is affected by water content and foam volume. Although the manufacturer of the superplasticizer used (Kao Chemical GmbH) suggested that the dosage should be 0.25%-1.0% of powder, they recommended that trial mixes should be performed to confirm the proper dosage. From trials, it was found that 1.5% of binder is the minimum dosage to make the mortar slurry workable. Because this type of superplasticizer might produce air voids during mixing (as mentioned by the manufacturer) and to avoid

affecting the total air volume, this minimum dosage was adopted for all relevant mixes.

It has been well documented that the use of silica fume as a partial replacement of cement in combination with superplasticizer provides a significant increase in the strength and decrease in the permeability of concrete (Toutanji and El-Korchi, 1995), and proportions up to 10% by mass of cement have been reported (Ramamurthy et al., 2009). Moreover and according to Giaccio, et al. (2007), when silica fume is used (usually no more than 10% of cement weight), there is no reduction in the fracture energy. In addition, based on the Taguchi method, Tanyildizi (2008) concluded that at 20°C the optimum for both compressive and flexural strength is 10% silica fume by mass; therefore, where used in this project, silica fume has been added to the mix at 10% of the cement weight.

Nambiar and Ramamurthy (2007b) stated that, in foamed concrete, because fly ash is a reactive material, replacement of sand with fly ash leads to increased strength. On the other hand, this will also lead to increased water absorption. In addition, according to Ramamurthy et al. (2009), mixes with fly ash exhibit higher carbonation than those with sand. Furthermore, using sand may lead to improved shear capacity between its particles and the paste resulting in higher tensile strength. For these reasons, a preliminary experimental programme was carried out at the lowest material density (FC3, 1300 kg/m³) to make the lightest mix suitable for structural purposes. Based on the results from this programme, in addition to adding silica fume and superplasticizer, fly ash replacement was limited to 20% by weight of fine sand (**Table 3-1**), giving a strength of over 17 MPa, and thereby bringing it into the range where it may be considered as a structural concrete, FCa3, (Neville, 2011). To enable sensible comparisons, this ratio was also adopted for the 1600 (FC6) and 1900 (FC9) kg/m³ mixes to produce mixes with additives (FCa6 and FCa9); see **Table 3-2** and **Table 3-3**.

In addition to the above mixes, some further mixes were designed to investigate the effect of additives, individually [10% silica fume (FCs), 20% fly ash (FCf) and 1.5% superplasticizer (FCp)] or together [silica fume and superplasticizer (FCsp)], on the properties of foamed concrete. With the same added foam and target density, four mixes (FCs3, FCf3, FCp3 and FCsp3) of 1300 kg/m³ density (**Table 3-1**) and also four mixes (FCs6, FCf6, FCp6 and FCsp6) of 1600 kg/m³ (**Table 3-4**) were designed.

Lightweight aggregate (LWA) has low weight with high volume. Therefore to leave enough space for foam bubbles, only 25% by weight of sand was replaced by lightweight aggregate (FCL6) to examine the effect of it on certain properties, particularly damage behaviour, of foamed concrete. In addition, all the selected additives were added to this mix to produce a modified mix (FCLa6), **Table 3-4**. **Figure 3-6** illustrates the mixes designed for this project.
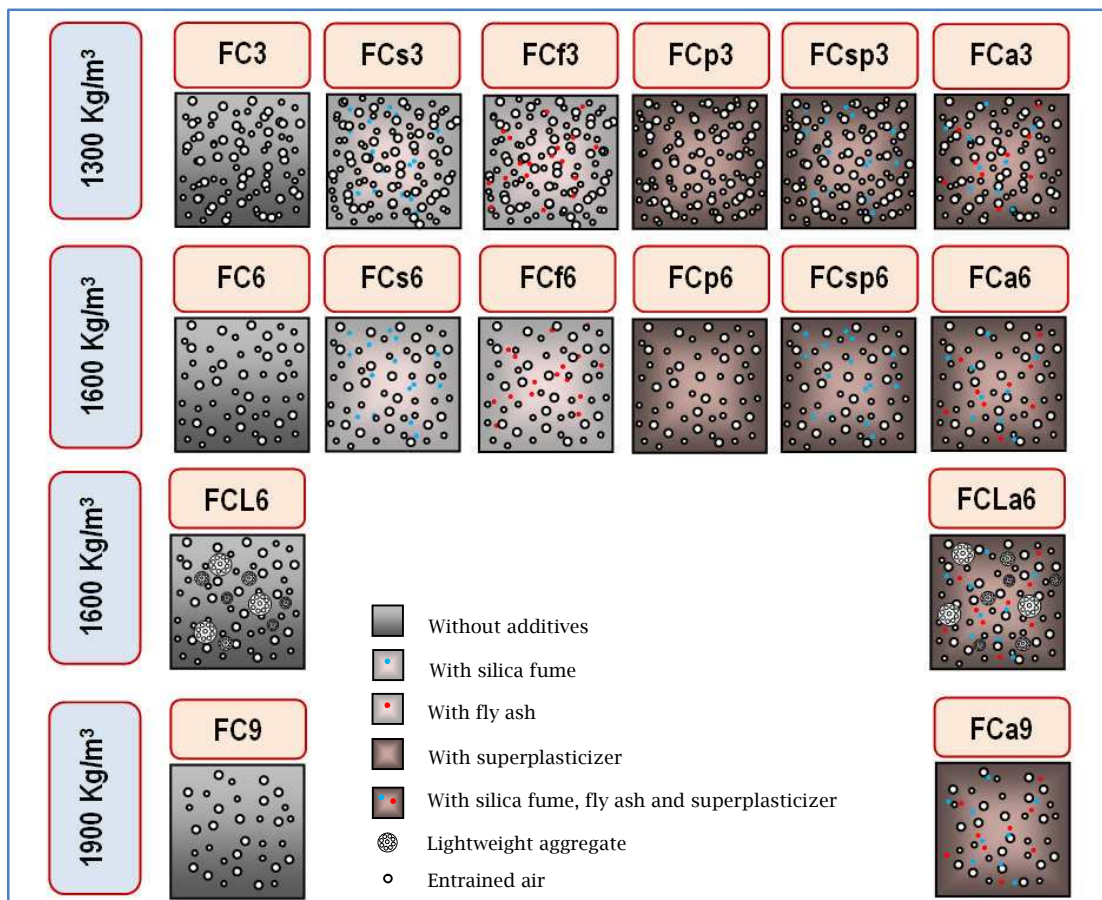
Figure 3-6 The mixes designed for this project

Table 3-1 Mix proportions of 1300 kg/m³ foamed concrete mixes

	Mixes					
	FC3	**FCs3**	**FCf3**	**FCp3**	**FCsp3**	**FCa3**
Target density (kg/m³)	1300	1300	1300	1300	1300	1300
Cement content (kg/m³)	500	450	500	500	450	450
Silica Fume (kg/m³)	-	50	-	-	50	50
W/b ratio*	0.475	0.475	0.475	0.3	0.3	0.3
Superplasticizer (kg/m³)	-	-	-	7.5	7.5	7.5
Water content (kg/m³)	237.5	237.5	237.5	150	150	150
Sand content (kg/m³)	562	562	450	642.5	642.5	514
Fly Ash (kg/m³)	-	-	112	-	-	128.5
Foam (kg/m³)	19.4	19.4	19.4	19.4	19.4	19.4
Foam (m³)	0.424	0.424	0.424	0.424	0.424	0.424

*w/b ratios required to achieve a density ratio of about unity for the selected mixes

Table 3-2 Mix proportions of selected foamed concrete mixes

	Mixes					
	FC3	**FCa3**	**FC6**	**FCa6**	**FC9**	**FCa9**
Target density (kg/m³)	1300	1300	1600	1600	1900	1900
Cement content (kg/m³)	500	450	500	450	500	450
Silica Fume (kg/m³)	-	50	-	50	-	50
W/b ratio*	0.475	0.3	0.5	0.325	0.525	0.35
Superplasticizer (kg/m³)	-	7.5	-	7.5	-	7.5
Water content (kg/m³)	237.5	150	250	162.5	262.5	175
Sand content (kg/m³)	562	514	850	744	1137.5	974
Fly Ash (kg/m³)	-	128.5	-	186	-	243.5
Foam (kg/m³)	19.4	19.4	13.3	13.3	7.6	7.6
Foaming agent (kg/m³)	0.35	0.35	0.24	0.24	0.13	0.13
Foam (m³)	0.424	0.424	0.295	0.295	0.166	0.166

*w/b ratios required to achieve a density ratio of about unity for the selected mixes

Table 3-3 Mix proportions of selected foamed concrete mixes (by volume)

	Mixes					
	FC3	**FCa3**	**FC6**	**FCa6**	**FC9**	**FCa9**
Target density (kg/m³)	1300	1300	1600	1600	1900	1900
Cement content m³/m³	0.158	0.142	0.158	0.142	0.158	0.142
Silica Fume m³/m³	-	0.0227	-	0.0227	-	0.0227
Superplasticizer m³/m³	-	0.0068	-	0.0068	-	0.0068
Water content m³/m³	0.237	0.15	0.25	0.162	0.262	0.175
Sand content m³/m³	0.212	0.193	0.32	0.28	0.429	0.367
Fly Ash m³/m³	-	0.061	-	0.088	-	0.116
Foam m³/m³	0.424	0.424	0.295	0.295	0.166	0.166
Foaming agent L/m³	0.339	0.339	0.236	0.236	0.133	0.133

Table 3-4 Mix proportions of 1600 kg/m³ foamed concrete mixes

	Mixes					
	FCs6	**FCf6**	**FCp6**	**FCsp6**	**FCL6**	**FCLa6**
Target density (kg/m³)	1600	1600	1600	1600	1600	1600
Cement content (kg/m³)	450	500	500	450	500	450
Silica Fume (kg/m³)	50	-	-	50	-	50
W/b ratio*	0.5	0.5	0.325	0.325	0.5	0.325
Superplasticizer (kg/m³)	-	-	7.5	7.5	-	7.5
Water content (kg/m³)	250	250	162.5	162.5	250	162.5
Sand content (kg/m³)	850	680	930	930	637.5	511.5
Fly Ash (kg/m³)	-	170	-	-	-	186
LWA (kg/m³)	-	-	-	-	212.5	232.5
Foam (kg/m³)	13.3	13.3	13.3	13.3	10.5	10.5
Foaming agent (kg/m³)	0.24	0.24	0.24	0.24	0.19	0.19
Foam (m³)	0.295	0.295	0.295	0.295	0.233	0.233

3.4.1 Examples of Mix Design

The mix proportioning begins with the selection of the unit weight of the concrete (wet density), the cement content, and the water-binder ratio (w/c) required to achieve a density ratio of about unity for the designed mix. Then, the mix is proportioned by the method of absolute volumes.

The mix design steps are explained in the following two examples:

Example 1: <u>For 1m³ of FC3 Mix</u>:

- ❖ Wet density of foamed concrete required =1300 kg/m³
- ❖ Cement content = 500 kg/m³
- ❖ Water–Binder ratio (w/b) =0.475
- ❖ Specific gravity of cement = 3.15
- ❖ Specific gravity of sand = 2.65
- ❖ Unit weight of water = 1000 kg/m³
- ❖ Unit weight of foam = 45 kg/m³

The total mass of raw materials = 1m³ ×1300 kg/m³ =1300 kg

Material	Weight		Absolute Volume
Cement	500 kg	$500 kg \times \dfrac{1}{3.15 \times 1000}$	0.158 m³
Water	(0.475×500) kg	$(0.475 \times 500) kg \times \dfrac{1}{1000}$	0.237 m³
Total	738 kg		0.395 m³
Dry sand required	$1300 - 738 = 562$ kg 562 kg	$562 kg \times \dfrac{1}{2.65 \times 1000}$	0.212 m³
Absolute volume of cement, water and sand			0.607 m³
Air volume required		1m³-0.607m³	0.393 m³

The air content in foam produced by using EABASSOC foaming agent is about 95%, therefore

Foam Volume $\dfrac{0.393}{0.95}$ 0.414 m^3

The amount of foaming agent required to produce (414) litre foam is:

$$\frac{0.8\text{ml} \times 414\text{L}}{1\text{L}} = 331.2\text{ml} = 0.347\text{kg}$$

The amount of water required to produce (414) litre foam is:

$$\frac{45\text{g} \times 414\text{L}}{1\text{L}} = 18630\text{g} = 18.63\text{kg}$$

Example 2: <u>For 1m³ of FCa3 Mix</u>:

- ❖ Wet density of foamed concrete required = 1300 kg/m³
- ❖ Cement content = 500 kg/m³
- ❖ Water–Binder ratio (w/b) = 0.3
- ❖ Specific gravity of cement = 3.15
- ❖ Specific gravity of superplasticizer = 1.1
- ❖ Specific gravity of silica fume = 2.2
- ❖ Specific gravity of sand = 2.65
- ❖ Specific gravity of fly ash = 2.09
- ❖ Unit weight of water = 1000 kg/m³
- ❖ Unit weight of foam = 45 kg/m³

The total mass of raw materials = 1m³ ×1300 kg/m³ =1300 kg

Material	Weight		Absolute Volume
Cement	450 kg	$500kg \times \dfrac{1}{3.15 \times 1000}$	0.1428 m³
Silica fume	50	$50kg \times \dfrac{1}{2.2 \times 1000}$	0.0227 m³
Water	(0.3×500) kg	$(0.3 \times 500)kg \times \dfrac{1}{1000}$	0.15 m³
Superplasticizer	(0.015×500) kg	$7.5kg \times \dfrac{1}{1.1 \times 1000}$	0.0068 m³
Total	657.5 kg		0.3223 m³
		$1300 - 657.5 = 642.5$ kg	
Dry sand required	(0.8×642.5) kg	$514kg \times \dfrac{1}{2.65 \times 1000}$	0.193 m³
Fly ash	(0.2×642.5) kg	$128.5kg \times \dfrac{1}{2.09 \times 1000}$	0.0614 m³
Absolute volume of C, S, W, P, F and sand			0.5767 m³
Air volume required		1m³-0.5635m³	0.4233 m³

The air content in foam produced by using EABASSOC foaming agent is about 95%, therefore

Foam Volume	$\dfrac{0.4223}{0.95}$	0.444 m³

The amount of foaming agent required to produce (444) litre foam is:

$$\frac{0.8\text{ml} \times 444\text{L}}{1\text{L}} = 355\text{ml} = 0.355\text{kg}$$

The amount of water required to produce (444) litre foam is:

$$\frac{45\text{g} \times 444\text{L}}{1\text{L}} = 19980\text{g} = 19.98\text{kg}$$

It should be noted here that for mixes with the same density, since the differences in the foam volume (design) required to reach the target density are small and to make logical comparisons between mixes, a single value of added foam volume was adopted. Note that this had a little effect on the density. The added foam volumes used were 42.4%, 29.5%, 16.6% and 23.3% for 1300, 1600, 1900 and 1600 with lightweight aggregate, respectively, **Table 3-1**, **Table 3-2** and **Table 3-4**.

3.5 Production

The production of foamed concrete on a small scale is a simple process and it does not involve any expensive or heavy machinery. By using the preformed foam method, except for the foam generator, equipment that is already available for normal concrete or mortar production can be used for production of foamed concrete.

The raw materials used to produce conventional foamed concrete and the additives for this research were listed in **Section 3.2**.

Component materials were added into the mixer in the following sequence: dry materials (including additives, if any), water with dissolved admixture to produce the unfoamed mix and then foam was added to produce the foamed concrete. The mixing procedure of Nambiar and Ramamurthy (2008) was adopted in this study as follows: after the quantity of raw materials has been worked out, dry constituents are mixed in an ordinary mixer for 2 minutes. Then, mixing water is added in stages until a homogenous unfoamed mix was achieved. After thorough mixing, the appropriate volume of preformed foam is added to the wet slurry and mixed until there was no physical sign of the foam on the surface, i.e. the foam was uniformly distributed and incorporated into the mix.

In moulding the specimens, the foamed concrete mix was placed in two approximately equal layers. The sides of the moulds were lightly tapped after placing each layer until the surface of the layer had subsided approximately to level (ASTM C796, 1997); see **Figure 3-7**. After filling the moulds, the surfaces of the specimens were levelled by using a trowel. All specimens were covered with thick nylon to prevent evaporation. All specimens were removed from moulds after 24 hours. After that and to investigate the effect of curing regime on strength of foamed concrete, water curing, **Figure 3-8**, and sealed-curing (wrapped in cling film), **Figure 3-9**, were adopted on the same mix. Since the results reveal that there

is no large difference in the compressive strength of specimens cured in the two curing regimes and sealed-curing reflects typical industry practice for foamed concrete (Jones and McCarthy, 2005), it was decided to adopt sealed-curing for all investigated mixes.

Figure 3-7 Moulding process of cubes and slab specimens

Figure 3-8 Moist curing (in water)

Figure 3-9 Sealed curing (wrapped in cling film)

3.6 Consistency

As described in Chapter Two (**Section 2.4.4.1**), the stability of foamed concrete relates to the consistency of the unfoamed mix. For each mix, the water-binder ratio w/b required to produce a stable mix and achieve a design density was determined by trials. For the investigated mixes (FC and FCa), water-binder ratios required to achieve a density ratio of unity or near it are presented in **Figure 3-10a, b**. This density ratio was calculated by comparing the fresh density, measured by weighing a filled standard container of known volume, with the designed density. For FC mixes, it is observed that at lower w/b ratios the density ratios are higher than unity due to bubbles breaking during mixing of a stiff mix. On the other hand, at higher w/b ratio, because the slurry was too thin to hold the bubbles, the density ratio also increases. However, the behaviour of FCa mixes at lower consistency, lower w/c ratios, was similar to that of FC mixes, while different behaviour was noticed at higher w/b ratios. The reason for the decreasing density ratio for FCa mixes at higher w/b ratios is the presence of a superplastisizer which may be helping not only by preventing bubbles segregation but also by producing entrained air bubbles resulting in reduced fresh density.

To enable sensible comparisons, for a given density, it was decided to adopt the required w/b ratio of the FC mix for FCs, FCf and FCL mixes and that of FCa mix for FCp, FCsp and FCLa mixes. Also, from the trials, it was found that these w/b ratios did not significantly affect the density ratios of mixes with individual additives and hence there was little effect on the fresh density, but it remained within a tolerance on plastic density ±50 kg/m^3 of the target density value which is typical of industry practice for foamed concrete production (Jones and McCarthy, 2005).

The consistency of both the unfoamed mix and foamed concrete was quantified by measuring the spread diameter of a cylinder of material of initial diameter 75 mm and 150 mm height (**Figure 3-11**) (Nambiar and Ramamurthy, 2008, Brady et

al., 2001b). The spreadability variation with mix density before and after addition of foam is illustrated in **Figure 3-12**. It seems that for the three densities adopted, the spreadability of unfoamed and foamed concrete mixes was 200-250 mm and 140-180 mm, respectively, for the conventional mixes (FC) while it was 400-450 mm and 290-350 mm, respectively, for the mixes with additives (FCa). It is evident that for a given mix, the spreadability reduces when the foam is added and for the selected mixes it also reduces with a reduction in design density; similar behaviour has been reported in the literature (Nambiar and Ramamurthy, 2006, Nambiar and Ramamurthy, 2008). Nambiar and Ramamurthy (2006) suggested that the reason for this may be that the adhesion between the bubbles and solid particles in the mixture increases the stability of the paste resulting in reduced spreadability, noting that there are more bubbles at the lower densities, **Figure 3-13**.
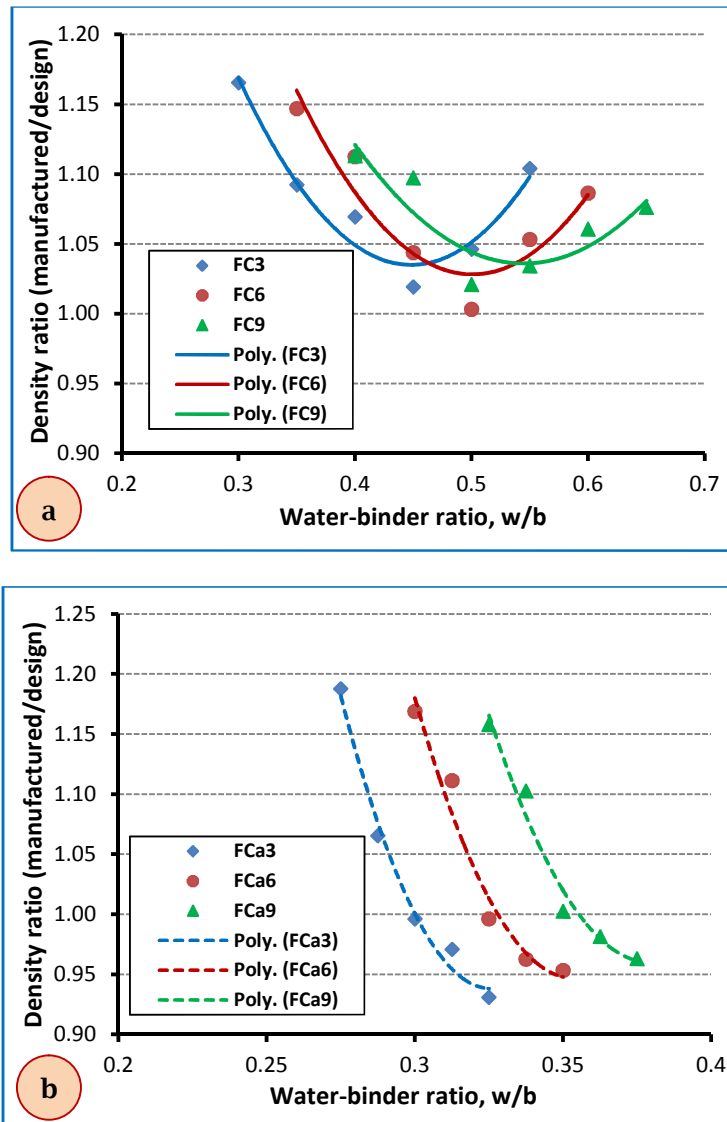
Figure 3-10 Variation of density ratio with water-binder ratio for (a) FC mixes (b) FCa mixes
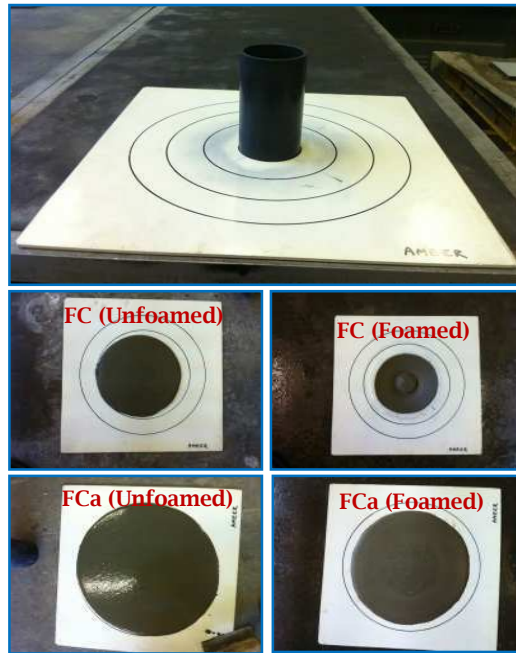
Figure 3-11 Test of the spreadability of the unfoamed mix and foamed concrete
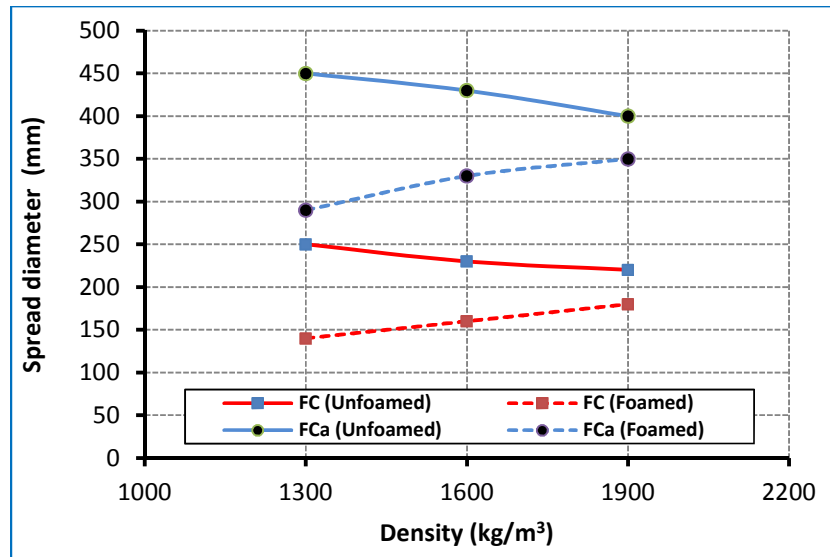
Figure 3-12 Variation of spreadability with density of the unfoamed and foamed concrete mixes
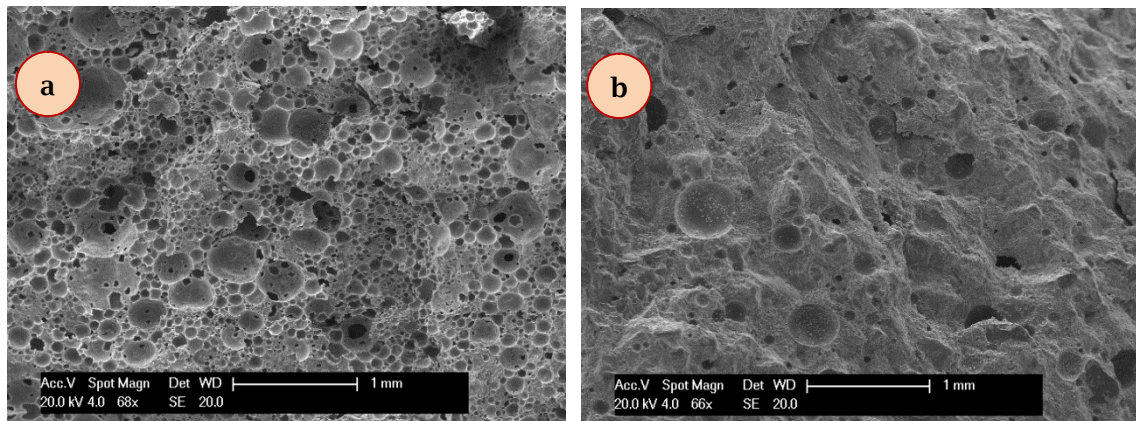
Figure 3-13 Air voids in foamed concrete: (a) 1300 kg/m³ density (b) 1900 kg/m³ density

3.7 Density

Wet density, after cling film curing, Υ_{wet} was determined from the following equation and its value was adopted as the mean average value of three 100 mm cubes.

$$\gamma_{wet} = \frac{W_a}{W_a - W_w} \times (1000 \frac{kg}{m^3}) \qquad (3\text{-}1)$$

where W_a is the weight of specimen in air and W_w is the weight of specimen in water.

   Table 3-5 summarises the wet and oven- dry, after drying at $105\,^{\circ}$C until a constant weight had been achieved, densities of the selected mixes of nominal densities 1300, 1600 and 1900 kg/m³.

Table 3-5 Wet and dry densities of the selected foamed concrete mixes

Mixes	Wet density, Υ_{wet} (kg/m³)		Oven- dry density, Υ_{dry} (kg/m³)	
	Average	Standard deviation	Average	Standard deviation
FC3	1305	13.23	1137	24.06
FCs3	1313	10.41	1139	13.43
FCf3	1291	11.24	1125	9.29
FCp3	1313	10.07	1155	14.73
FCsp3	1315	7.77	1159	10.02
FCa3	1307	15.28	1147	18.18
FC6	1621	11.00	1466	20.30
FCs6	1610	8.08	1470	8.54
FCf6	1582	10.41	1450	10.44
FCp6	1621	8.62	1480	15.95
FCsp6	1615	10.15	1476	9.61
FCa6	1609	12.86	1475	10.50
FCL6	1603	7.09	1457	4.36
FCLa6	1605	12.86	1468	14.00
FC9	1874	14.57	1778	19.76
FCa9	1877	8.14	1797	6.11

3.8 Raw Materials Cost

According to Jones and McCarthy (2005), it has been estimated that the cost per unit volume of foamed concrete is approximately 1.3 times that of normal concrete. In addition, RONEZ Company (RONEZ, 2011) stated guide prices without delivery charge of certain foamed concrete mixes (2:1 sand: cement with w/c=0.5) as follows: C3 (compressive strength of 3 MPa) for void filling with 1350 kg/m³ density at £111.54/m³, C7 for trench reinstatement with 1500 kg/m³ at £118.93/m³ and C12 for sewer surrounds and reinstatement with 1650 kg/m³ at £123.83/m³. However, in the same guide but for normal concrete mixes (2450 kg/m³) designed with 4/20 mm aggregate and CEM I cement, the costs for C15, C25, C35 and C45 were £131/m³, £147/m³, £159/m³ and £166/m³ respectively. In this study, by knowing the costs of raw materials, the costs of some of the investigated foamed concrete mixes were estimated as shown in **Table 3-6**. However, the costs of normal concrete mixes, made with the same materials used for producing the foamed concrete mixes, with compressive strengths of 25 MPa to 55 MPa ranged between £270/m³ and £285/m³ depending on the composition of the mix and the type of cement used. It can be seen that, excluding FC3, FCa3 and FC6, the cost per unit volume of foamed concrete mixes produced in this study is about 1.15- 1.32 times that of normal concrete with the same strength.

Table 3-6 Estimated costs for some foamed concrete mixes

Material	Cement	Silica fume	Water	Super-plasticizer	Sand	LWA	Fly ash	Foaming agent
Cost (£/kg)	0.1908	0.425	0.00285	2.24	0.199	0.171	0.21	4.266
Mix	FC3	FC6	FC9	FCa3	FCa6	FCa9	FCL6	FCLa6
Total Cost (£/m³)	209.5	266.2	323.1	255.1	312.5	370	260.1	305.8

3.9 Test Programme

The aim of this research is to produce foamed concrete mixes which are suitable for semi-structural or structural purposes with good insulation and durability properties and to evaluate its damage behaviour. Therefore, a test programme was carried out within the following areas:

❖ **Void Structure Properties**

   Porosity (total air volume), air void distribution, shape factor and connectivity were investigated.

❖ **Mechanical Properties**

   Density, compressive strength, splitting tensile strength, flexural strength and modulus of elasticity (static and dynamic) were measured.

❖ **Thermal Properties**

   Thermal conductivity and heat capacity values were found.

❖ **Permeation Properties**

   Water absorption, sorptivity and air permeability were investigated.

❖ **Damage Evaluation**

   The quantification of micro and macrocracks and the effects of the microstructure on them were examined.

   It should be noted here that these tests will be discussed in detail in the following chapters. In addition, because foamed concrete is a porous material, studying its pore structure characteristics and their influence on the other properties is a significant objective.

3.10 Summary

Portland cement CEM I, natural fine aggregate (sand) with additional sieving to remove particles greater than 2.36 mm, 45 kg/m^3 foam and water were used in the production of conventional foamed concrete. MIGHTY 21 EG Superplasticizer which is compatible with the EABASSOC foaming agent, Elkem silica fume and CEMEX fly ash (class S) were added, individually and together, to the conventional mixes to enhance certain properties of foamed concrete. For the 1600 kg/m^3 mix, LYTAG lightweight aggregate (4-10mm size) was added to investigate its effect on the damage of foamed concrete. Because the aim of this research was to produce foamed concrete suitable for semi-structural or structural purposes, it was decided to produce mixes within the density range 1300- 1900 kg/m^3. Therefore, three groups were selected, namely 1300, 1600 and 1900 kg/m^3. The absolute volume method was adopted to design the constituent proportions of all mixes taking into account that the binder (cement and silica fume) and the foam volumes are equal for all mixes with the same density (conventional and with additives) and that the filler (sand, fly ash) volume is equal for mixes with the same water to binder ratio. The fresh properties testing was mainly focused on the consistency and spreadability measurement of mixes without foam (unfoamed) in order to investigate the amount of water required to produce foamed concrete with a fresh density close to the target density. The cost per unit volume of foamed concrete mixes produced in this study is about 1.15- 1.32 times that of normal concrete with the same strength.

Chapter 4: Air-void Structure Characterisation

4-1 General

The air-void structure of foamed concrete is a significant characteristic since it affects properties such as strength and durability. To investigate these properties, the determination of total air voids content is not sufficient as the shape, size and distribution of air voids may also be influential. Thus, this chapter presents the experimental work that was carried out to characterise the air-void structure of foamed concrete mixes in terms of the porosity (voids content), void size distribution, void shape and the connectivity of voids. Additionally, to understand the formation of voids after hardening, an investigation of the bubble size distribution of foam (before adding to the mixture) and the pore size distribution of the foamed concrete mixes (after hardening) is discussed in this chapter. Techniques used to characterise the voids structure are described. The effect of additives on the air-void structure of foamed concrete mixes is investigated by examining their size and shape parameters. In addition, the relationships between dry density and parameters of air-void structure are presented. Finally, the main findings are summarized.

4.2 Techniques Used

4.2.1 Mercury Intrusion Porosimetry (MIP)

Mercury intrusion porosimetry characterizes a material porosity by applying a pressure to a sample immersed in mercury. The size of the accessible pores that will be filled by mercury is inversely proportional to the pressure applied. For each externally applied pressure, the pore diameter (mercury–pore space interface) is determined by the Washburn equation:

$$P_c = -\frac{4\rho \times cos\theta}{d} \qquad\qquad (4\text{-}1)$$

where P_c is the capillary pressure, ρ is the surface tension, θ is the contact angle and d is the diameter of the pore space (Katz and Thompson, 1986, Yen, 2007). In this project, MIP tests were performed using a Micromeritics AutoPore IV mercury porosimeter, **Figure 4-1**, with a maximum 414 MPa (60000 psi) injection pressure and applied over a capillary range of 0.004 to 400 μm. A contact angle of 142˚ and a mercury surface tension of 485×10^{-3} N/m were used to convert applied pressure to pore diameter (Goual et al., 2006).

Figure 4-1 Micromeritics AutoPore IV mercury porosimeter

In a review of mercury porosimetry (MIP), Diamond (2000) concluded that this technique is an inappropriate method for the measurement of pore size distributions in cement-based materials. However, he added that MIP measurements are useful to provide threshold diameters and intrudable pore volume which may be helpful as comparative indices of the cement paste or concrete pores. This is

because the Washburn equation is applicable to a pore system characterized by percolative chains with ever finer pores at each step from the surface to the middle of sample; **Figure 4-2a**. From this Figure, the larger pore (open to the exterior) fills with mercury at pressure P_1 while the smaller pore (open to the large pore) will not fill until a higher pressure P_2, corresponding to its smaller diameter, is reached.

In a hydrated cement system, a pore structure illustrated in **Figure 4-2b** is likely to occur leading to mistakenly allocating a large pore the diameter of a small pore at high pressure step P_2. Therefore, the MIP technique was used in this project to determine the total porosity, the characteristic length (lc) and the conductivity factor of the selected mixes not to investigate the pore size distribution of them.
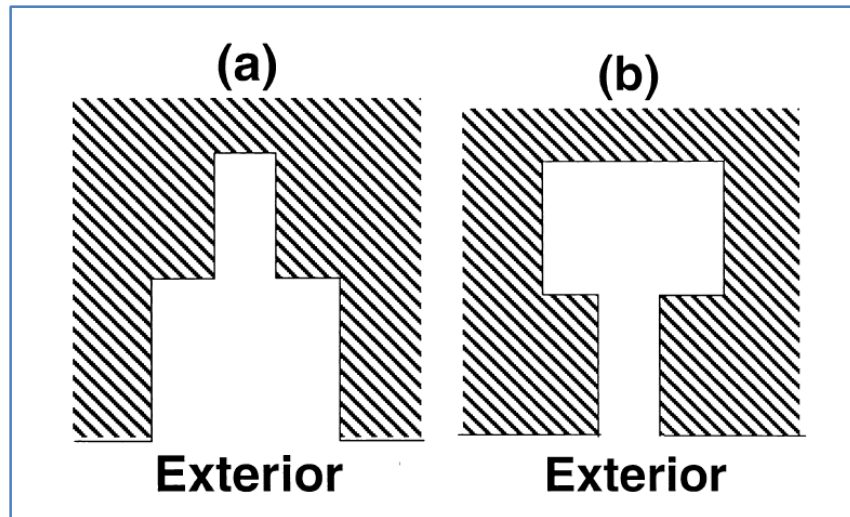
Figure 4-2 (a) A small cylindrical pore connected to the exterior of a specimen through a large cylindrical pore (MIP model is applicable) (b) A large cylindrical pore connected to the exterior of a specimen through a small cylindrical pore (the large diameter pore will not be detected) (Diamond, 2000)

4.2.2 Optical Microscopy (OM)

Optical and electron microscopies are the two principle microscopy techniques widely used for study of cementitious materials. An optical microscope uses normal (visible) light and a system of lenses to magnify images of small samples. It has been extensively used for the studying of cementitious materials due to its easy use

and rapid operation. However, the main limitation of this technique is the resolution (Hemavibool, 2007).

In this project, in order to investigate the void size distribution and shape factor of both foam and foamed concrete mixes, a charge-coupled device (CCD) camera connected to an optical microscope (MCA NIKON SMZ-10 STEREO) and a computer, see **Figure 4-3**, was used to capture the images. These images were then digitized, converted into binary form and analysed using ImageJ software.
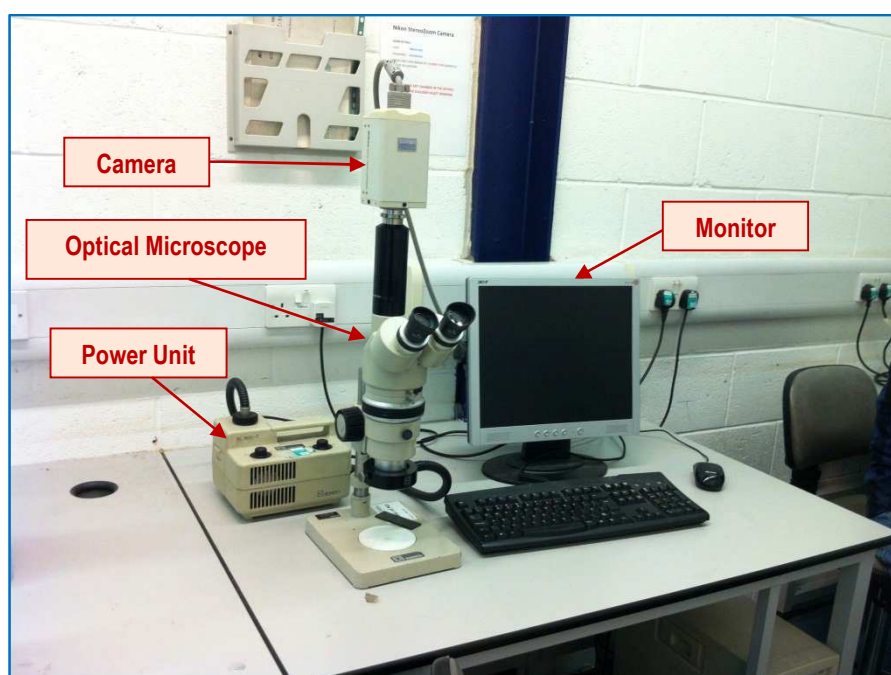
Figure 4-3 An optical microscope (MCA NIKON SMZ-10 STEREO)

4.2.3 Scanning Electron Microscopy (SEM)

In general, the SEM consists of an electron gun, condenser lenses (to de-magnify the electron beam), objective lenses (to focus the probe onto the specimen surface), a control system for the beam movement, platform for specimen, electron detector, signal amplifier and display unit (Hemavibool, 2007). A XL30 Scanning Electron Microscope (SEM) (OXFORD INCA INSTRUMENTS) was used in this project; **Figure 4-4**.

The SEM principle can be described briefly as follows: when the electron beam (primary electrons) hits the specimen surface, it may elastically change its direction with no loss of energy (elastic scattering process), or a detectable amount of the primary electron energy may be absorbed resulting in most of the primary electrons being stopped while a few of them are backscattered (inelastic scattering process). In general, these processes produce other types of electrons which are useful for the materials analysis, as illustrated in **Figure 4-5**, (Hemavibool, 2007). However, only secondary electrons (SE) and backscattered electrons (BSE) will be used in this project.

In the elastic scattering process, most of the primary electrons will stop in the specimen forming a volume of a tear drop shape below the specimen surface known as the interaction volume which affects the lateral resolution of the image produced from each signal. The depth and shape of the interaction volume depends on both the average atomic number of the sample and the accelerating voltage. The secondary electrons are used to describe those having energy less than about 50 eV (electronvolts). Being close to the specimen surface, they will be able to leave the specimen giving information about the first very thin layer below the surface. Thus, they are very useful for investigating the topography of the material surface. For this reason, the secondary electron mode (SE) was used in this project to qualify, analyse and investigate the microstructure of the selected foamed concrete mixes.

Backscattered electrons (BSE) are primary electrons leaving the specimen surface with energy greater than 50 eV (from 50 eV to that of the primary electrons). Compared to secondary electrons, they have very high energy. The BSE mode, in combination with the ImageJ software, was used in this project to perform quantitative image analysis of the void structure and the ITZ of the selected mixes.
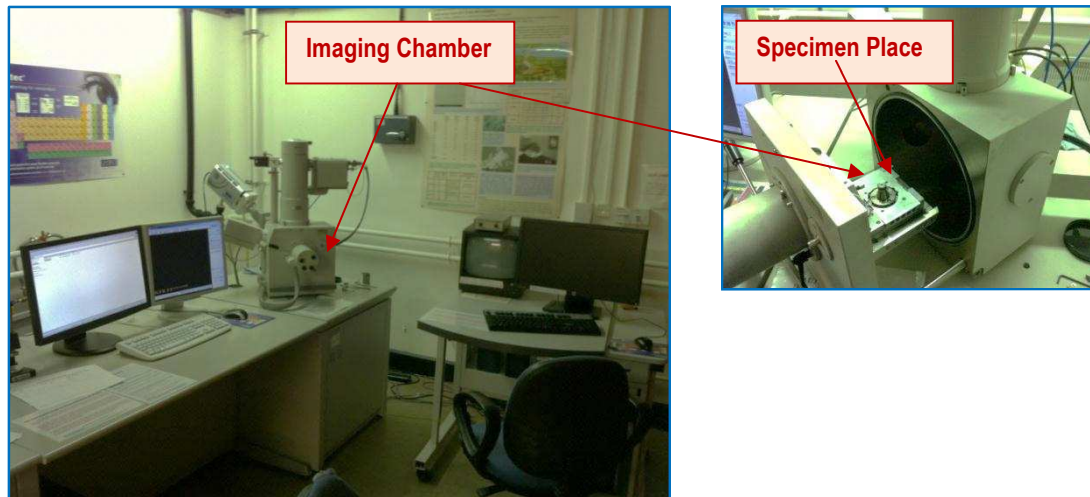
Figure 4-4 XL30 Scanning Electron Microscope (SEM)
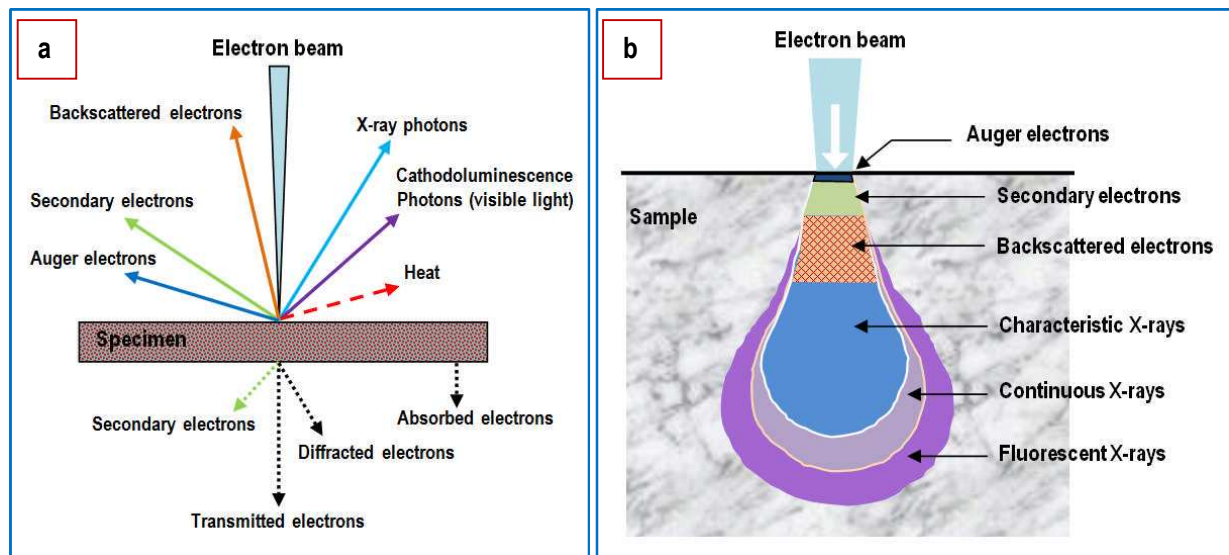
Figure 4-5 (a) The results of interaction of electron beam with specimen (b) The interaction volume and the regions of the various signals that may be detected [After Hemavibool (2007)]

4.2.4 Micro Computed Tomography (μCT)

A μCT scanner consists of a source for the X-ray beam with a collimator. The beam is transmitted through the sample and then detected by a detector; as shown in **Figure 4-6**. This technique utilises the ability of X-rays, which are produced by accelerated electrons striking the X-ray tube target (e.g. tungsten), to penetrate objects and measures the intensity before and after passing through the objects. Its principle is: when an X-ray beam passes through a sample, some of the X-ray

radiation is absorbed and scattered (with intensity I_o), while the rest penetrates through the sample (with intensity I); see **Figure 4-7**. The amount of penetration depends on the X-rays' energy, molecule atomic number and the density and thickness of the object. Depending on the material density, the amount of absorption is a function of the linear attenuation coefficient (L_{att}) at each point. The denser the material the more the absorbed radiation. The L_{att} can be expressed as $L_{att}(x,y)$ where x and y are the Cartesian coordinates of the locations within the scanned section. The raw data of a series of intensity measurements, at different orientations around the sample, is converted to form a 2-D slice image by a mathematical process within the software indicating the different internal features and their distribution within the scanned section. Depending on the differences in density within the scanned object, the image consists of a range in the grey spectrum [0 (black) to 255 (white) for an 8-bit image]. Within the composite material, the higher the difference in component densities the better the identification and distinguishing between them. Finally, the 2-D images may be converted to a 3-D image to observe the location of voids, defects or inclusions without sectioning the sample, i.e. allowing the three-dimensional internal structure of a specimen to be determined non-destructively (Maire et al., 2007, Khan, 2010, Abdul Hassan, 2012).

Figure 4-8 illustrates the SCANCO MEDICAL micro computed tomography device (μCT 40) used in this project.
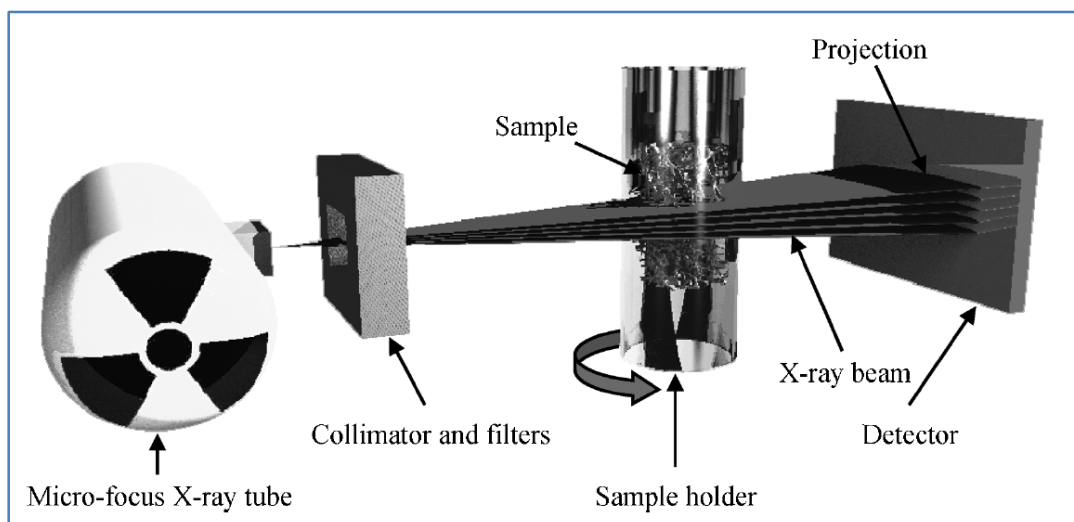
Figure 4-6 The key Components of µCT scanner (Bouxsein et al., 2010)
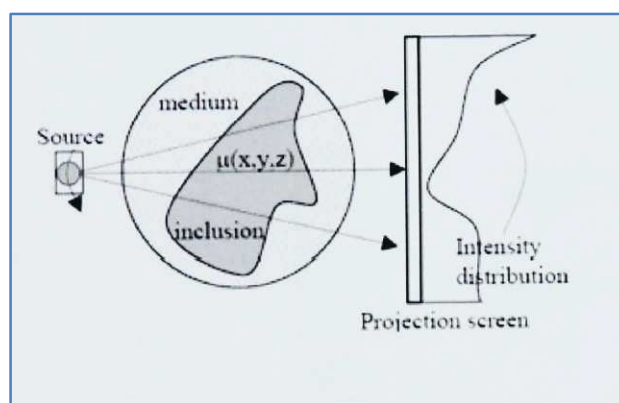
Figure 4-7 Intensity distribution in X-ray tomography (Khan, 2010)
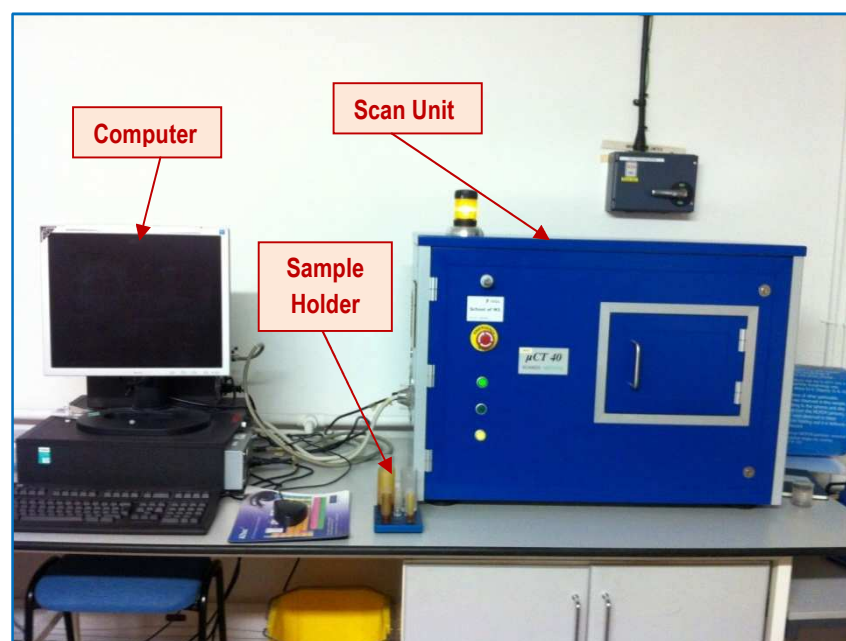
Figure 4-8 SCANCO MEDICAL micro computed tomography (µCT 40)

4.3 Air-Void Structure Characterisation

This section presents the experimental work that was carried out to characterise the air-void structure of foamed concrete mixes in terms of the porosity (voids content), void size distribution, void shape and the connectivity of voids.

4.3.1 Porosity

In this project, calculation and measurement methods for determining the porosity of selected foamed concrete mixes were adopted, as follows:

4.3.1.1 Theoretical Porosity

The porosity of foamed concrete is the sum of the entrained air voids (artificial air voids) and the voids within the paste, i.e. the gel and capillary pores (Nambiar and Ramamurthy, 2007b, Kearsley and Wainwright, 2001b, Yen, 2007, Kearsley and Wainwright, 2002). The paste should theoretically have a porosity of about 28% of the total volume of gel (the solid products of hydration and the gel water) (Kearsley and Wainwright, 2001b). The solid products of hydration should occupy a volume equal to the sum of anhydrous cement volume and the volume of water, less 25.4% of the volume of non-evaporable water (Neville, 2011), while the total water, with the situation of 100% hydration, represents the sum of the non-evaporable water (23% of the mass of anhydrous cement) and gel water and capillary water. To calculate the theoretical porosity for each mix, the calculated paste porosities, gel and capillary pores, were added to the corresponding design foam volumes, as illustrated in the Fv+ϕ_{paste} column in **Table 4-1**.

Kearesley and Wainwright (2002) have successfully used the Hoff equation to estimate the total porosity of foamed concrete. This equation expresses the theoretical porosity of cellular concrete containing cement, water and foam, being the volume of voids expressed as a fraction of the total volume. To derive the

equation, the mass of non-evaporable (hydrated) water was taken, as above, as 20% of the mass of anhydrous cement (by weight) assuming full hydration:

$$\emptyset_{th} = 1 - \frac{\gamma_c(1 + 0.2G_c)}{(1 + w/c)G_c\gamma_w} \qquad (4\text{-}2)$$

where $\emptyset_{th}$ is the theoretical porosity, Υ_c is the concrete density, G_c is the specific gravity of the cement, Υ_w is the water unit weight and w/c is the water to cement ratio (by weight). In addition, Lian et al. (2011) reported an equation proposed by Zheng (2004) to estimate the total porosity of porous concrete which was similar to the Hoff equation but with incorporated the aggregate proportions for porous concrete, as follows:

$$\gamma_{th} = \frac{100 + R_{ca} + 0.25R_{ca}}{\frac{100}{G_a} + \frac{R_{ca}}{G_c} + (0.25R_{ca} \times 0.75)} \times \gamma_w \qquad (4\text{-}3)$$

where Υ_{th} is the theoretical density, R_{ca} is the cement to aggregate ratio by weight, G_c is the specific gravity of cement, Υ_w is the water density, and G_a is the specific gravity of aggregate. It can be seen that 25% is taken in Zheng's equation as the ratio of hydration water to cement by weight and the volume of this water therefore reduces to approximately 75% of the original volume after chemically hydrating the cement (Lian et al., 2011).

The total porosity can now be calculated as:

$$\emptyset_T = 1 - \frac{\gamma_b}{\gamma_{th}} \qquad (4\text{-}4)$$

where $\emptyset_T$ is the total porosity and Υ_b is the bulk density of the sample. **Table 4-1** includes porosities calculated using both the Hoff and Zheng (2004) equations.

Table 4-1 Theoretical and measured porosity results

Mix	Υ_{dry} kg/m^3	(Fv) design % of Vol.	Porosity (%)							
			Theoretical			Measured				
			Fv+φ_{paste}	Hoff Eq.	Zheng Eq.	ϕ_{app}	ϕ_{vac}	Φ_{MIP}	Φ_{OM}	Φ_{SEM}
FC3	1130	42.4	53.2	55.2	51.8	17.77 (0.3)	51.63 (0.2)	44.84 (1.8)	36.71 (3.9)	47.14 (4.0)
FC6	1460	29.5	40.6	44.8	39.5	20.23 (0.8)	40.76 (0.3)	36.36 (0.6)	26.65 (2.1)	35.21 (3.3)
FC9	1785	16.6	28.1	36.5	29.4	20.65 (0.9)	28.73 (0.7)	28.01 (1.6)	15.10 (2.1)	25.03 (3.1)
FCa3	1145	42.4	50.5	49.0	51.6	13.41 (1.4)	49.07 (0.3)	42.05 (1.1)	37.40 (4.1)	47.53 (4.7)
FCa6	1470	29.5	37.9	37.7	39.7	12.43 (0.5)	38.60 (0.6)	35.72 (1.3)	25.87 (2.1)	36.30 (4.8)
FCa9	1790	16.6	25.3	27.9	29.0	11.28 (0.5)	27.75 (0.5)	27.19 (1.1)	15.44 (2.2)	25.24 (4.7)
FCL6	1455	23.3	38.3	45.3	40.1	21.46 (0.8)	39.23 (0.3)	31.33 (1.2)	19.12 (2.8)	25.33 (3.8)
FCLa6	1465	23.3	36.0	37.9	39.9	13.54 (0.1)	38.41 (0.7)	30.29 (1.1)	18.10 (2.9)	29.56 (5.9)

() The standard deviation

4.3.1.2 Measured Porosity

i. Apparent Porosity

For the selected foamed concrete mixes, the apparent porosity was determined from the average of three specimens, see **Table 4-1**, by drying 28-day old specimen (100×100×70 mm) at 100±5°C for 2 days, until constant mass, immersing it in water for 7 days (until constant weight) and then measuring its weight in air and water and applying the following equation:

$$\emptyset_{app} = \frac{W_{s,a} - W_{dry}}{W_{s,a} - W_{s,w}} \times 100 \qquad (4\text{-}5)$$

where ϕ_{app} is the apparent porosity (%), $W_{s,a}$ is the weight of a saturated sample in air, $W_{s,w}$ is the weight of the saturated sample in water and W_{dry} is the weight of the oven-dried sample.

ii. Total Porosity

The total porosity of the selected foamed concrete mixes was determined from the average of three specimens (see **Table 4-1** using the vacuum saturation approach,

as explained by Kearsley and Wainwright (2002). Porosity measurements were conducted on 28-day old samples of (100×100×70 mm) that were dried at 100±5°C until a constant weight had been achieved and then placed in a desiccator under vacuum for at least 3 hours. After that, the desiccator was filled with de-ionised water to 30mm above the samples and left under a vacuum pump for another 3 hours. Then, the samples remained under water over night (Kearsley, 1999). Finally, the samples were weighed in air and water to calculate the total (vacuum determined) porosity (ϕ_{vac}) from **Eq. (4-5)** assuming them to now be fully saturated.

iii. Mercury Intrusion Porosimetry (MIP)

The MIP test was also used to determine the total porosity of the selected mixes, see **Table 4-1**. The test was performed on fully dried (10×10×20mm) specimens cut from three positions (top, centre and bottom) of tested porosity samples (Goual et al., 2006). The porosity percentage was computed once the total accessible pore volume (i.e. total volume of mercury intruded) and the bulk volume (specimen weight over bulk density) were determined.

iv. Optical Microscopy (OM)

For each foamed concrete mix, 3 slices ($50 \times 50 \times 15$mm) were cut from the centres of three cured specimens, perpendicular to the cast face, and used for air-void structure investigation.

To make the boundaries between the air voids and the matrix sharp and easily distinguishable, the specimens were first polished and cleaned to remove any residues. Then, to enhance the contrast, the specimen surfaces were treated by applying two coats of permanent marker ink to them. After placing them in an oven at 50°C for 4 hrs, a white powder (Sodium bicarbonate) with a minimum particle size 5 μm was pressed into the surfaces of the specimens and forced into the voids. This left the concrete surface black and the voids white, resulting in specimens with

excellent properties for image analysis, **Figure 4-9**. This technique is described more fully in EN 480-11 (2005) and Nambiar and Ramamurthy (2007a).

For all mixes, a magnification of (23×) was selected with a pixel representing 6 μm and an image size of 178.52 mm^2 (15.43mm × 11.57mm). This magnification was chosen in order that air voids with diameters in excess of 20 μm could be easily identified, **see Section 4.3.2.2**.

Ten images were captured for each mix and then digitized, converted into binary form and analysed. For this study, only two phases, air voids and solid, were of interest. A histogram of gray levels from the optical microscope image was used to select the threshold value, below which all pixels were considered voids and above which they were considered as solid, creating the final binary image required for analysis. Although the gray-scale histograms did not have a sharp boundary between the two phases (voids and matrix), there was always a minimum in the boundary region and this was set as the threshold for analysis of the images in this project, see **Figure 4-10**. Although software operations such as dilation, erosion, opening, closing and hole filling have all been suggested as being useful in application to concrete microscopy (Nambiar and Ramamurthy, 2007a), in this project, it was found that the simple operation of hole filling was sufficient since there is a sharp contrast between the white coloured air voids and the surrounding black coloured matrix. Typical binary images for the three investigated mixes are shown in **Figure 4-11**. The porosity results from the optical microscopy technique are illustrated in **Table 4-1**.

To check if the number of images used is sufficient to give representative results for porosity investigation, a statistical consideration that the average value of the porosity (Ø$_{average}$) should be within 10% of the true average (e= 0.1*Ø$_{average}$) and assuming a normal distribution with a 97.5% confidence interval was adopted (Elsharief et al., 2003). For this, the equation [N$_{images}$= ((Sn*Sd)/e)^2] was used, where

N_{images} is the required images number, Sn is the standard normal variable, Sd is the standard deviation and e is the error corresponds to 10% of the average of porosity (Elsharief et al., 2003). For 97.5% confidence interval, Sn equals to 1.96 and by substitution the porosity and standard deviation values for each mix (**Table 4-1)** in the above equation, it was noticed that the largest value of N_{images} was 8.6. Therefore, for this study, ten images are sufficient to give representative results.

Figure 4-9 Some samples after preparation for optical microscope investigation
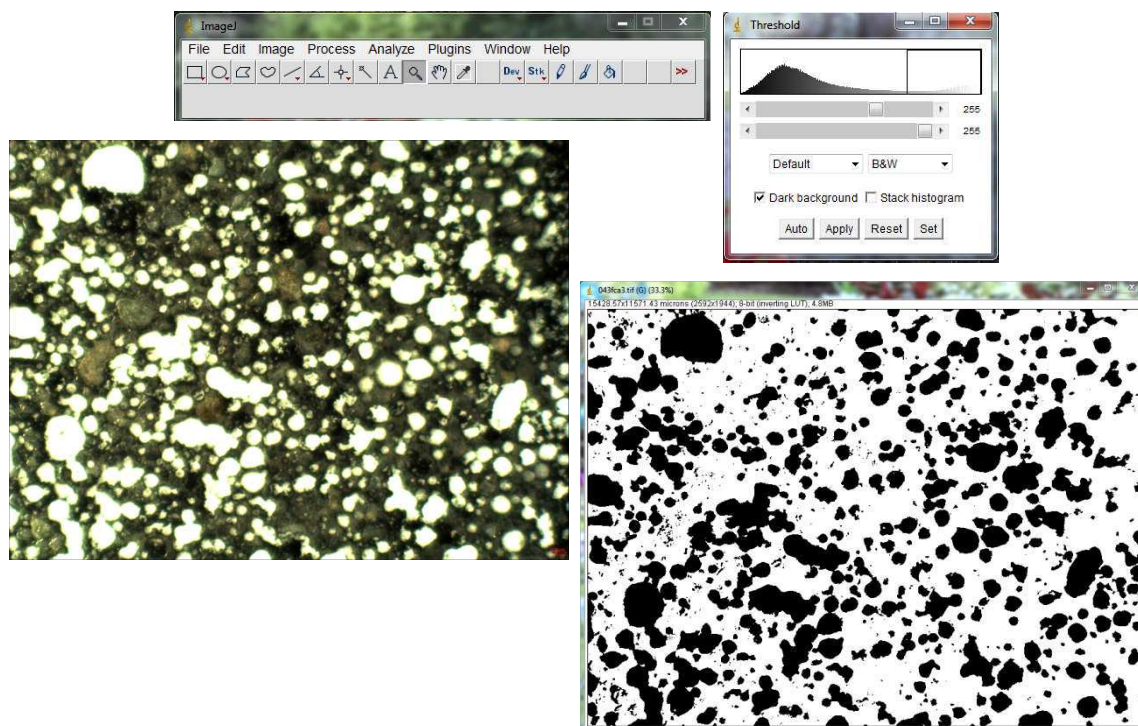
Figure 4-10 Analysis of OM image with ImageJ software [15.43mm × 11.57mm]
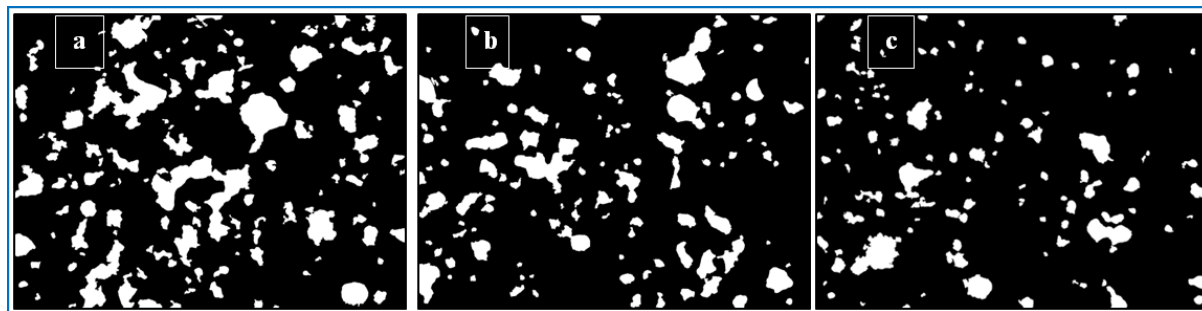
Figure 4-11 Typical binary images [15.43mm × 11.57mm] (a) FC3, (b) FC6 and (c) FC9

v. Scanning Electron Microscopy (SEM)

For this technique, specimens of about 20×20 mm size with a minimum thickness of about 12 mm were cut from the middle of two (100×100×70 mm) samples, as used for the porosity test, using a diamond cutter. The faces of the specimens were cut perpendicular to the cast face (parallel to the casting direction) (ASTM C457, 1998). After drying for 2 days at 105°C and to ensure the stability of the air void walls during polishing, the cooled specimens were vacuum impregnated with a slow setting epoxy (Epo Fix Resin). Then, the impregnated specimens were polished with 240#, 400#, 800# and 1200# silicon carbide abrasive (58.5, 35, 21.8 and 15.3 micron, respectively) using a rotating grinder and then a final stage was with 5 micron abrasive (4000#). During polishing, when changing to a finer abrasive, all surfaces of the specimens were gently and thoroughly cleaned, with a soft brush under running water, to remove all grinding compound (ASTM C457, 1998). Then, polished and cleaned specimens were dried at room temperature for at least 12 hours before testing (Babu, 2008). In order to avoid the distortion of the SE or BSE images due to a negative charge which may have built up on the sample surface under a high energy incident electron beam, the samples, nonconductive materials, were then coated with a thin film of conductive material before investigating with the SEM. In this project, for the analysis in BSE mode, coating with carbon was used, while coating with gold was used for the SE mode. Finally, the coated samples were

stored in the desiccators before and after investigation in the electron microscope, see **Figure 4-12**.

For porosity investigation, the specimens were studied through backscattered electron images which are captured using an XL30 Scanning Electron Microscope (SEM) (OXFORD INCA INSTRUMENTS), to capture 2D-images. The images were captured at 75× magnification and each one contains 712×484 pixels. ImageJ software was used to analyze these images. The porosity of the foamed concrete specimens was determined from analysis of 10 SEM images. In this procedure, the pore areas as obtained from the thresholded images (binary images) using the analysis features in the image processing software (ImageJ) were summed and divided by the total image area to obtain the area fraction of pores (the porosity), **Table 4-1**.

In this study, the simplest threshold was adopted to create a binary image in which one number (gray scale value) is selected; below it all pixels are considered void while above it they are considered non void (matrix). It is obvious that there are many methods to identify the threshold value (the ImageJ software has 17 of them). However, the question is: which of these methods could best segment the data? To answer this, all options have been tried and by visually comparing the obtained binary image with the original one, it has been decided that the IsoData method is the best one for thresholding the SEM images of this study, **Figure 4-13**. By applying an iterative selection method (IsoData or iterative intermeans), a histogram of the distribution of gray levels in the Backscattered Electron (BSE) image was used to select the threshold value to create the final binary image required for image analysis. The principle of this method has been described by Ridler and Calvard (1978).

Figure 4-12 Coated samples for BSE and SE mode
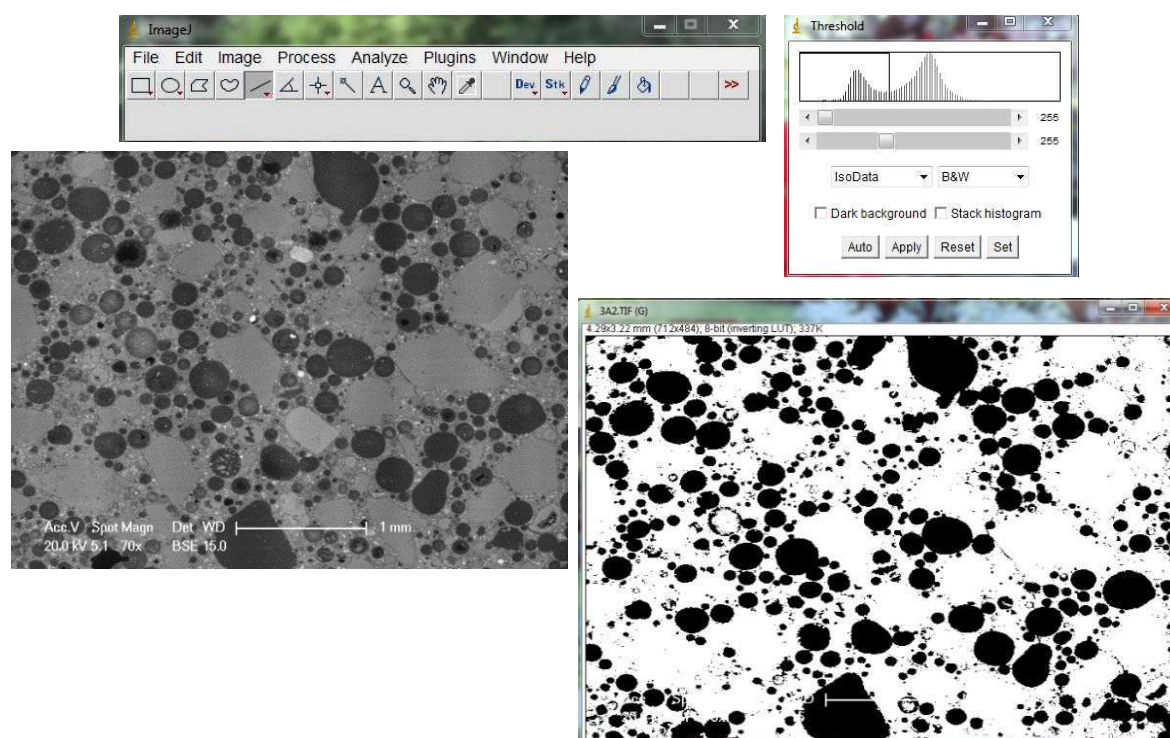
Figure 4-13 Analysis of SEM image with ImageJ software

vi. Overall Discussion on Porosity

In order to make this discussion easy to understand, **Figure 4-14** was drawn to illustrate the limitations of each technique used in measuring the porosity of the investigated foamed concrete mixes.

As mentioned before, both theoretical computations and measurements were used to determine the porosity of foamed concrete at 28 days and the results are shown in **Table 4-1**. For all selected mixes, it can be seen that the apparent porosity at normal condition is lower than that determined by the vacuum saturation method. This difference shows that not all the entrained pores (air-voids) are taking part in conventional water absorption although they are interconnected via small capillary pores, see **Figure 4-15**. In addition, the contribution to water absorption being by the capillary pores, which depend on the paste content (Nambiar and Ramamurthy, 2007b, Nambiar and Ramamurthy, 2006) and the entrained pores contribute little to water absorption since their capillary suction is much weaker compared to the capillary pores. Because the MIP technique only determines pore diameters accessed through voids of 400 μm or less and because the OM and SEM data show that some pores were larger than 400 μm, the porosity obtained from MIP was lower than the total porosity as measured by vacuum saturation for all mixes. The total porosity averaged from voids area fractions of 10 SEM 2D-images was also less than ϕ_{vac} since the SEM technique only determines pore diameters larger than about 6 μm, resulting in a loss of the smallest void areas, i.e. a reduced porosity will be obtained. In terms of the porosity measured from the optical microscope images, it was close to the volume of the added foam since by this technique and with this magnification, only pore diameters larger than 20 μm can be determined. For mixes with LWA, FCL6 and FCLa6, none of the MIP, OM and SEM techniques are appropriate to measure their porosity since the samples or the captured images are not sufficiently representative of the whole specimen.

On the basis of the measured results, the most appropriate test to obtain a relatively accurate porosity for foamed concrete (conventional, with additives and with LWA) is therefore the vacuum saturation method.

Theoretically, it has been determined that the equation derived by Zheng (2004) can be used to predict the porosity of foamed concrete mixtures whereas, in spite of that, Kearsley and Wainwright (2002) have successfully used the Hoff equation to estimate the total porosity of foamed concrete; however, using it in this study gave values higher than those of the vacuum saturation method. In addition, by knowing the foam volume and the porosity of cement paste (φ_{paste}), a theoretical total porosity has been estimated with a close match to the most reliable measured value (φ_{vac}).

It should be noted that the porosities measured by vacuum saturation method were used to decide the threshold values of the different corresponding mixes after subtracting the corresponding theoretical paste porosities in order to obtain their connectivity values, **Section 4.3.4**. Therefore, the porosities obtained from the µCT technique are close to the volume of added foam since pore diameters larger than 16 µm were determined from this technique.
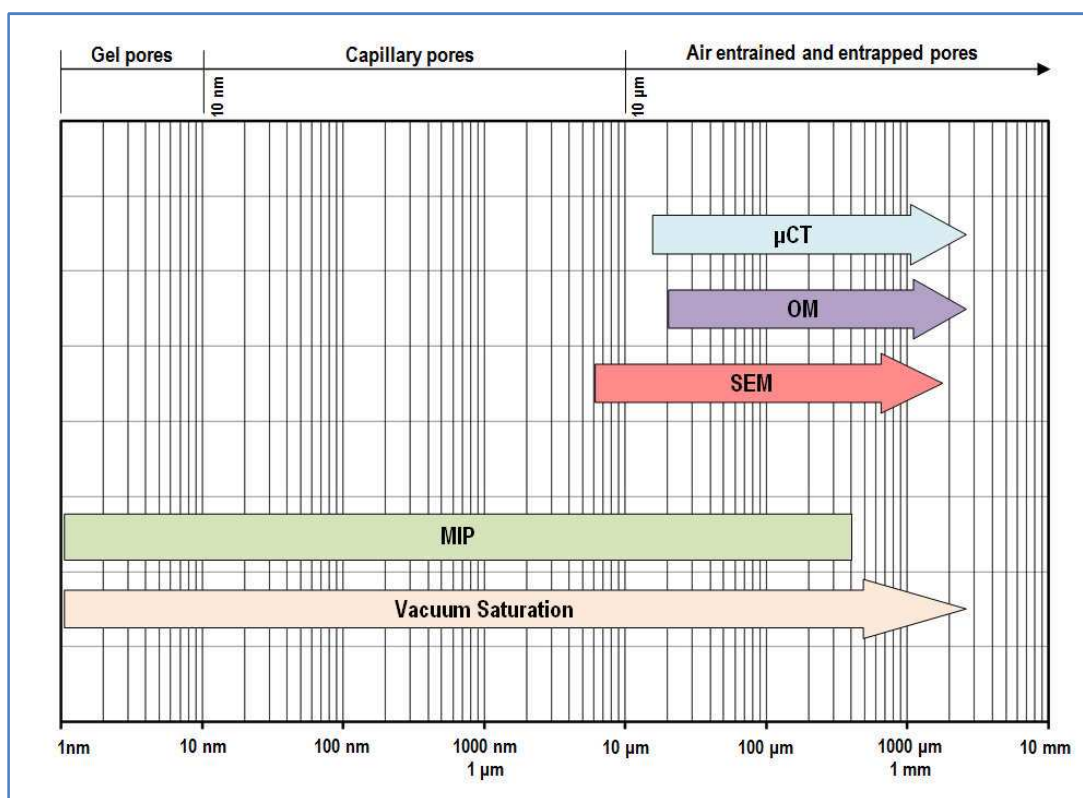
Figure 4-14 The limitations of techniques used for porosity measurements
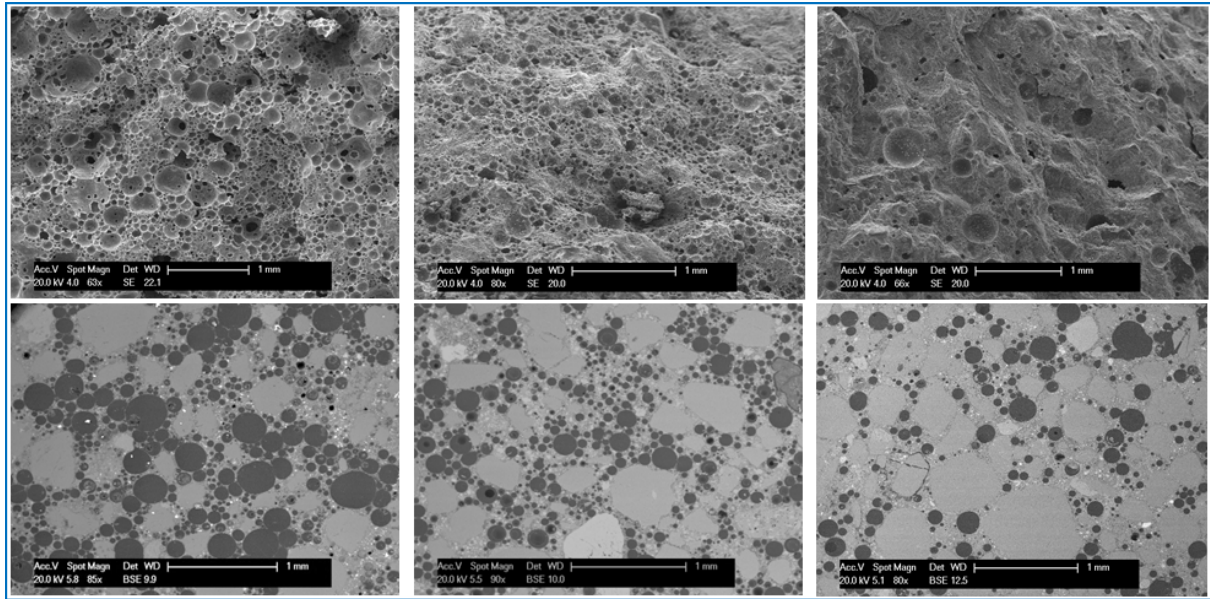
Figure 4-15 Air-void structure of some mixes; left: FC3; middle: FC6; right: FC9

4.3.2 Void Size Distribution

Although the void size distribution of foamed concrete has to some extent been investigated, a great deal remains to be understood, so this section, in addition to characterizing the air-void structure of mixes, aims to investigate the formation of the voids during mixing. This is achieved by:

1) Determining and comparing the size distributions of air voids in the foamed concrete mixes (after hardening) to those of bubbles in the preformed foam based on both number and area of bubbles/voids.

2) Investigating the circularity of the voids within the mixes.

4.3.2.1 Foam

For foam investigation, about a litre of foam has been taken from the foam generator and then put in a cylindrical plastic container (50mm diameter and 20mm height) for foam surface microscopic investigation; **Figure 4-16**. Due to the impossibility of capturing a clear image of the foam in its natural state using an optical microscope with low magnification, it was decided to impregnate it with a very small dose of bitumen emulsion, see **Figure 4-17**. Bitumen emulsion was

chosen since it contains carbon which, when using an optical microscope, gives an image with good clarity and contrast between the edges and surfaces of individual foam bubbles, **Figure 4-18**. In addition, the production process of bitumen emulsion involves a surfactant (emulsifier) which surrounds individual bitumen droplets (of size <10 μm) within the water, which is essentially the same mechanism as used in foam production, see **Figure 4-19**. The result is that the bitumen emulsion will be compatible with the foam and spread easily through the bubble membranes, giving them colour.

A magnification of (56×) was selected, with a pixel representing 2.34 μm and an image of 28.3 mm^2 (6.14mm × 4.60mm). However, it proved impossible to derive a binary image suitable for automated analysis (in ImageJ) and manual measurements were therefore carried out to determine the void diameters (around 200 voids in each image) from the captured foam images.

The bubble size distribution and the corresponding cumulative frequencies (on the basis of number of bubbles) for the foam images are shown in **Figure 4-20**. From this, it can be seen that the minimum bubble diameter is about 100 μm and the largest is 875 μm with a median diameter D_{50} of 325 μm and a 90th percentile (D_{90}) of 600 μm. However, it was observed that the natural surface of the foam formed in such a way as to conceal some of the smaller bubbles, and a second set of ten images was therefore captured from the same foam samples after applying a microscope glass slide to the surfaces; see **Figure 4-21**. From this figure, the membrane thickness between two bubbles is about 100 μm and since the individual bitumen droplets are less than 10 μm, little effect on the observed bubble diameters is anticipated.

The numeric cumulative frequency curves for the foam with and without glass plate application are shown in **Figure 4-22**.
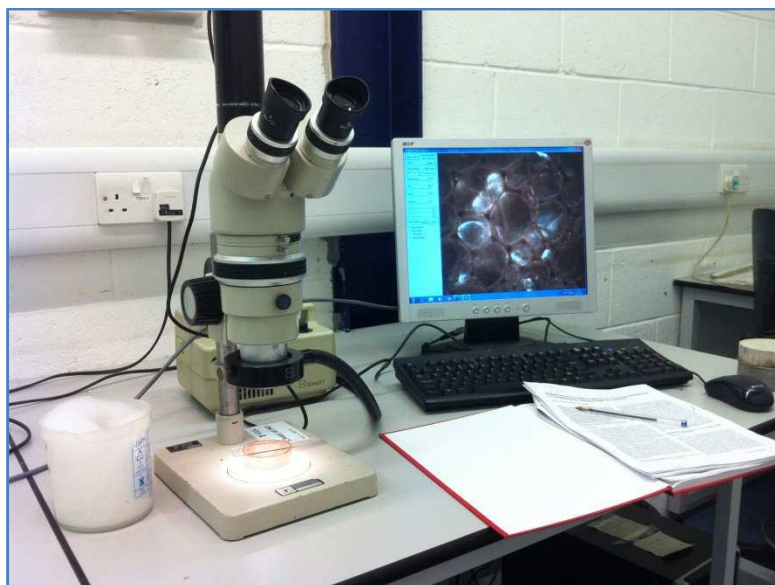
Figure 4-16 Foam during microscopy investigation
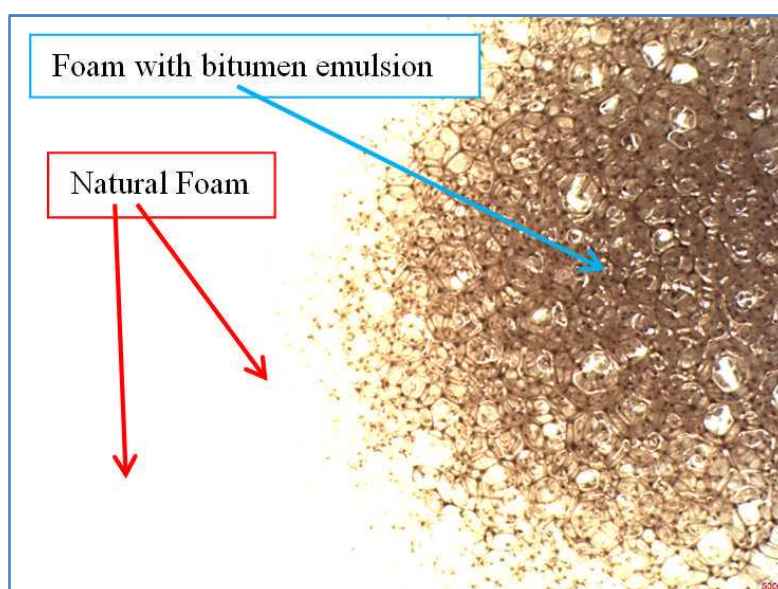
Figure 4-17 Image of foam during bitumen emulsion application [15.43mm × 11.57mm]
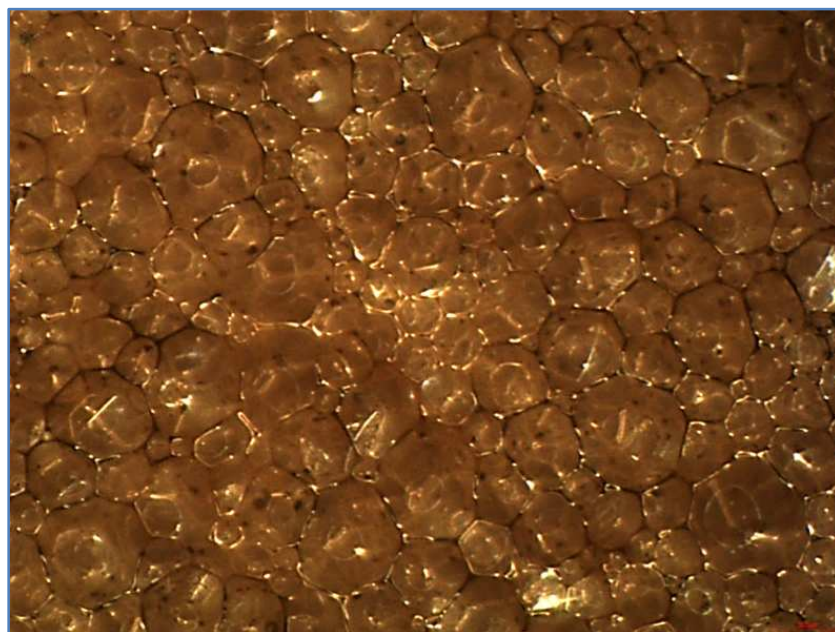
Figure 4-18 Foam after treating with bitumen emulsion [6.14mm × 4.60mm]
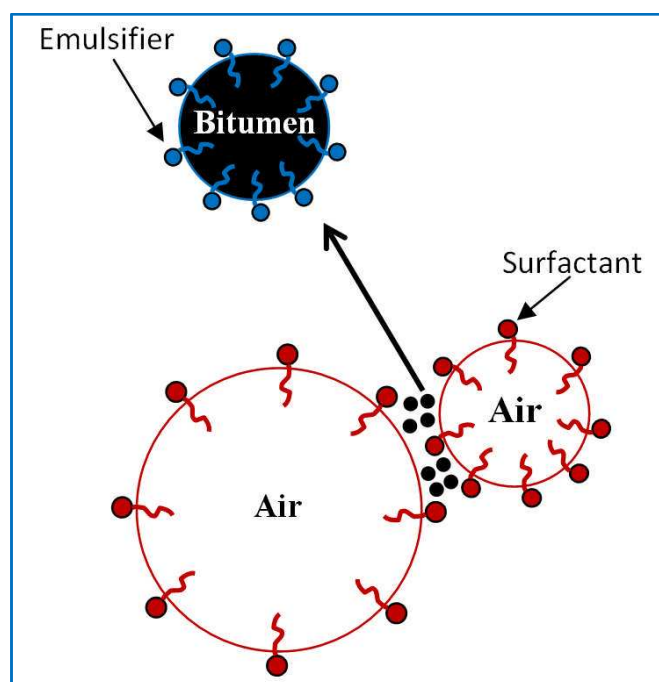
Figure 4-19 The interaction between foam bubbles and bitumen emulsion
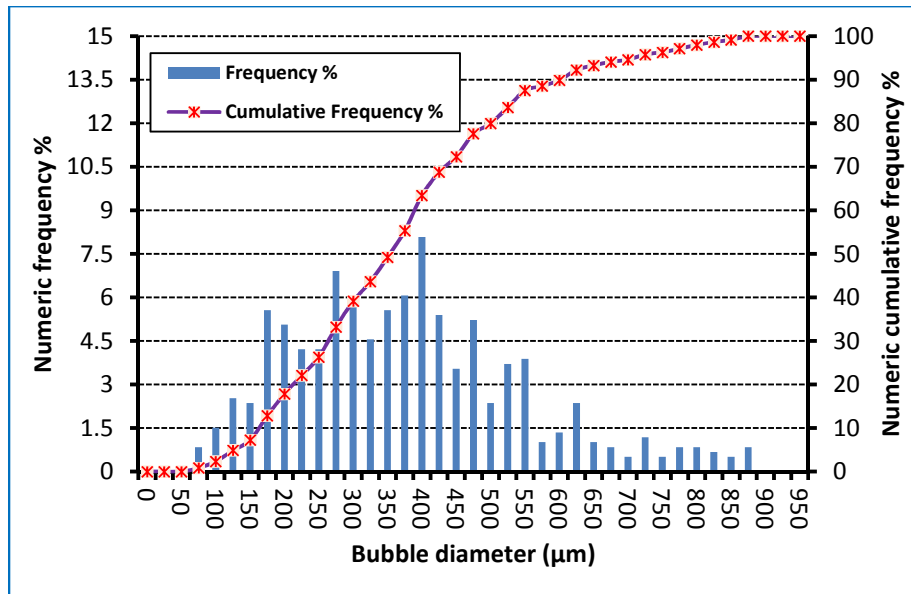
Figure 4-20 Numeric bubble size distribution and cumulative frequency of foam
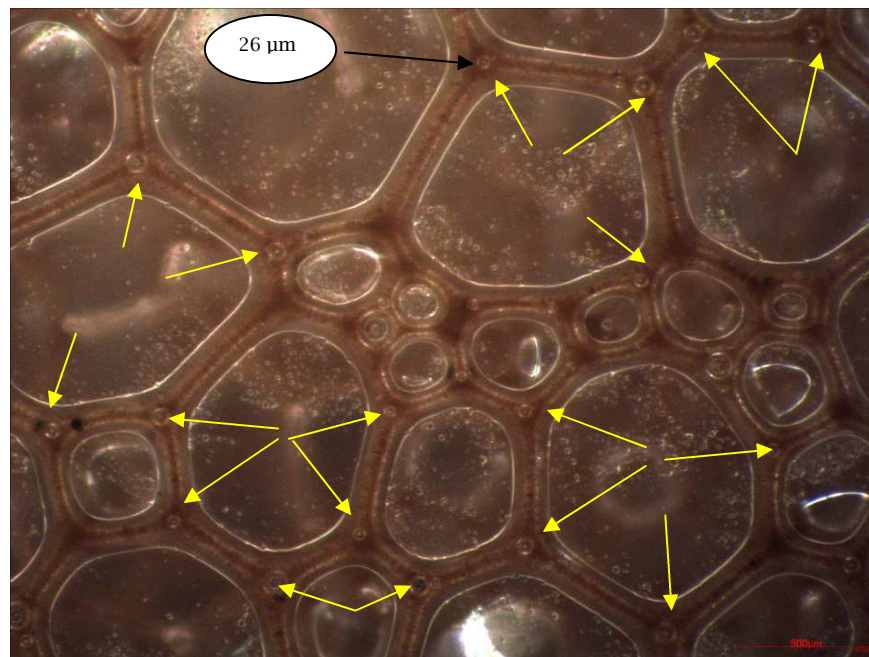
Figure 4-21 Foam image showing constrained surface bubbles with diameters less than 100 μm when sandwiched beneath a microscope glass slide [2.30mm × 2.06mm]
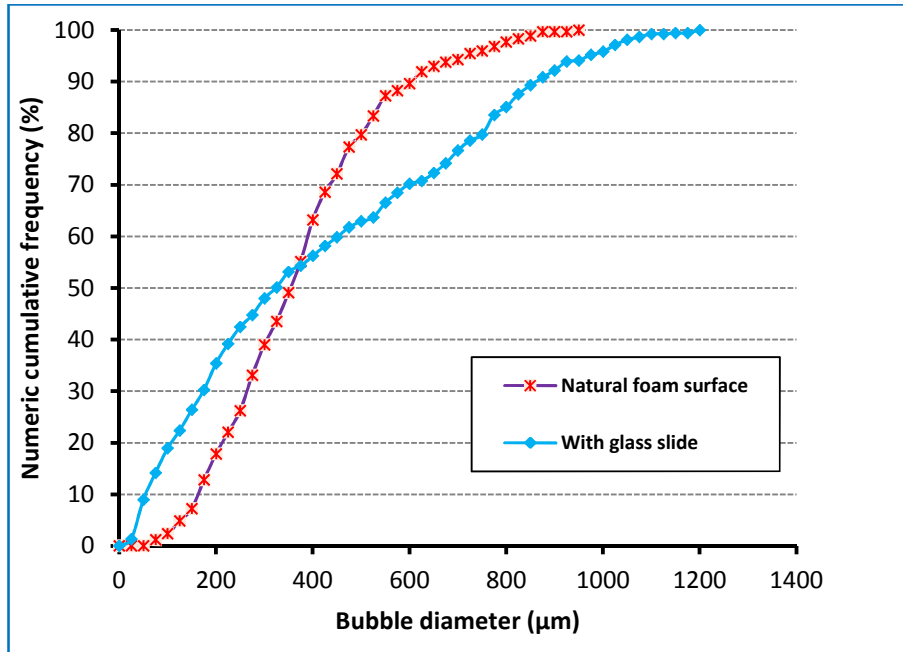
Figure 4-22 Numeric cumulative frequency of foam with and without glass slide application

4.3.2.2 Foamed Concrete

For each mix, the same ten optical microscope images used for porosity investigation were used also for void size distribution.

For each void, an effective diameter was calculated by measuring the void area and assuming it to be perfect circle (Kearsley, 1999).

Figure 4-23 shows the resulting pore size distributions for conventional foamed concrete mixes with nominal densities of 1300, 1600 and 1900 kg/m^3 (mixes FC3, FC6 and FC9 respectively), where it may be seen that sizes vary between approximately 20 and 2000 μm. It is clear that at higher density, the proportion of the larger voids decreases leading to a narrower air void size distribution. In order to quantify and compare the air void distribution of different mixes, the parameters O_{50} (median opening pore size) and O_{90} (90th percentile) were calculated on the basis of number of voids, see **Table 4-2**; O_{50} varied from 165 to 180 μm, O_{90} from 525 to 750 μm, and both O_{50} and O_{90} increased with foam proportion. The smallest air void diameter identified was about 20 μm. To check that these smallest pores came from

the added foam (entrained air voids) rather than from the manufacturing process (entrapped air voids), SEM images were captured from mixes both with and without added foam, **Figure 4-24** and **Figure 4-25**. In **Figure 4-25**, it can be seen that there are very few entrapped air voids in the 20 μm size range, leading to the conclusion that all pores in excess of 20 μm, clearly apparent in **Figure 4-24**, are foam pores.
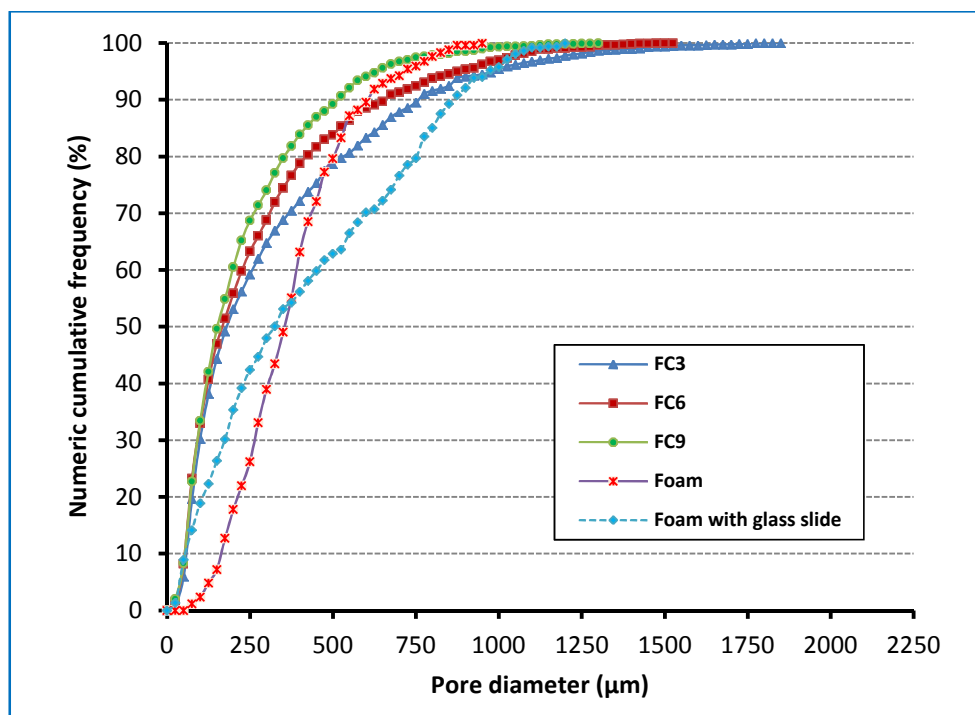
Figure 4-23 Numeric cumulative frequency of bubble/pore diameters of foam and conventional foamed concrete mixes

Table 4-2 Parameters of pores sizes and circularity of foam and conventional foamed concrete mixes

	Foam	FC3	FC6	FC9
(D or O)$_{50}$* (μm)	325	180	175	165
(D or O)$_{90}$* (μm)	600	750	650	525
(D or O)$_{50}$** (μm)	470	770	685	550
(D or O)$_{90}$** (μm)	765	1425	1225	990
F_{circ50}		0.53	0.59	0.65
F_{circ10}		0.25	0.29	0.35

Note: Diameter of bubbles (D) and voids (O) derived either from cumulative distribution based on numeric of bubbles/voids[*] at each size or on area of bubbles/voids[**] at each size.
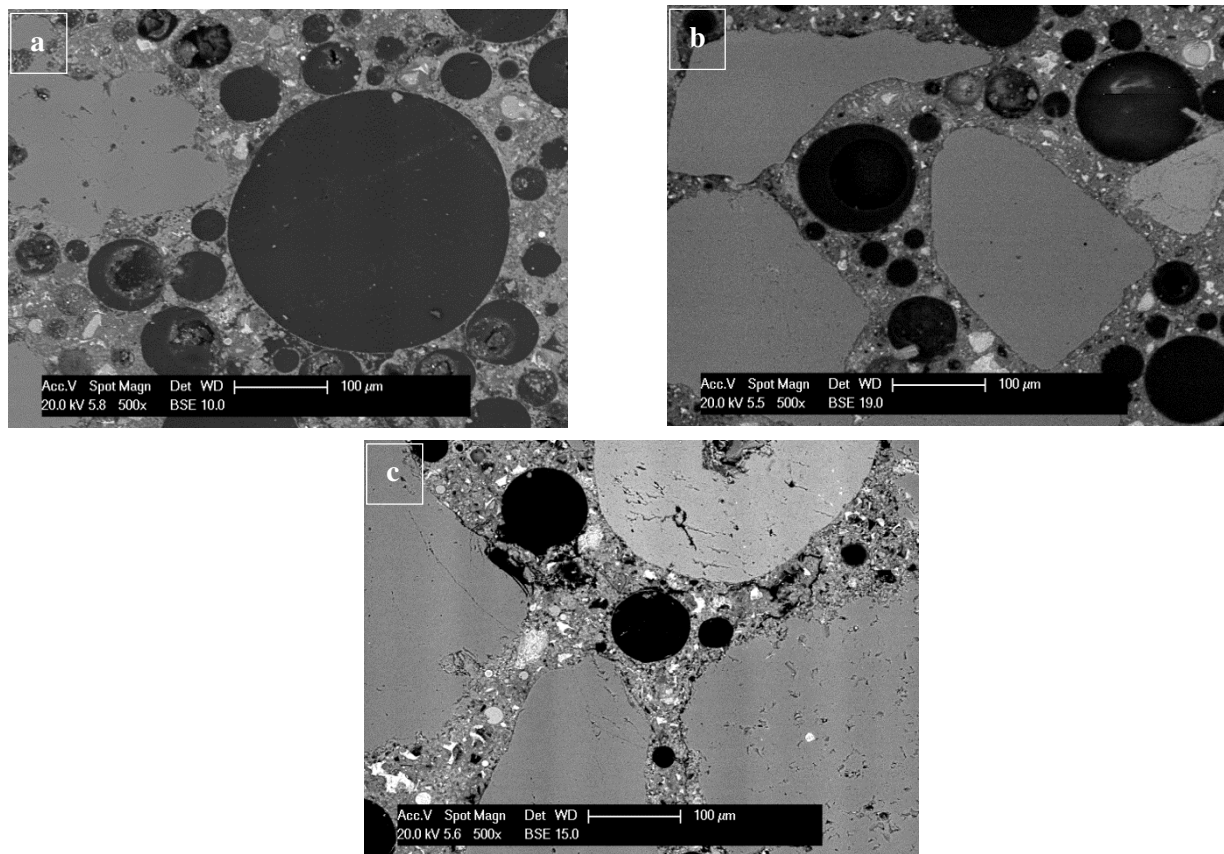
Figure 4-24 SEM images of foamed concrete mixes (a) FC3, (b) FC6 and (c) FC9
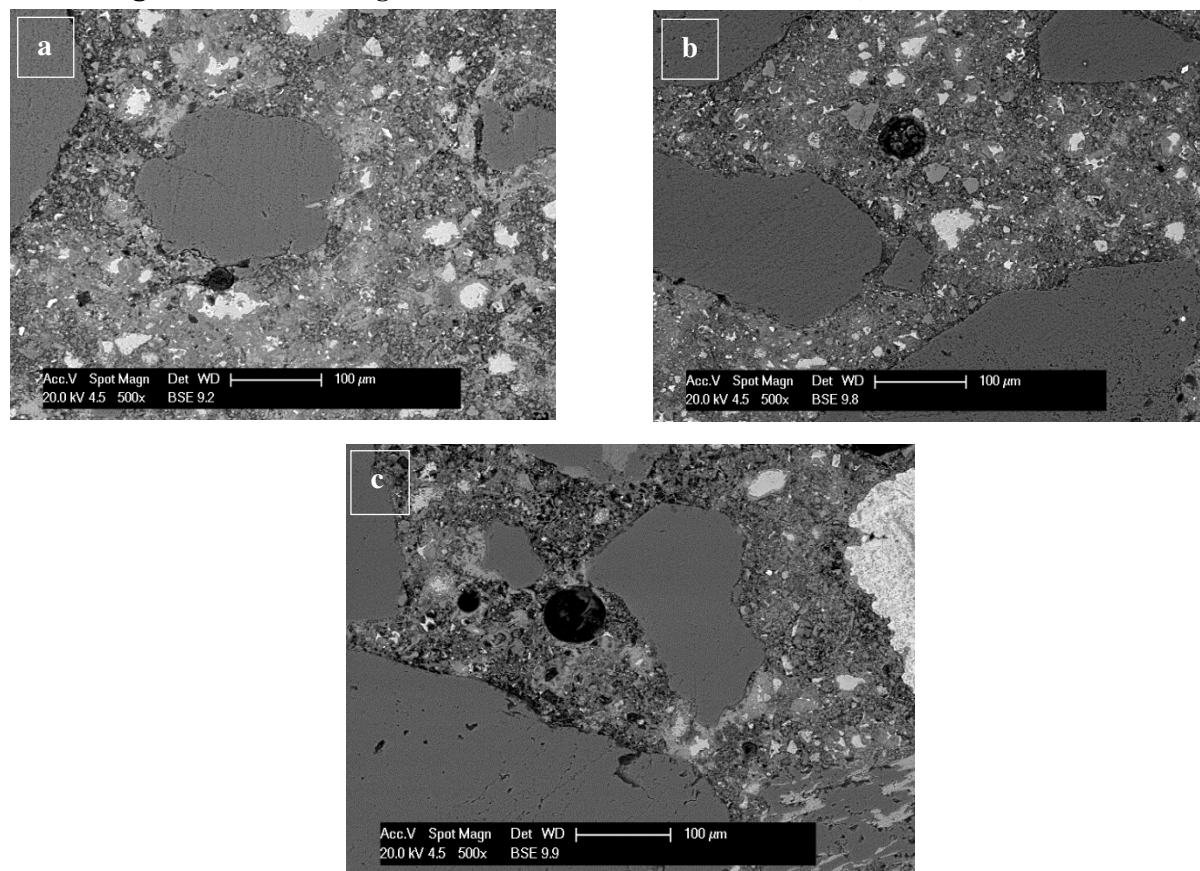
Figure 4-25 SEM images for mixes without foam (a) 1300 (b) 1600 and (c) 1900 kg/m³

4.3.2.3 Comparison

Figure 4-23 illustrates the cumulative frequency of bubble/ pore diameters in the foam and the foamed concrete mixes (on the basis of number of bubbles/voids). Two very clear differences are apparent. First, foamed concrete mixes contain some larger sized pores than those in the foam itself and the number of such pores increases with the increase in added foam volume. This is logical due to the combining of foam bubbles during and possibly after mixing. However, the second difference is much more substantial. From **Figure 4-20**, the smallest bubble diameter in the foam was about 100 μm, while in the foamed concrete mixes there were many voids with sizes lower than this value. Even when the microscope glass slide was pressed into the foam surface, **Figure 4-21**, no more than 20% of bubbles were found to be smaller than 100 μm (**Figure 4-22**) and it could be argued that this technique leads to bubble distension and an overestimation of bubble diameters. In contrast, 30-40% of voids in the mixes had a diameter less than 100 μm. Looking at the D_{50} values, that for foam was 300-325 μm, depending on the observational technique used, compared to 165-185 μm for the mixes.

There are two possible reasons for this. Firstly; merging of large bubbles, by reducing the number of larger voids, reduces the total number of voids compared to that of foam leading to an increase in the numeric proportion of the smallest voids and positioning the numeric cumulative curve for the mix above the curve for the foam. Secondly, from a vacuum saturation test, it was found that the porosities of the mortars (without foam) are 13.6, 13.1 and 12.9% for FC3, FC6 and FC9 respectively. While for the FC3, FC6 and FC9 foamed concrete, they are 51.63, 40.76 and 28.73%. By knowing the added foam (**Table 4-1**) and the difference between foamed concrete and corresponding unfoamed porosities, it was found that there is foam volume loss of about 4.3, 1.8 and 0.8% for FC3, FC6 and FC9 respectively. This loss is probably because foam bubbles collapse or the air in them is lost to the

atmosphere, and this is most likely with the large bubbles. This will have the same effect of merging leading to the median diameter of foam bubbles (D_{50}) being larger than those of the voids (O_{50}) in the mixes. Another possible interpretation is that the loss of foam bubbles (by collapse) during the mixing process leaves a solution (foaming agent with water) which works as an air-entraining agent and produces, during mixing, other smaller bubbles. In this context, the addition of a foam stabilizer could usefully be investigated and the bubble size distribution in the hardened concrete examined.

In place of analysis of numbers of bubbles at each diameter, the same data was considered from the prospective of the area of the bubbles in the foam and the concrete images. **Figure 4-26** shows the frequency and cumulative frequency by area of the bubbles in the foam. This may be contrasted with the numeric frequency previously presented in **Figure 4-20**. A low number of larger bubbles (**Figure 4-20**) means that the area contained within these bubbles comprises a significant proportion of the space occupied by the foam, as seen in **Figure 4-26** between 550 and 875 μm. This has the effect of increasing the D_{50} calculated on the basis of area (470 μm) from the value of 325 μm calculated on the basis of number of bubbles (**Table 4-2**). Because in concrete the larger bubbles are more implicated in the development of cracking and, hence, strength reduction, the characterisation by bubble area is probably to be preferred. Continuing this argument, characterization by, for example, D_{90} may be more germane.

A comparison of foam bubble area and concrete mix pore area is included in **Table 4-2**. It shows that both median and large characteristic voids are significantly greater in area than in the foam. This implies that there has been significant merging of small voids into a few larger voids during the concrete mixing process. This behaviour is most pronounced in the least dense mix.

Considering this observation with the earlier one that median pore size based on number of pores reduces, comparison of **Figure 4-23** and **Figure 4-27** allows us to deduce that bubble merging is prevalent in all mixes. In the less dense mixes, bubble merging takes place at all sizes (the cumulative area void curve for the concrete is always beneath that for the foam). In the most dense mix the area contained in small pores does not change much at all, indicating that the small bubbles result in small pores without much loss to merged bubbles.

Since the voids merging of larger voids in the most dense mix is less than in the lighter mixes, loss of voids must be more effective than their merging in making the mix curve lie above the foam curve within the small diameter range (**Figure 4-27**).
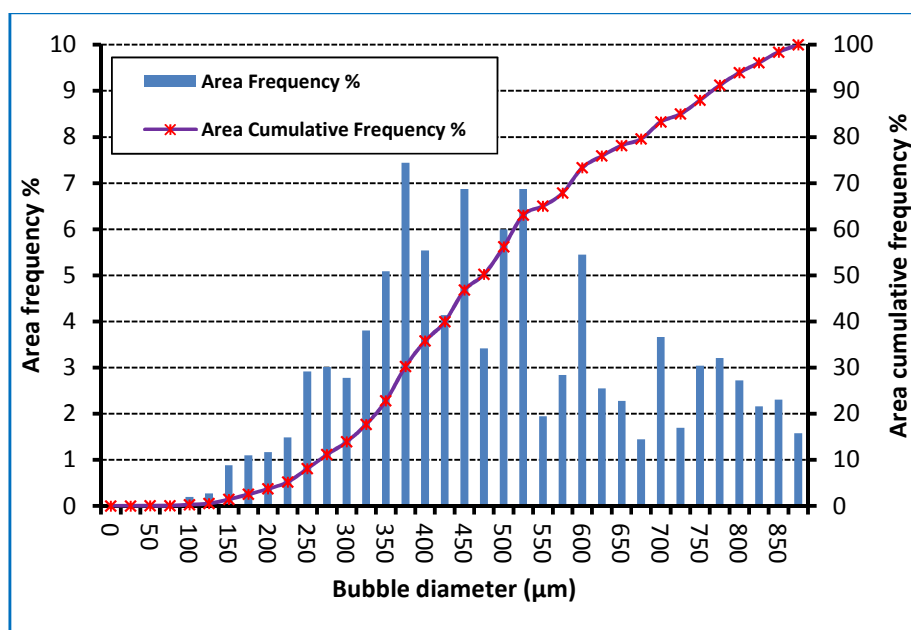
Figure 4-26 Area bubble size distribution and cumulative frequency of foam
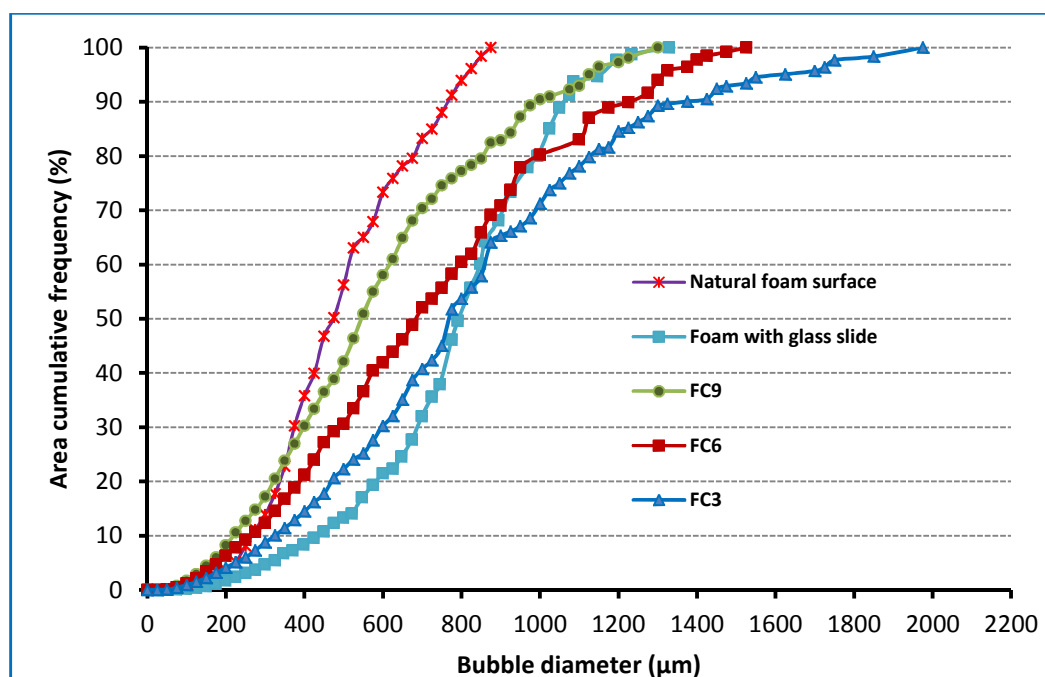
Figure 4-27 Area cumulative frequency of bubble/pore diameters of foam and foamed concrete mixes

4.3.3 Void Shape

The circularity factor (Fcirc) is a function of the perimeter and surface area of each pore, defined as follows;

$$F_{circ} = 4\pi \left[\frac{Area}{Perimeter^2} \right] \qquad (4\text{-}6)$$

Circularity factor equals 1 for a perfect circular pore and it is smaller for irregular shapes (Scheffler and Colombo, 2005), see **Figure 4-28**.

From the SEM images for foamed concrete mixes, **Figure 4-24**, it can be seen that the shape of the smaller voids, at high magnification (>500×), is almost circular which means that their circularity factor should be near to 1. However, with the optical microscope (at low magnification, <25×), larger voids with irregular shapes, formed due to bubble merging, can clearly be seen; see **Figure 4-11** supported by lower magnification SEM images in **Figure 4-29**. From image analyses results, **Figure 4-30** shows that void merging is more evident with increased added foam volume.

Thus, the F$_{circ50}$ (median circularity factor) and F$_{circ10}$ (circularity factor at which 10% are less) show that irregularity of voids for FC9 is less than for FC3; see cumulative frequency curves in **Figure 4-30** and **Table 4-2**. This effect, bubble merging, is likely to be a primary reason that the porosity values (36.71, 26.65 and 15.1 for FC3, FC6 and FC9 respectively) calculated by image analysis from optical microscopy were lower than the added foam volumes (42.4, 29.5 and 16.6), a reason also suggested by Nambiar and Ramamurthy (2007a), and the difference increases with increased added foam (decrease in density).
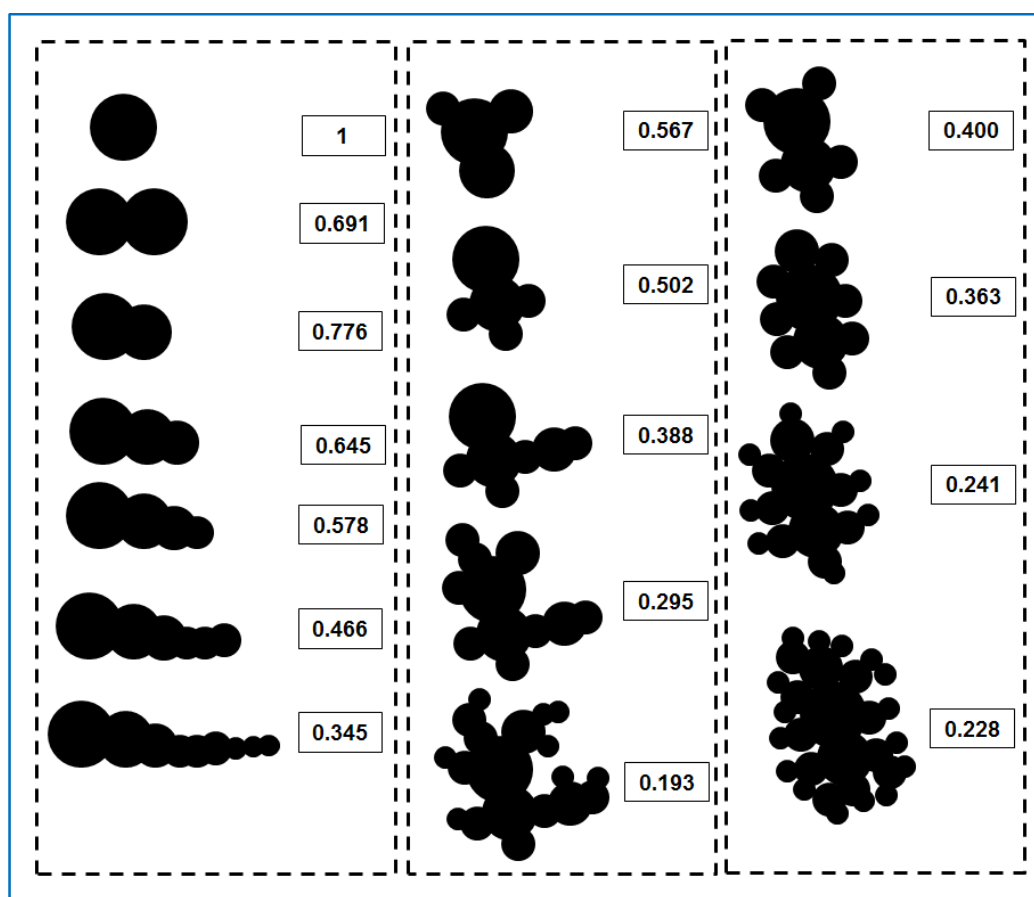
Figure 4-28 Circularity factors of different shapes calculated by using ImageJ
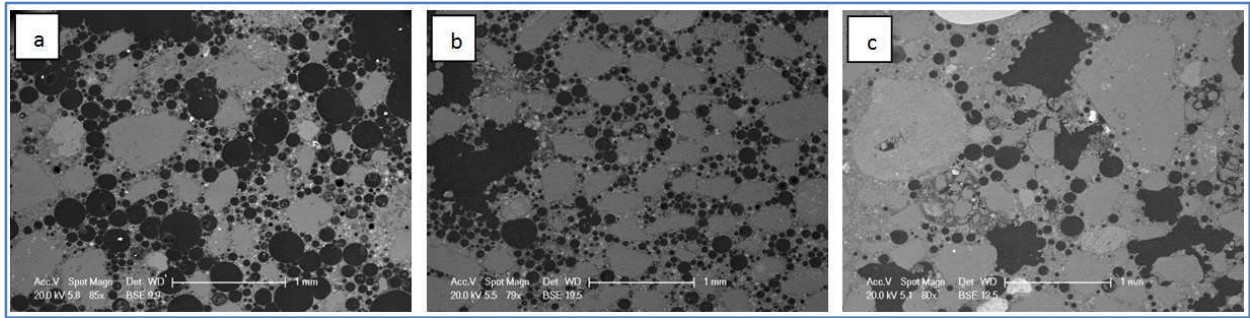
Figure 4-29 SEM images of foamed concrete mixes showing the bubble merging (a) FC3, (b) FC6 and (c) FC9
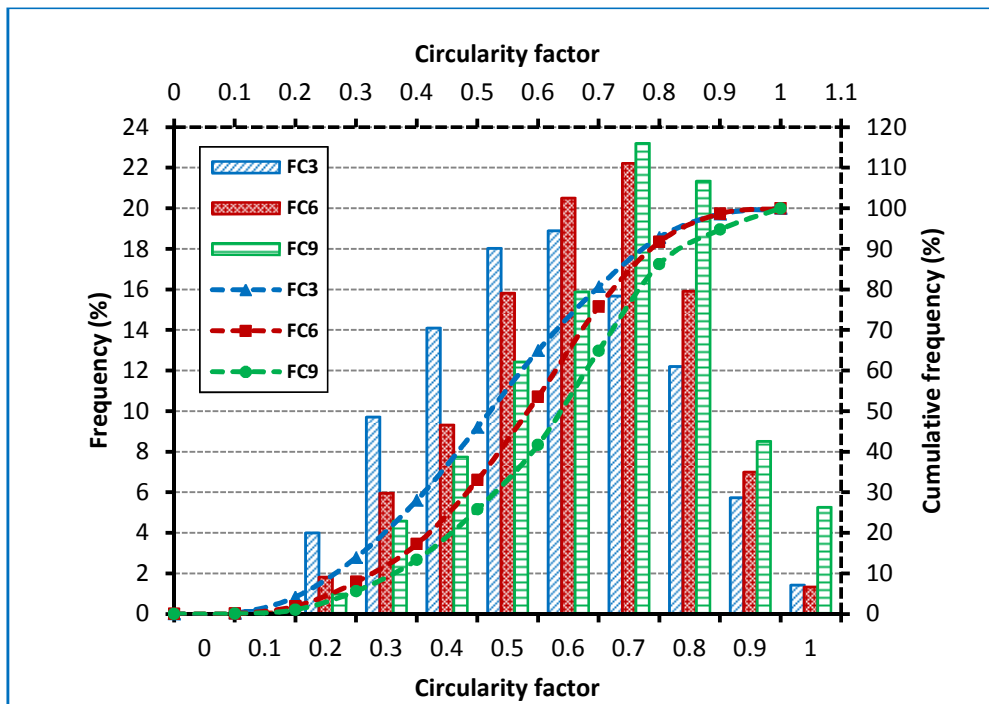
Figure 4-30 Circularity factor of foamed concrete mixes

4.3.4 Connectivity of Voids

Scheffler and Colombo (2005) stated that Micro Computed Tomography (μCT) has been used to compute the connectivity density (Conn. D.) of ceramic foams from different preparation methods by using the Conn-Euler principle.

From the SCANCO MEDICAL μCT manual, the connectivity density (Conn. D.) obtained from its data is calculated with the Conn-Euler method which is described by Odgaard and Gundersen (1993) in their study on quantification of connectivity in cancellous bone, with special emphasis on 3-D reconstructions.

The Conn-Euler method uses the Euler characteristic (χ) of three dimensional structure (as an expression of connectivity) which reports the number of particles of a structure plus the number of enclosed cavities minus the connectivity. Determination of connectivity is based on the Euler characteristic since it is relatively simple to determine and it has a known relation to connectivity.

Odgaard and Gundersen (1993) defined the connectivity as a measure of the degree to which a structure is multiply connected. To illustrate this, given a network consisting of nodes and branches (points connected to lines). If only one path from any node (say, **P**) to any other node (say, **Q**) exists then this network is simply connected, **Figure 4-31a**. In **Figure 4-31b**, an additional branch is added causing some nodes to be connected by more than a single path resulting in generating a multiply connected structure. In other words, if a branch in a tree is broken with a simply connected structure, the structure will fall apart; while in a multiply connected network the structure will not separate into isolated parts even by cutting some of the branches.
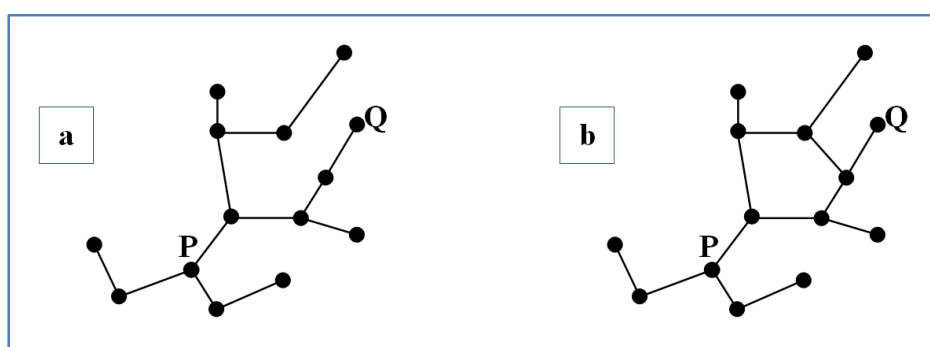
Figure 4-31 (a) Simply connected node-and-branch network [one path exists from P to Q] (b) Multiply connected network [two paths exist from P to Q], after (Odgaard and Gundersen, 1993)

Figure 4-32 illustrates some examples of determination of the Euler characteristic (χ) for an examination volume of a 3×3×3 cube of voxels by using **Eq. (4-7)** which is particularly suited for 3-D digital images.

$$\chi(X) = \sum (-1)^i \, n_i = n_0 - n_1 + n_2 - n_3 \ldots \ldots \ldots \tag{4-7}$$

where n_i is the number of convex bodies of dimension i in the decomposition of **X** into convex bodies. In these examples, n_3 is the number of voxels, n_2 is the number of voxel faces, n_1 is the number of edges and n_0 is the number of voxel corners.

The Euler characteristic (χ) of the union of two sets A and B is given by the sum of the Euler characteristics of the two sets minus the Euler characteristic of the intersection of the sets, as follows;

$$\chi(A \cup B) = \chi(A) + \chi(B) - \chi(A \cap B) \tag{4-8}$$

This is known as the addition theorem which indicates that when the structure is divided into parts, the sum of the Euler characteristics for each of the parts differs from the Euler characteristic of the entire structure. As a result, the Euler characteristic of the intersection of two sets (**Eq. (4-8)**) should be taken into consideration.

Finally, the Euler-Poincare formula states that for a 3-D structure (**X**),

$$\chi(X) = \beta_0 - \beta_1 + \beta_2 \tag{4-9}$$

where the zeroth Betti number, β_0, reports the number of separate particles of the structure, the first Betti number, β_1, reports the connectivity and the second Betti number, β_2, reports the number of cavities enclosed within the structure.

From **Eq. (4-9)**, the connectivity of the structure, β_1, can be determined as follows:

$$\beta_1 = \beta_0 + \beta_2 - \chi(X) \tag{4-10}$$
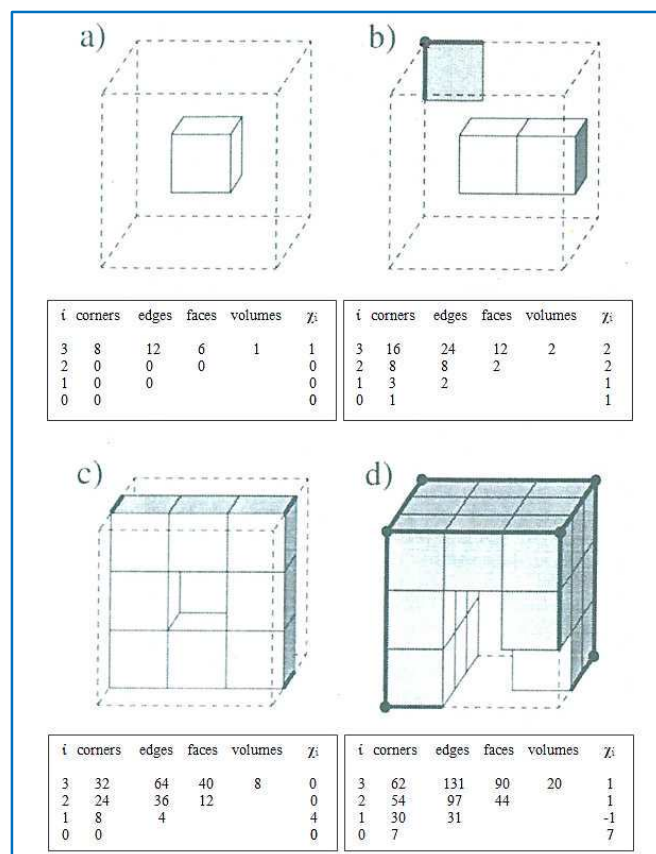
Figure 4-32 Examples of determination of the Euler characteristic (χ) for an examination volume of a 3×3×3 cube of voxels, after Odgaard and Gundersen (1993)

For this project, tomographic scans were performed for all investigated cylindrical samples (10×20mm) using a SCANCO MEDICAL micro computed tomography (μCT 40). The x-ray energy was set to values of 55 kV and 144 μA. The pixel resolution was 16 μm. The tomographic reconstruction was performed using SCANCO software.

The connectivity density (Conn. D.) was obtained from the μCT data and to convert it to the connectivity value (β_1) it should be multiplied by the corresponding examination volume.

Figure 4-33 shows 2-D images and 3-D reconstruction images of the selected mixes. **Table 4-3** shows the connectivity values of the investigated mixes (FC and FCa mixes). From the table, it is clear that the connectivity reduces with increase in density and with using additives for the same density.

It should be noted here that there is no possibility to compare these values with other studies since there are currently no available results for connectivity, either in normal concrete or in lightweight concrete, particularly foamed concrete. However, knowledge of the connectivity values may constitute a useful comparative index for the different investigated mixes.
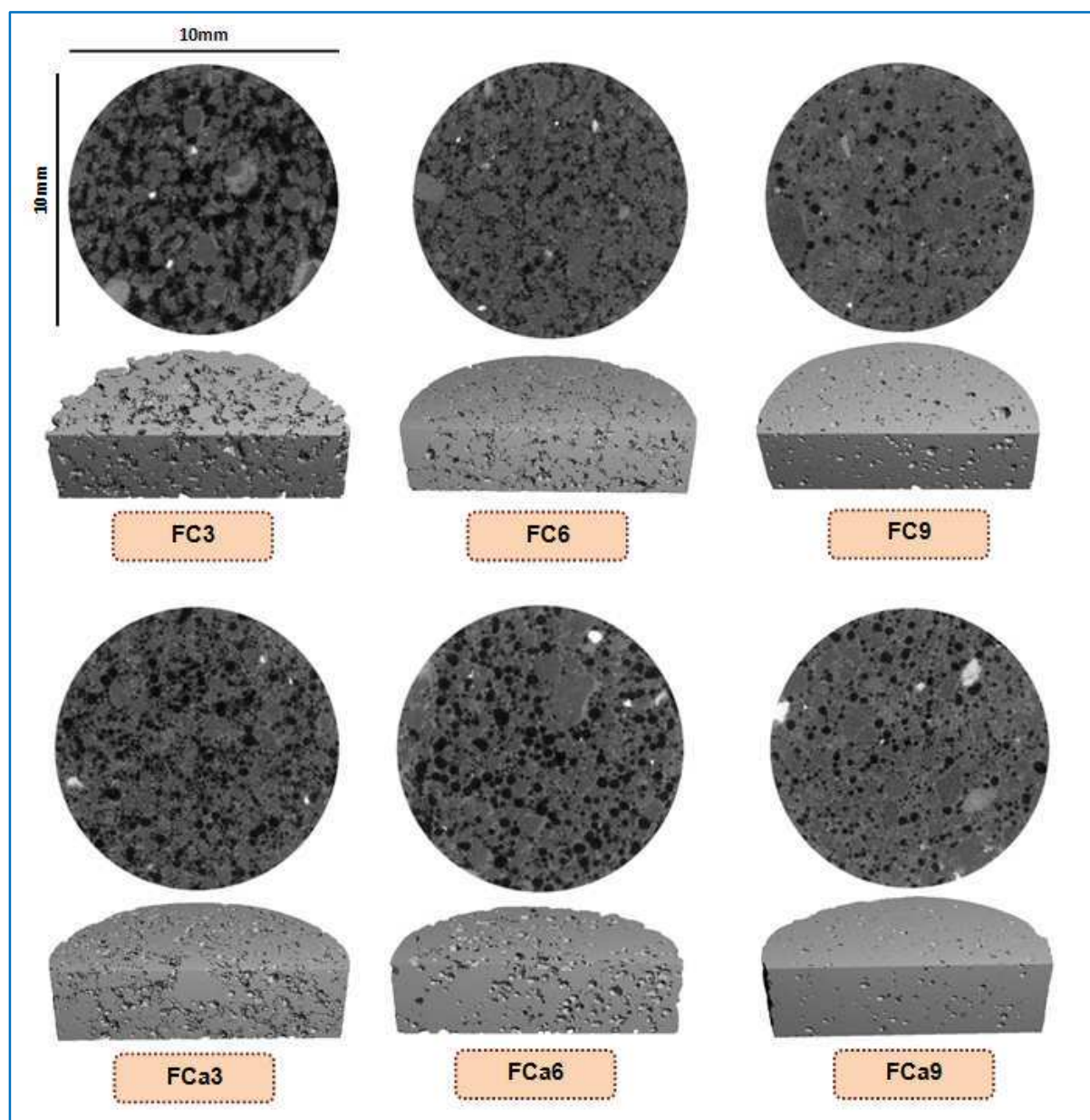
Figure 4-33 2-D images and three-dimensional reconstruction images of the selected mixes

Table 4-3 Connectivity values of the investigated mixes

Mix	FC3	FC6	FC9	FCa3	FCa6	FCa9
Volume (mm^3)	302.9	317.4	569.5	261.6	300.5	291.2
Conn. D. (1/mm^3)	81.2	64.5	3.8	65.6	17.5	1.3
Connectivity, β_1	24586.3	20483.9	2123.9	17174.9	5257.4	383.4

4.4 Effect of Additives on Air-void Structure

In this section, the effect of additives on the air-void structure of the selected foamed concrete mixes has been described by optical microscopy images and quantified by size and shape parameters obtained from the analysis of these images.

Figure 4-34 shows binary images for all mixes selected to investigate the air-void structure and the effect of the additives on it. It is clear that at higher density (less added foam) the proportion of larger voids decreases leading to a narrower air void size distribution; see also **Figure 4-35**. In addition, for a given density, the additives in combination led to increased void numbers by preventing their merging and producing a narrower void size distribution compared to a corresponding conventional mix, **Figure 4-35**.

To investigate the effect of additives, individually and in combination, on void structure, **Figure 4-36** shows the void size distributions of 1600 kg/m^3 mixes. In order to quantify and compare the air void distribution of selected mixes, the parameters O_{50} and O_{90} were calculated on the basis of number of voids, see **Table 4-4**. It can be seen that both O_{50} and O_{90} increased with foam volume while they decreased significantly with additives in combination (FCa mixes) suggesting that the inclusion of these additives helps in achieving more uniform distribution of air voids (less merging) than FC mixes. This is also obvious from the circularity results since reducing void merging resulted in less irregularity in the shape of voids,

pushing the circularity factors (F_{circ50} and F_{circ10}) toward 1, see **Table 4-4**. Compared to FC6, using the additives individually slightly deceased O_{50}, while O_{90} was significantly decreased implying that additives helped in reducing the merging of voids and so reduced the areas of the larger voids.

It can be seen from **Table 4-4** that superplasticizer on its own achieves the smallest pores when compared to the effect of other additives and significantly smaller pores when used in combination with other additives. By comparing **Figure (4-34/FCp6)** to **Figure (4-34/FCa6)** and by comparing **Figure (4-37d)** and **Figure (4-37e)**, it can be seen that shape of voids is not much altered by combining additives over use of superplasticizer alone, compare FCp6 and FCa6 in **Table 4-4**; the shape is largely unchanged. Taken together, this implies that the superplasticizer has the most beneficial influence on void structure.

The addition of LWA instead of part of the sand also helps in improving the air-void structure of the mixes compared to those without LWA. From **Figure 4-36** it is clear that the void size distributions for mixes with LWA are narrower than those without it with the same density. There are two possible reasons for this; firstly, by adding LWA the amount of added foam has been reduced, **Table 3-4**, leading to reduced void merging and thereby increased circularity factors. Secondly, additional small pores within the LWA led to a decrease in the size parameters, **Table 4-4**.
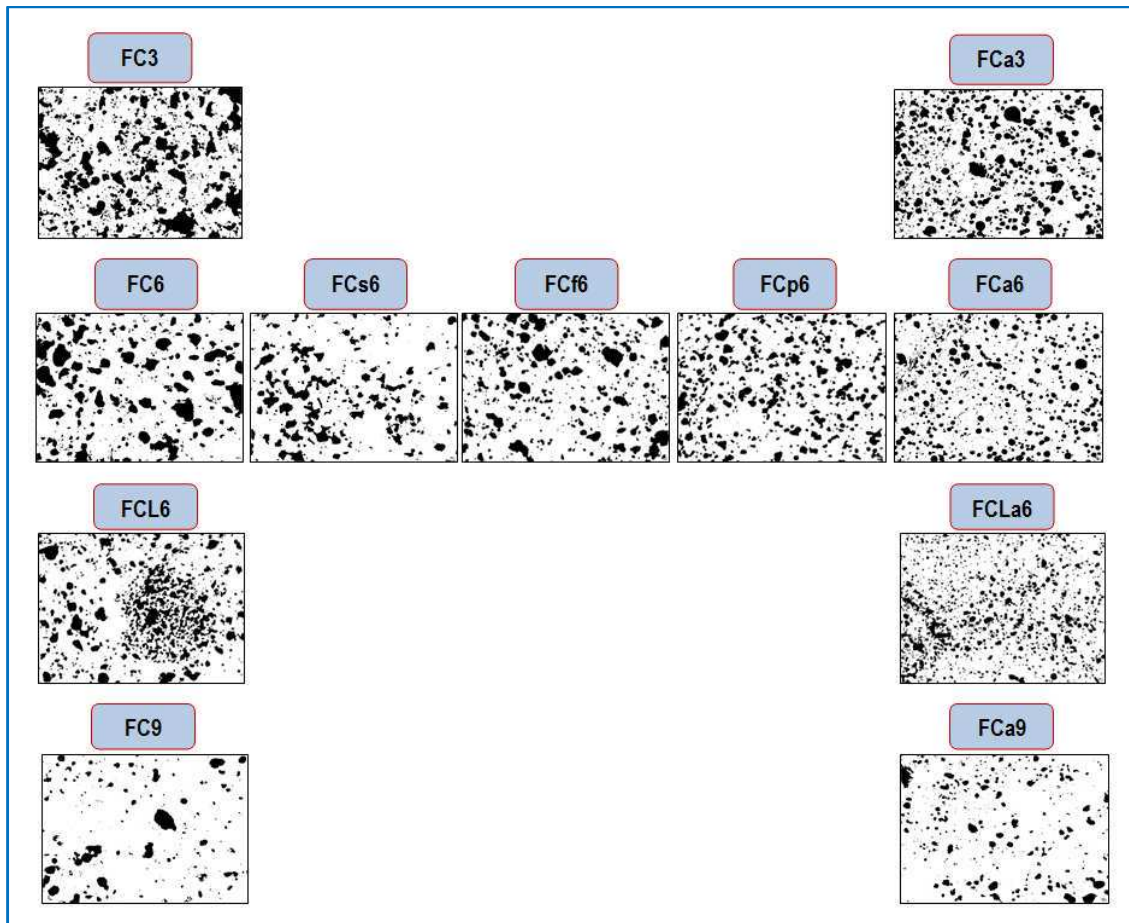
Figure 4-34 Typical binary images [15.43mm × 11.57mm] for the selected mixes
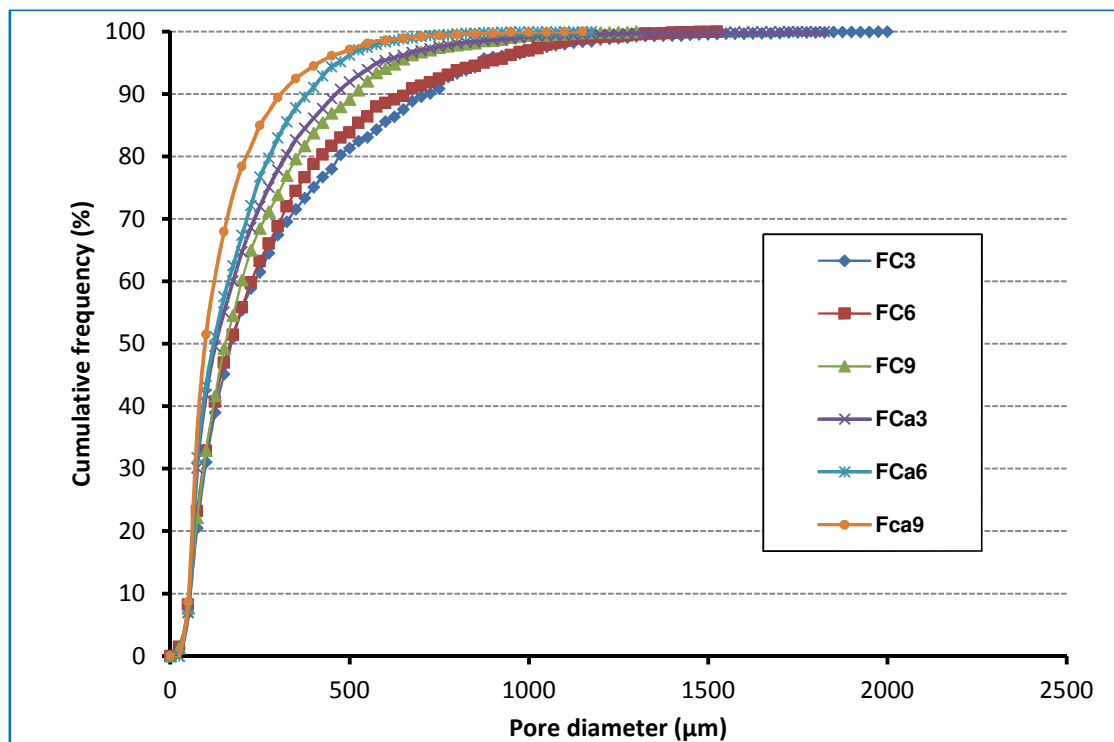
Figure 4-35 Numeric cumulative frequency (%) of pore diameters of FC and FCa foamed concrete mixes
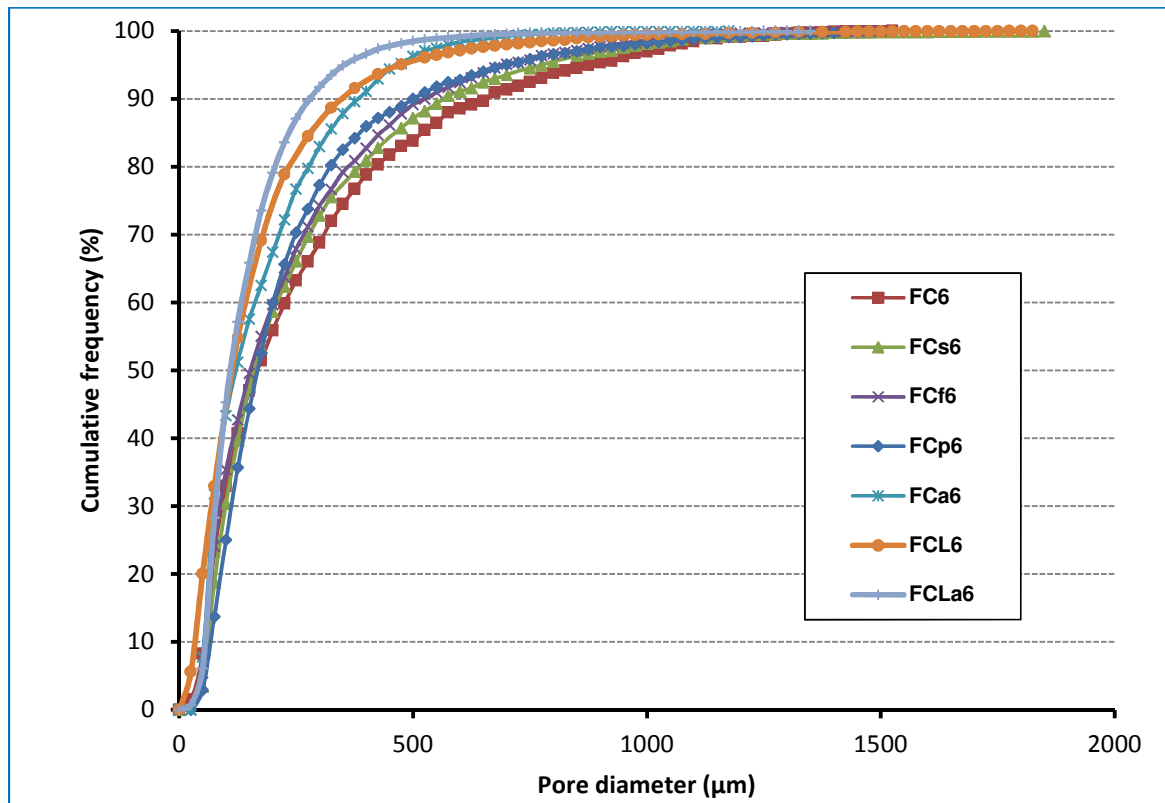
Figure 4-36 Numeric cumulative frequency (%) of pore diameters of 1600 kg/m^3 mixes
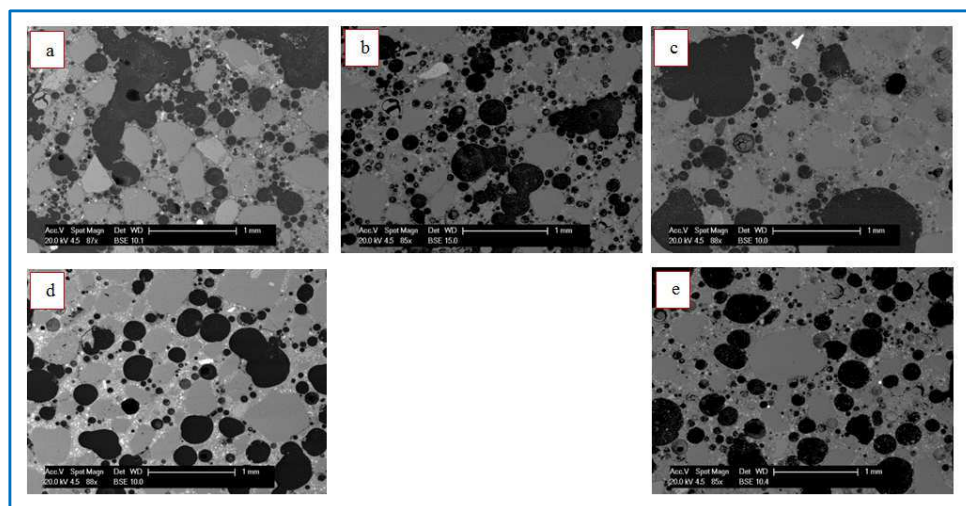
Figure 4-37 SEM images for the selected median density mixes (a) FC6 (b) FCs6 (c) FCf6 (d) FCp6 and (e) FCa6

Table 4-4 Parameters of pores sizes and circularity of selected foamed concrete mixes

Parameter Mixes	O_{50} (µm)	O_{90} (µm)	F_{circ50}	F_{circ10}
FC3	180	750	0.53	0.25
FC6	175	650	0.59	0.29
FC9	165	525	0.65	0.35
FCa3	125	465	0.57	0.31
FCa6	120	385	0.63	0.37
FCa9	95	315	0.69	0.41
FCs6	160	565	0.58	0.30
FCf6	165	510	0.53	0.27
FCp6	165	500	0.61	0.31
FCL6	125	350	0.63	0.32
FCLa6	115	300	0.66	0.35

4.5 Dry Density vs Voids Structure Parameters

The influence of dry density on the equivalent air-void diameter for both FC and FCa mixes is shown in **Figure 4-38**. From this graph, it can be seen that the voids are smaller in the most dense mixes. Both the median and 90th percentile void diameter decrease with increasing dry density. However, there is a noticeable decrease with O_{90} indicating that the void merging (irregular voids) reduces with increase in dry density. In addition, using additives helps in decreasing both O_{50} and O_{90} compared to those of FC mixes with the same density. This is attributed to the uniform distribution of bubbles with less merging and overlapping in mixes containing additives.

The variation of circularity factors with dry density is shown in **Figure 4-39** for all FC and FCa mixes. Compared to air-void structures of FC mixes, those of FCa mixes exhibit more uniform void shape. This is for the same reasons mentioned above.
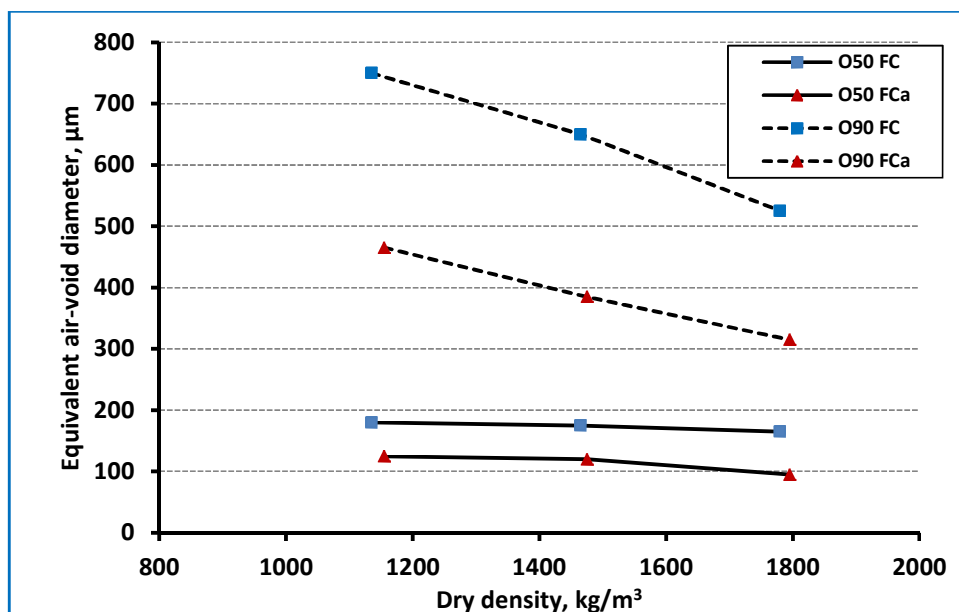
Figure 4-38 Effect of dry density on the size parameters
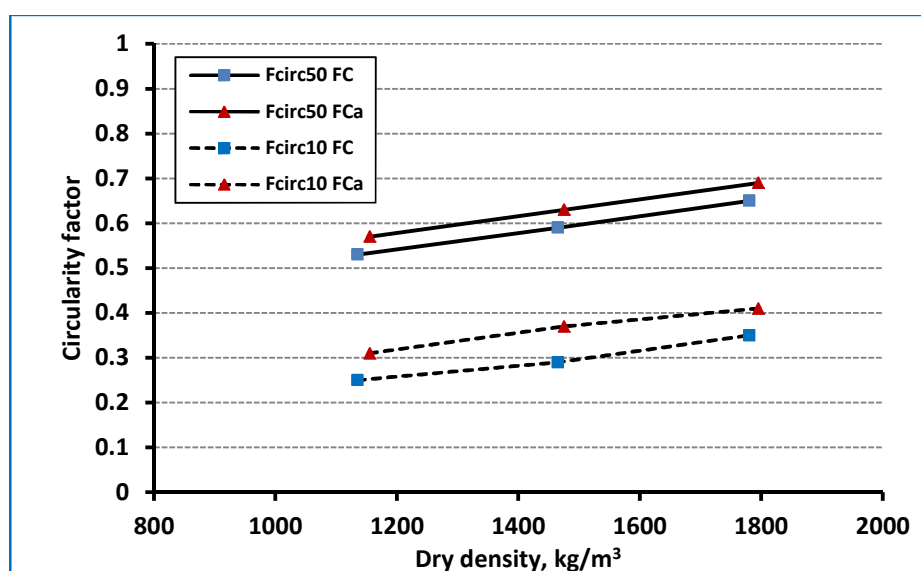
Figure 4-39 Effect of dry density on the shape parameters

4.6 Summary

This chapter has presented the experimental work that was carried out to characterise the air-void structure of foamed concrete mixes in terms of the porosity (voids content), void size distribution, void shape and the connectivity of voids. Eleven different mixes were investigated with varying density (nominally 1300, 1600 and 1900 kg/m³) with and without additives (silica fume, fly ash and

superplasticizer), used either individually or together, as well as with lightweight aggregate.

Different measurement [apparent, total vacuum saturation, mercury intrusion porosimetry (MIP), optical microscope (OM) and scanning electron microscopy (SEM)] and calculation [Hoff and Zheng equations] methods were adopted to determine the porosity and a comparison between them was done. On the basis of the measured results, the most appropriate test to obtain a relatively accurate porosity for foamed concrete (conventional, with additives and with LWA) is the vacuum saturation method. Theoretically, it has been determined that the equation derived by Zheng can be used to predict the porosity of foamed concrete mixtures. In addition, to characterize the air-void structure of mixes and investigate the effect of additives on it, this study aimed to investigate the formation of voids during mixing. An investigation of the bubble size distribution of foam (before adding to the mixture) and the pore size distribution of the foamed concrete mixes (after hardening) was presented. In order to investigate the foam structure before adding to the mix, it was found that by treating the foam with bitumen emulsion, a clear image of its structure can be captured using an optical microscope. Using this technique, a significant difference was found between the size distribution of foam bubbles and those of air pores within foamed concrete mixes.

For all mixes, higher foam volume (nominally 1300 kg/m^3) resulted in a greater degree of void merging, leading to large irregular voids which resulted in a wide distribution of void sizes. However, it was found that the effect of additives (both individually and in combination) was significant. For a given density, although the additives in combination led to increased void numbers, both void size and connectivity were reduced by preventing their merging and this resulted in a narrow void size distribution. From circularity factor results, the evidence for bubble merging is higher with increased added foam volume (decreased density).

Chapter 5: Mechanical and Thermal Properties

5.1 General

As mentioned previously, the ultimate aim of this investigation is to push back the limits of foamed concrete achieving strengths suitable for semi-structural or structural purposes but with enhanced strength/weight ratio and excellent thermal properties. Therefore, the mechanical and thermal properties of foamed concrete are discussed in this chapter. The mechanical properties discussed include compressive strength, tensile (flexural and splitting) strength and modulus of elasticity (static and dynamic), while the thermal properties include thermal conductivity and heat capacity. In addition, the properties of the foamed concrete mixes in this study are compared to normal weight, lightweight and foamed concretes produced in other studies. Moreover, the effect of additives and void structure characterisation on the strength and thermal properties is investigated. Finally, a summary is presented at the end of the chapter.

5.2 Mechanical Properties

5.2.1 Compressive Strength

As explained in **Chapter 3**, to develop the selected foamed concrete mixes, superplasticizer, silica fume and fly ash at specified ratios were added as a proportion of the mixture. To identify the effect of additives, individually or together, on the strength, a preliminary experimental programme was carried out at the lowest material density (nominally 1300 kg/m^3), see **Table 3-1**. The results are shown in **Figure 5-1**, where it may be seen that adding silica fume (FC3s) or fly ash (FC3f) individually improved the 28-day compressive strength by about 10% and 60% respectively. In addition, the use of superplasticizer (FC3p) improved the compressive strength by 115% (at 28 days); this increased to 125% with a combination of silica fume and superplasticizer (FC3s+p). Further addition of fly

ash (FCa3) achieved a large increase in strength (215%) making even this lightest mix potentially suitable for structural purposes.
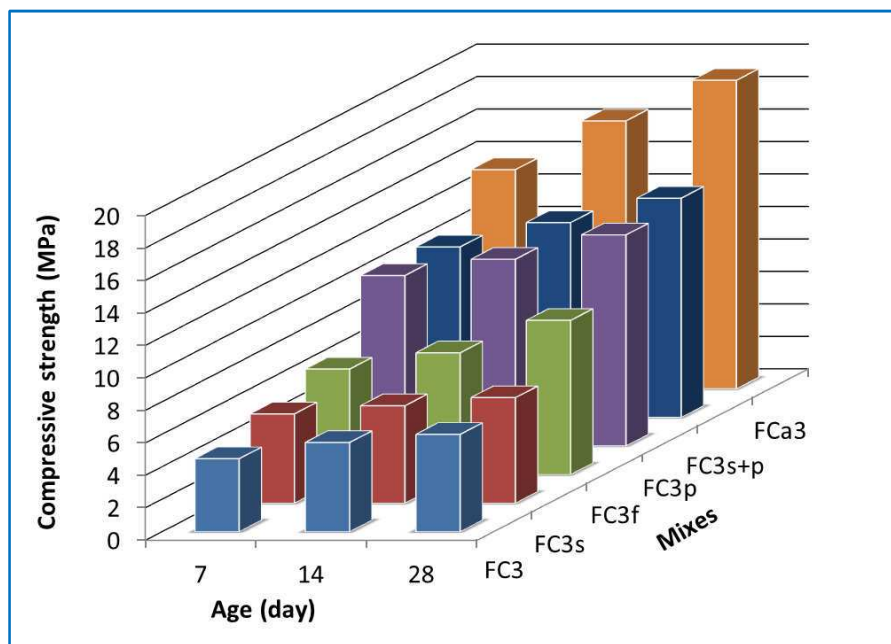
Figure 5-1 Effect of used additives on the compressive strength of 1300 kg/m³ mix

Compressive strength testing was carried out on 100 mm cubes in accordance with BS EN 12390-3 (2002) and in each case the results quoted are the average of three specimens. As expected (Jones and McCarthy, 2005, Nambiar and Ramamurthy, 2006), the compressive strength of foamed concrete decreases dramatically with a reduction in density, as shown in **Figure 5-2**. As illustrated in **Figure 5-3**, the use of additives (silica fume SF, fly ash FA and superplasticizer) greatly improves compressive strength development at all test ages. This is because of the reduction in water content due to use of a superplasticizer and the pozzolanic characteristics of both SF and FA, leading to an improved aggregate-matrix bond associated with the formation of a less porous interfacial zone and a better interlock between the paste and the aggregate (Toutanji and El-Korchi, 1995), (see **Figure 5-4a, b**). In addition, using FA as filler may help in achieving more uniform distribution of air-voids by providing uniform coating on each bubble

thereby preventing merging of bubbles, leading to an increase in strength (Jitchaiyaphum et al., 2011, Ramamurthy et al., 2009), (**Figure 5-4c, d**).

In general, it is reported that foamed concrete with fly ash as filler has a higher strength to density ratio for all densities (Nambiar and Ramamurthy, 2006). A comparison of strength to density ratios between FC and FCa mixes, at 28 days, with foamed concrete mixes from the literature (Jones and McCarthy, 2005, Nambiar and Ramamurthy, 2006, Pan et al., 2007) is shown in **Figure 5-5**. Based on this comparison, it would appear that the FCa mixes showed higher strength to density ratios than any of the foamed concrete mixes in other studies produced by using sand and/or fly ash as a filler material. Overall, except for mixes FC3 and FC6, the results suggest that the remaining mixes are all potentially suitable for use as a lightweight concrete for semi-structural or structural purposes since their densities of not exceed 2000 kg/m^3 and their 28-day compressive strengths are in excess of 17 MPa (Kosmatka et al., 2002, Neville, 2011).

It has been found that the use of lightweight aggregate (LWA) in combination with artificially introduced air void in the mortar matrix (lightweight aggregate foamed concrete) to be advantageous (Weigler and Karl, 1980). Weigler and Karl mentioned that with the inclusion of foam it was possible to attain dry density ranging from 700 to 1200 kg/m^3 with compressive strengths of 5 to 30 MPa using LWA with a particle density between 600 and 900 kg/m^3. In a further study of lightweight aggregate foamed concrete, compressive strengths of 6.4 and 15 MPa were obtained for densities of 842 and 1133 kg/m^3, respectively, by combining a foamed cement matrix with LWA (Regan and Arasteh, 1990). In this study, it was found that the 28-day compressive strength of foamed concrete mix with LWA (FCL6) was 22.5 MPa, and it was 36.5 MPa for FCLa6 (with additives in combination). Comparing these values with those of FC6 (15 MPa) and FCa6 (33.5 MPa), it can be seen that adding LWA helped to increase the compressive strength (Kayali, 2008) by

enhancing the ITZ between the cement paste and LWA (Zhang and Gjørv, 1990) and reducing the volume of added foam, which replaces the air pores in the LWA to gain similar density.
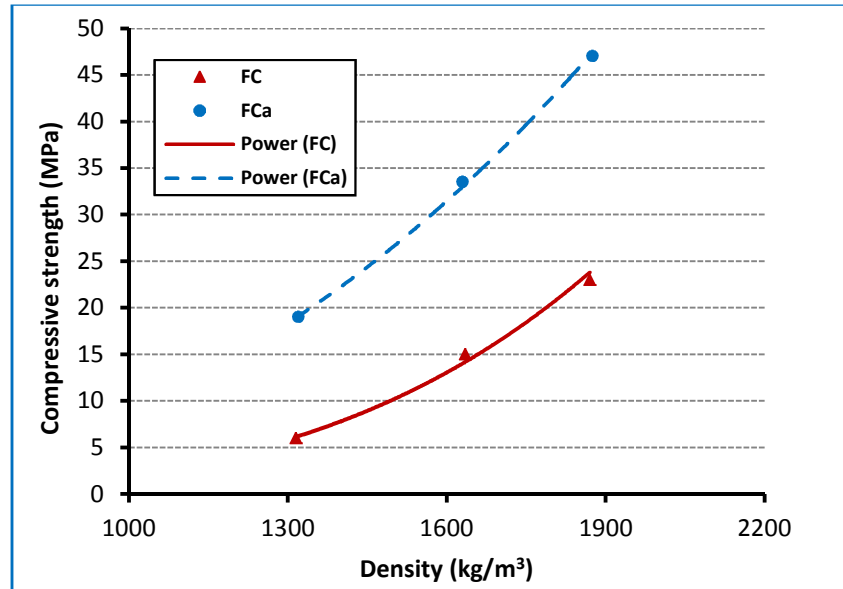
Figure 5-2 28 day compressive strength density variation for FC and FCa mixes
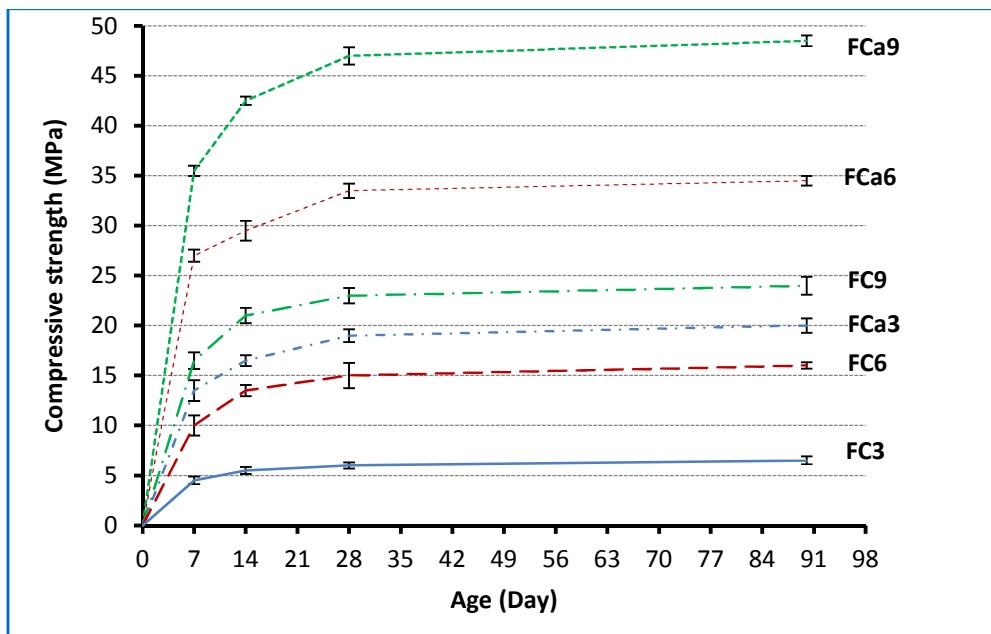
Figure 5-3 Development of 100mm cube sealed-cured compressive strength
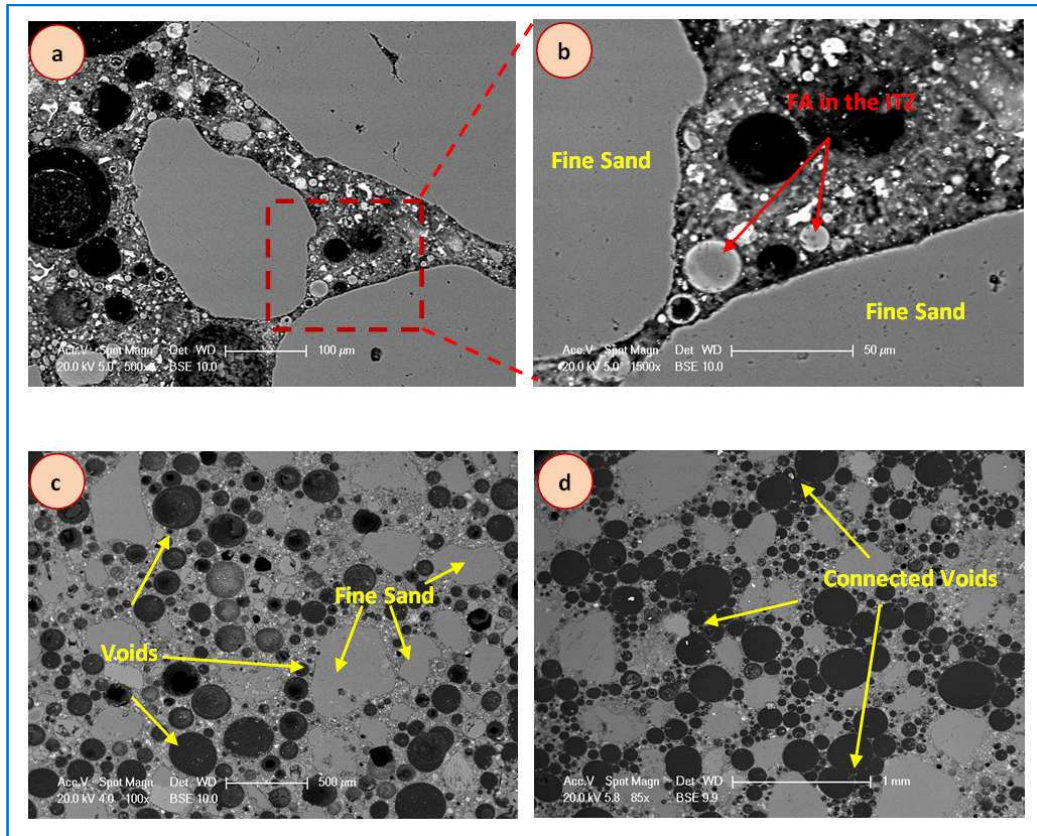
Figure 5-4 Scanning Electron Microscopy images of 1300 kg/m³ foamed concrete (a, b and c) with additives (FCa3), (d) conventional
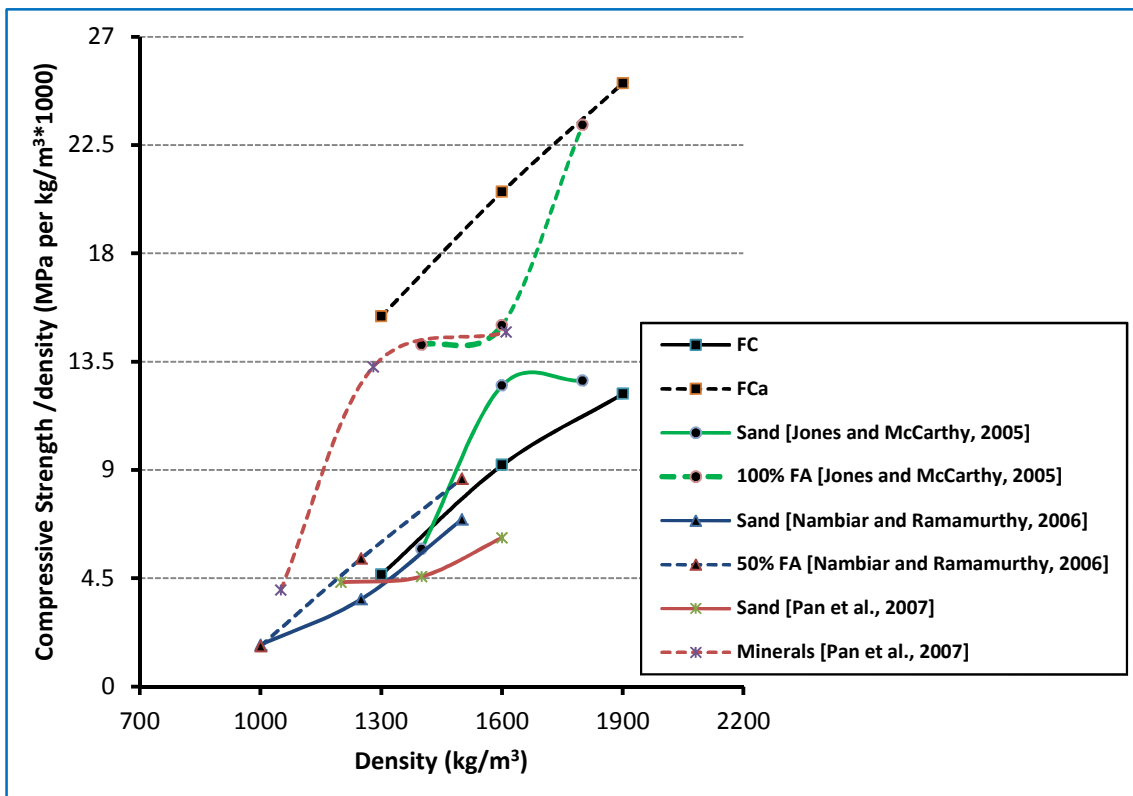
Figure 5-5 Strength to density ratios for different foamed concrete mixes

5.2.2 Tensile (Flexural and Splitting) Strength

The structural properties of concrete such as shear resistance, bond strength and resistance to cracking depend on the tensile strength; the higher the tensile strength the better the structural properties (Babu, 2008). Flexural strength testing (three-point loading) was conducted on two 100×100×500 mm prisms at ages of 7,14 and 28 days to determine the modulus of rupture (f_r) in accordance with BS EN 12390-5 (2000). Splitting tensile strength (f_{sp}) testing was also undertaken, in accordance with BS1881-117 (1983) and in each case the mean of three tested values at each test age was recorded. The averaged values of f_r and f_{sp} are summarized in **Table 5-1**. Those at 28 days are compared with corresponding 28-day compressive strengths in **Figure 5-6** and **Figure 5-7**, respectively. Note that in **Figure 5-6** the FC, LWC and NWC graphs were plotted from equations $f_r=0.31(f'_c)^{0.83}$, $f_r=0.46(f'_c)^{2/3}$ and $f_r=0.438(f'_c)^{2/3}$ respectively (Babu, 2008, Fédération internationale de la précontrainte, 1983, Ahmad and Shah, 1985), and that in **Figure 5-7** the LWC and NWC graphs were plotted from equations $f_{sp}=0.28(f'_c)^{0.69}$ and $f_{sp}=0.2(f_c)^{0.7}$ respectively (Babu, 2008, Oluokun, 1991). It can be seen from the two figures that, for a given 28-day compressive strength, the conventional mixes (FC) produced higher indirect tensile strengths, flexural and splitting, than those with additives (FCa). The reason for this may be the improved shear capacity between the sand particles and the paste phase (Jones and McCarthy, 2005) noting that, for a given density, the sand content is lower in the mixes with additives (FCa). However, f_{sp}/f_{cu} ratios for both FC and FCa mixes were slightly higher than those reported in the reviewed studies, while, the tensile (f_r or f_{sp})/compressive strength (f_{cu}) ratios of both FC and FCa mixes were slightly lower than those investigated by Babu (2008), probably because of the presence of lightweight aggregate in these mixes which may lead to improved tensile strength. As illustrated in **Figure 5-8**, at an age of 28 days, f_r values of about 16-23 % and 11-15 % of f_{cu} were observed for FC and

FCa mixes respectively, while the ranges for f_{sp} were about 10-14 % and 7-9 % of f_{cu}.

The same observation of enhancing the compressive strength by adding LWA was noticed in terms of flexural and splitting strengths compared to mixes of similar density but without LWA, namely FC6 and FCa6, see **Table 5-1**.

Table 5-1 Flexural strength and prism splitting tensile strength results

Mixes	Test Age (day)								
	7			**14**			**28**		
	Density (kg/m³)	f_r **(MPa)**	f_{sp} **(MPa)**	**Density (kg/m³)**	f_r **(MPa)**	f_{sp} **(MPa)**	**Density (kg/m³)**	f_r **(MPa)**	f_{sp} **(MPa)**
FC3	1280	1.2 (0.06)	0.65 (0.05)	1295	1.3 (0.05)	0.75 (0.06)	1285	1.4 (0.03)	0.85 (0.01)
FCa3	1320	2.1 (0.17)	0.85 (0.06)	1323	2.6 (0.06)	1.35 (0.07)	1316	2.8 (0.02)	1.65 (0.05)
FC6	1615	2.3 (0.05)	0.9 (0.02)	1620	2.7 (0.01)	1.5 (0.04)	1625	2.9 (0.04)	1.8 (0.08)
FCa6	1605	3.4 (0.09)	1.7 (0.80)	1620	3.8 (0.05)	2.35 (0.09)	1630	4.1 (0.14)	2.65 (0.09)
FC9	1870	2.9 (0.08)	1.5 (0.04)	1880	3.2 (0.13)	2.15 (0.07)	1865	3.7 (0.07)	2.35 (0.05)
FCa9	1870	4.1 (0.34)	2.5 (0.07)	1875	4.5 (0.08)	3.1 (0.11)	1880	5.3 (0.21)	3.5 (0.06)
FCL6	-	-	-	-	-	-	1595	3.1 (0.39)	2.0 (0.18)
FCLa6	-	-	-	-	-	-	1610	4.2 (0.33)	2.75 (0.26)

() the standard divaition
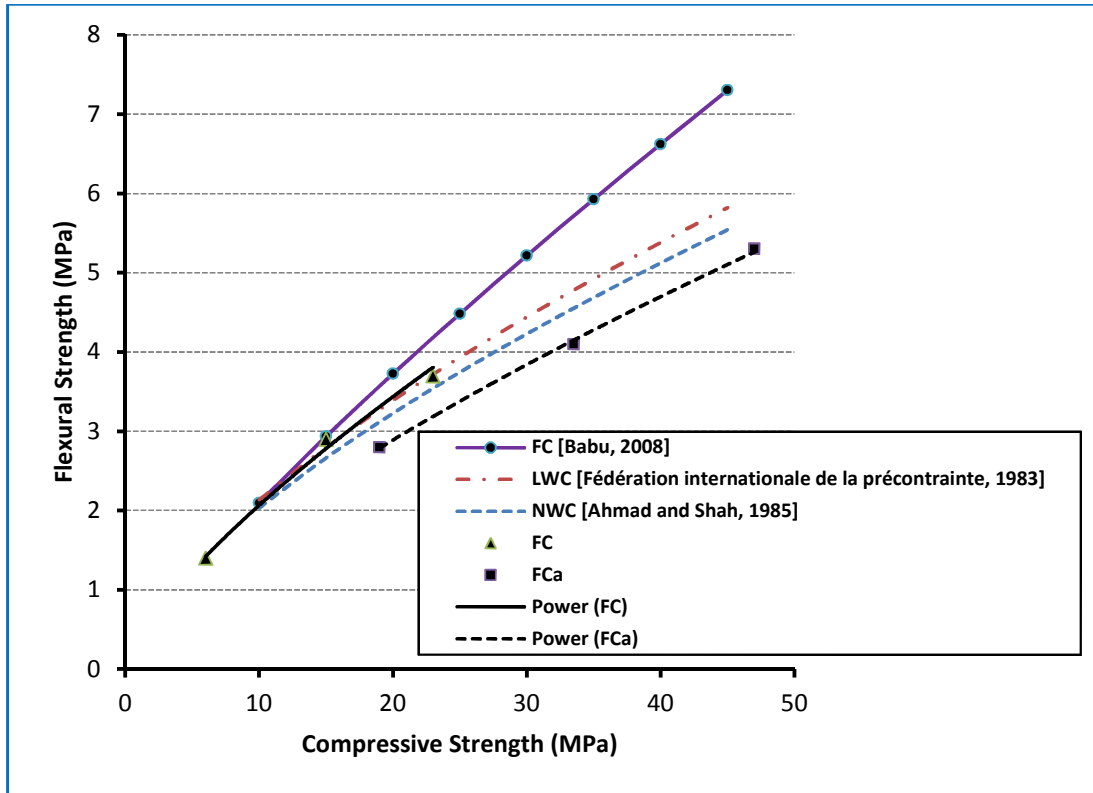
Figure 5-6 Relationship between flexural strength and 28 day compressive strength of foamed, LW and NW concretes
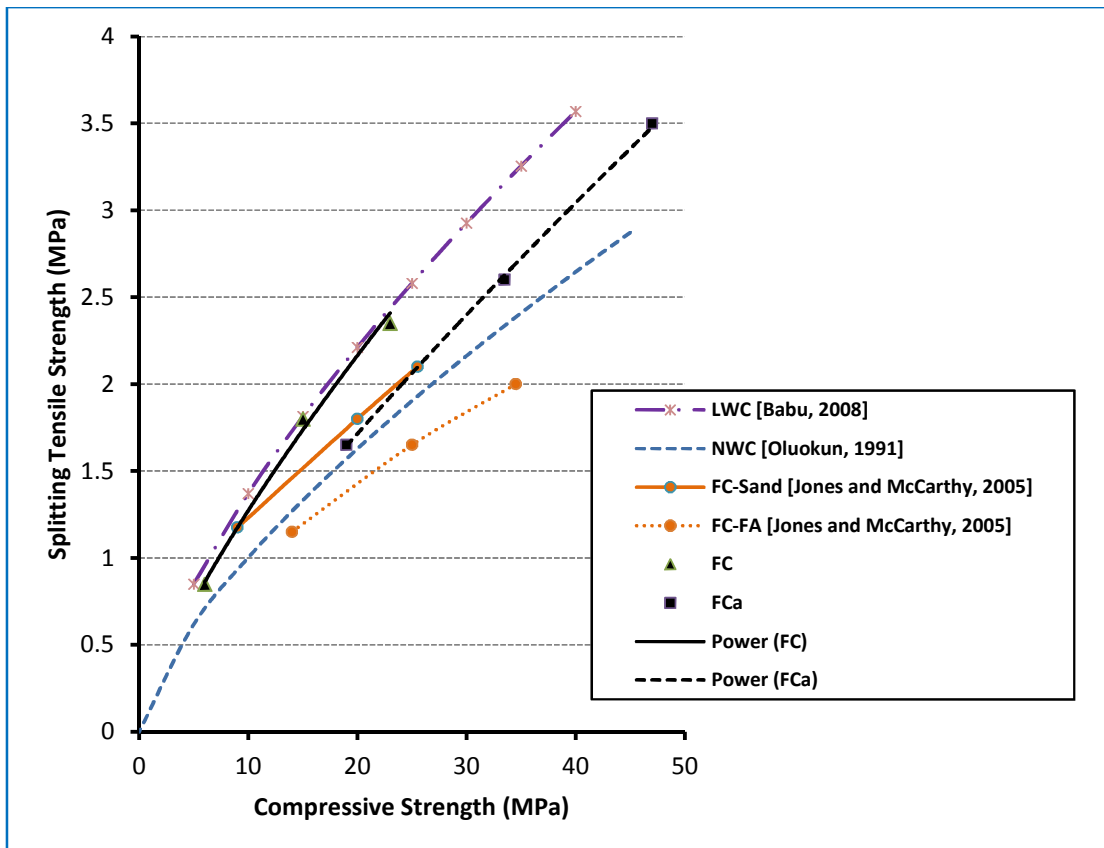
Figure 5-7 Relationship between splitting tensile strength and 28 day compressive strength of foamed, LW and NW concretes
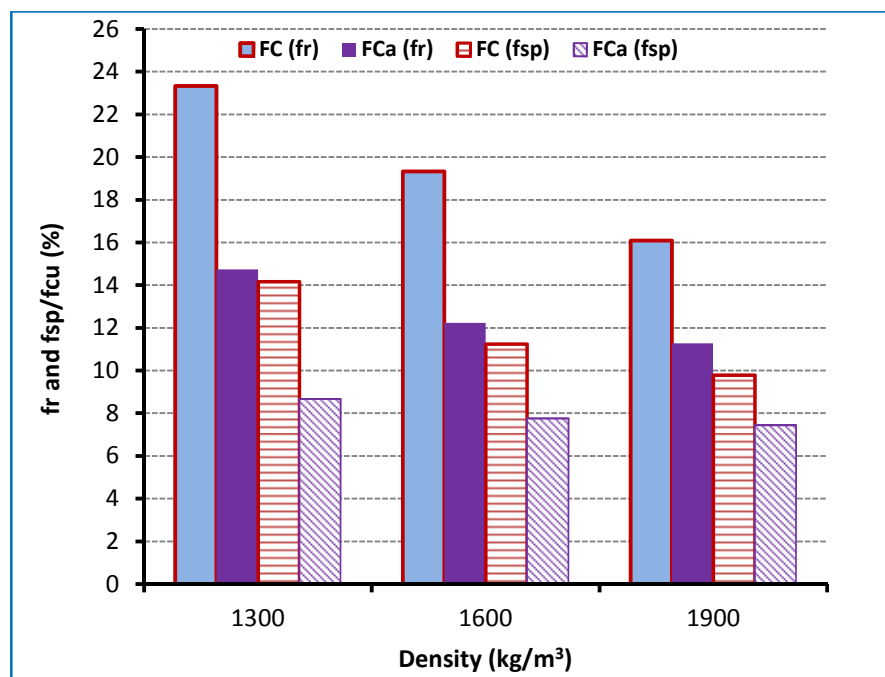
Figure 5-8 The ratios of tensile strength (f_r and f_{sp}) to compressive strength of the selected mixes at 28 day

5.2.3 Modulus of Elasticity

5.2.3.1 Static Modulus of Elasticity

The static modulus of elasticity (E_s) of the conventional mixes (FC) and mixes with additives in combination (FCa) was determined using 150 × 300 mm cylinder specimens. Two specimens were tested for each mix at an age of 28 days in accordance with BS 1881-121 (1983). Each specimen was fitted with four potentiometers at different quadrants to measure the axial deformation, see **Figure 5-9**. During the testing, all specimens were loaded in the form of cyclic loading as follows: after placing the test specimen in the machine, a basic stress σ_b of 0.5 MPa was applied and the strain gauge reading at each potentiometer was recorded. Then, the stress was increased steadily at a constant rate (0.5 MPa/s) until reaching one-third of the compressive strength, σ_a, (estimated from the 100mm cube strength assuming that the cylinder strength is about 0.8 times the cube strength (Neville, 2011)). After that, the stress was maintained for 60s before reducing the load at the same rate (0.5 MPa/s) to the level of the basic stress σ_b to finish the first

cycle. After completion of the second cycle and a waiting period of 60s under stress σ_b, the strain readings ε_b were recorded at the four potentiometers. Then, the specimen was reloaded to stress σ_a at the specified rate and the strain reading ε_a was averaged from the four readings. When the elasticity measurements were completed, the load was increased at the same rate to failure. This loading process is illustrated in **Figure 5-10**.

Es (in MPa) is given by (**Eq. 5-1**).

$$E_s = \frac{\Delta_\sigma}{\Delta_\epsilon} = \frac{\sigma_a - \sigma_b}{\epsilon_a - \epsilon_b} \tag{5-1}$$

where: σ_a is the upper loading stress (MPa), (σ_a=f'c/3);

σ_b is the basic stress (i.e. 0.5 MPa);

ε_a is the strain under σ_a;

ε_b is the strain under σ_b.

The relationships with corresponding 28-day sealed-cured cube compressive strengths are given in **Figure 5-11**. Note that the FC-FA, FC-Sand, LWC and NWC graphs were plotted from equations $E=0.99(f_{cu})^{0.67}$, $E=0.42(f_{cu})^{1.18}$, $E=1.7\times10^{-6}(\Upsilon)^2(f_{cu})^{0.33}$ and $E=11.71(f'_c)^{0.33}$-8.355, respectively (Jones and McCarthy, 2005, BS 8110, 1985, Rashid et al., 2002). It can be seen that for a given compressive strength, the FCa mixes exhibited lower Es values than the FC mixes, while Es for NWC was higher than for both FC and FCa. The same behaviour was observed by Jones and McCarthy (2005) leading then to conclude that a direct substitution of foamed concrete for the same compressive strength grade of normal concrete will not in reality give similar structural performance.

Due to the internal curing of LWA, the ITZ with the surrounding cement paste may be enhanced by an increased degree of cement hydration (Zhang and Gjørv, 1990), also see **Section (2.4.6)**. Therefore, mixes with LWA (FCL6 and FCLa6) develop

a smaller amount of cracking compared to FC6 and FCa6, respectively. However, the ascending part of the stress-strain curve for mixes with LWA is not steeper and linear up to a higher proportion of the ultimate strength making these mixes more ductile than those without LWA, with a higher strain and a higher static modulus of elasticity, 11.4 GN/m^2 for FCL6 and 12.9 GN/m^2 for FCLa6.

Figure 5-9 Elastic modulus test set up
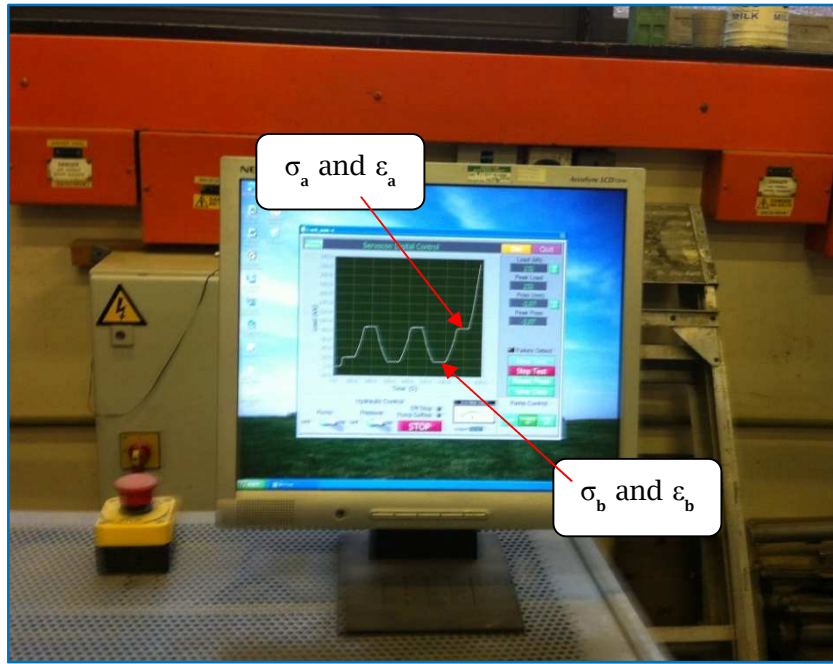
Figure 5-10 Load-time realtionship during static modulus test
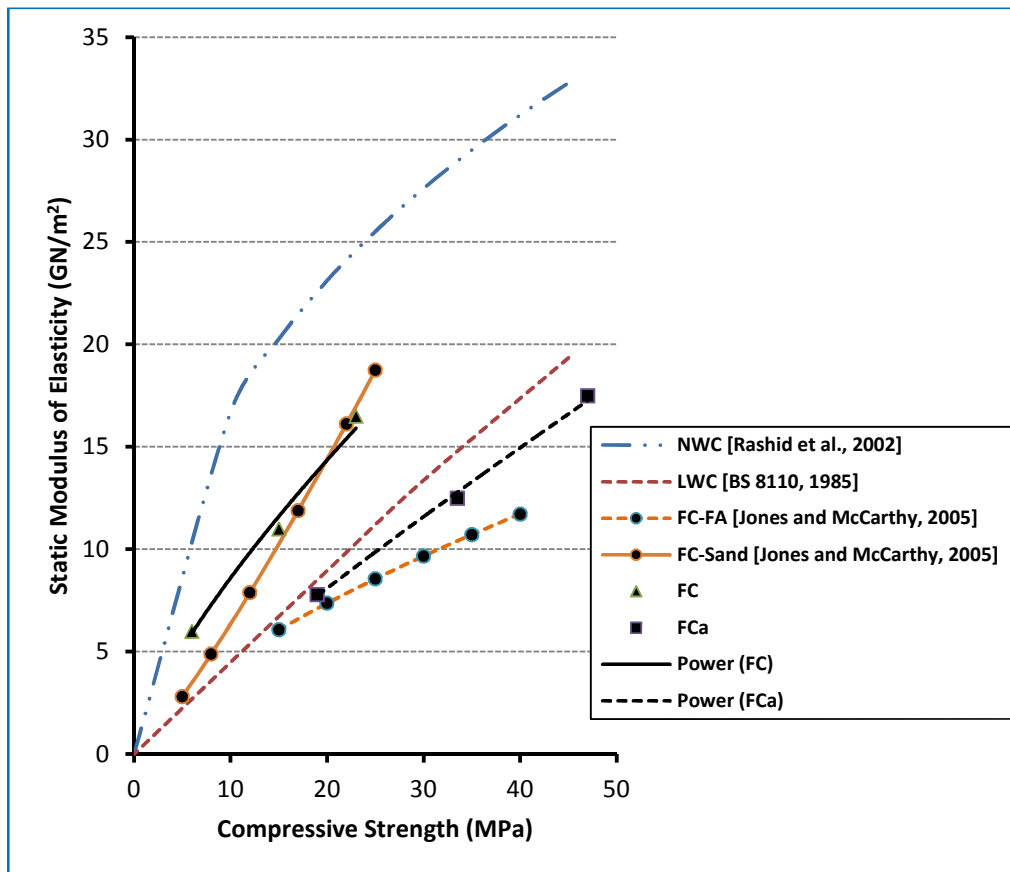
Figure 5-11 Relationship between E-values and 28 day compressive strength of foamed, LWC and NWC concretes

5.2.3.2 Dynamic Modulus of Elasticity

The dynamic modulus of elasticity E_d was measured using a CNS Farnell PUNDIT, Portable Ultrasonic Non-destructive Digital Indicating Tester, on sealed-cured (wrapped in cling film) 100 mm cube samples at 28 days old, and the average of three samples was recorded. The E_d defines as the ratio of the stress to that part of the strain corresponding to elastic deformation only. It here refers to the initial tangent of the non-linear stress/strain relationship for the concrete. It is normally greater than the static modulus of elasticity and is commonly used for comparative testing to examine different types of concrete in the laboratory. The E_d (in GN/m²) for each specimen was calculated from the formula:

$$E_d = \frac{(1 + v)(1 - 2v)}{(1 - v)} \cdot \left(\frac{\gamma}{g}\right) \cdot v^2 \qquad (5\text{-}2)$$

where v is Poisson's ratio and (γ/g) is mass density of the material.

The relationships between the static (E_s) and dynamic (E_d) moduli of elasticity for both FC and FCa mixes are shown in **Figure 5-12**. In this study (as in many others), the E_d appears higher than the E_s in all selected mixes. This is usually ascribed to the use of a 100% non-destructive approach for determining E_d which provides very small applied stress and hence there is neither micro crack formation nor creep during the test (Najim and Hall, 2012).
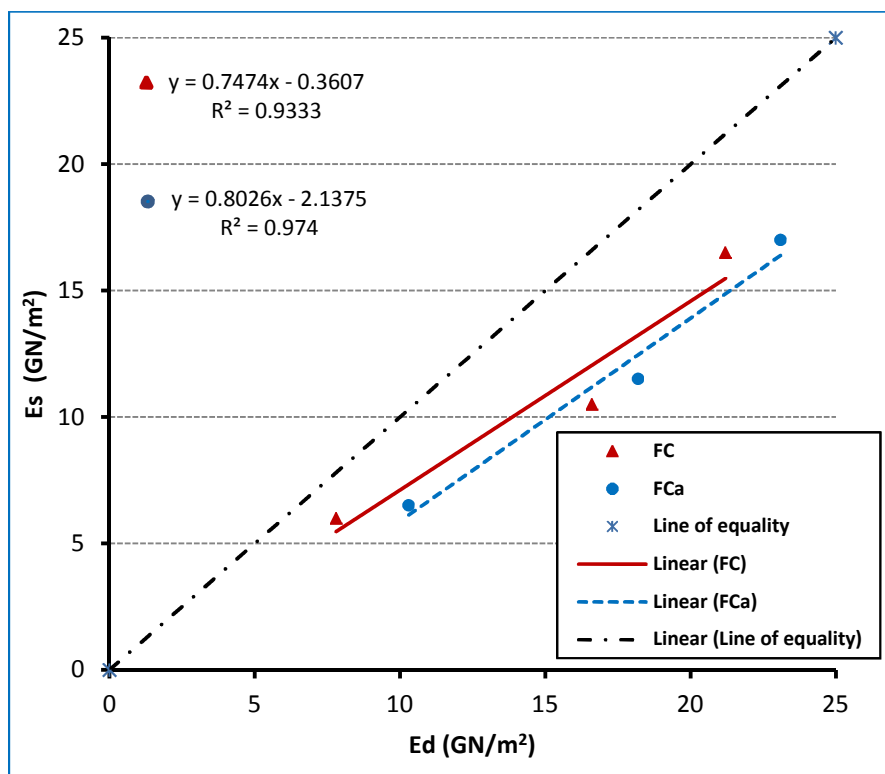
Figure 5-12 Relationship between static and dynamic modulus of elasticity at 28 days of foamed concrete mixes

5.3 Effect of Voids Structure Characterisation on Strength

Foamed concrete is a porous material; therefore its pore structure plays a dominant role in controlling its properties.

Figure 5-13 shows the effect of void size distribution parameters on compressive strength of FC and FCa mixes. Meanwhile, **Figure 5-14** illustrates the effect of these parameters on compressive strength of 1600 kg/m³ mixes. It can be seen that for all mixes, higher foam volume (FC3 and FCa3) resulted in a greater degree of void merging, see **Figure 4-34**, leading to larger irregular voids which resulted in a wider distribution of void sizes and lower strength. In addition, a reduction in O_{50} and O_{90} is clearly linked to an increase in strength for each density implying that the effect of additives (both individually and in combination) was significant. However, it is known that changes to the cement paste microstructure due to additives, **Figure 5-15** and **Figure 5-16**, will also contribute to strength gain. It was found that the

paste porosities (capillary and gel pores) calculating from the BSE images (**Figure 5-16**) using ImageJ software were 12.6%, 12.1%, 13.2%, 11.3%, 10.5% for FC6, FCs6, FCf6, FCp6 and FCa6, respectively. Therefore for a given density, the questions are these; does this strength improvement come from the enhancement of void structure or the paste microstructure improvement due to additives and to what extent does each affect the strength?

To answer the above questions, the compressive strengths of unfoamed mixes were investigated and compared to those of foamed concrete, see **Figure 5-17**. It is evident that the compressive strengths of the most dense unfoamed mixes (FC9 and FCa9) are higher than unfoamed FC3 and FCa3 mixes. The reason is the higher aggregate/binder ratio (agg/b) in the FC9 and FCa9 which may lead to reduced damage in the interfacial transition zone (ITZ) between the aggregate and cement paste by reducing shrinkage and bleeding. In addition, with high a/b ratio the cement paste would be less, resulting in, on the one hand, reduced thermal changes from hydration of cement and, on the other hand, a smaller voids fraction and so less adverse effect on strength (Neville, 2011). In addition, some water may be absorbed by a larger amount of aggregate in FC9 and FCa9 leading to reduce the effective w/b ratio. Neville (2011) also stated that strength of a mix decreases as the proportion of aggregate increases from 0 to 20% but it increases for aggregate proportions from 40% to 80%. He added that the same behaviour was noticed at different w/c ratios but the reason for this pattern of behaviour is not clear.

Similar strength increases is seen in the foamed concrete mixes FC9 and FCa9 being stronger than the comparable FC3/6 and FCa3/a6 mixes, although the rate of strength increases with density appears somewhat greater for foamed version compared to unfoamed version.

It can be seen from **Figure 5-17** that inclusion of additives (individually or in combination) helps to improve the strength of both unfoamed and foamed mixes.

This is due to the additional reduction in porosity of cement paste and an improved interface between it and the aggregate by:

- A substantial reduction in the mixing water (using a superplastisizer);
- Forming calcium silicate hydrate (C-S-H) from a pozzolanic reaction of fly ash with the lime produced from the hydration of cement and water;
- Acting as fine filler (silica fume).

From **Figure 5-15** it can be seen that the microstructure of FCa mix is more homogenous than that of FC mix due to the physical and chemical contribution of the additives (SF and FA) as well as being less porous owing to reduced w/c ratio with the addition of a superplasticizer. This improved matrix microstructure can also be deduced from the difference between the vacuum saturation porosity (entrained air voids and capillary voids) and the entrained (> 20μm) void content calculated from analysis of optical microscopy images. It was found that the capillary porosity of FCa is less than that of FC at all investigated densities. Secondly, micro-hardness values of the ITZ at 30μm distance from the aggregate surface (five readings averaged from a Vickers micro-hardness test, square base pyramid indenter, with test load 10g and contact time 15s) were 39.66, 59.3 and 91.13 HV for FC3, FC6 and FC9 respectively while for FCa3, FCa6 and FCa9 they were 54.83, 85.56 and 111.43, respectively (1 HV=1 kgf/cm^3=0.09806650 MPa).

The compressive strength reduction from unfoamed and foamed concrete for each mix is shown in **Figure 5-18**. It can be seen that this reduction decreases with increase in density for both FC and FCa mixes. For the same density, the reduction was lower in the case of FCa indicating that the void structure improvement helped in increasing the strength. This is also evident from the results for individual additives (silica fume, fly ash and superplastisizer) at the same density (1600

kg/m³). However, this is not the case in terms of FCL6 and FCLa6 since adding LWA reduced the strength of their unfoamed mixes compared to FC6 and FCa6 mixes.

A similar interpretation can be made from **Figure 5-19** which illustrates the reduction for both unfoamed and foamed concretes between a mix with additives (individual or in combination) and a conventional mix. The difference between values of unfoamed and foamed concrete reductions implies that not only the enhancement of cement paste microstructure but also improvements in the void structure of foamed concrete both will contribute to strength gain. In addition, the effect of each variable, i.e. unfoamed strength (changes to cement paste microstructure) and void size parameters (O_{50} and O_{90}), were examined from a statistical point of view using the Chi Squared Test which is the sum of the squared difference between observed and expected data divided by the expected data. With a degree of freedom equal to 8 (the number of all categories minus 1) and a probability value α=0.1 (which means that there is a 10% probability that any deviation from expected results is due to change), the value of χ^2 equals 13.362. It was found that the greatest effect was for O_{90} (with a power relation with compressive strength, χ^2=6.535) followed by unfoamed strength (with a linear relation with foamed concrete strength, χ^2=10.933). Meanwhile, with a power relationship, χ^2=16.841, O_{50} does not have any significant effect on the strength of the investigated foamed concrete. These relationships are shown in **Figure 5-20** which demonstrates that O_{90} correlates better than O_{50} with strength of foamed concrete implying that it is the larger pores that influence the strength. Similar behaviour was noticed by Nambiar and Ramamurthy (2007a).
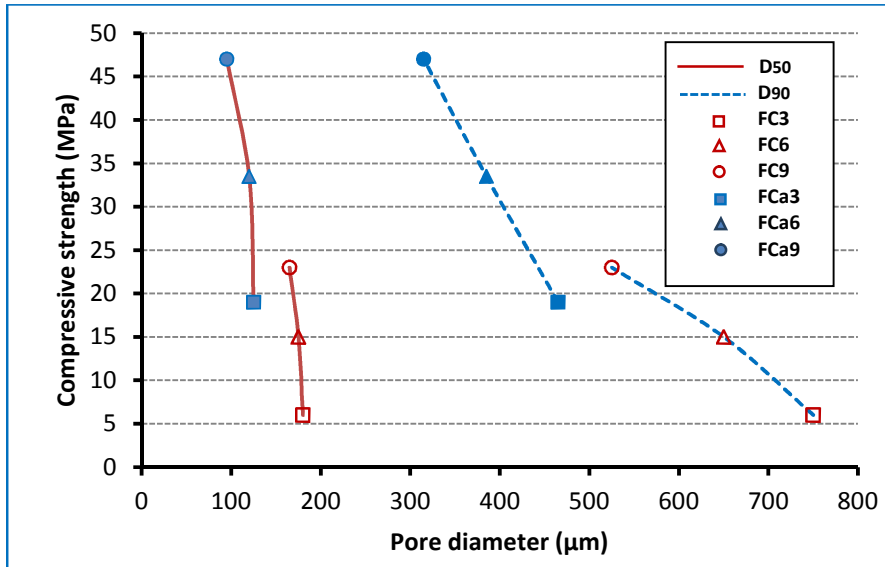
Figure 5-13 Compressive strength versus void size distribution parameters
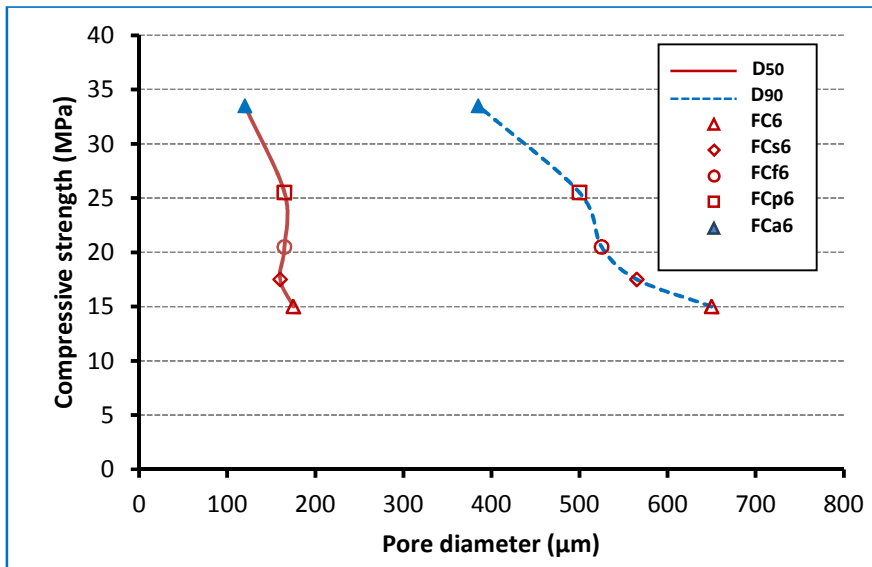
Figure 5-14 Compressive strength versus void size distribution parameters of 1600 kg/m^3 mixes
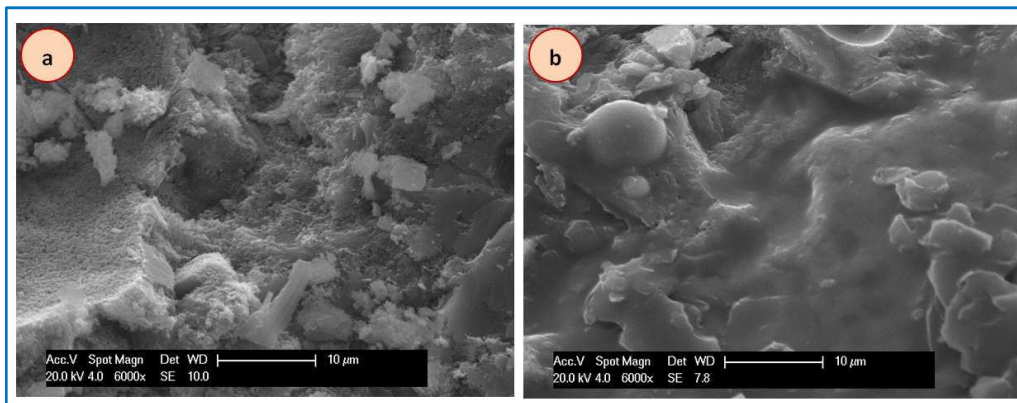
Figure 5-15 Microstructure of two 1600 kg/m^3 foamed concretes (a) Conventional, FC6 (b) with additives, FCa6
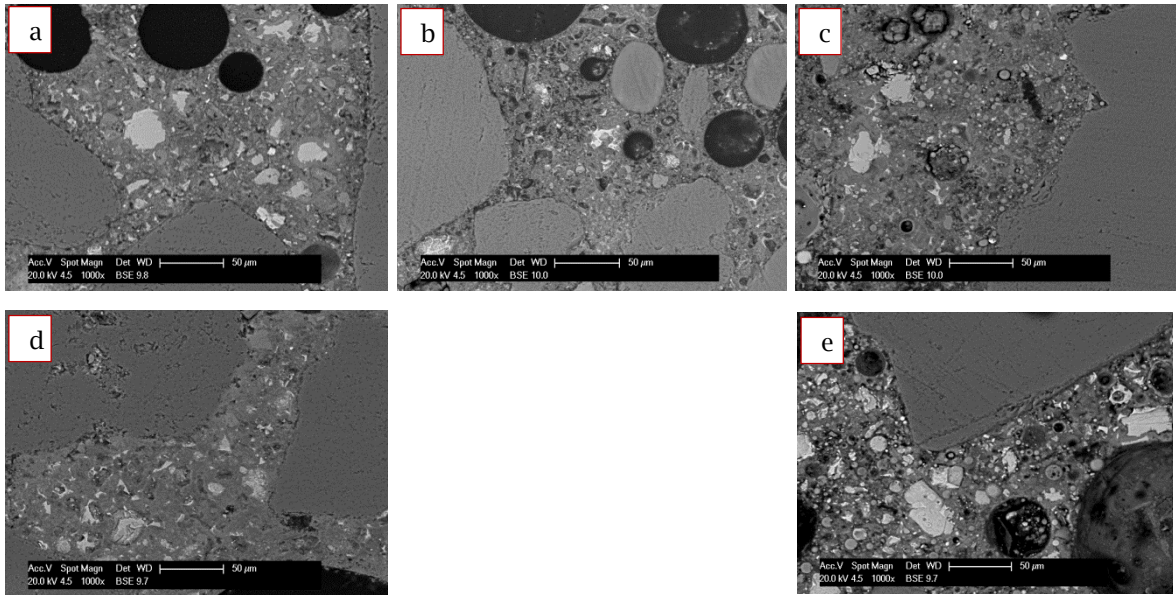
Figure 5-16 Effect of additives on the cement paste microstructure (a) FC6 (b) FCs6 (c) FCf6 (d) FCp6 and (e) FCa6
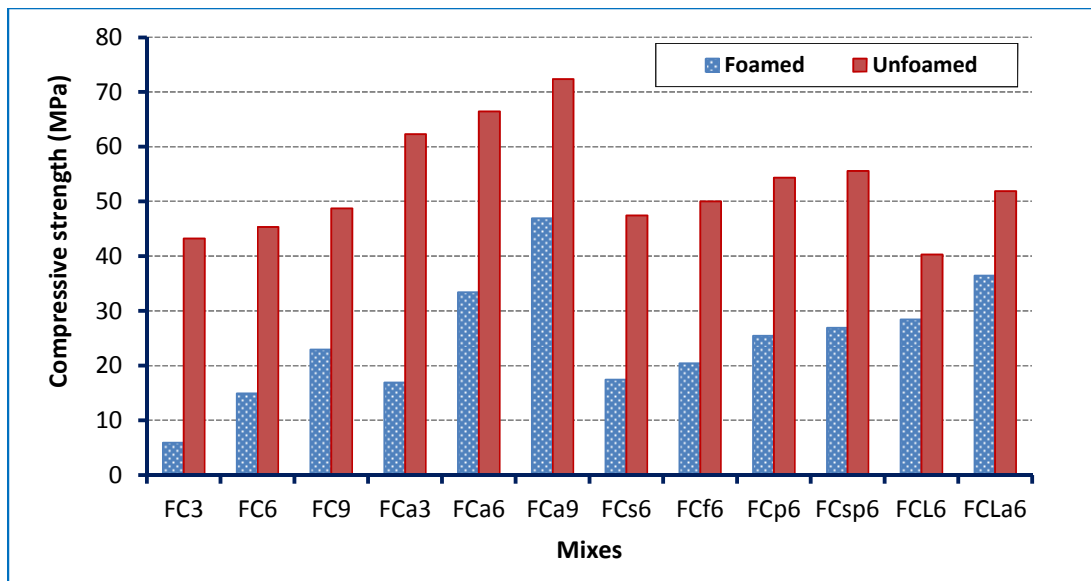
Figure 5-17 28-day Compressive strength of unfoamed and foamed concrete mixes
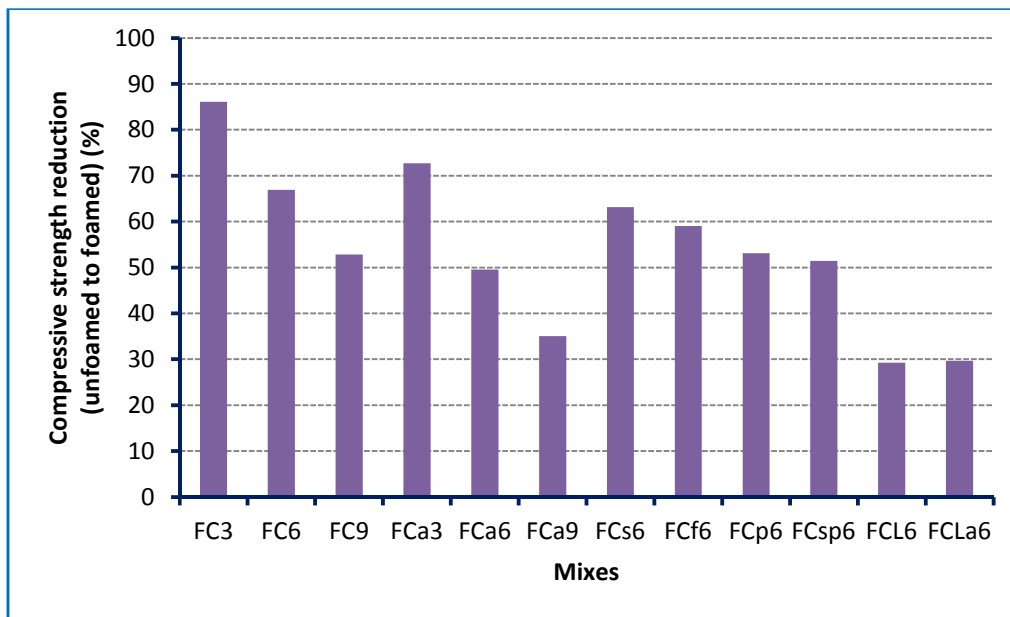
Figure 5-18 Compressive strength reduction (%) of unfoamed to foamed concrete for the same mix
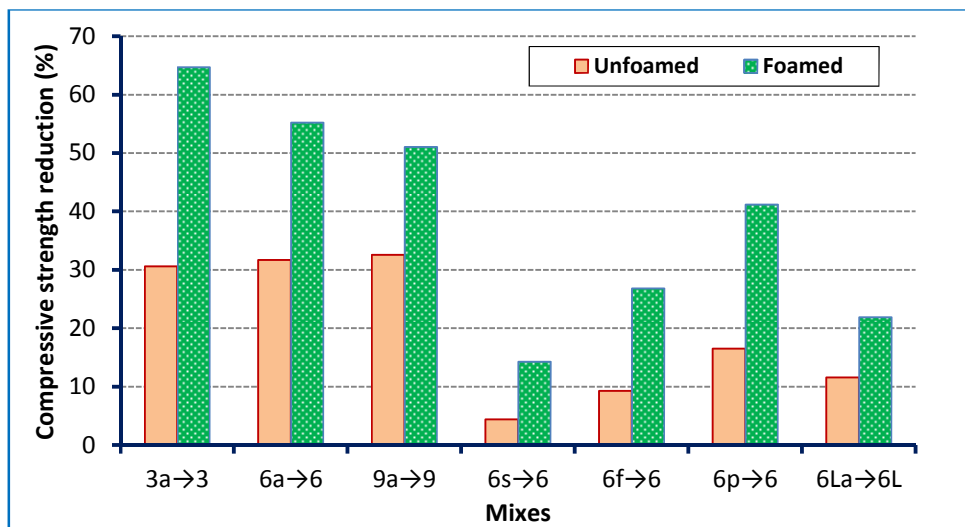
Figure 5-19 Compressive strength reduction (%) of unfoamed and foamed concrete mixes (from with additives to conventional)
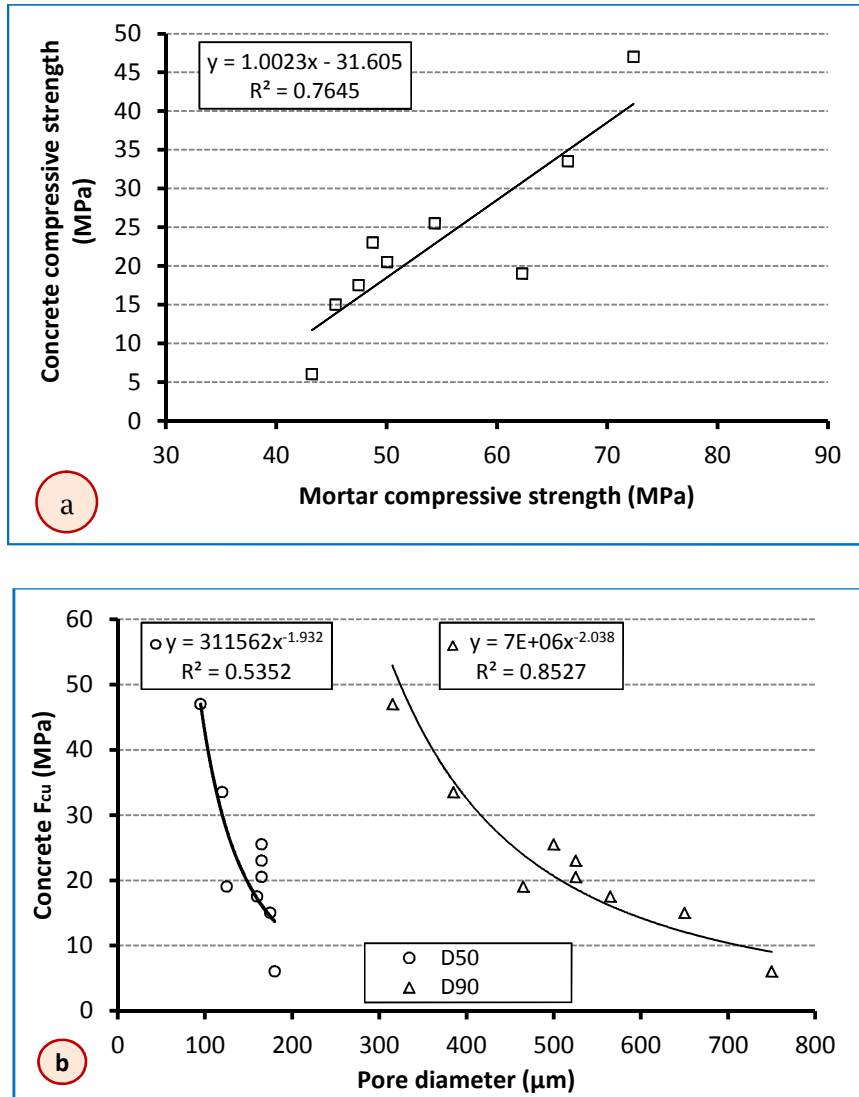
Figure 5-20 (a) unfoamed strength and (b) pore size parameters versus foamed concrete strength for all investigated mixes

5.4 Thermal Properties

Heat can be defined as "the form of energy that can be transferred from one system to another as a result of temperature difference". Heat always transfers from the higher to lower temperature medium in three different modes (Cengel, 2002), see **Figure 5-21**:

- **Conduction**: is "the transfer of energy from the more energetic particles of a substance to the adjacent less energetic ones as a result of interactions between the particles".

- **Convection**: is "the mode of energy transfer between a solid surface and the adjacent liquid or gas that is in motion".

- **Radiation** is "the energy emitted by matter in the form of electromagnetic waves (or photons) as a result of the changes in the electronic configurations of the atoms or molecules".
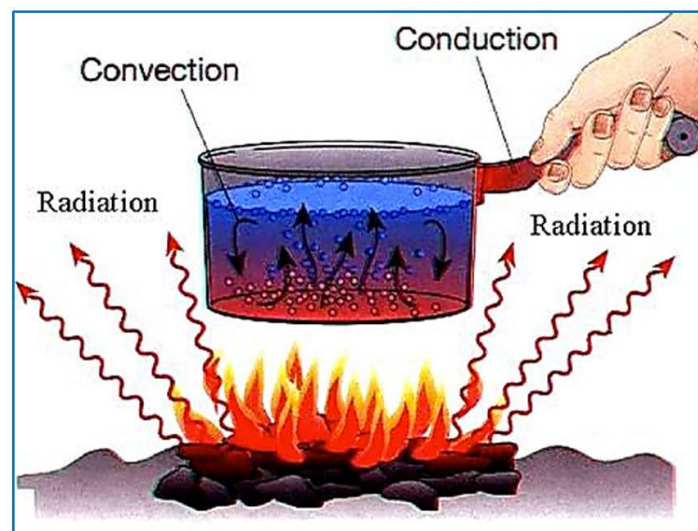
Figure 5-21 Modes of heat transfer (Holcomb, 2012)

According to Cengel (2002), experiments have shown that the rate of heat transfer Q through a wall is doubled when the temperature difference ΔT across the wall is doubled, but is halved when the wall thickness L=Δx is doubled. Thus, the rate of heat conduction through a plane layer is proportional to the temperature

difference across the layer and the heat transfer area, but is inversely proportional to the thickness of the layer. That is,

$$Rate\ of\ heat\ conduction \propto \frac{(Area)(Temperature\ difference)}{Thickness}$$

or,

$$Q_{cond} = \lambda A \frac{(T_1 - T_2)}{\Delta x} = -\lambda A \frac{\Delta T}{\Delta x} \qquad (5\text{-}3)$$

where the constant of proportionality λ is the thermal conductivity of the material which is a measure of the ability of a material to conduct heat.

5.4.1 Thermal Conductivity

Thermal conductivity (λ) of concrete is expressed as the ratio of the heat flow to the temperature gradient. Thermal conductivity is measured in Watts per square meter of area of body when the temperature difference is 1°K per metre: $(W/m^2) \times (m/K)$ or (W/mK). Two classes of method are normally used to measure the thermal conductivity of building materials; steady-state methods, in which the temperature across a sample does not change with time, and transient methods, in which a measurement is performed during the process of heating up (Keikhaei Dehdezi, 2012). Somerton (1992) reported that though the steady-state methods require long periods of time to achieve an equilibrium condition, their results are generally more accurate than transient methods.

For porous construction materials, the most dominant mechanism of heat transfer is likely to be conduction through the solid skeleton and fluid in the voids. In addition, evaporation and condensation of moisture within the voids would also affect the thermal conductivity when these voids are partially saturated with water. As mentioned earlier, heat transfer occurs through three mechanisms, however, for

pore diameters smaller than 3 mm, the effect of radiation, from solid surfaces of pores, and convection, through the fluid of pores, can be neglected (Han, 2006). Therefore under normal ambient conditions, conduction heat transfer through the solid and fluid in the pores is likely to be the controlling mechanism affecting the effective thermal conductivity of the porous construction materials in both dry and fully saturated states (Han, 2006).

In this study, the Heat Flow Meter (HFM) method, introduced in ISO 8301 (1996), was adopted to determine the thermal conductivity of all selected mixes. In the HFM technique, the specimen (305×305×50 mm) is placed between a hot plate and the HFM which is attached to a cold plate. A Thermal Conductivity of Building and Insulating Materials Unit (B480), shown in **Figure 5-22**, was used for this test.

The thermal conductivity of the specimen was calculated Under steady-state conditions by using the following equation (Hilton Ltd, 1994).

$$\lambda = \frac{l_s.\left[\{(k_1 + (k_2.\bar{T})\} + \{(k_3 + (k_4.\bar{T})).HFM\} + \{(k_5 + (k_6.\bar{T})).HFM^2\}\right]}{dT} \qquad (5\text{-}4)$$

$k_1 \rightarrow k_6$: calibration constants of the apparatus determined separately from testing a sample of known thermal conductivity;

$\bar{T} = \frac{T_{hot} - T_{cold}}{2}$: average temperature of hot & cold plate (˚C);

$dT = T_{hot} - T_{cold}$;

HFM: heat flowmeter output (mV);

l_s: thickness of the specimen (mm).

A range of thermal conductivity of different insulation materials is illustrated in **Table 5-2**, while **Figure 5-23** shows the relationship between the thermal conductivities of different kinds of lightweight concretes, including cellular, aerated, lightweight foamed and lightweight aggregate concretes, and their dry

densities (Weigler and Karl, 1980). It was found that an inclusion of 20% of entrained air reduced the concrete dry density by 20% and the thermal conductivity by 25%.

For this project, the results of thermal conductivity (average of two specimens) for both dry (λ_d - oven-dried at 105°C until constant weight) and saturated (λ_s - immersed in water for 7 days) states are shown in **Table 5-3**.

As expected, for a given mix, it was found that the higher the density the higher the thermal conductivity, and that thermal conductivity increases with increased moisture ($\lambda_s > \lambda_d$), since air has lower thermal conductivity than water. For a given density, the thermal conductivity in the dry state of mixes with additives in combination (FCa) is slightly higher than that for conventional mixes. The reason for this is that in the case of foamed concrete, its thermal conductivity depends not only on the air volumetric fraction but also on the thermal conductivity of the solid materials (mortar or cement paste) which is made denser by the physical and chemical contribution of the additives (SF and FA) as well as having less porosity owing to reduced w/c ratio with the addition of a superplasticizer, as shown in **Figure 5-15**. In addition, the pore structure of a material plays a dominant role in controlling its thermal conductivity, and it is noticed the additives in combination led to a more uniform voids distribution resulting in reduced void connectivity and consequent increase in thermal conductivity. In contrast, in the saturated state and for a given density, the results illustrate that compared to conventional mixes (FC), the thermal conductivities were slightly lower for FCa mixes. This is because the water absorption of FCa mixes is less than that for FC mixes leading to the water content being lower, which results in reduced thermal conductivity. In other words, the water absorption in foamed concrete is mainly influenced by the paste phase which is denser in the case of FCa mixes, and not all artificial pores take part in

water absorption since their suction is weaker than that of capillary pores (Ramamurthy et al., 2009), (**Figure 5-4c**).

In terms of mixes with LWA, it can be seen from **Table 5-3** that the values of thermal conductivities of FCL6 and FCLa6 in the dry state are close to those of mixes with the same density but without LWA, FC6 and FCa6. However, in the saturated state and since adding LWA increases the water absorption, it was found that the values of thermal conductivity for FCL6 and FCLa6 are higher than those of FC6 and FCa6.
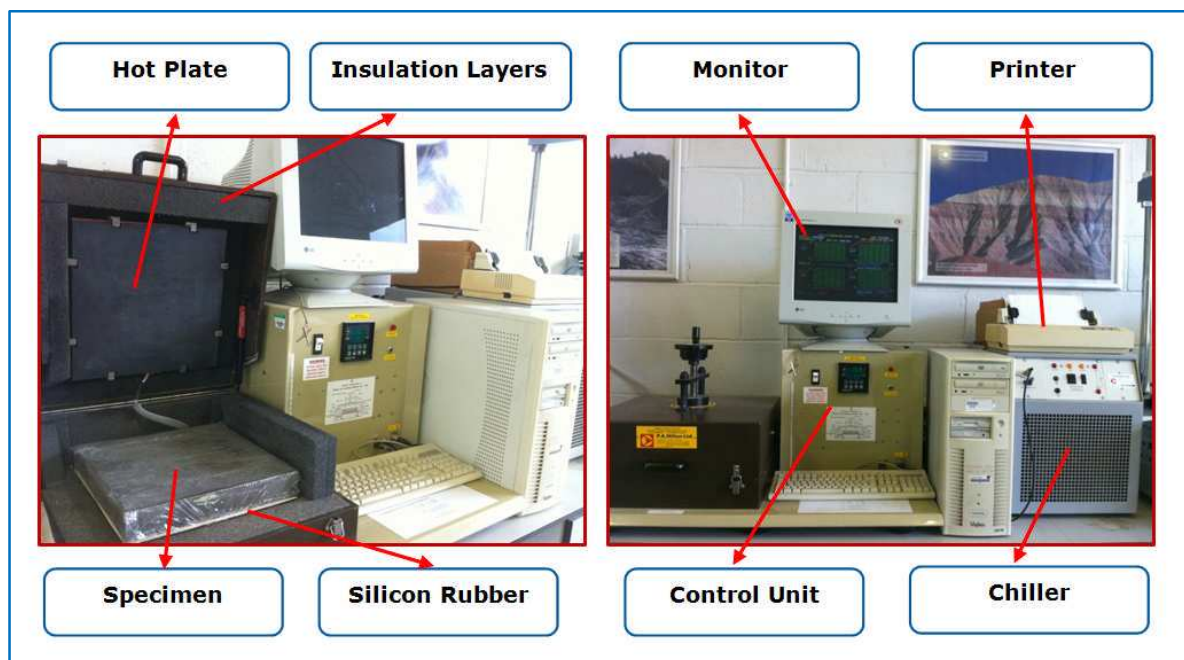
Figure 5-22 Thermal conductivity machine (Hilton LTD)

Table 5-2 Thermal conductivity of some insulation materials (Han, 2006)

Material	k-value (W/m.K)	ρ_d, dry density (kg/m^3)
Polyurethane foam	0.02	32
Polystyrene	0.037	30
Glass Wool	0.041	65 ~ 160
Polyethylene	0.0348	32 ~ 38
Rock Wool	0.04	40 ~ 130
Foamed concrete	0.065	300
	0.08	400
	0.095	500
	0.115	600
Perlite Concrete	0.194	870
	0.28	1315
Vermiculite Concrete	0.1	400
Normal weight concrete with granite	2.6-2.7	2400
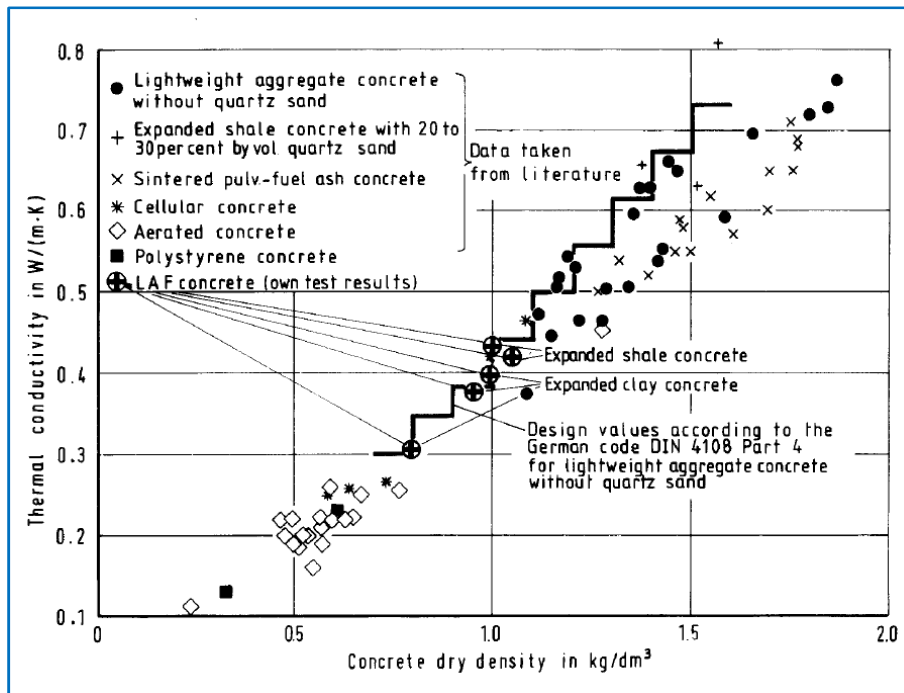
Figure 5-23 Thermal conductivity of different kinds of lightweight concretes (Weigler and Karl, 1980)

Table 5-3 The results of thermal conductivity for both of dry and saturated states

Mixes		FC3	FCa3	FC6	FCa6	FC9	FCa9	FCL6	FCLa6
λ (W/mK)	Dry	0.475	0.498	0.775	0.789	0.951	0.962	0.785	0.793
		(0.007)	(0.005)	(0.013)	(0.014)	(0.014)	(0.017)	(0.015)	(0.009)
	Saturated	0.635	0.599	1.08	0.986	1.185	1.112	1.121	1.074
		(0.012)	(0.014)	(0.015)	(0.016)	(0.015)	(0.017)	(0.019)	(0.021)

() standard deviation

5.4.2 Specific Heat Capacity

The C-THERM TCi (Thermal Conductivity Analyzer) is a non-destructive thermal conductivity and effusivity testing instrument with broad testing capabilities (0 to 220 W/mK) in a wide range of temperatures (–50° to 200°C). It is based on the Transient Plane Source (TRS) method with a one-sided heat reflectance sensor which applies a constant heat source to the sample. The principle of its operation is: a small amount of heat is provided by applying a known current to the sensor's heating element resulting in a rise in temperature at the interface between the sensor and the sample. This temperature rise induces an increase in the sensor voltage which is used to determine the thermo-physical properties, thermal conductivity and effusivity, of the sample as shown in **Figure 5-24** (C-THERM TCi, 2014).

To calculate the specific heat capacity in this study, the C-THERM TCi™ system, shown in **Figure 5-25**, was utilised to measure the thermal conductivity and effusivity of the selected foamed concrete mixes. The effusivity, also known as the coefficient of heat storage, is a measure of a material's ability to exchange heat with its surroundings. The test was performed on three individual samples (50×50×15 mm) of each mix on which five independent readings were obtained.

The specific heat capacity C_p, a measure of a material's ability to store thermal energy, (in J/kg.K) is calculated using the following equation (Keikhaei Dehdezi, 2012).

$$C_p = \frac{\beta^2}{\gamma_{dry} \times \lambda_d} \qquad (5\text{-}5)$$

where: β is the thermal effusivity (J/s$^{0.5}$ m^2 K), γ_{dry} is the dry density (kg/m^3) and λ_d is the thermal conductivity (W/m.K) at dry state.
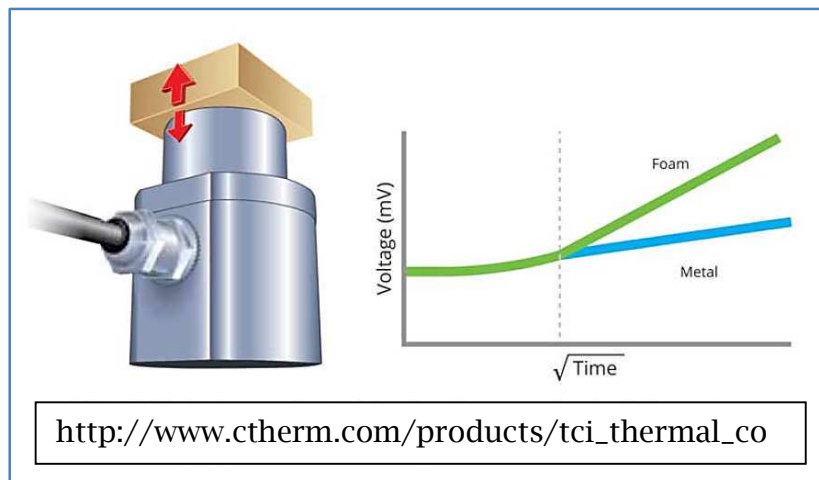
Figure 5-24 The work principle of C-THERM TCi

Figure 5-25 C-THERM TCi (Thermal Conductivity Analyzer) system

Neville (2011) stated that the common range of specific heat values for ordinary concrete is between 840 and 1170 J/kg.K and specific heat increases with increase of temperature or decrease of density of the concrete. **Figure 5-26** shows that, for FC and FCa mixes, the specific heat C_p decreases as the density increases (decrease of porosity) owing to enhanced inter-particle contact when the void ratio is minimised. However, for a given density, C_p is similar for mixes with additives in combination (FCa) compared to conventional mixes (FC). This observation and that from the C_p values of 1600 kg/m³ mixes with individual additives implies that, unlike normal concrete, the density does appreciably affect the thermal properties of lightweight concrete due to the low conductivity of air (Neville, 2011). It should be noted here that since the C-THERM TCi measurement is performed on an area of about 12mm diameter, the sample of mixes with LWA is not representative, therefore the calculated C_p values for FCL6 and FCLa6 may not represent the actual values.

Figure 5-27 shows the thermal conductivities of the selected mixes by adopting the two techniques, Helton and C-THERM TCi. In general, the values from the TCi technique are higher than those of the Helton technique. However, as mentioned earlier, the results of the steady state method (Helton) are generally more accurate than those of the transient method since the latter works with the sample surface and may not give a representative thermal conductivity value for the whole nonhomogeneous sample (concrete).
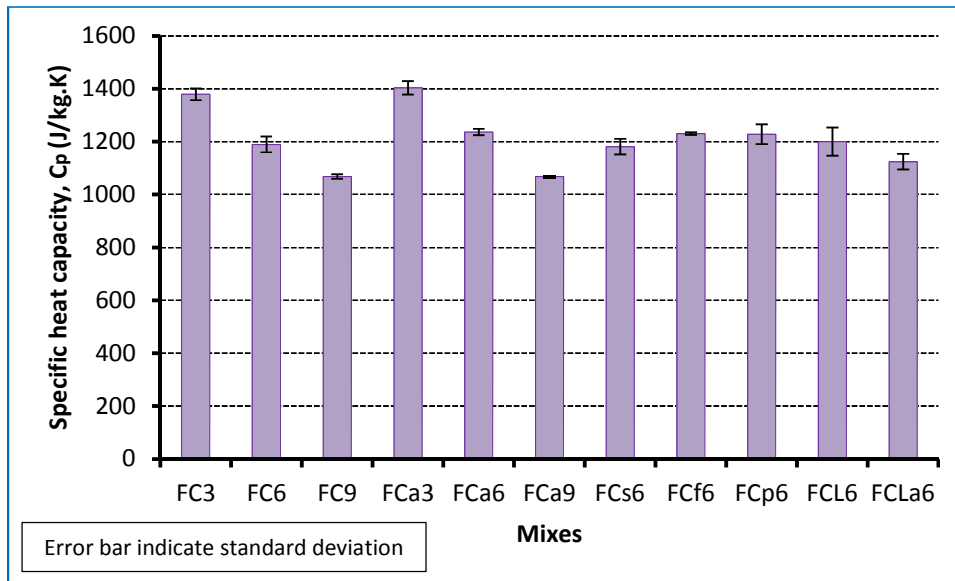
Figure 5-26 Specific heat capacity of investigated mixes
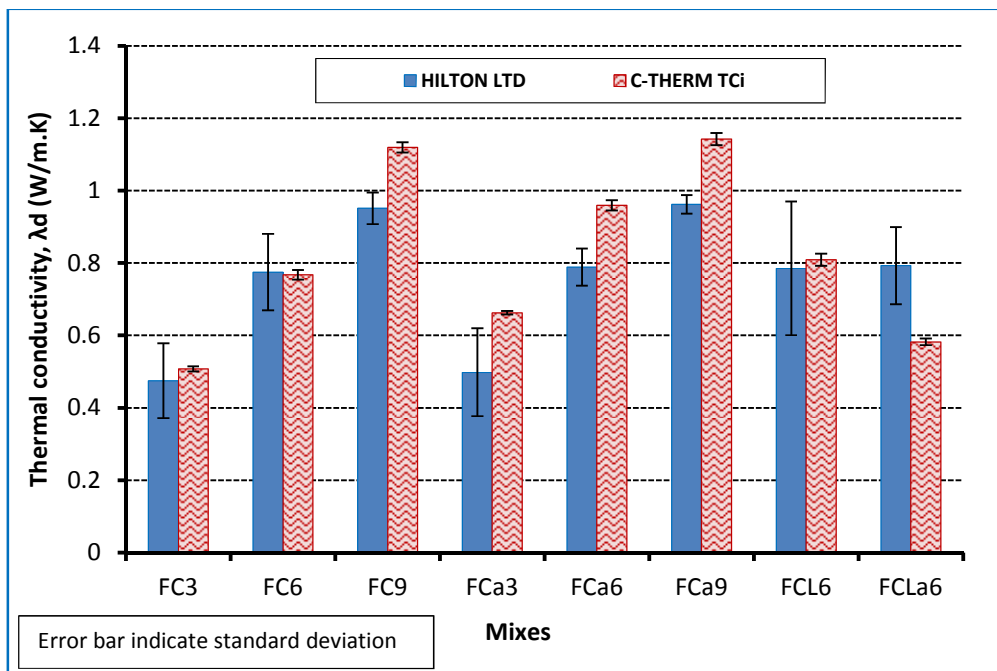
Figure 5-27 The thermal conductivities of selected mixes by utilising the two techniques

5.5 The Structural Efficiency

In concrete construction, it is not only beneficial to reduce the thermal conductivity of a material, but also to increase its structural efficiency (f_c/λ). **Figure 5-28** illustrates that, for all mixes, there is an increase in the (f_{cu}/λ_d) ratio with increase of density while, for the same density, this ratio increases with the presence of additives. These increases are gained as a result of improvements in the cementitious matrix either due to reducing the foam volume or by reducing the w/c ratio by adding a water reducer and the incorporation of high quality pozzolana (SF and FA). A comparison of thermal conductivity and (f_{cu}/λ_d) for the selected mixes with other mixes (NWC, LWC and FC) from the literature (Pan et al., 2007, Keikhaei Dehdezi, 2012) [*, **] is shown schematically in **Figure 5-28**.
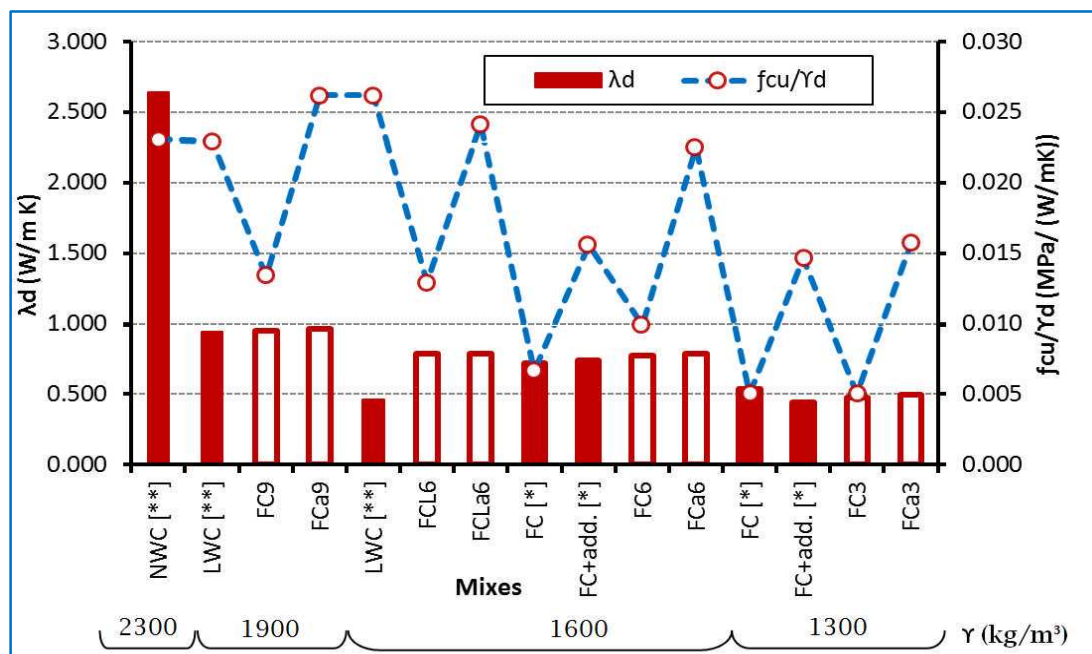
Figure 5-28 The comparison of (λ_d) and (f_{cu}/λ_d) for the selected mixes with other mixes (NWC, LWC and FC) [(Pan et al., 2007)*, (Keikhaei Dehdezi, 2012)**]

5.6 Summary

This chapter has described an experimental study of the enhancement of mechanical and thermal properties of pre-formed foamed concrete, 1300-1900 kg/m³, by utilising two types of additives, silica fume and fly ash, to partially replace Portland cement and fine sand as well as a superplastisizer. It has focused on mechanical and thermal properties as well as presenting a comparison with normal weight, lightweight and foamed concretes from the literature.

From the results presented in this chapter, the following conclusions can be drawn:

- The mineral admixtures (SF and FA) and superplasticizer combination provides improvement in the strength properties of foamed concrete.

- Compared to other studies on foamed concrete produced by using sand and/or fly ash as a filler material, the results from the mixes investigated in this study showed higher strengths (for a given density), higher tensile to compressive strength ratios and higher moduli of elasticity.

- A reduction in air void size parameters (O_{50} and O_{90}) is clearly linked to an increase in strength for each density implying that the effect of additives (both individually and in combination) was significant. However, it is noted that changes to the hydrated microstructure also contribute to strength gain.

- Due to their making the cement paste denser and less porous, addition of additives and superplasticizer leads to slightly increased thermal conductivity in the dry state. However, owing to reduced water absorption, the thermal conductivity in the saturated state was slightly lower for FCa mixes than FC mixes.

- Adding LWA instead of part of the sand helped in increasing the strength and modulus of elasticity without significantly increasing the thermal conductivity compared to mixes with the same density but without LWA.

Chapter 6: Permeation Properties

6.1 General

In general, the durability of concrete is affected by fluids (gas or liquid) transported through its pore system resulting in its deterioration. The transport of aggressive liquids into concrete depends on its permeation characteristics such as permeability, water absorption and sorption (Nambiar and Ramamurthy, 2007b) which represent the most important factors affecting the service life of a concrete structure (Sanjuan and Munoz-Martialay, 1996b).

In this project, measurements of water absorption, the ease with which water can penetrate foamed concrete, sorptivity, a rate of the absorption of water by capillary suction, and permeability, a measure of the flow of fluid (air) under pressure, were carried out to determine the permeation characteristics. Then, the effect of the void structure on permeation properties was investigated.

6.2 Water Absorption

Absorption is usually measured by drying a specimen to a constant mass, immersing it in water and then measuring its mass increase as a percentage of dry mass (Neville, 2011). Nambiar and Ramamurthy (2007b) reported that various procedures, different drying temperatures and/or immersion periods, have been adopted in measuring the water absorption resulting in widely different results. Examples are immersion in water for 24h (ASTM C796, 1997), immersion for 7 days/till a constant mass (Kearsley and Wainwright, 2001b) and adopting a vacuum saturation method. Neville (2011) stated that one reason for the variation in absorption is that drying at ordinary temperature may be ineffective in removing all the water; while drying at high temperature may remove some of the chemically combined water.

In this project, the ease with which water can penetrate foamed concrete was determined by measuring the water absorption on (100×100×70 mm) specimens which had been cured under sealed conditions for 28 days. These specimens were oven-dried at 105 °C (to a constant mass) and then immersed in water for 7 days (to a constant mass). Although absorption of normal concrete is usually expressed as the increase in mass as a percentage of oven dry mass, for foamed concrete it is here expressed as a percentage of volume to avoid misleading results because of the large differences in density between mixes (Kearsley and Wainwright, 2001b, Nambiar and Ramamurthy, 2006, Nambiar and Ramamurthy, 2007b). However, in mixes without foam, where density variation is normally less, the results of water absorption are not affected by the way in which it is expressed. Thus, the water absorption (to the nearest 0.5 %), Ab_w, was expressed as a percentage of the volume of the whole specimen as follows, (ASTM C796, 1997).

$$Ab_w = \frac{V_w}{V_c} \times 100 \qquad (6\text{-}1)$$

$$V_w = \frac{W_{w,a} - W_{dry}}{\gamma_w} \qquad (6\text{-}2)$$

where V_w is the volume of water absorbed, V_c is the specimen volume, W_w is the weight of saturated specimen in air, W_{dry} is the weight of oven dry specimen and γ_w is the unit weight of water.

Figure 6-1 and **Figure 6-2** show the variation in water absorption due to simple immersion with time for foamed concrete (conventional and with additives in combination), respectively % by weight and % by volume. An important observation is that the water absorption of foamed concrete, represented as a percentage by weight, increases with a reduction in density (Kearsley and Wainwright, 2001b), while when it is represented as a percentage of volume, it is seen that it is lower at

lower densities (Nambiar and Ramamurthy, 2007b, Nambiar and Ramamurthy, 2006), see **Figure 6-3**.

Although the porosity increases with a reduction in density of foamed concrete (increase in foam volume), the water absorption (% by volume) exhibits a reduction, **Figure 6-4**. Since the total porosity represents the sum of capillary pores and entrained air voids (Narayanan and Ramamurthy, 2000), this shows that not all the artificial pores are taking part in water absorption. As the foam volume increases the volume of entrained air pores increases reducing the paste content and therefore causing a reduction in the volume of capillary pores and this results in a decreasing trend of water absorption (Nambiar and Ramamurthy, 2007b). This is supported by another study on properties of foamed concrete (Nambiar and Ramamurthy, 2006), where it was shown that some mixes without foam showed higher water absorption than foamed concrete mixes. Thus, the water absorption of mixes with and without foam is mainly influenced by the paste phase. This will be discussed in detail in the next section.
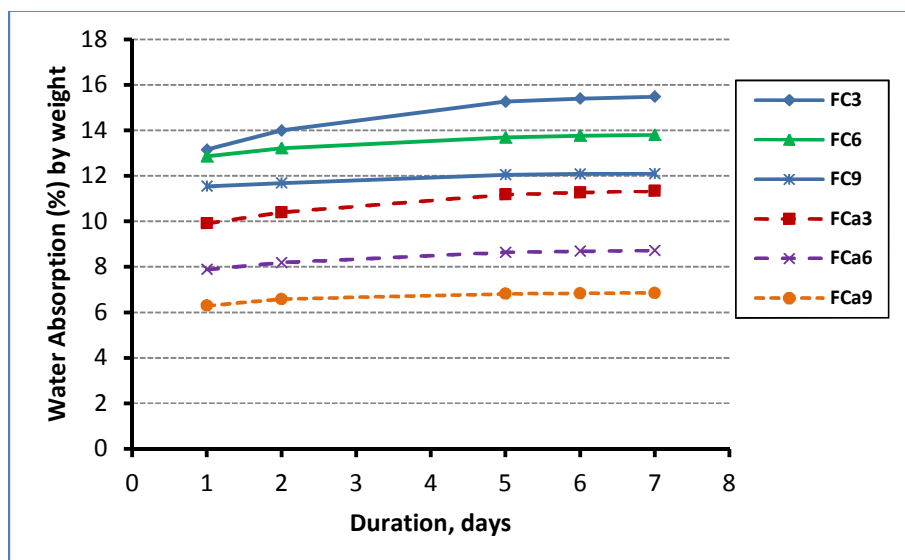
Figure 6-1 Variation in water absorption (%) by weight with time
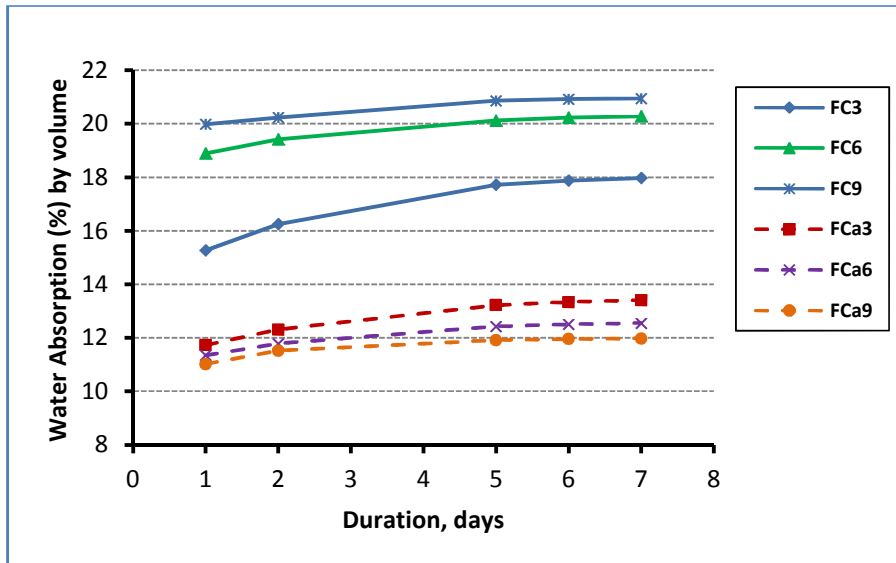
Figure 6-2 Variation in water absorption (%) by volume with time
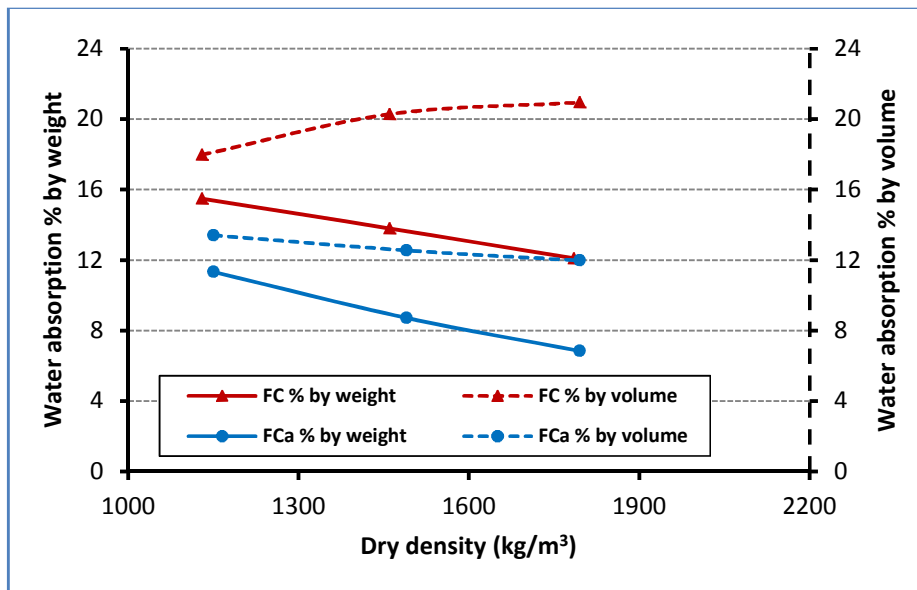
Figure 6-3 Water absorption percent of mass and volume as a function of dry density
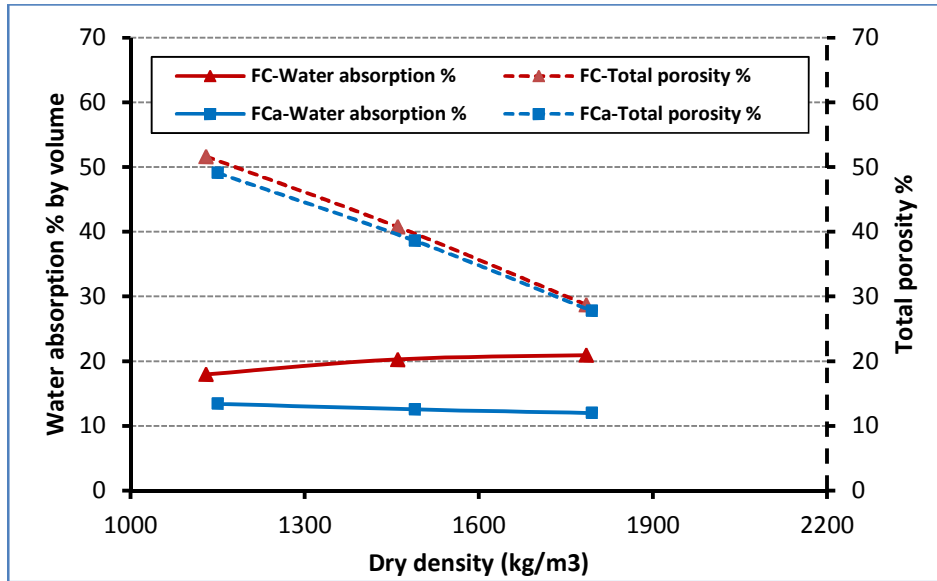
Figure 6-4 Water absorption percent of volume and porosity (%) as a function of dry density

6.3 Sorptivity

Sorption characteristics, absorption and sorptivity, express the tendency of a material to absorb and transmit water. From these properties, an indication of the penetration of detrimental materials such as chloride and sulphate ions, which cause long term deterioration in concrete, can be identified. Therefore, an understanding of moisture transport in concrete is significant to optimise its quality and to estimate its service life as a building material (Nambiar and Ramamurthy, 2007b).

The following square-root-time relationship describes the movement of water into foamed concrete (Nambiar and Ramamurthy, 2007b) and lightweight aggregate concrete (Lo et al., 2006):

$$i = B + St^{0.5} \tag{6-3}$$

where i is a cumulative volume absorbed per unit area of inflow surface [in mm³/mm²] in time t [min], B is a constant term representing the y-intercept at t=0

and *S* is the sorptivity of the material obtained from the i versus $t^{0.5}$ curve using a best fit linear regression [in $mm/min^{0.5}$].

Three cubical specimens of 100 mm dimension were cast for each foamed concrete mix while a further three 70 mm cubes were produced for the corresponding unfoamed mix (without foam). To ensure uniformity in the suction surface in contact with water during testing, a slice was cut from the bottom of the unfoamed specimen using a diamond rotary cutter; this left an unfoamed specimen size of 70×70×50 mm. Meanwhile for foamed concrete specimens, the 100 mm cubes were cut into two equal halves (100×100×48 mm) and these cut surfaces were submerged in the water during testing (Lo et al., 2006). All specimens were dried in an oven at 105 ˚C until a constant weight was achieved and then cooled to room temperature. To achieve unidirectional flow, the lowest 30 mm of the specimen sides were sealed with aluminium foil, see **Figure 6-5**. After that, the specimens were immersed in a tray, **Figure 6-5**, and rested on steel bars, to permit free access of water to the inflow surface, in a manner such that approximately the lowest 3 mm of the sealed faces were submerged in water at a constant level throughout the test. In the test, several weight measurements (to the nearest 0.01 g) were taken over a period of up to 7 hours.

Figure 6-5 Foamed concrete specimens during a sorptivity test

Figure 6-6 and **Figure 6-7** show that the sorptivity of conventional foamed concrete mixes (FC) increases with the decreasing foam volume. As sorptivity is caused by capillary suction (Nambiar and Ramamurthy, 2007b), its reduction is due to the reduction in unfoamed mixture volume (i.e. the reduction in capillary pore volume) with a reduction in density (i.e. increase in foam volume), see **Figure 6-8**. This led Nambiar and Ramamurthy (2007b) to conclude that the entrained air voids do not contribute to this transport mechanism which depends on those pores that participate in capillary suction. However, from the same figures, it can be seen that mixes with additives in combination (FCa) exhibit lower sorptivity than the conventional mixes. This is because of the reduction in water content due to use of a superplasticizer and the pozzolanic characteristics of both SF and FA lead to enhanced microstructure of cement paste by making it less porous, see **Figure 5-15** and the difference (capillary porosity) between the ϕ_{MIP} and the added foam in **Table 4-1**. In addition, from the MIP data, the partial porosity of pores <1 μm (capillary pores) were 27.5, 39.9, 44.4, 17.5, 20.6 and 22.3 % for FC3, FC6, FC9, FCa3, FCa6 and FCa9 respectively. Note that these partial porosities do not represent the actual values since by using the MIP technique most of pores appear smaller than they are in reality (Diamond, 2000). However the partial porosities provide useful comparative indices about the pore system of the selected mixes. Unlike FC mixes, the sorptivity of FCa mixes reduces with decreased foam volume (increased density). The same behaviour was noticed from the water absorption results (% volume); see **Figure 6-2**. This is because the inclusion of fly ash (20% of fine sand for all mixes) was higher for the denser mix (FCa9) due to the higher sand content in FCa9 than in the FCa3 mix (see **Table 3-2**) which, with the same cement content, made the cement paste micropores of FCa9 less connected resulting in reduced sorptivity, see **Figure 6-9**. In general, though the variation in sorptivity is marginal in the case of FCa mixes, it varies considerably in the case of FC mixes.

From **Figure 6-7**, it can be seen that foamed concrete mixes (FC and FCa) exhibit lower sorptivity than the corresponding unfoamed mixes (without foam) indicating clearly the effect of unfoamed mixture volume and thus the capillary porosity on the sorptivity. The other reason is the increase in the average path length of water movement owing to the presence of the entrained air voids (Nambiar and Ramamurthy, 2007b), see **Figure 6-10**.
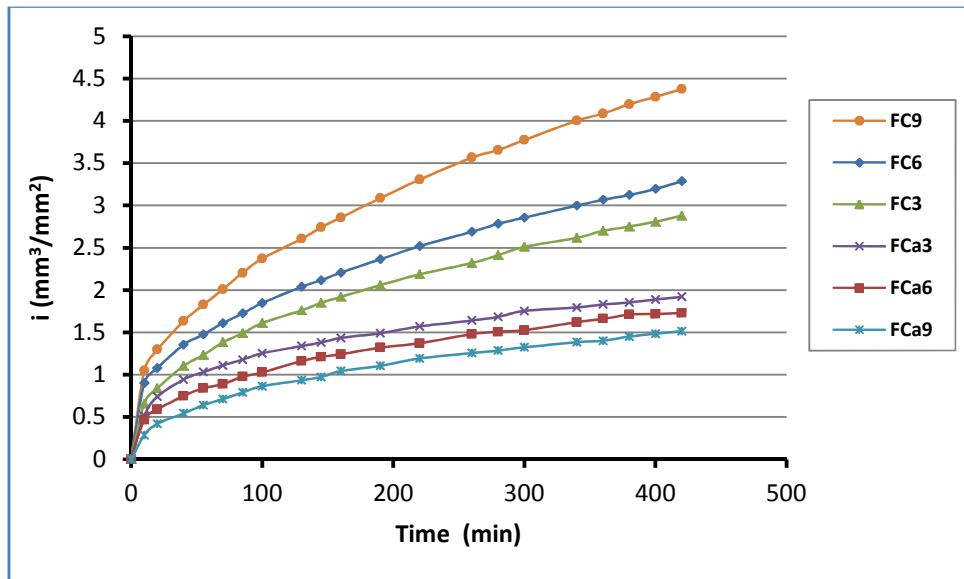
Figure 6-6 Evolution in the cumulative volume of water absorbed of FC and FCa mixes with time
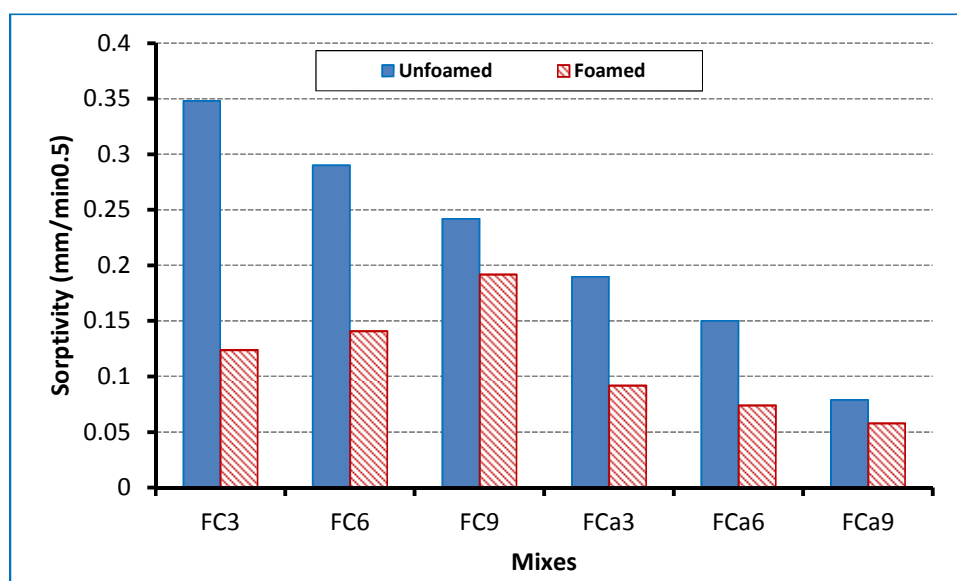
Figure 6-7 Comparison of sorptivity of foamed concretes with unfoamed mixes
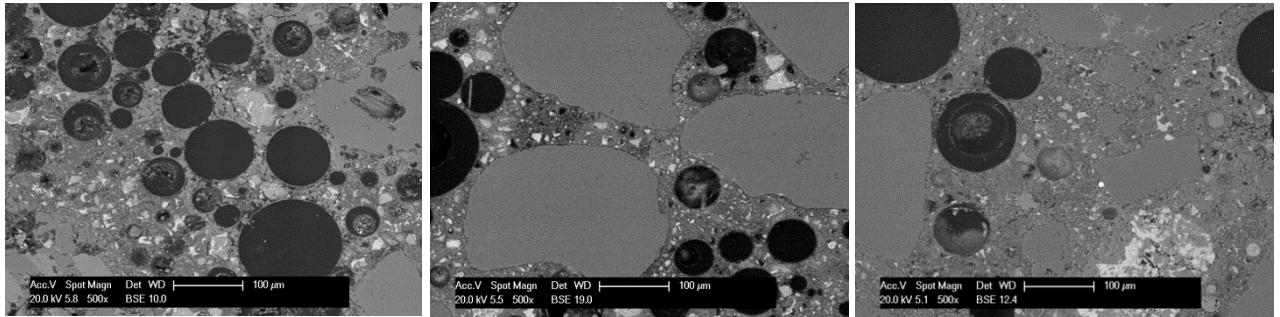
Figure 6-8 SEM images of foamed concrete mixes (left) FC3 (middle) FC6 (right) FC9
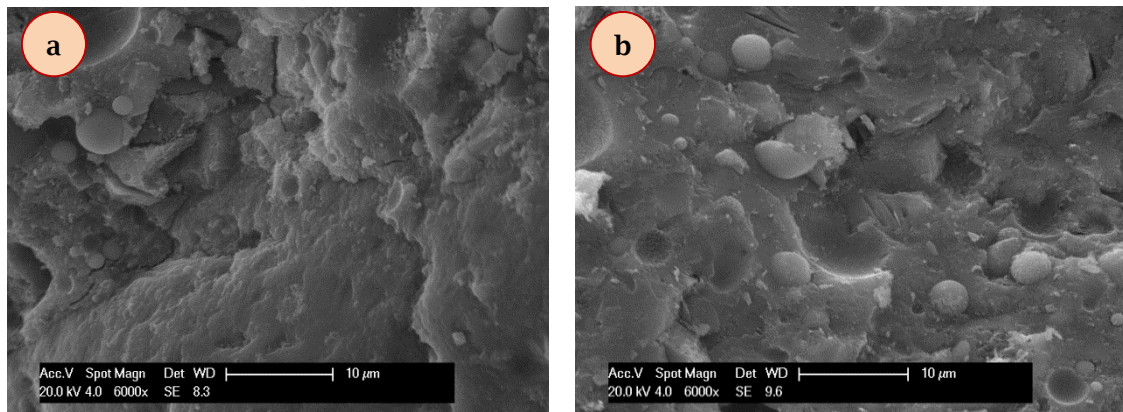
Figure 6-9 Microstructure of two foamed concretes with additives (a) FCa3 (b) FCa9
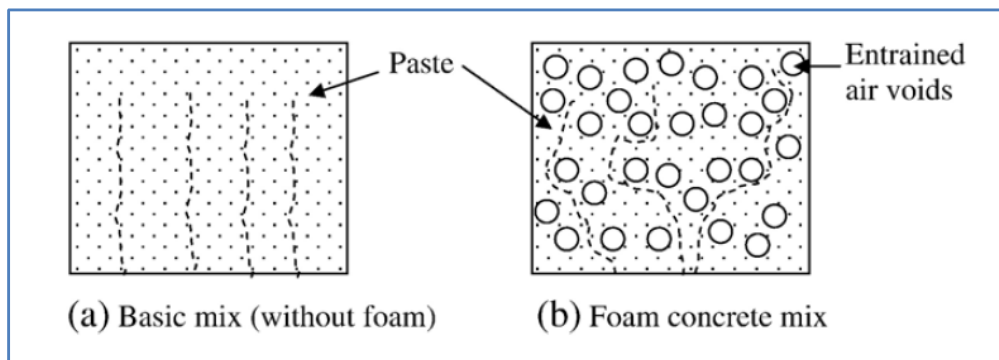
Figure 6-10 Movement of water into unfoamed and corresponding foamed concrete (Nambiar and Ramamurthy, 2007b)

It has been reported that incorporation of fly ash (30% and 40% of cement) results in less sorption than that of a control concrete with the same water/binder ratio (Nath and Sarker, 2011). However, owing to their higher water-solids ratio with a given density, foamed concrete mixes with fly ash exhibit relatively higher sorptivity than those without fly ash (Nambiar and Ramamurthy, 2007b). Note that

in this project a unique water/binder ratio was found to produce a stable 1600 kg/m^3 foamed concrete (with density ratio, measured fresh density divided by design density, close to unity) for FC6, FCs6 and FCf6 mixes, **Table 3-4**. Therefore, the data from this research clearly shows that the sorptivity reduces with inclusion of silica fume or fly ash compared to the conventional mix, FC6; **Figure 6-11**.

It can be seen from **Figure 6-11** that the sorptivity of the unfoamed mixes reduces considerably by adding the superplasticizer on its own or in combination with the other additives (FCp6, FCsp6 and FCa6). This is because of the enhancement of the microstructure of cement pastes which results from reducing the water, by adding the superplasticizer, as well as the physical and chemical contributions of the silica fume and fly ash (**Figure 5-15**). On the other hand, Kearsley and Wainwright (2001b) mentioned that in the case of foamed concrete the entrained air voids can be considered as an aggregate and their inclusion might reduce the permeability not only by obstructing flow but also because of the absence of microcraking at the interface between air voids and the mortar. In this study, comparing the unfoamed (mortar) and corresponding foamed concrete mixes, **Figure 6-11**, the reduction in sorptivity with foam addition was found to be much greater for the FC6, FCs6 and FCf6 mixes than for mixes with superplasticizer (FCp6, FCsp6 and FCa6). This may be for two reasons. The first is due to enhancement of the microstructure of the cement paste and the interfacial transition zone between it and the foam by the internal curing. From **Figure 6-12**, it is obvious that this enhancement (reducing the porosity and hence pore connectivity) is better in the conventional mixes than the mixes with a superplasticizer in combination with the other additives since the presence of the defects, microcracks and micropores (black features in **Figure 6-12**), in the microstructure of cement paste might be little in the unfoamed mixes with a superplasticizer (before adding foam). Secondly, reducing void merging by adding a

superplasticizer (FCp6, FCsp6 and FCa6) results in reducing the void sizes, see **Table 4-4** and **Figure 4-34**, and thus decreasing the average path length of water migration compared to FC6, FCs6 and FCf6 mixes, making the difference between the foamed concrete sorption and the corresponding unfoamed sorption smaller in the case of mixes with a superplasticizer.

Owing to its very fine pores, **Figure 6-13**, lightweight aggregate may contribute to the sorption mechanism. Therefore, the FCL6 mix exhibits more sorptivity than the FC6 mix for both unfoamed and foamed concrete phases and the same observation was noticed for FCLa6 comparing to FCa6.
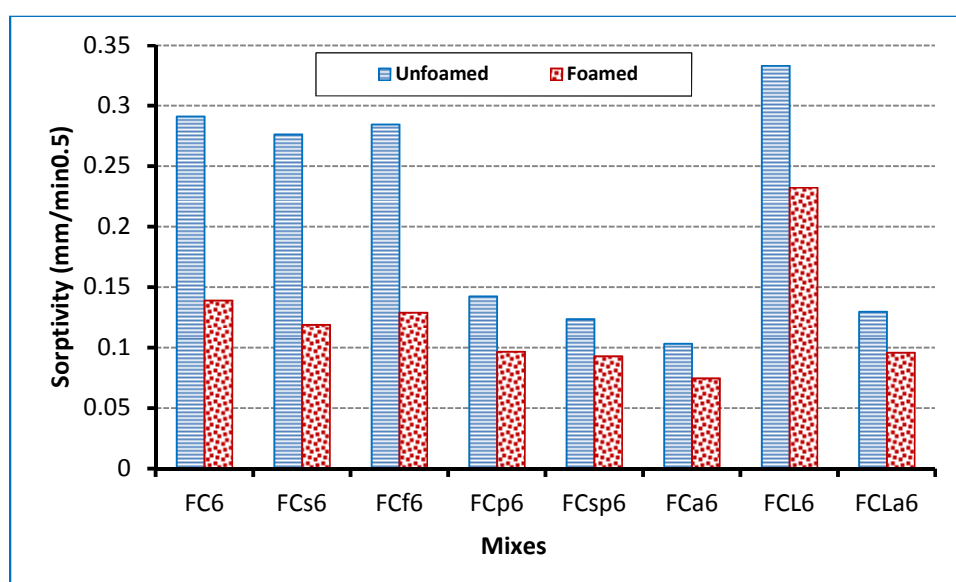
Figure 6-11 Comparison of sorptivity of 1600 kg/m³ foamed concretes mixes with corresponding unfoamed mixes
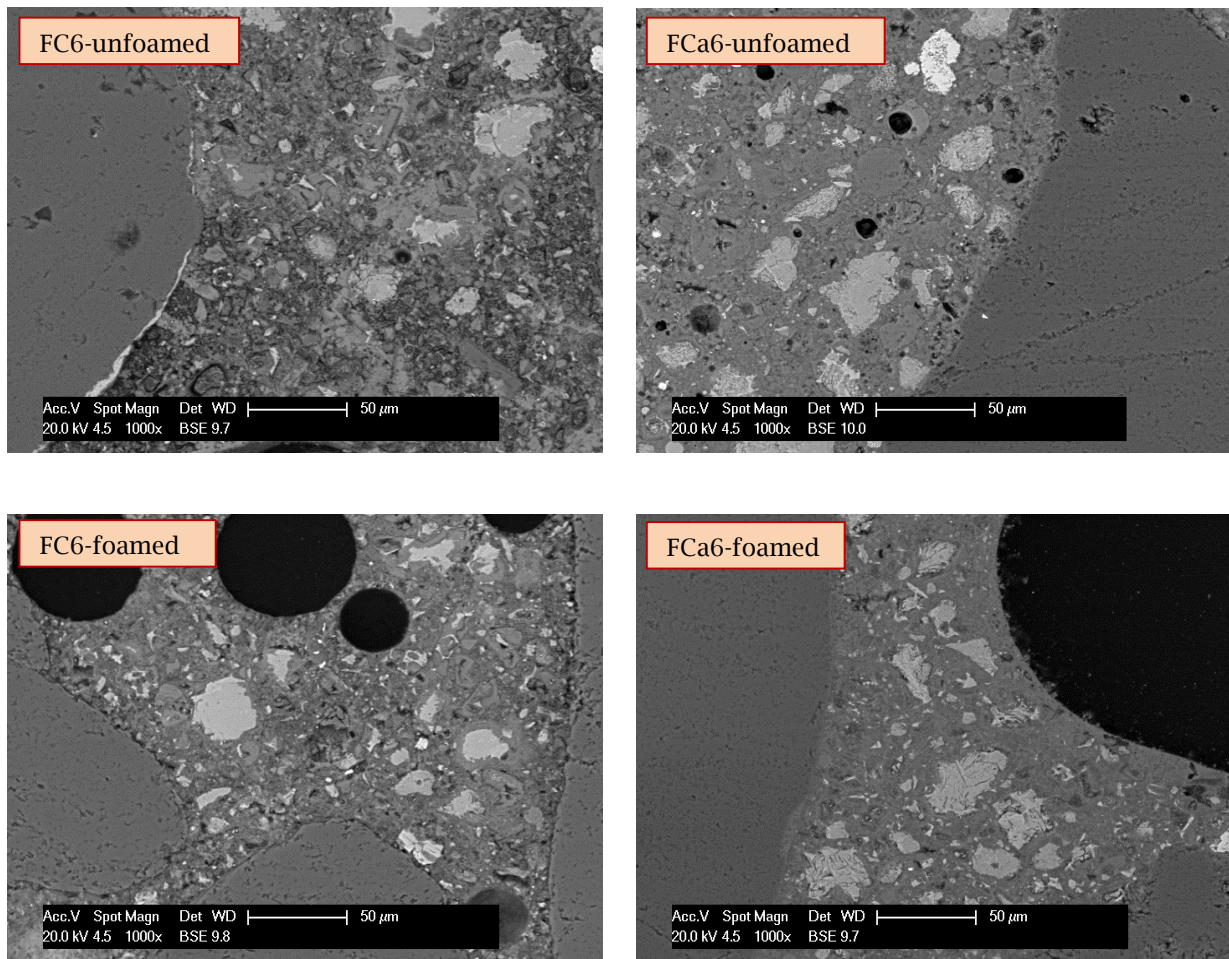
Figure 6-12 SEM images of 1600 kg/m³ foamed and unfoamed mixes
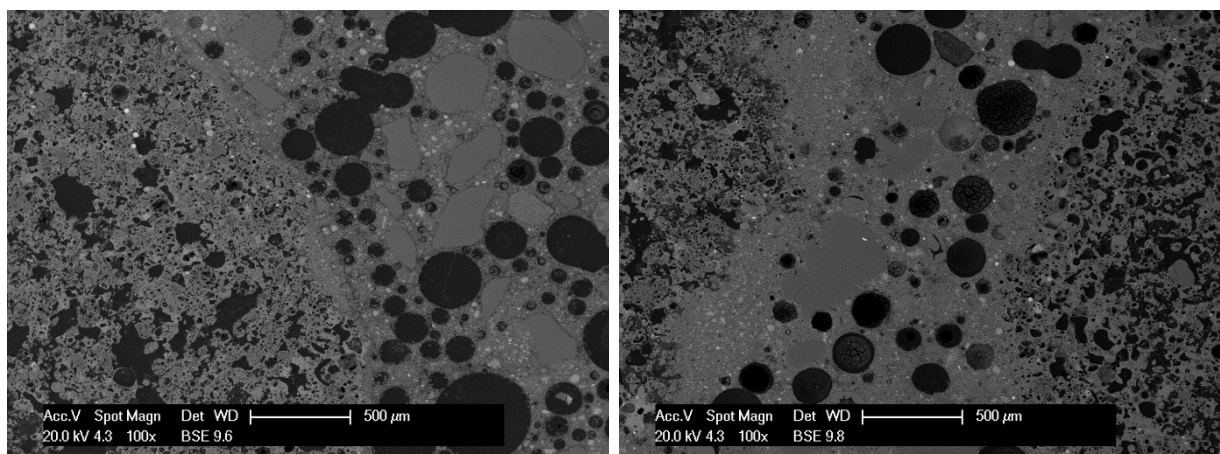
Figure 6-13 SEM images of 1600 kg/m³ foamed concrete mixes with lightweight aggregate left) FCL6 right) FCLa6

For normal concrete with a w/c ratio of 0.4, the sorptivity is expected to be 0.09 mm/min$^{0.5}$ and 0.17 mm/min$^{0.5}$ at a w/c ratio of 0.6 (Neville, 2011). Meanwhile, Lo et al. (2006) mentioned that the sorptivity of ordinary Portland cement concrete with a w/c ratio of 0.4-0.5 is about 0.23 mm/min$^{0.5}$. However, in their study on the effect of air content on permeability of lightweight aggregate concrete, the sorptivity ranged between 0.124 and 0.128 mm/min$^{0.5}$ at 28-day age with a w/c ratio of 0.4. In this study, the sorptivity was 0.126-0.194 mm/min$^{0.5}$ for conventional foamed concrete (FC) with w/b ratio between 0.475 and 0.525 and 0.067-0.092 mm/min$^{0.5}$ for mixes with combined additives (FCa) with w/b ratio between 0.3 and 0.35. Meanwhile, it was 0.232 mm/min$^{0.5}$ and 0.095 mm/min$^{0.5}$ for mixes with lightweight aggregate FCL6 and FCLa6 respectively. This indicates that the sorptivity values of all investigated mixes were not particularly high compared to normal weight concrete of the same w/c ratio.

6.4 Permeability

An important indicator of concrete long term durability is its permeability which is the relative ease with which an aggressive substance can penetrate into concrete (Sanjuan and Munoz-Martialay, 1996b, Alshamsi and Imran, 2002, Neville, 2011). Because the durability of concrete is governed by its resistance to penetration by external aggressive agents, the property of permeability is a logical estimator of its quality (Sanjuan and Munoz-Martialay, 1996a, Sanjuán and Muñoz-Martialay, 1997). In this project, permeability was measured by constant and falling head methods and calculated by the Katz and Thompson model.

6.4.1 Measurement Methods

6.4.1.1 Constant Head Method

Foamed concrete cylinders (100Ø×140mm) were produced and then sealed-cured (wrapped in cling film) for 28 days. After that, 60 mm thick disks were cut from the middle of each cylinder, 30mm above and below the central line thereby excluding regions of non-representative porosity. These disks were dried at 105°C for 2 days to reach capillary dry conditions and tested at 30 days after mixing. The air permeability coefficient, k_{air} (m²), was calculated according to the Hangen-Poiseuille equation for a laminar flow in steady-state conditions of a compressible fluid (Sanjuan and Munoz-Martialay, 1996a);

$$k_{air} = \frac{2QPZ\mu}{A(P^2 - P_a^2)}$$ (6-4)

where; Q is the air flow rate (m³.s⁻¹), μ is the air dynamic viscosity (1.8×10⁻⁵ N.s.m⁻² at 20°C), P is the absolute inlet pressure (N.m⁻²), P_a and $P_。$ are outlet and measuring pressure, respectively, (both are equal to the atmospheric pressure, 0.101 MPa), A is the cross-section area (0.00785 m²) and Z is the specimen thickness (0.06 m).

The test steps of this method were as follows: a specimen was sealed in a hollow rubber cylinder for around 20 hours before the test to avoid the possibility of edge leakage. During testing, a specified inlet air pressure (0.6, 0.5, 0.4, 0.3, 0.2, 0.15 MPa) was applied to the specimen in an apparatus. For each applied pressure an air flow Q (m³ s⁻¹) was obtained by a flow meter connected at the end of the outlet tube, **Figure 6-14a, b**. From, the relationship between the air flow rate and the pressure difference ($P^2 - P_a^2$) for each mix, the air permeability coefficient, k_{air} (m²), was obtained by multiplying the slope of this straight line by ($2P_。Z\mu$).
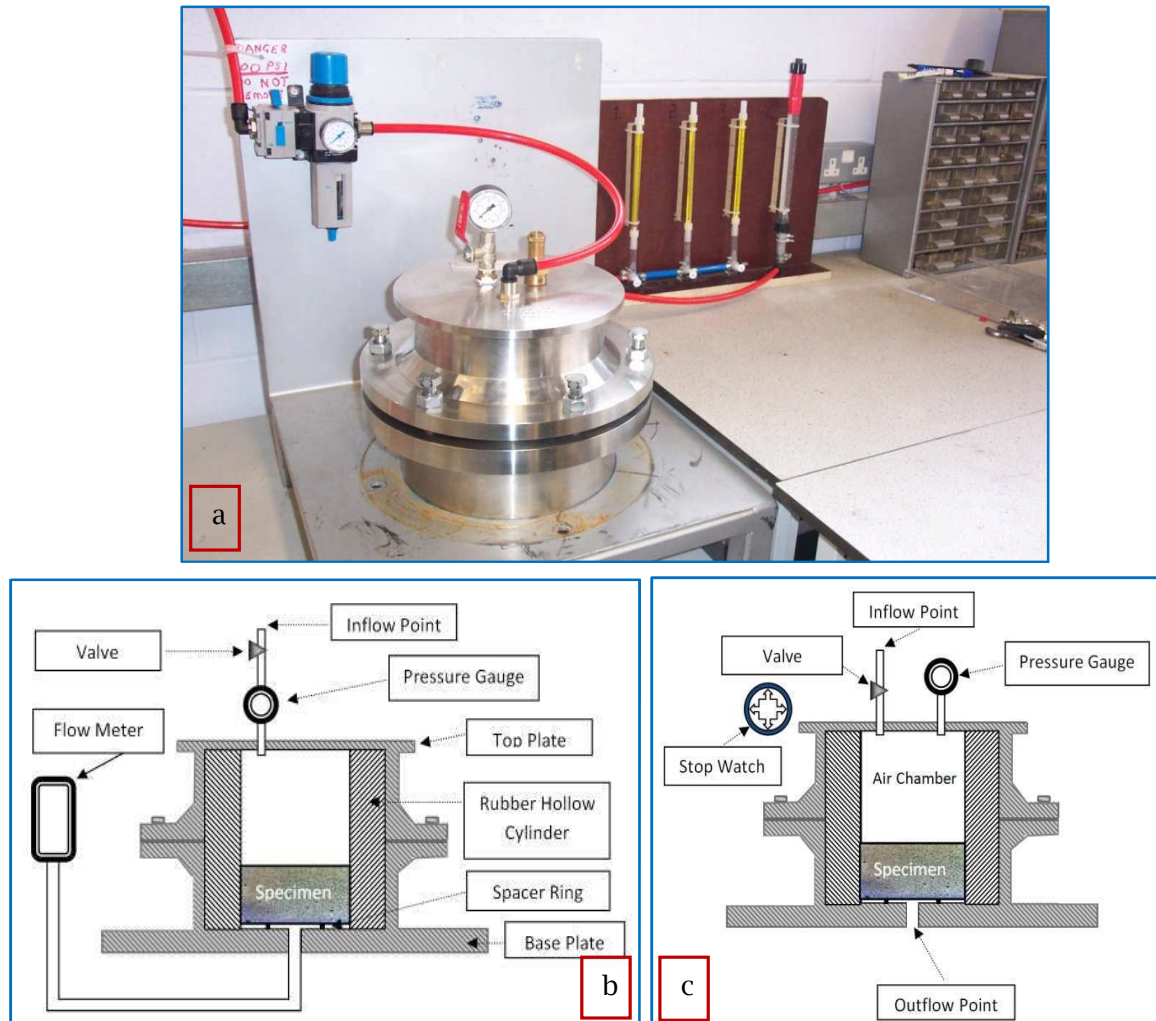
Figure 6-14 (a) Permeameter used (b) Schematic of a constant-pressure air permeameter (c) Schematic of a falling-pressure air permeameter

6.4.1.2 Falling Head Method

Figure 6-14c describes the apparatus used for testing the air permeability of the selected mixes by the falling-pressure method. From this figure, it can be seen that the upper surface of the specimen and the top plate form an air chamber while the specimen's lower surface is open to the atmosphere. Compressed air is used through the air inlet to pressurize the air chamber until reaching a specified pressure, 603.3 kPa (87.5 psi), measured by a pressure gauge connected to the air chamber. After that, the air inflow valve is closed so that the air in the chamber can only leak out through the specimen to the atmosphere from the outflow point. The time starts at zero when the pressure is 603.3 kPa (87.5 psi), then as the pressure

drops by steps of 17.2 kPa (2.5 psi) the time is recorded with a maximum number of 35 drops (from 603.3 to 17.2 kPa). The same size cylindrical specimen as used in the constant head method was used in this test by sealing it in a hollow rubber cylinder with a silicone sealant thereby forming an air chamber of 120 mm height.

From mathematical models based on Darcy's law for gases, Li et al. (2004) present an analytical solution for estimating air permeability using the test data obtained by the falling pressure method, as follows:

$$k_{air} = -\frac{V_{ch}.Z.\mu.m}{A.P_{atm}} \qquad (6\text{-}5)$$

where: k_{air} is the air permeability (cm²), V_{ch} is the air chamber volume (cm³), Z is the specimen thickness (cm), μ is the dynamic viscosity of air (g cm⁻¹ s⁻¹), A is the cross-section area (cm²), P_{atm} is the atmospheric pressure (g cm⁻¹ s²) and m is the slope of the $\ln[c(P_{(t)}-P_{atm})/(P_{(t)}+P_{atm})]$ versus t straight line. In addition, $P_{(t)}$ is the pressure at any time, t, and c is a constant given by:

$$c = \frac{P_{(0)} + P_{atm}}{P_{(0)} - P_{atm}} \qquad (6\text{-}6)$$

In addition, Li et al. (2004) derived a theoretical prediction of $\ln[c(P(t)-Patm)/(P(t)+Patm)]$ versus t as follows;

$$ln\left(c\frac{P_{(t)} + P_{atm}}{P_{(t)} - P_{atm}}\right) = -\frac{AP_{atm}k}{V_{ch}Z\mu}t \qquad (6\text{-}7)$$

In this study, their method has been adopted to measure the air permeability of the selected mixes using the falling pressure method.

The validity of this analytical method is based on the assumption that $\delta \ll 1$ where δ is defined as:

$$\delta = \frac{n_a\mu Z^2}{kP_m} \times \frac{P(t)}{P^2(t) - P^2_{atm}} \times \left|\frac{dP}{dt}\right| \qquad (6\text{-}8)$$

where n_a is the air-filled porosity and P_m is the main air pressure defined as the average of the minimum and maximum pressure in the test.

Based on **Eq. (6-5)**, Li et al. (2004) derived a theoretical prediction for the pressure $P_{(t)}$ at any time t > 0, as follows:

$$P_{(t)} = \frac{(c + e^{-mt})P_{atm}}{c - e^{-mt}}$$

(6-9)

where m is as in **Eq. (6-5)**.

6.4.2 Calculation Method

Many models and theories have been developed to predict the permeability of a porous medium by linking its transport properties to microstructural parameters such as porosity, pore surface area and critical pore diameter (Yen, 2007). Moreover, it has been reported that a theory of pore structure transport should be based on an experimental characterisation of the pore structure which is directly relevant to the transport properties. Yen (2007) listed some of the models used to predict the permeability of concrete as follows: Kozeny-Carmen theory, Katz-Thompson theory, statistical modelling, computer network model and composite model theory (general effective media, GEM).

6.4.2.1 Katz and Thompson Model

The approach used in this project is that of Katz and Thompson (1986), which is particularly suitable for the permeability of a porous material, k, in units of m², as follows:

$$k = \frac{1}{226} \cdot \frac{\sigma}{\sigma_{\circ}} \, l_c^2$$

(6-10)

where σ is the electrical conductivity of the saturated porous material (S/m) (Siemens per metre), $\sigma_{\circ}$ is the conductivity of the solution in the pores (S/m) (1.02*10⁶ S/m at 20˚C for mercury) and l_c is the characteristic length scale of the material. Katz and Thompson reported that, as can be seen from **Eq. (6-10)**, the

conductivity term reflects the connectedness of the pore space, whereas the length term sets the scale for the permeability. However, it has been shown that l_c, the maximum continuous length scale or the critical pore diameter, can be generated from an MIP experiment (Katz and Thompson, 1986, Christensen et al., 1996), representing the pore dimension corresponding to the inflection point in the cumulative intruded volume vs. pore diameter plot (maximum in log differential intrusion volume vs. equivalent pore diameter plot, dV/dlog D vs. D) (Cui and Cahyadi, 2001, Mindess et al., 2003).

In this project, the values of conductivity factor ($\sigma/\sigma_\circ$) were obtained from MIP data and were not computed directly from electrical measurements.

6.4.3 General Discussion on Permeability

The air permeability was measured by adopting the constant and falling head methods and was calculated by applying the Katz and Thompson equation. The results are listed in **Table 6-1**. In terms of the constant head method, **Figure 6-15a-c** shows the relationship between the air flow rate and the pressure difference ($P^2-P_a^2$) for the selected foamed concrete mixes. For each mix, the air permeability coefficient, k_{air} (m^2), was obtained by multiplying the slope of this straight line by ($2P_\circ Z\mu$). The driving pressure was found to have a significant influence on the coefficient of permeability k, it being higher when the applied pressure is lower, as observed by other authors (Christensen et al., 1996, Yen, 2007); i.e. a non-Darcy response is obtained. The decrease in measured air permeability with increase in applied pressure is due to a gas slippage phenomenon at wall pores. This phenomenon can be described as follows: gas molecules are colliding with each other during travelling with an average distance called a mean free path. At lower pressure, the mean free path is greater resulting in reducing the contact between the gas molecules and pore walls leading to easily gas movement and then increased of permeability.

With regard to the falling head method, **Figure 6-16** shows how the pressure function $\ln[c(P_{(t)}-P_{atm})/(P_{(t)}+P_{atm})]$ changes with time for the average of three repeated tests for the FC9 mix and that the theoretical prediction (**Eq. (6-7)**) gives a satisfactory match. By using the slope of the straight line, the air permeability of the sample was estimated based on **Eq. (6-5)**. In addition, by using this slope and applying **Eq. (6-9)**, a theoretical prediction of the pressure at any time can be drawn, **Figure 6-17**. From this figure, it is observed that there is a good fit between the data and the theoretical prediction. It should be noted that the validity of this method has been checked by using **Eq. (6-8)** obtaining values of δ between 0.032 for FC9 and 0.065 for FC3. Thus the condition $\delta \ll 1$ of **Eq. (6-8)** is satisfied.

The MIP test was carried out to obtain the conductivity factor and the critical pore diameter for foamed concrete specimens. The σ or $\sigma_{\circ}$ is the proportionality constant between electrical current per unit cross-sectional area (i/A) and the gradient of the electrical potential V $[i/A = \sigma \nabla V]$ according to Ohm's law (Friedman and Seaton, 1998). Meanwhile, as explained above that the l_c is defined as the smallest size of pores that remain interconnected. As it is practically impossible to determine this size directly, an indirect assessment is usually achieved by the MIP technique. The l_c is taken to be the pore size at which the mercury enter the pores at its fastest rate as this must represent the point at which the pores become largely interconnected (El-Dieb and Hooton, 1994). This size corresponds to the steepest part of the plot of cumulative intruded volume versus pore diameter (also the pore size at which the dV/d(log D) versus D plot reaches its maximum value) (see **Figure 6-18**) is interpreted as the critical pore diameter (the maximum continuous length scale) (l_c) being 9.89, 1.93, 1.27, 3.49, 1.28 and 0.49 μm for FC3, FC6, FC9, FCa3, FCa6 and FCa9, respectively (**Figure 6-19a, b**), while the conductivity factor, respectively, was 0.159, 0.085, 0.055, 0.118, 0.079 and 0.034 for FC3, FC6, FC9, FCa3, FCa6 and FCa9. Note that the MIP test was not done on mixes with LWA (FCL6

and FCLa6) since the specimen size (10×10×20mm) will not be representative of these mixes with coarse LWA (4-10mm) size.

The question whether or not the Katz and Thompson theory can be applied to cementitious material has been answered by Cui et al. (2001) by thoroughly examining the pore structure of cement paste and comparing it with that of stone, since it was concluded that this equation is suitable for porous rock (Katz and Thompson, 1986). They found that the difference in pore structure between stone and cement paste is due to the existence of gel pores in the latter. Moreover, when the cement paste is very porous, capillary pores form a continuous network throughout the whole material. In this case and by ignoring the contribution of gel pores, capillary pores control the permeability leading to the conclusion that the Katz and Thompson theory could be used. However, for low porosity, another model considering the roles of both capillary and gel pores should be adopted, since in this case the capillary pores may be blocked by the hydration products so that the gel pores may play a more significant role in fluid transport.

Figure 6-20 shows a comparison between the measured and calculated permeability values for this study and studies from the literature. It can be seen that applying the Katz and Thompson equation [**Eq. (6-10)**] to foamed concrete (this study) or very porous cement pastes (Christensen et al., 1996) yielded a good correlation with the experimental values. Howerver, for cementitious materials with low porosity, El-Dieb and Hooton (1994) concluded that the Katz and Thompson equation is not suitable (large difference between the experimental and calculated results). Halamickova et al. (1995), found that the Katz and Thompson equation provided a good permeability estimation at w/c=0.5 but the predicted permeabilities were overestimated at w/c=0.4, see **Figure 6-20**, suggesting that this relationship may be applied better with interconnected capillary systems rather than systems where the gel pores dominate the transport. In addition, **Figure 6-20**

shows that the general effective media model (GEM) is not suitable for a porous material (this study) but it appears to be a suitable tool for cementitious materials with low porosity (Cui and Cahyadi, 2001). Note that for this study, the procedure proposed by Cui and Cahyadi (2001) was employed to calculate foamed concrete permeability by the GEM model with capillary porosities (a difference between the total porosity and the added foam) of 9.23%, 11.23% and 12.13% for FC3, FC6 and FC9, respectively.

Table 6-1 Measured and calculated permeability results

Mixes	Dry Density (kg/m^3)	Permeability (m^2)		
		Measured		Calculated
		Constant	Falling	Katz
FC3	1135	$5.58*10^{-14}$	$6.40*10^{-14}$	$6.80*10^{-14}$
FC6	1455	$1.10*10^{-15}$	$1.25*10^{-15}$	$1.22*10^{-15}$
FC9	1790	$2.89*10^{-16}$	$5.10*10^{-16}$	$3.92*10^{-16}$
FCa3	1155	$2.25*10^{-15}$	$1.37*10^{-15}$	$6.38*10^{-15}$
FCa6	1470	$1.90*10^{-16}$	$2.37*10^{-16}$	$5.72*10^{-16}$
FCa9	1795	$3.19*10^{-17}$	$1.14*10^{-17}$	$3.47*10^{-17}$
FCL6	1425	$6.56*10^{-15}$	$7.98*10^{-15}$	-
FCLa6	1450	$3.34*10^{-16}$	$5.12*10^{-16}$	-
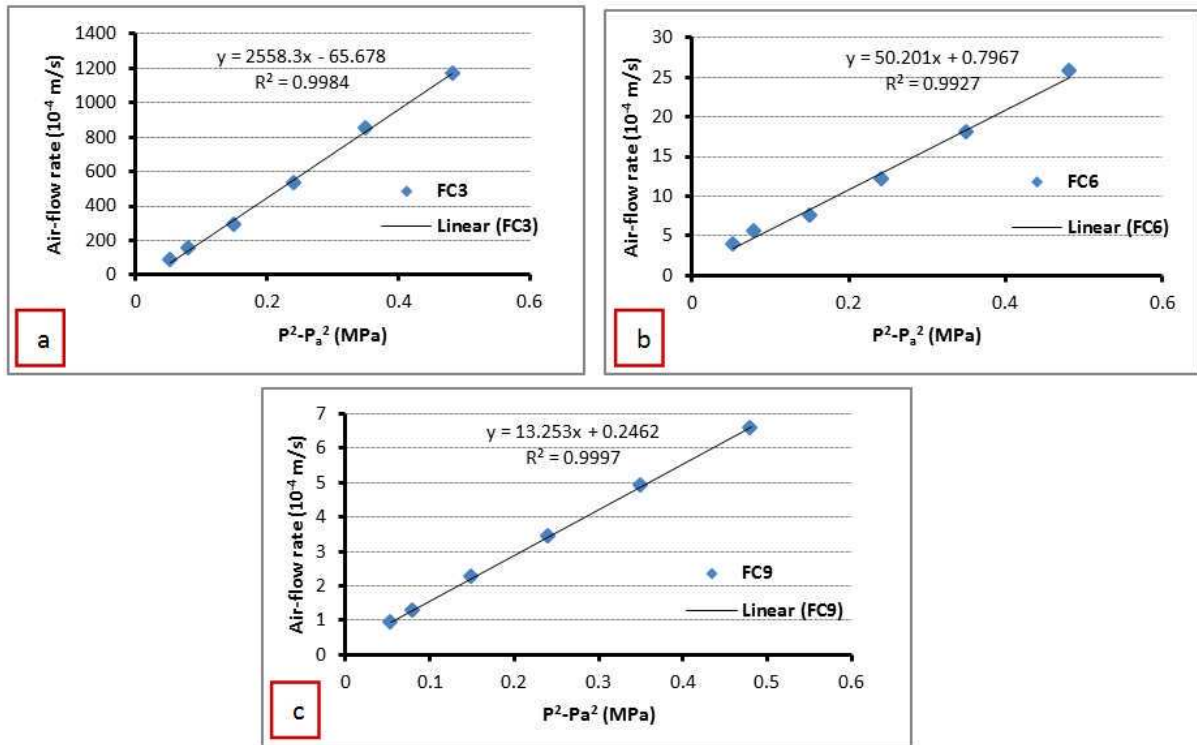
Figure 6-15 Relationship between the air-flow rate and the pressure difference ($P^2-P_a^2$) for the three selected mixes (a) FC3, (b) FC6 and (C) FC9
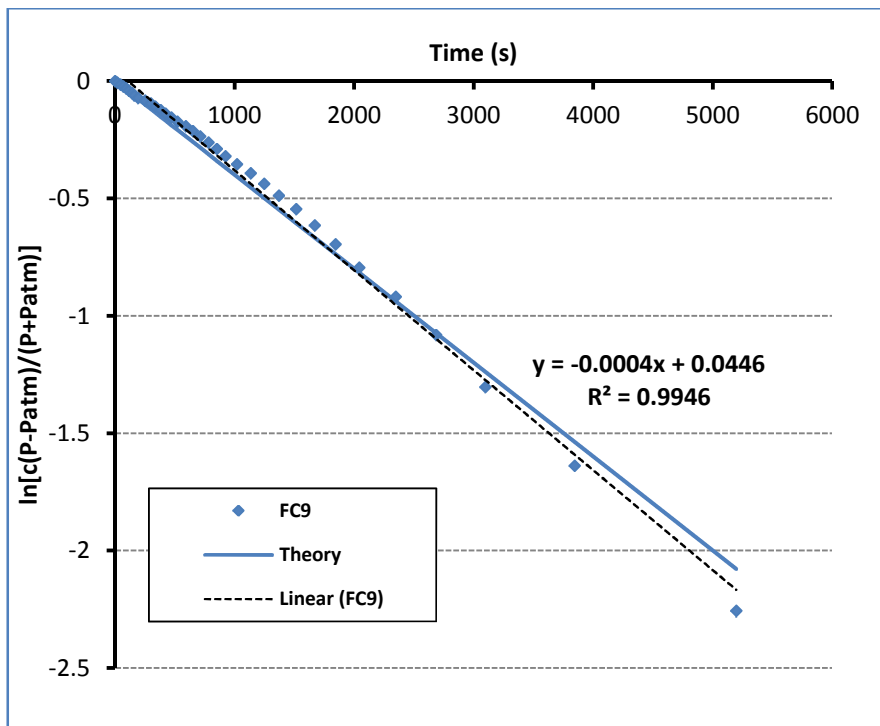
Figure 6-16 ln [$c(P-P_{atm})/(P+P_{atm})$] versus time test data for FC9 and its linear analytical prediction by Eq. (6-7)
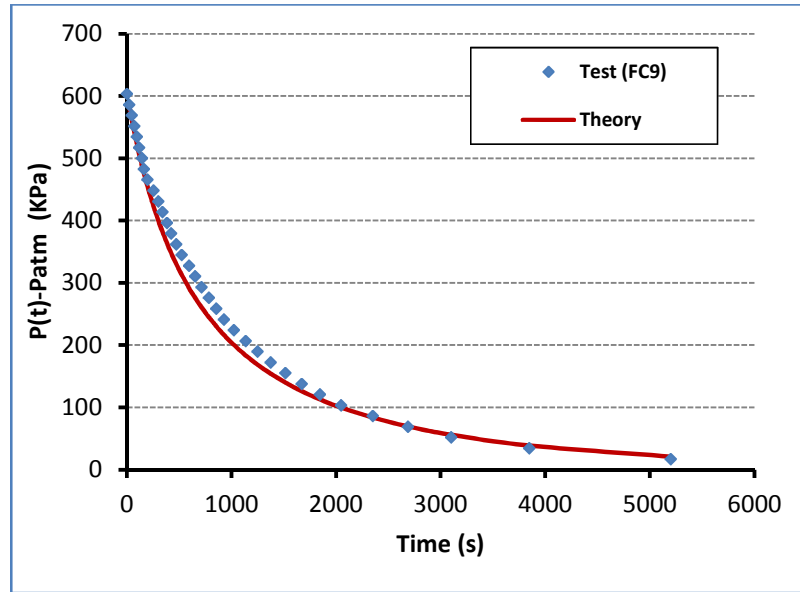
Figure 6-17 $(P_{(t)} - P_{atm})$ versus time test data for FC9 and its linear analytical prediction by Eq. (6-9)
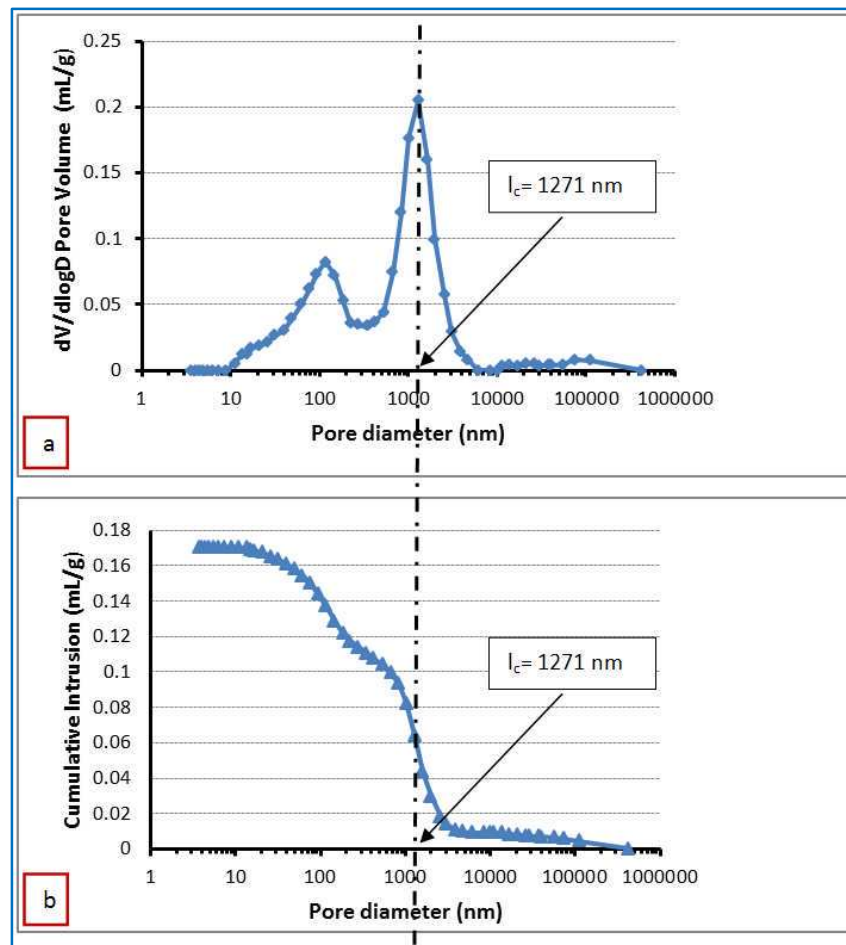
Figure 6-18 (a) Critical pore diameter of FC9 mix; (b) the variation of cumulative intrusion mercury volume of FC9 mix
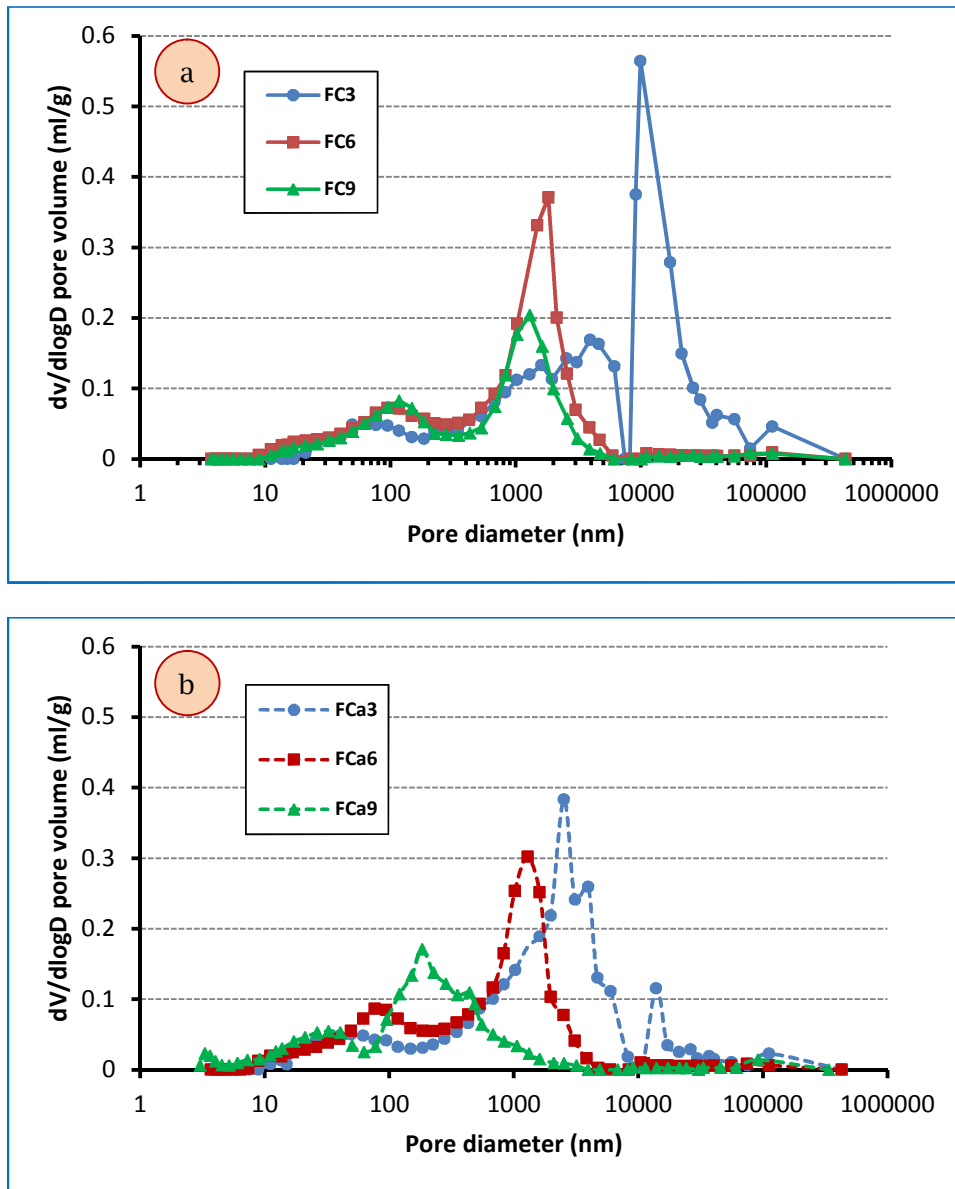
Figure 6-19 Critical pore diameter of (a) Conventional (b) with additives foamed concrete mixes
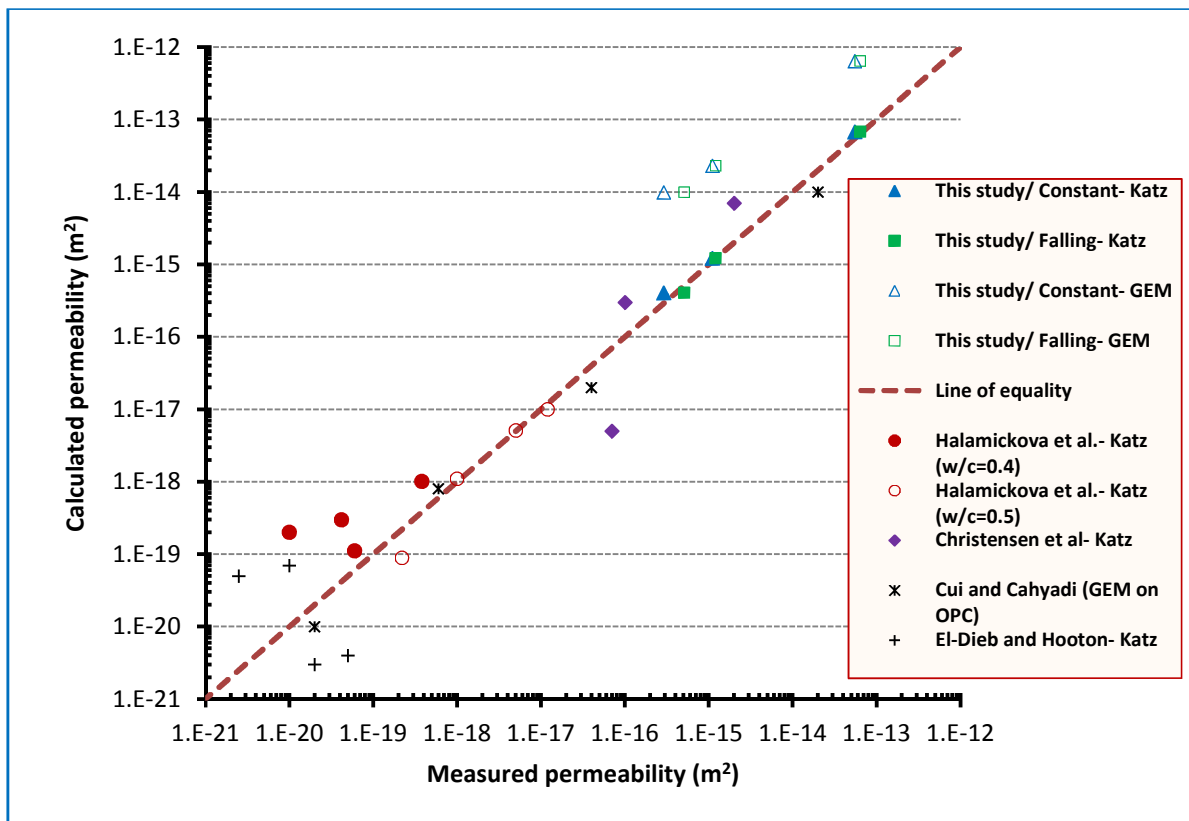
Figure 6-20 Comparison between the measured and calculated permeability values

6.5 Effect of Voids Structure Characterisations on Permeation Characteristics

It is well known that the durability of concrete depends on its transport properties which are affected by the pore structure (Yang et al., 2006). The relationship between porosity and water vapour permeability was studied in foamed concrete and cement pastes by Kearsley and Wainwright (2001b). In their study, it was concluded that water vapour permeability increases with increased porosity, or decreased density, with similar trend lines for mixtures both with and without foam. Kearsley and Wainwright (2001b) concluded that porosity of foamed concrete is largely dependent on dry density. This type of relationship can also be seen in **Figure 6-21** with the relationship of permeability with dry density. It can be seen

that, there are inverse relationships for both porosity and permeability with dry density leading to a positive relationship between porosity and permeability, **Figure 6-22**. From these two figures, it is obvious that the air permeability coefficient decreases with an increase in the density or decrease in the amount of added foam (porosity). Moreover, by decreasing the porosity from about 52% for FC3 to 29% for FC9 the permeability decreases by about 200 times indicating a highly non-linear relationship between them. This means that not only the volume of voids but also their connectivity (usually higher with increased added foam, see **Table 4-3**) is controlling the air permeability. From **Table 6-1**, the inclusion of LWA resulted in increasing the air permeability (both constant and falling methods) of FCL6 and FCLa6 mixes compared to the same density mixes, FC6 and FCa6. This may be due to increased void connectivity of the mixes owing to the connected pores nature of LWA, see **Figure 6-13**.

In order to determine the distribution of pores and their relationship to permeability from the intrusion curves (determined by the MIP test) and after adding the difference in voids volume between the vacuum and MIP tests (voids of size higher than 400 μm), the porosity in a specified range of pore sizes was normalized by the total porosity into two ranges of pore width, <200 nm, and >200 nm, **Figure 6-23**. The second range is mainly related to the permeability of cementitious material (Yang et al., 2006, Akçay, 2007). From **Figure 6-23**, it is obvious that the pore range with diameter >200 nm decreases with increase in the density of foamed concrete resulting in decreasing permeability, **Figure 6-24**.

In a study on permeability and pore structure of ordinary Portland cement paste, Cui et al. (2001), defined a critical pore diameter (l_c) as the pore diameter above which a connected path could form through a sample and added that the smaller the l_c, the finer the pore structure. Since the critical pore diameter (l_c) represents the grouping of the largest fraction of interconnected pores (Yang et al., 2006), it

can be expected to influence the transport properties such as permeability and from **Figure 6-24**, it can be seen that there is a positive relationship between the critical pore diameter and the permeability of foamed concrete.
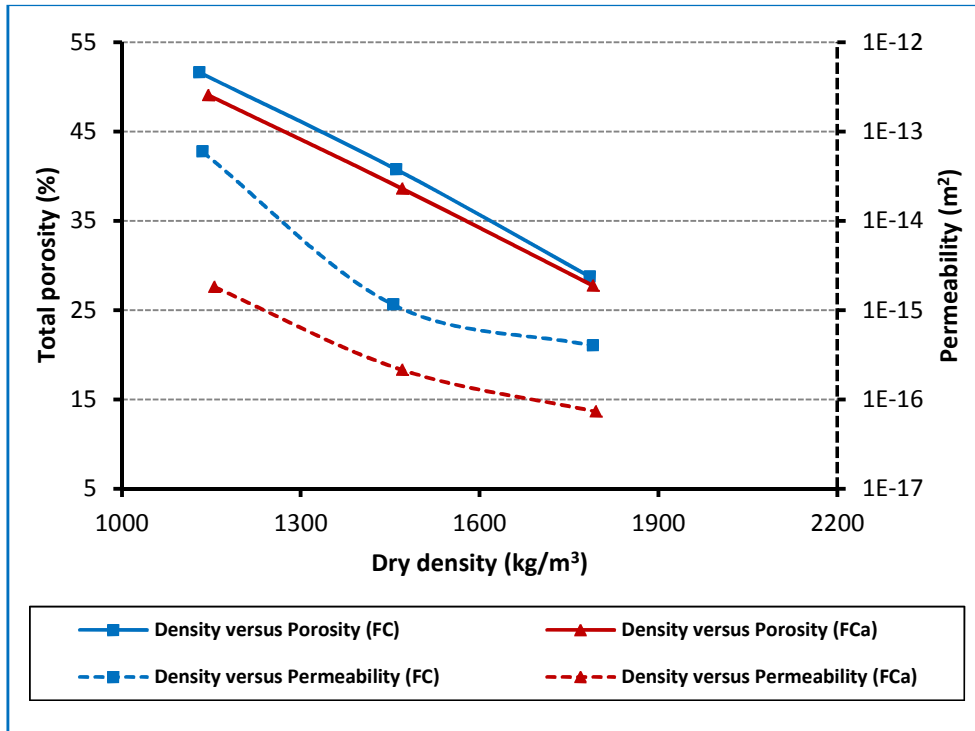
Figure 6-21 Porosity and permeability as a function of dry density
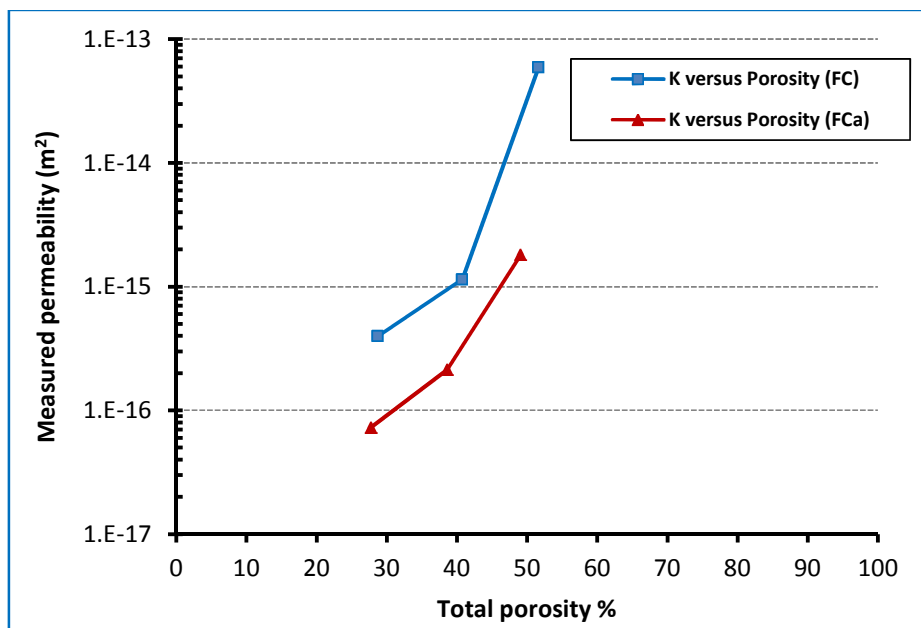
Figure 6-22 Air permeability versus porosity of the selected mixes
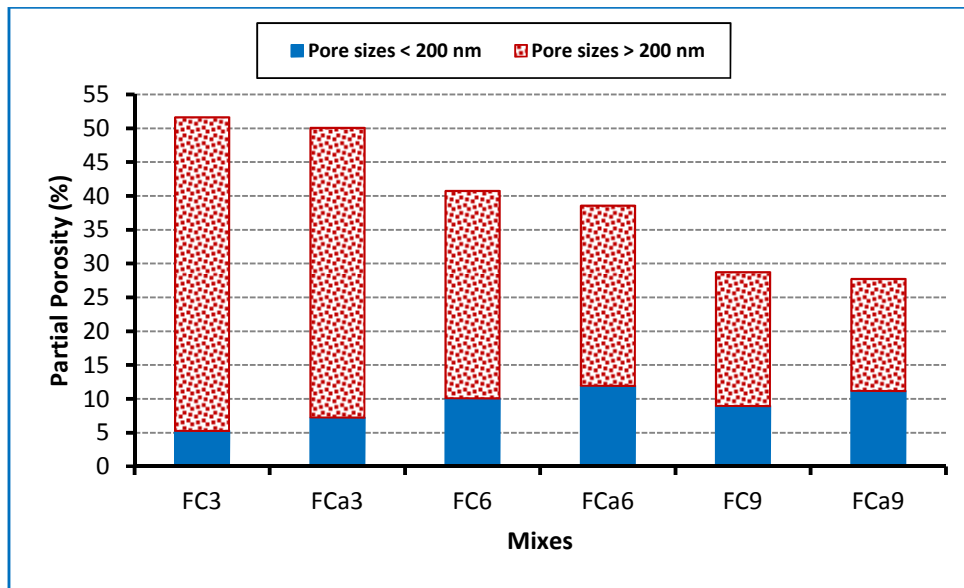
Figure 6-23 The distribution of pores as a partial porosity (%)
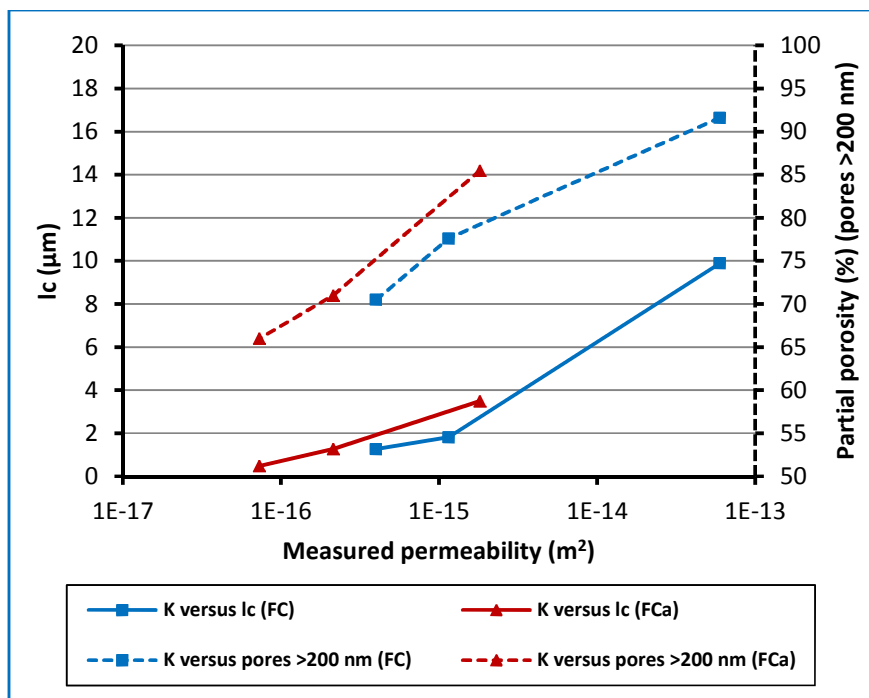
Figure 6-24 The relationships between measured permeability and both critical pore diameter (lc) and partial porosity (pores >200nm)

6.6 Summary

This chapter has presented the work undertaken to investigate the permeation properties (water absorption, sorptivity and permeability) of pre-formed foamed concrete with a nominal density between 1300 and 1900 kg/m³ and to examine the effect of the void structure characterisation (porosity and critical pore diameter) on these properties.

Different measured and calculated methods were adopted to determine the above properties and a comparison between them was done. Permeability was measured (by constant and falling head methods) and calculated (by the Katz and Thompson model).

From the tests carried out on the selected mixes and based on the results and discussion, the following conclusions can be drawn:

- For conventional foamed concrete mixes, although porosity increases with a reduction in density (due to an increase of the foam volume), the water absorption (% by volume) exhibits a reduction. Therefore, many of the artificial pores due to the added foam are not taking part in water absorption due to their weaker suction compared to that of capillary pores.

- Adding additives (individually or in combination) helped in reducing the sorptivity of foamed concrete. However, inclusion of LWA resulted in increased sorptivity compared to the same density mixes, conventional or with additives in combination.

- For all investigated mixes, the sorptivity values of unfoamed mixes were higher than those of corresponding foamed concrete mixes and the sorptivity reduction (from unfoamed to foamed mixes) was greater for mixes without a superplastisizer than those with it.

- The predictive permeability equation derived by Katz and Thompson best fits the air permeability results determined in this study. However, the general effective media model (GEM) is not suitable for a porous material but it appears to be a suitable tool for cementitious materials with low porosity.

- The critical pore diameter (from the MIP test) and the pore volume >200nm are found to be closely related to the permeability of foamed concrete.

Chapter 7: Damage Evaluation

7.1 General

In this chapter, damage of foamed concrete mixes is evaluated at both macro and micro levels under compressive and tensile loading using different techniques. The Digital Image Correlation (DIC) technique was adopted to investigate macrocrack initiation and propagation and to measure the strains on the surface of a specimen under uniaxial compressive load. In addition, Scanning Electron Microscopy (SEM) with image processing software (ImageJ) was employed to investigate the microcracks formed under compressive load both quantitatively (density, distribution and orientation) and qualitatively (formation and propagation) in order to understand the cracking phenomena. Moreover, the ductility of the investigated mixes is examined from the elasticity, fracture and fractal points of view. Finally, a summary is presented at the end of this chapter.

7.2 Digital Image Correlation (DIC)

Nemati et al. (1998), stated that there are several methods to study microcracking in concrete such as acoustic emission, microscopic techniques with dye, x-ray, optical and electron microscopy. However, it was concluded that some of these techniques may not allow appropriate observation of large areas, have limited resolution or are not precise in crack detection. In addition, other methods are not suitable for examining the specimens during loading or may require special sample preparation which results in altered the behaviour of the material.

The DIC technique has been used in various aspects by many researchers because it is simple, full-field and contactless. It is a technique for large deformation/strain measurements at thousands of points on the specimen surface. Lecompte et al. (2006) defined DIC as an optical-numerical full-field displacement

measuring technique which is based on a comparison between pictures taken during specimen loading.

The displacements can be computed between two selected images, a reference and a deformed image, captured at different loading stages by using a charge-coupled device (CCD) camera. To compute the displacement values in X and Y directions, firstly, a subset image is selected on the reference image. Then, this subset image is found on the deformed image (**Figure 7-1**) by using a mathematical function (a correlation coefficient of cross or normilized correlation terms). This correlation coefficient depends on the intensity (I) of both the pixel at (x,y) in the reference image (Image 1) and the pixel at (x+Δx, y+Δy) in the deformed image (Image 2) as well as the number of pixels in the subset image. It gives a higher value when the patterns of the two subset images are more similar and it becomes 1 if these subset images are exactly the same, while if there is no correlation it becomes zero. Thus the idea is to track a point by finding its correlation coefficient from the intensity (grey level) point of view. By repeating this process on a large number of subset images, full-field deformation or displacement data can be obtained (Choi and Shah, 1997, Lawler et al., 2001, Wang et al., 2010). It should be noted that, in this study, it was assumed that every visible strain concentration indicated a crack.
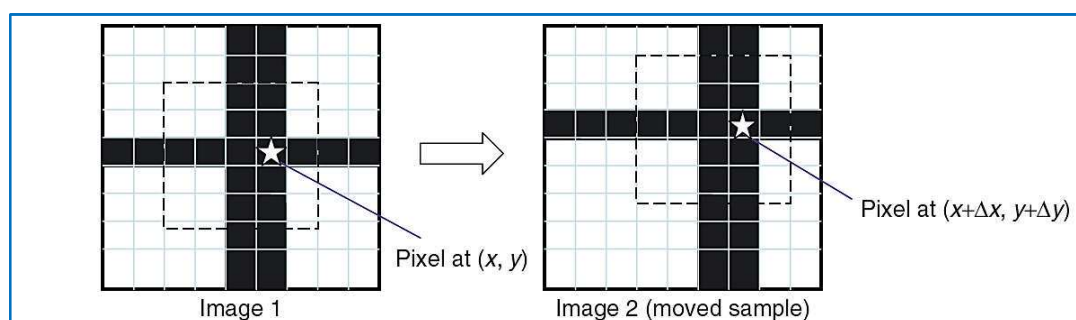
Figure 7-1 Images taken before and after deformation (Wang et al., 2010)

Compared to other methods, there are some important advantages to using DIC in studying the fracture of cementitious materials. Firstly, it does not have technical limitations relating to multiple cracks. Secondly, measured values would not be disturbed by the development of a crack because there is no need to attach gauges to the specimen and therefore the measurements are not disturbed while failure progress. Thirdly, due to the use of different subset images for each measurement, displacement by this technique can be measured on the specimen while it is fractured into multiple parts during a loading test. Finally, unlike some sensitive techniques, the DIC method is not affected vibration problems which are often generated by hydraulic testing machines (Shah and Choi, 1999).

For compressive tests, two $50{\times}50{\times}100mm^3$ prisms, cut from a $100{\times}100{\times}100mm^3$ cube, were used. Since the concrete surface is a homogenous region, images on it cannot be reliably matched. Therefore to make the surface heterogeneous, all specimens were painted first with white spray and then a black paint sprayed directly on the white surface as black dots, see **Figure 7-2**.
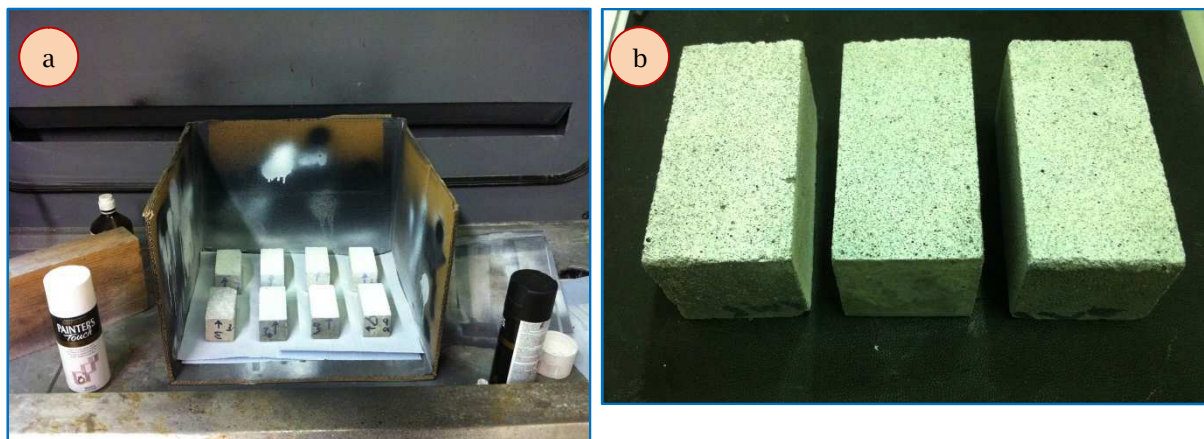
Figure 7-2 Specimens preparation for DIC test (a) during painting (b) after painting

During testing, the compressive load was applied using an INSTRON machine, having a load capacity of 250 kN, by maintaining a constant rate of vertical deformation 0.0025 mm/s. Two digital cameras (CCD) were used to acquire digital images of the specimen surface during each test. These images were sent to an image-processing computer with the capability of image storage, display and graphics. The test setup is shown in **Figure 7-3**.
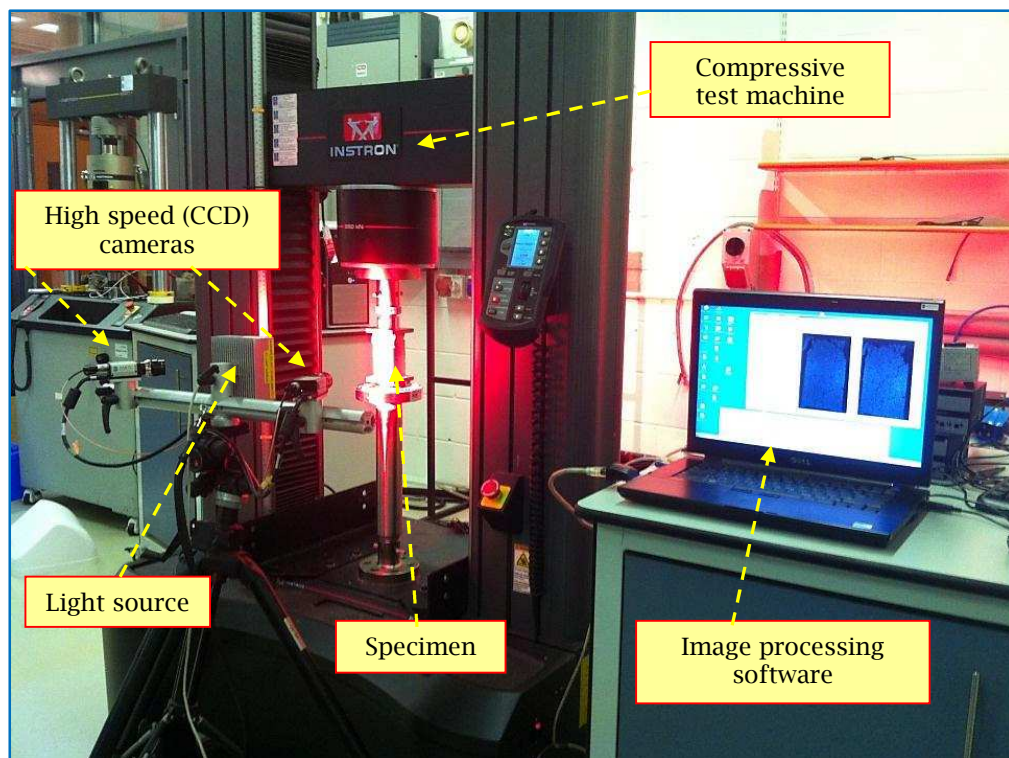
Figure 7-3 DIC setup at the testing site

In this project, the DIC technique was used to measure the displacement and the strain on foamed concrete specimens under uniaxial compressive load and to investigate the crack failure development during loading, see **Figure 7-4**.
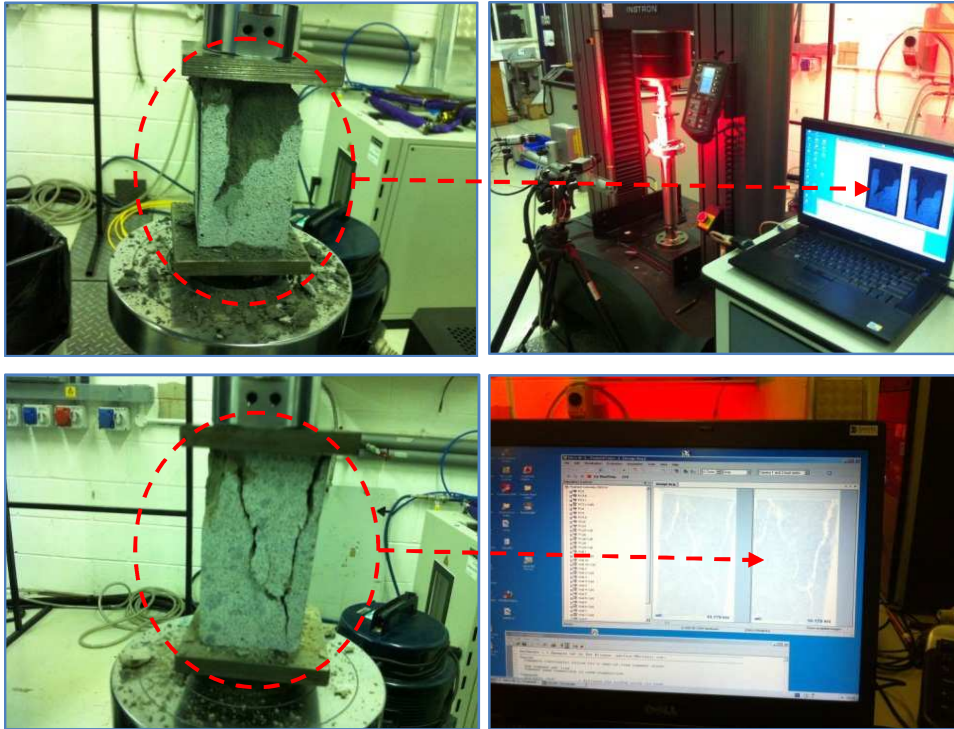
Figure 7-4 Actual failure and that capturing by the high speed cameras

7.3 Fracture Energy and Brittleness

Because of its stable pre-peak crack growth and strain-softening post peak, concrete is typically classified as a quasi-brittle material. Fracture mechanics has become a popular tool to quantify the brittleness of concrete (Babu, 2008). Brittleness is commonly understood to be the tendency for a material to fracture suddenly before significant irreversible (plastic) deformation has developed. A parameter used to describe the brittleness of cementitious materials is the characteristic length l_{ch} (mm) which is defined as:

$$l_{ch} = \frac{E.G_f}{f_c^2} \qquad\qquad (7\text{-}1)$$

where E, G_f and f_c are the modulus of elasticity (MPa), fracture energy (N/mm) and compressive strength (MPa) of concrete, respectively. The l_{ch} is proportional to G_f (a high fracture energy leads to a tougher concrete) and also has inverse dependence

on f_c (strong concrete is brittle). Therefore, a balance between G_f and f_c is required to produce a ductile concrete (Rosselló et al., 2006). It has been stated that l_{ch} represents the size of the fracture zone and thus as it decreases a more brittle behaviour appears (i.e. the lower the l_{ch}, the lower the ductility) (Giaccio et al., 2007). On the other hand, depending on the toughness/strength ratio (G_f/f_c), a relative ductility of the mix can be determined (Chiaia et al., 1998).

Design of reinforced concrete structures is based on the ultimate strength capacity which includes a portion of the post-peak behaviour, i.e. strain-softening, of concrete in uniaxial compression. In addition, characterising the post-peak behaviour is necessary in predicting the ductility and ultimate axial deformation of concrete (Jansen and Shah, 1997).

In their study of measurement of deformation on concrete subject to compression, Choi and Shah (1997) found that a full-field measuring system based on digital image correlation, compared to linear variable differential transformers (LVDT), was successfully able to measure the surface deformation in compression. In the current study, the load-displacement diagram was used to examine the compression fracture energy. From the DIC data, **Figure 7-5** shows the full load-displacement relationship of different foamed concrete mixes, two prisms (50×50×100 mm) for each mix, under uniaxial compressive load. In this study, there is a wide variation in the maximum displacement of different specimens; therefore to estimate a comparable evaluation of fracture energy it was decided to calculate up to 33% of the peak load. The fracture energy (N/mm) was obtained by computing the work done W_f (the area under the load-displacement curve, kN.mm) up to 33% of the maximum load at the post-peak portion (Jansen and Shah, 1997) and dividing it by the cross-sectional area of the specimen (mm²).

Table 7-1 summarises the results of fracture energy G_f and characteristic length l_{ch} for the investigated foamed concrete mixes. The FCa9 mix shows the highest

peak load, whereas FCLa6 is characterised by the highest fracture energy. If the work done (W_f) represents a measure of toughness (Chiaia et al., 1998), the FCLa6 has the largest toughness. On the other hand, from the brittleness point of view, mixes without additives (FC) are more ductile compared to those with additives having a similar density. However, for all mixes, the lower the density the higher the ductility.

Compared to mixes without LWA, for a given density, inclusion of LWA leads to improved ductility of mix with and without additives, FCLa6 and FCL6, respectively (i.e. FC6 and FCa6 mixes were more brittle). This may be because of the weakness of LWA which causes a limited macro crack-arresting capacity and a stable manner of crack propagation through the LWA (Chiaia et al., 1998). The brittleness can also be deduced from the load-displacement curve; the steeper the slope of the descending branch, the more brittle is the material.
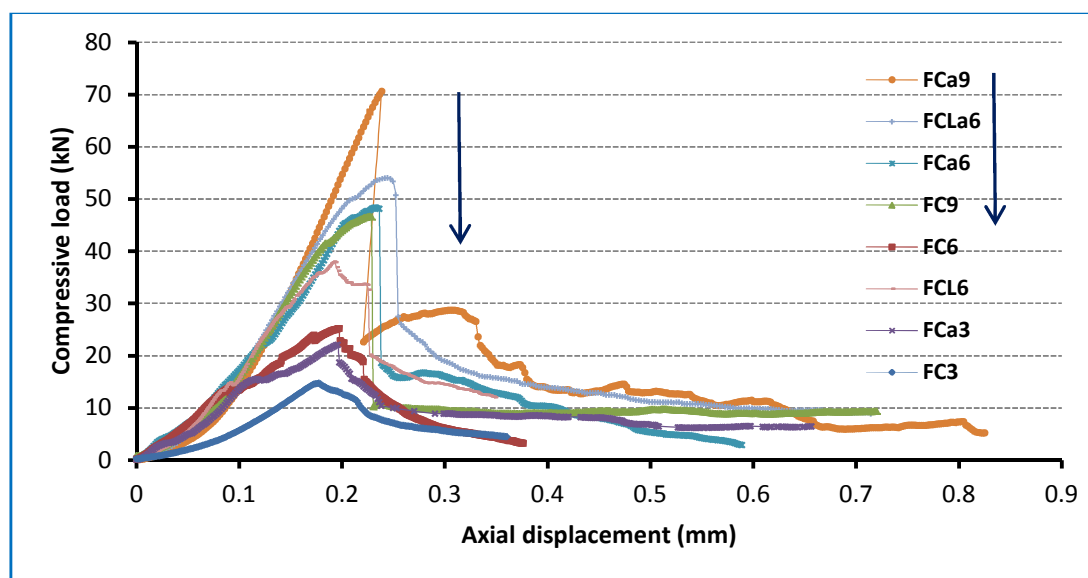
Figure 7-5 Load- axial displacement relationships

Table 7-1 Results of fracture energy and characteristic length

Mixes	FC3	FC6	FC9	FCa3	FCa6	FCa9	FCL6	FCLa6
W_f (kN.mm)	3.44	3.71	5.13	5.01	5.57	6.21	6.66	7.93
G_f (N/mm)	0.687	0.742	1.025	1.000	1.113	1.241	1.331	1.587
l_{ch} (mm)	0.119	0.066	0.049	0.083	0.034	0.026	0.076	0.044
Ductility	0.117	0.074	0.055	0.113	0.058	0.044	0.094	0.073

7.4 Load-deflection in Tension

Splitting tensile tests were conducted on discs (100Ø×25 mm) with a Stingray camera and image processing software (Imetrum-Video Gauge) to measure the horizontal deformation between two points located at the middle of the specimen as shown in **Figure 7-6**. This technique was used to avoid damage to Linear variable differential transformers (LVDTs) at specimen failure since it is a noncontact method. The principle of this technique is simillar to that of the DIC technique.
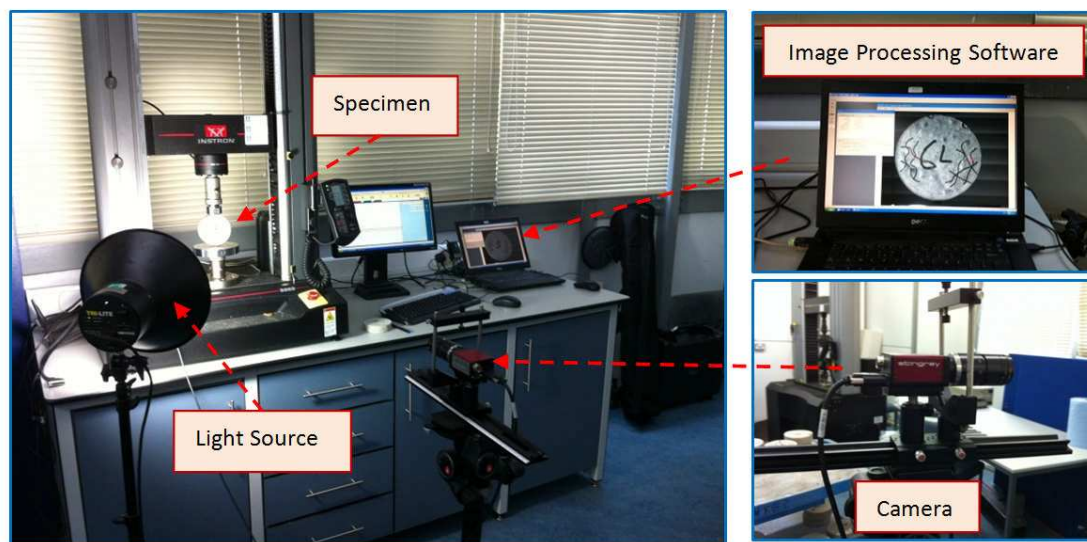
Figure 7-6 Splitting test set-up

Two specimens were tested for each mix and the fitting lines of the averaged results of the investigated mixes are shown in **Figure 7-7**. It can be seen that the curves for mixes with additives (FCa) are steeper than those for conventional mixes

(FC) and this is also the case for mixes with LWA. If the lateral displacement represents the crack width, it is obvious that the crack width at failure increases with increased density, and for a given density it increases with additives. In addition, using LWA helped to increase the crack width compared to a similar density mix without LWA. In general, for a given group (FC, FCa or FCL), the stronger the concrete the larger the lateral deformation before failure. During testing, it was noticed that, except for the FC3 mix, all investigated specimens were split into two parts at the peak load, see **Figure 7-8**. This prevented the complete load-deformation relationship to be obtained and thus there was no chance of calculating the fracture energy of the pre- and post-peak portions in tension.
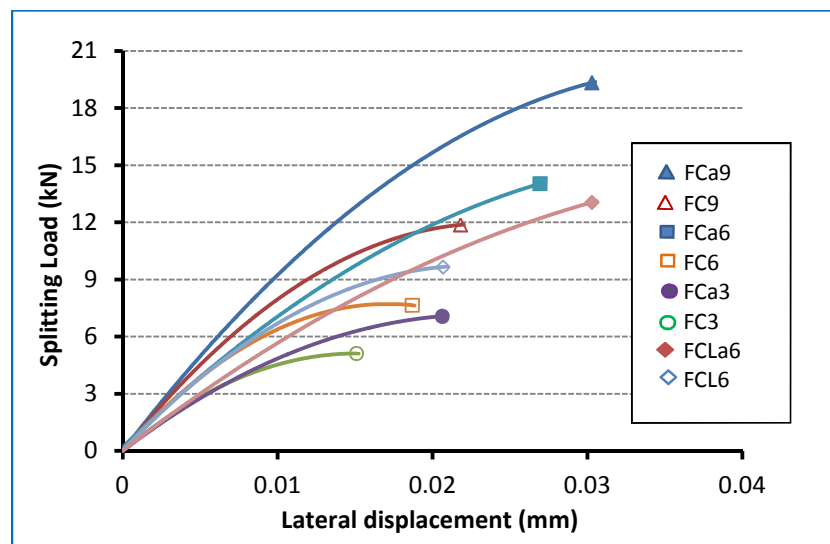
Figure 7-7 Splitting load versus lateral deformation of the investigated mixes
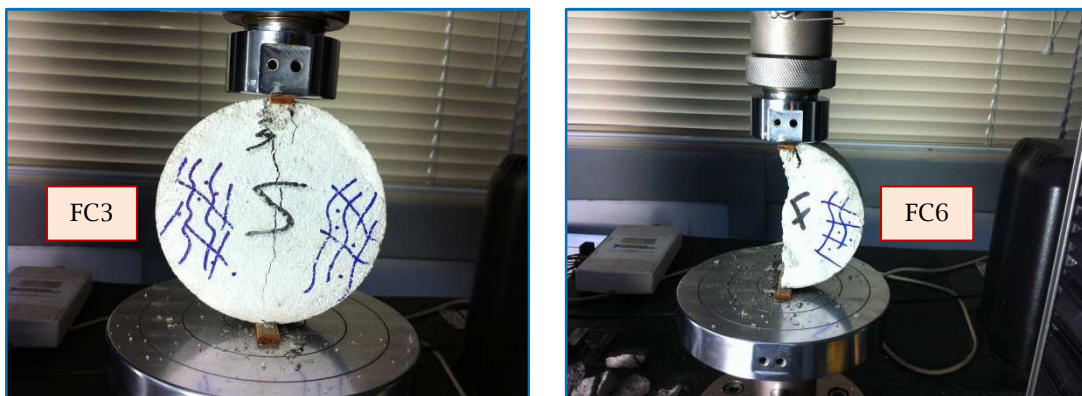
Figure 7-8 Specimen failure after splitting test

7.5 Stress-Strain Behaviour in Compression

The failure of concrete under uniaxial compression is either a tensile failure of cement crystals or of bond in a direction perpendicular to the applied load, or is a collapse caused by the development of inclined shear planes (Neville, 2011). Its mechanism involves the growth and propagation of ITZ and bond cracks which are reflected in the stress-strain behaviour (Giaccio et al., 2007). Neville (2011) stated that one view of concrete failure is to associate it with the discontinuity point at which the volumetric strain ε_v stops decreasing due to development of extensive mortar cracks. This point represents the beginning of instability and sustained loading above this point will lead to failure.

It should be noted here that to measure the axial ε_A and lateral ε_L strains, vertical and horizontal potentiometers were fixed, as an initial trial, on a 150Ø×300 mm cylinder as shown in **Figure 7-9a**. However, it was found that the lateral strain behaviour (**Figure 7-10**) was not compatible with that of brittle materials, such as concrete, even after changing the fixing method of the horizontal potentiometers, see **Figure 7-9a**, **b**). Therefore, it was decided to adopt another technique, namely Digital Image Correlation (DIC) which has been proved as a successful system to measure the deformation on a concrete surface in compression (Choi and Shah, 1997).

Based on the stress-strain curves obtained from the DIC data, **Figure 7-11**, the critical stresses can be obtained. The critical stresses represent the onset of unstable propagation of cracks in the concrete matrix and are defined as the stresses corresponding to the minimum peak of strains in the volumetric strain curves ($\varepsilon_v=\varepsilon_A+2\varepsilon_L$) (Giaccio et al., 2007). The results of critical stresses as percentages of the corresponding compressive strengths are shown in **Figure 7-12**. As can be observed from this figure, the percentage increases with increased density (reduced added foam) and for a given density it increases with inclusion of additives in

combination. This indicates that the period of unstable crack propagation through the mortar matrix (between the critical and peak stresses) is reduced, showing a tendency to a more brittle failure mechanism. In addition, adding LWA helped in decreasing the critical stress percentage leading to more ductile behaviour compared to mixes with the same density but without LWA.
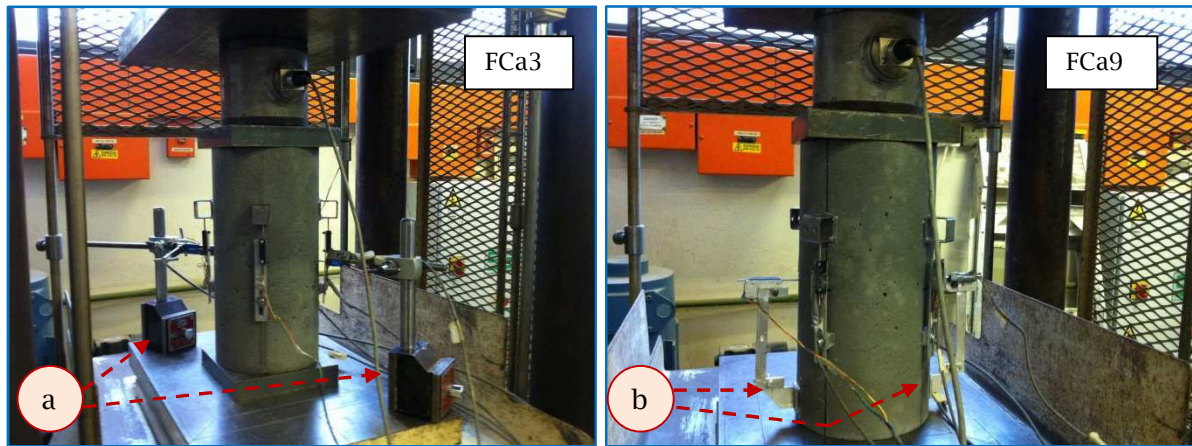
Figure 7-9 (a) Horizontal potentiometers fixed on the base (b) Horizontal potentiometers fixed on the specimen
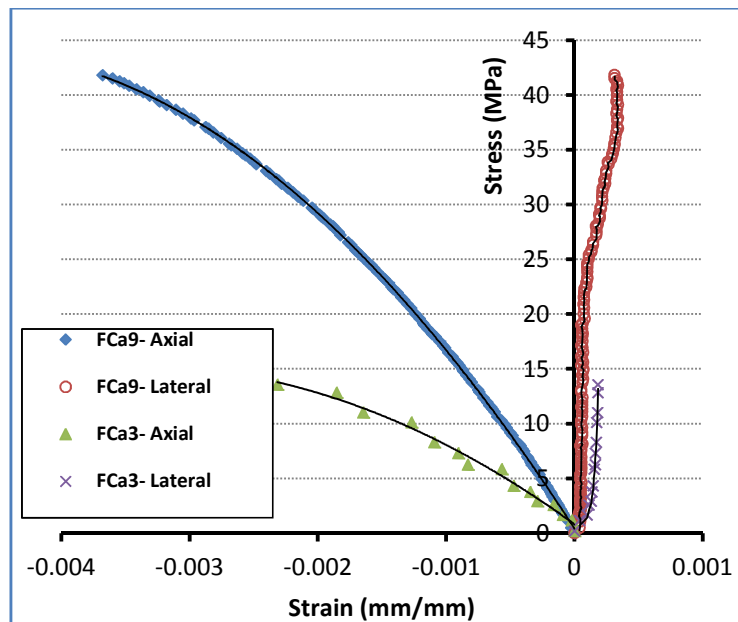
Figure 7-10 Stress versus axial and lateral strains in compression using horizontal and vertical potentiometers
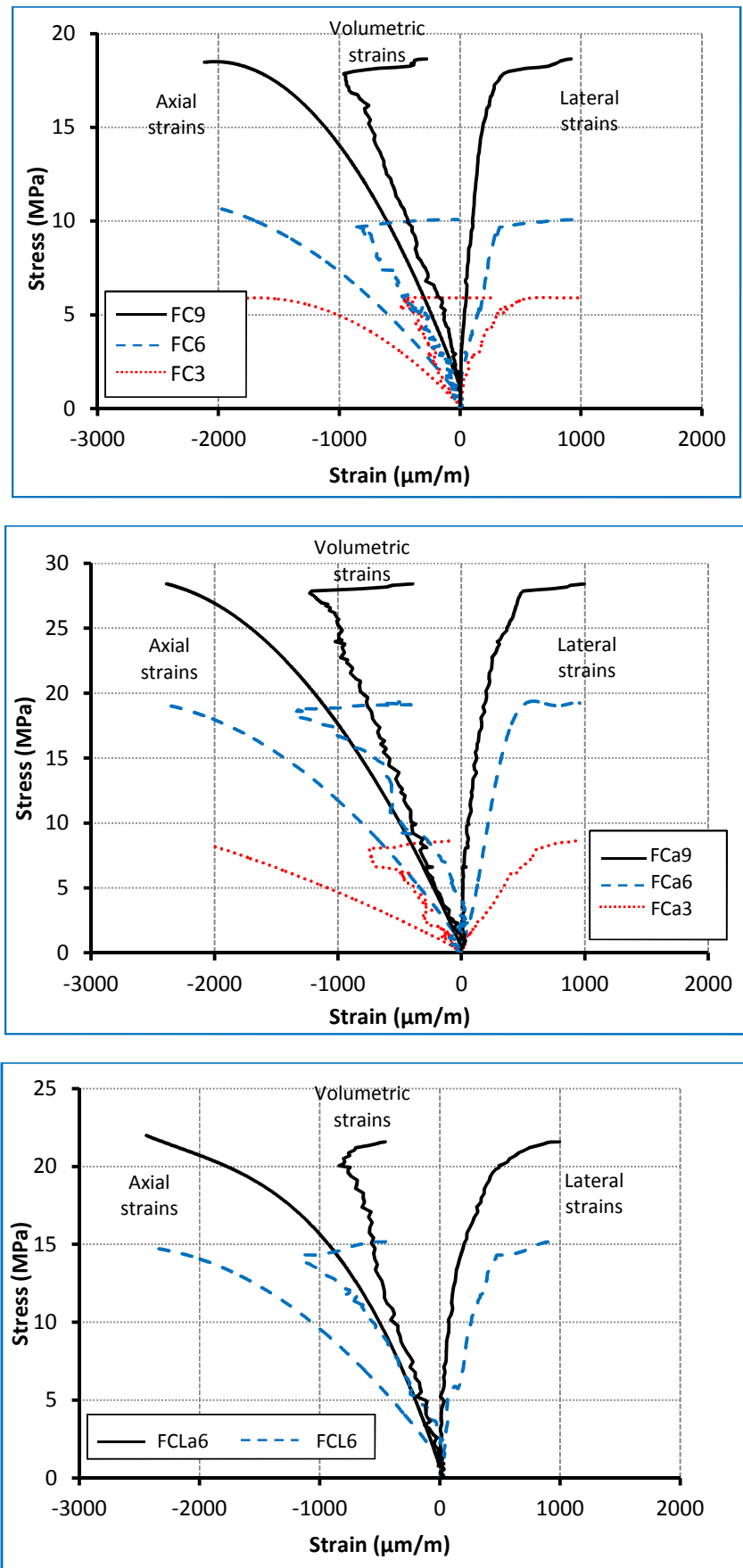
Figure 7-11 Stress versus axial, lateral and volumetric strains in compression using DIC technique
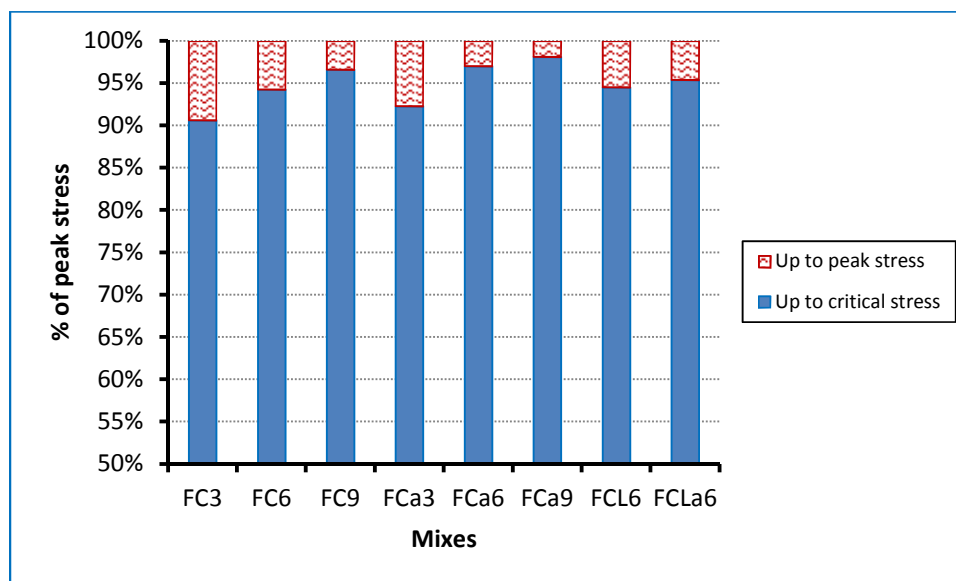
Figure 7-12 Critical stresses in the investigated mixes

7.6 Macro and Microcracks

7.6.1 Macrocracks in Compression

It is well known that cracks in concrete develop under load as a result of tensile stress. The data produced by the DIC technique provide insight into the mechanisms of crack propagation in foamed concrete at three stages: microcrack growth (before peak), peak and the stage of branching and bridging of macrocracks (after peak), see **Figure 7-13**.

From **Figure 7-14**, some points can be observed as follows: the DIC technique is a successful system at detecting very small cracks which are not visible to the naked eye. In terms of crack propagation, they seem to propagate from the specimen corners of the FC3 specimen, while they not only propagate from the corners but also along the edge of the FCa3 specimen. For the most dense mixes, the main crack seems to develop from the corner for the FC9 specimen, while the crack take a vertical orientation and does not initiate from the FCa9 specimen corner. However, the failure behaviour of FCa9 is quite comparable to that of FC9 since the longest cracks propagate over most of the length of the specimen. In general, more direct and vertically oriented cracks were detected within the most

dense mixes (less added foam) indicating fast crack propagation and more brittle behaviour. Meanwhile, in the lowest density mixes more tortuous cracks were detected leading to more ductile behaviour.

Figure 7-15 shows the failure pattern of 1600 kg/m³ mixes and it can be seen that the cracks in mixes with LWA are more tortuous indicting increased ductility compared to mixes without LWA.
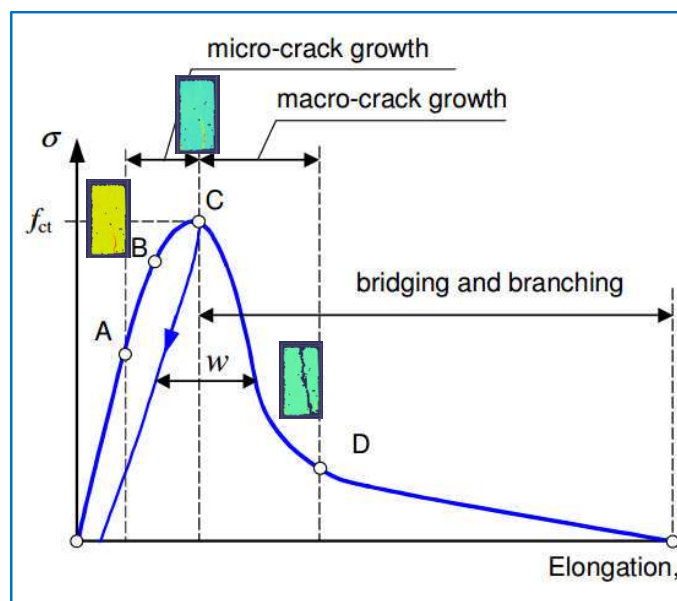
Figure 7-13 The selected stages at which cracks were investigated, after (Lofgren, 2005)
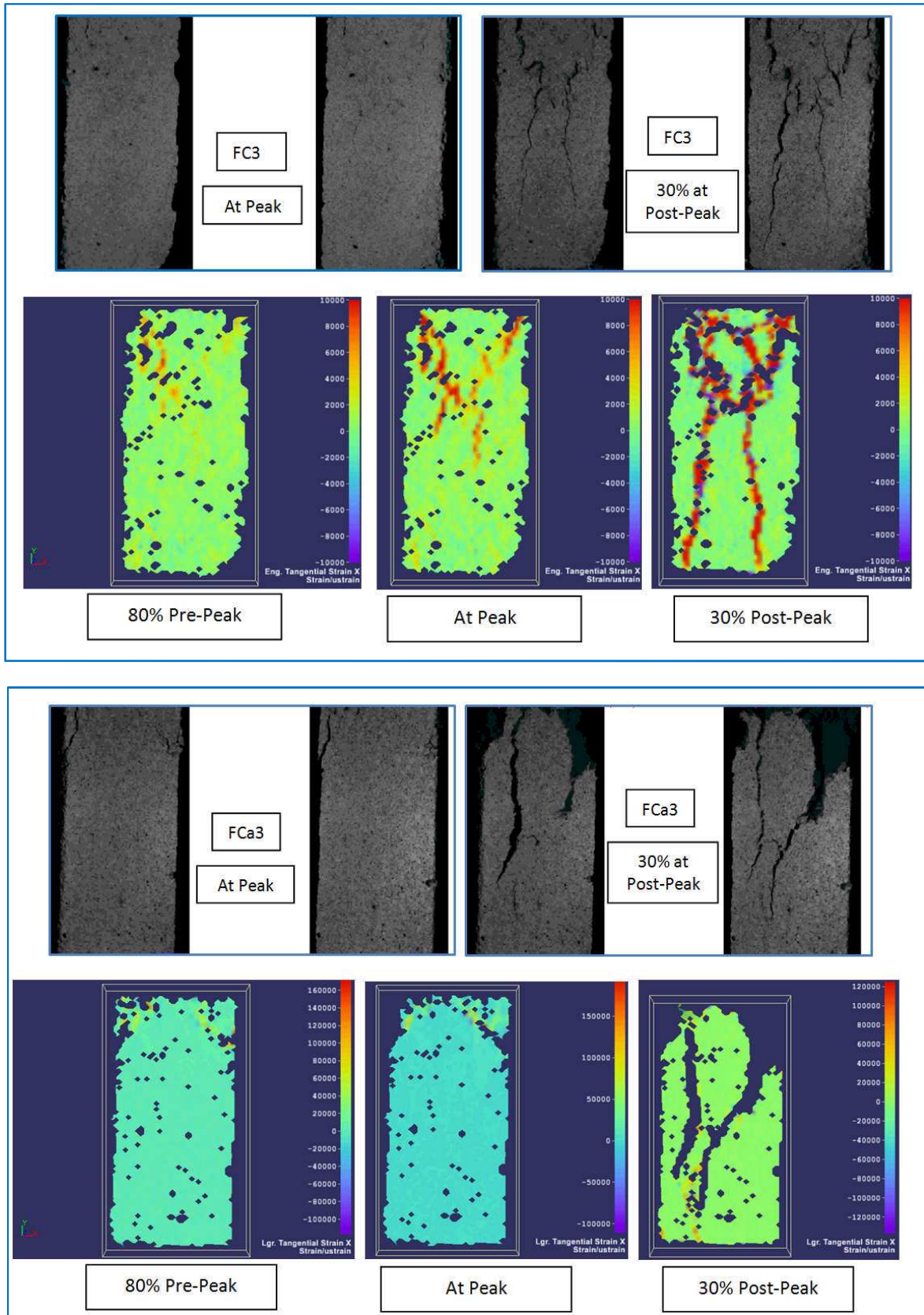
Figure 7-14 Cracks in selected foamed concrete specimens at different loading stages
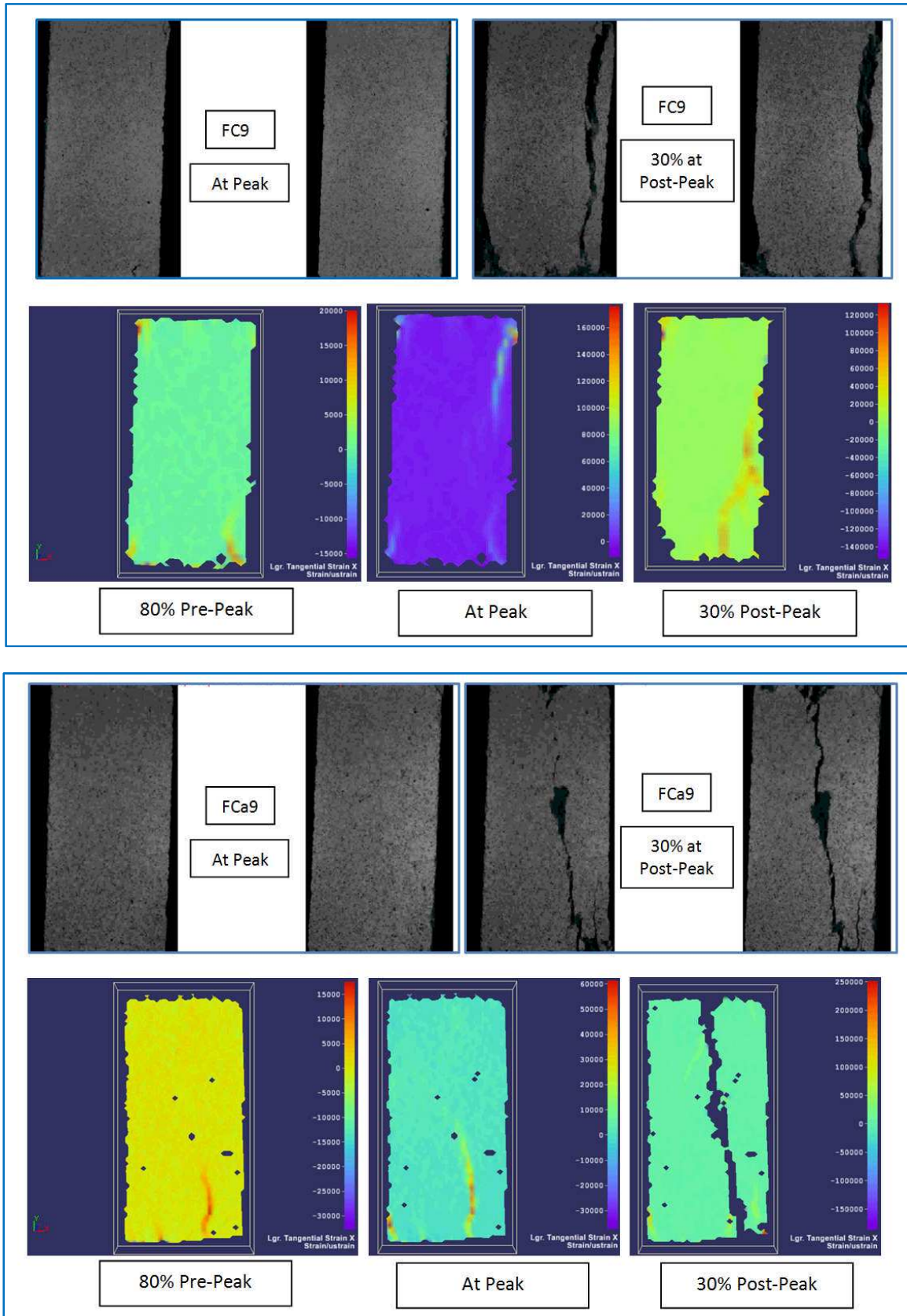
Figure (7-14) continued: Cracks in selected foamed concrete specimens at different loading stages
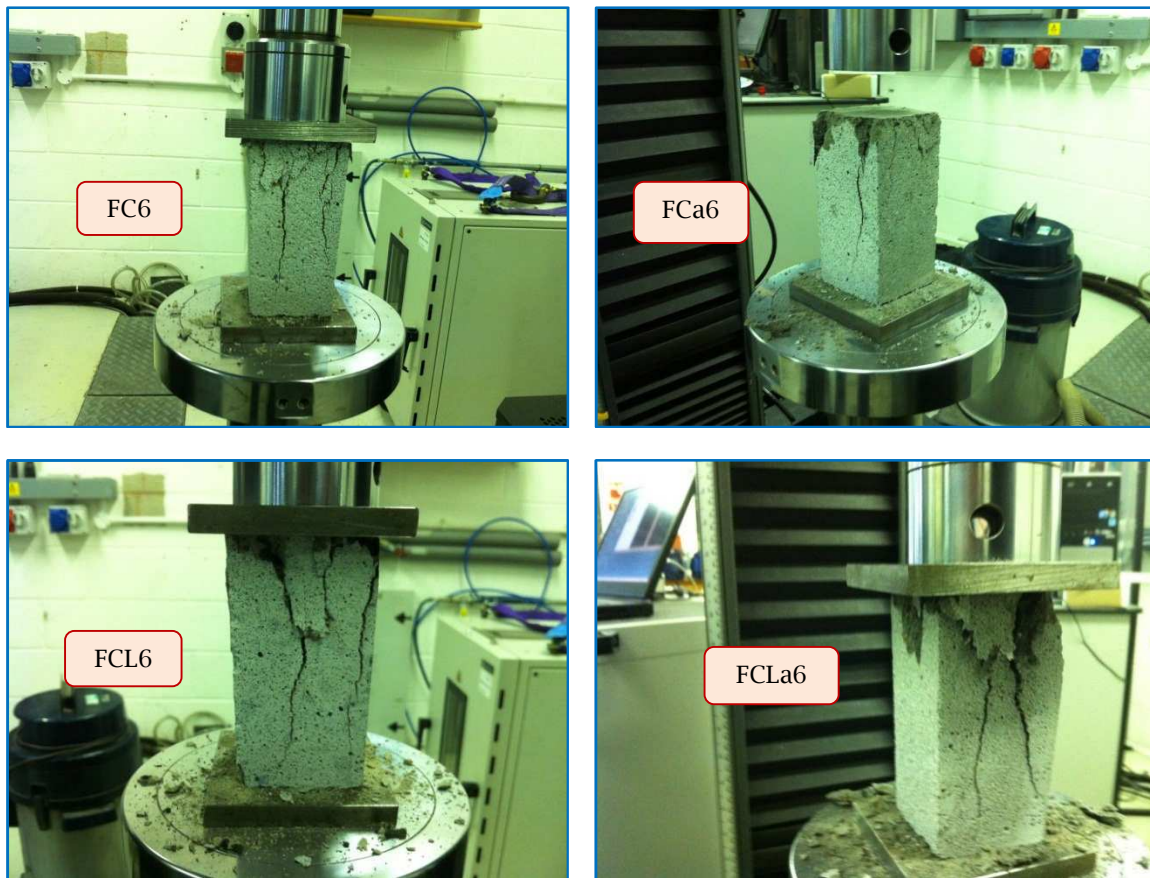
Figure 7-15 Failure pattern of 1600 kg/m³ mixes

7.6.2 Fractal Dimension

The 'zigzag' content of surface macrocracks may reflect the effect of additives (microstructural changes) on the fracture properties of foamed concrete. One method to estimate this influence is by the fractal dimension of surface macrocracks. The definition and determination of fractal dimension D are described in a study of the relationship between fractals and fracture by Charkaluk et al. (1998).

The fractal dimensions of cracks were computed by means of the box-counting method in ImageJ software. In this method, the digitized crack is covered with a rectangular mesh with different grid sizes (x_1, x_2, …). By varying x and counting the number of grids, a logarithmic plot of log(N) versus log(1/x) can be drawn. The

slope of the fitting line is the fractal dimension D (Guo et al., 2007), see **Figure 7-16**. As the appearance of the crack path becomes more complicated so the fractal dimension becomes larger.

$$D = \lim_{x_i \to 0} \left(\frac{logN(x_i)}{log(\frac{1}{x_i})} \right)$$
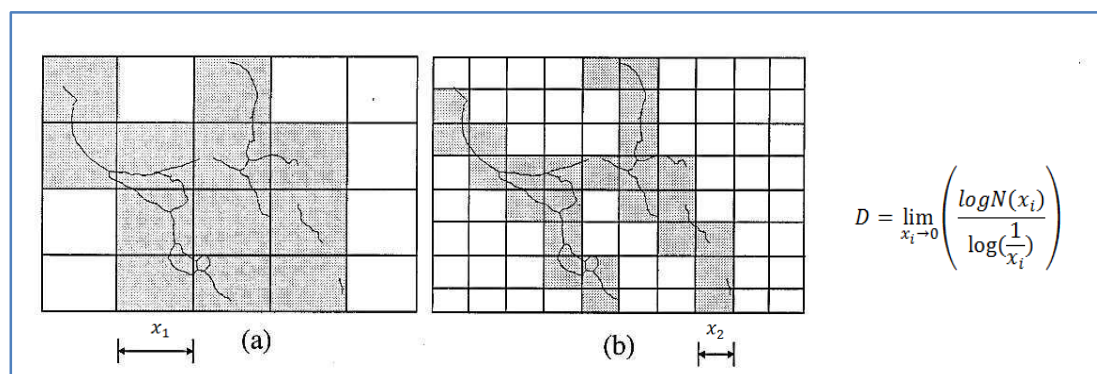
Figure 7-16 The box counting method applied to crack patterns, after (Chiaia et al., 1998)

Macrocracks on the surfaces of disc specimens (100Ø×25 mm, tested in splitting tensile mode) were examined by means of fractal dimension. It can be seen from **Figure 7-17** that with incorporation of additives, the surface macrocrack becomes more complicated making its fractal dimension higher than that of the conventional mix. **Figure 7-18** shows the fractal dimension results versus the fracture energies of the selected mixes. It can be seen that D decreases with increased added foam and with a given density it increases with additives or LWA. From **Figure 7-18**, it is evident that there is a good correlation between the fractal dimensions and the fracture energies of the foamed concrete mixes investigated in this research. However, Charkaluk et al. (1998) stated that a general conclusion cannot easily be drawn about the correlation of fractal dimension of fractured surfaces with fracture toughness since some workers reported a positive variation but others found it to be negative. The failure pattern of some of the specimens investigated is shown in **Figure 7-19**.
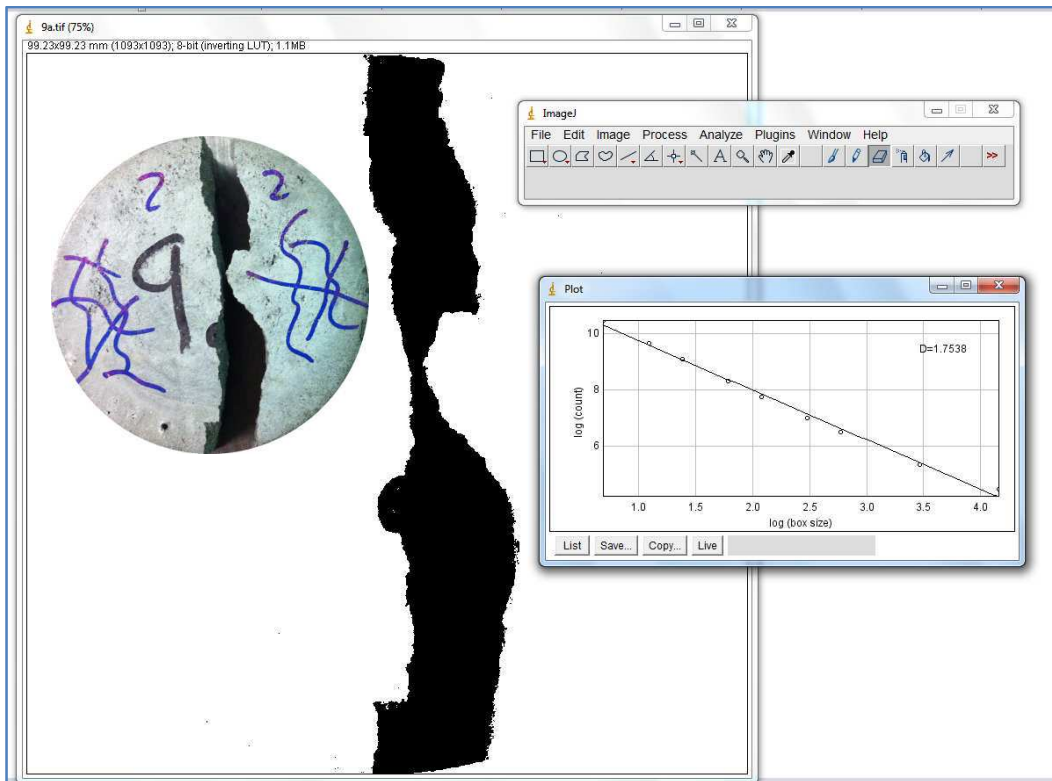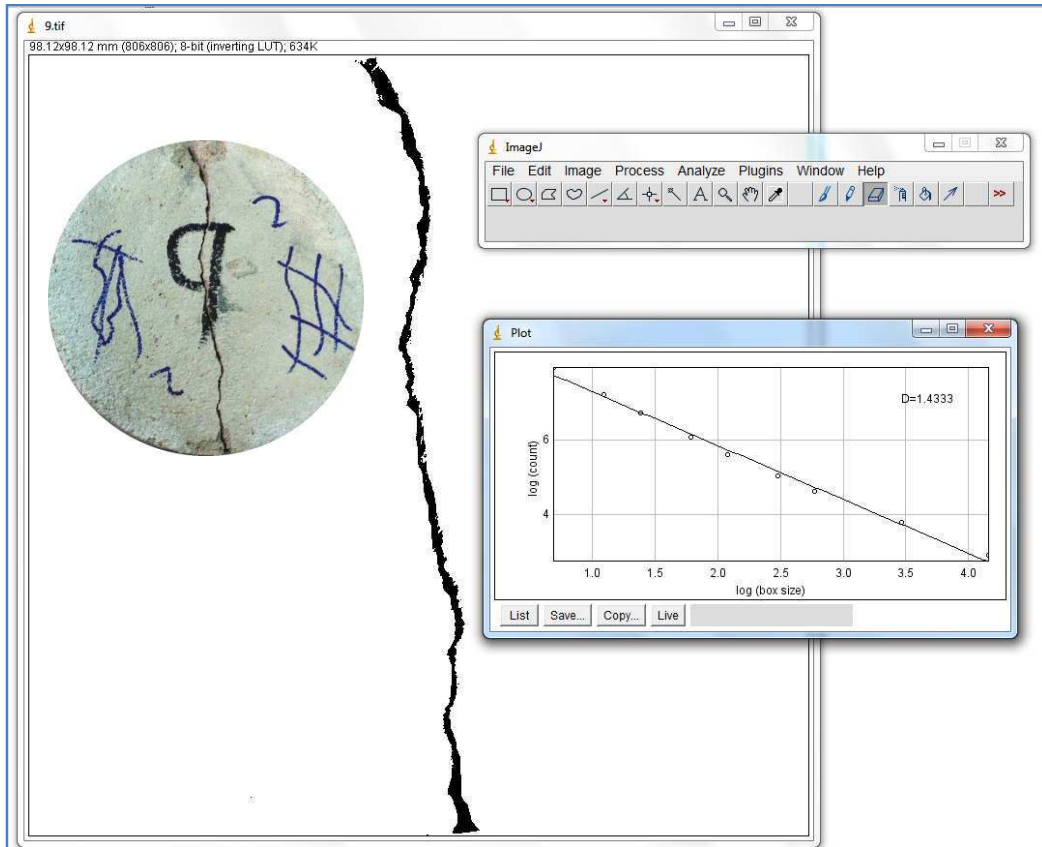
Figure 7-17 Fractal dimension of FC9 (above) and FCa9 (below) mixes
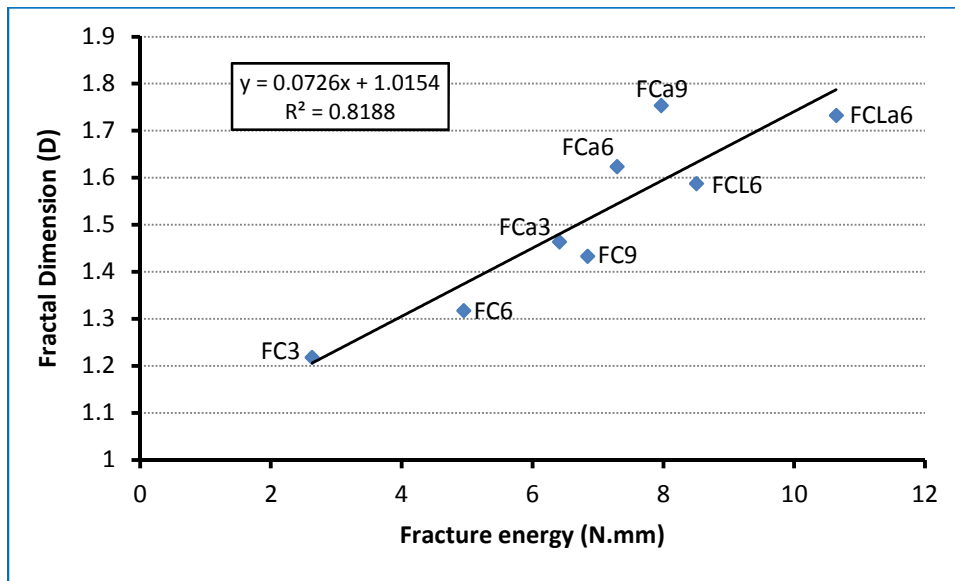
Figure 7-18 Relationship between the fractal dimension and the fracture energy
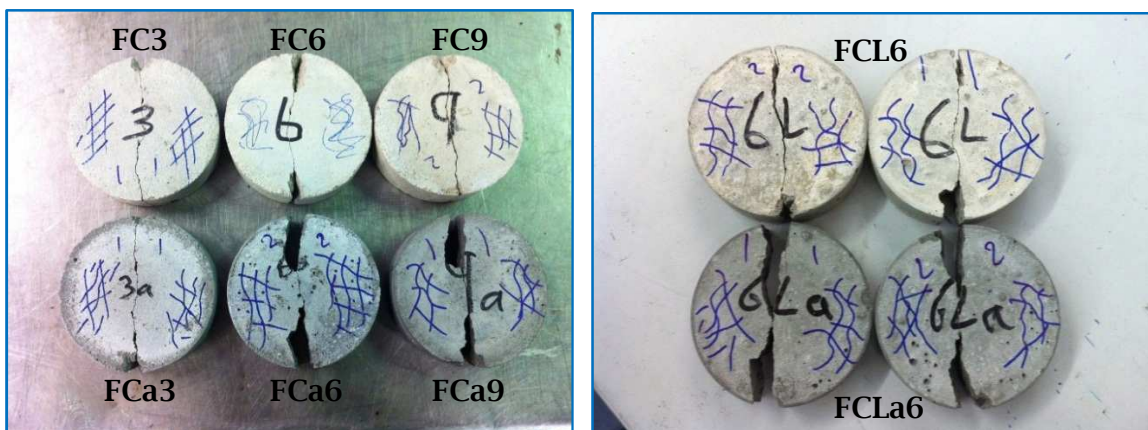
Figure 7-19 Failure pattern of selected specimens

7.6.3 Microcracks: Quantitative and Qualitative Investigations

Because of the tendency to utilise a higher proportion of the strength of the concrete, knowledge of the basic nature and behaviour of cracks formed in response to external loads is required (Raju, 1970). Neville (2011) stated that microcracks have not been defined in terms of size, however 100 μm has been suggested as an upper limit which is the smallest size that can be detected by the naked eye. On the other hand, a lower limit can be taken as the smallest crack

observable using a microscopic technique. Conventionally, microcracks in concrete can be defined as cracks with width less than 10 μm (Ammouche et al., 2001).

The nature of microcracks formed in foamed concrete under uniaxial compressive load was investigated by experiments on prismatic specimens (the same samples used in the DIC investigation). The distribution (into bond, matrix and aggregate) and orientation (to the direction of applied load) of formed microcracks were studied using SEM images (SE and BSE) and image processing software (ImageJ). In this investigation, polished and non-polished cracked specimens were investigated; see **Figure 7-20a, b**. It was noticed that a magnification between 200× and 1000× was appropraite to investigate the microcracks. There was no advantage in using a higher magnification due to the limited field of view and with a lower magnification it was difficult to detect the microcracks.

Various mixes were investigated to examine the effect of certain variables on the formation and propagation of microcracks under a compressive load, as follows:

- To examine the effect of added foam, unfoamed and foamed mixes were investigated.

- To examine the effect of the foam volume, FC3, FC6 and FC9 mixes were investigated.

- To examine the additives effect, FC6 and FCa6 mixes were investigated.

- To examine the LWA effect, (FC6 and FCL6) and (FCa6 and FCLa6) were investigated.

It should be noted here that to avoid the damaging effects of cutting on the nature of microcracks, pieces from the specimens after failure were impregnated with epoxy under vacuum and polished along their natural surface slopes, see **Figure 7-20b**, i.e. the final surface slopes of the polished samples are those of the cracked samples before impregnation.
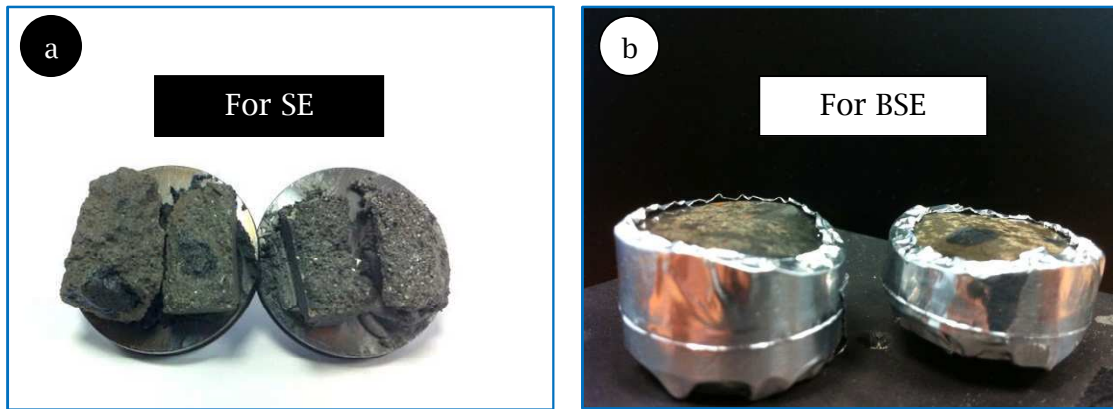
Figure 7-20 (a) non-polished (b) polished samples prepared for microcrack investigation

For a **quantitative** analysis, the formed microcracks were analysed into bond, matrix and aggregate *distribution*, see **Figure 2-19**, and *orientation* to the applied load. By using a straight tool in the ImageJ software, the lengths of microcracks were measured within the bond, matrix and aggregate and their distributions were calculated as ratios of the total length. Meanwhile, the density of microcracks was calculated by divided the total length by the areas of the examened images. The results of density, fractal dimension and *distribution* of the microcracks are listed in **Table 7-2**. From the table, it can be seen that:

- Matrix cracks formed the major percentage of the total length of cracks in all investigated foamed concrete mixes although it has been observed that under the uniaxial compression test bond cracks represented the major percentage in normal concrete (Raju, 1970). This is attributed to two possible reasons. Firstly, the presence of entrained voids or LWA led to a decrease in the sand volume (reduced number of sand particles) and thereby reduced the amount of bond cracks. Note that from all the captured images it was observed that there were no bond microcracks around the voids or the LWA, see **Figure 2-18** and then **Figure 7-21**. Secondly, because of their weakness, the voids and LWA induced cracks, which were formed first in the ITZ of the natural aggregates as bond

cracks, towards them through the matrix or export cracks from them to the mortar in a random manner depending on the nature of the nearest features.

- A difference was observed in the propagation of bond cracks formed in FC and FCa mixes and in mixes with LWA, FCL6 and FCLa6. In both cases, it was found that the bond crack percentage was larger in mixes with additives (FCa6 and FCLa6) than in those without additives (FC6 and FCL6). The reason may be as explained in **Section 2.4.7.3**, related to a bigger difference between the ITZ and mortar strengths resulting in a high tendency for forming bond microcracks; i.e. cracks confined within the ITZ may be bounded by a stronger mortar matrix. Note that due to additives the strength of the FCa mix is higher that of the FC mix. It was noticed that there were no fine aggregate (sand) cracks within all the investigated foamed concrete mixes.

- The results for fractal dimension (D) of microcracks formed under a compression test were in agreement with those of macro cracks under a splitting tensile test.

- More concentrated damage occurred in mixes without LWA compared to those with LWA. This is attributed to the arresting of microcracks in LWA particles and the absence of bond microcracks around them.

- It was noticed that the microcrack density (1/μm) decreased with increased material density, however the maximum crack widths were found within the most dense mixes.

Table 7-2 Density and distribution of microcracks formed under compressive load

Mixes	Crack density (1/μm)	Fractal dimension (D)	Crack distribution (%)		
			Bond	**Matrix**	**Aggregate**
FC6	0.0058	1.057	42.6	58.4	-
FCa6	0.0052	1.154	49.3	51.7	-
FCL6	0.0021	1.165	27.2	62.2	7.6
FCLa6	0.0017	1.262	33.6	55.9	10.5
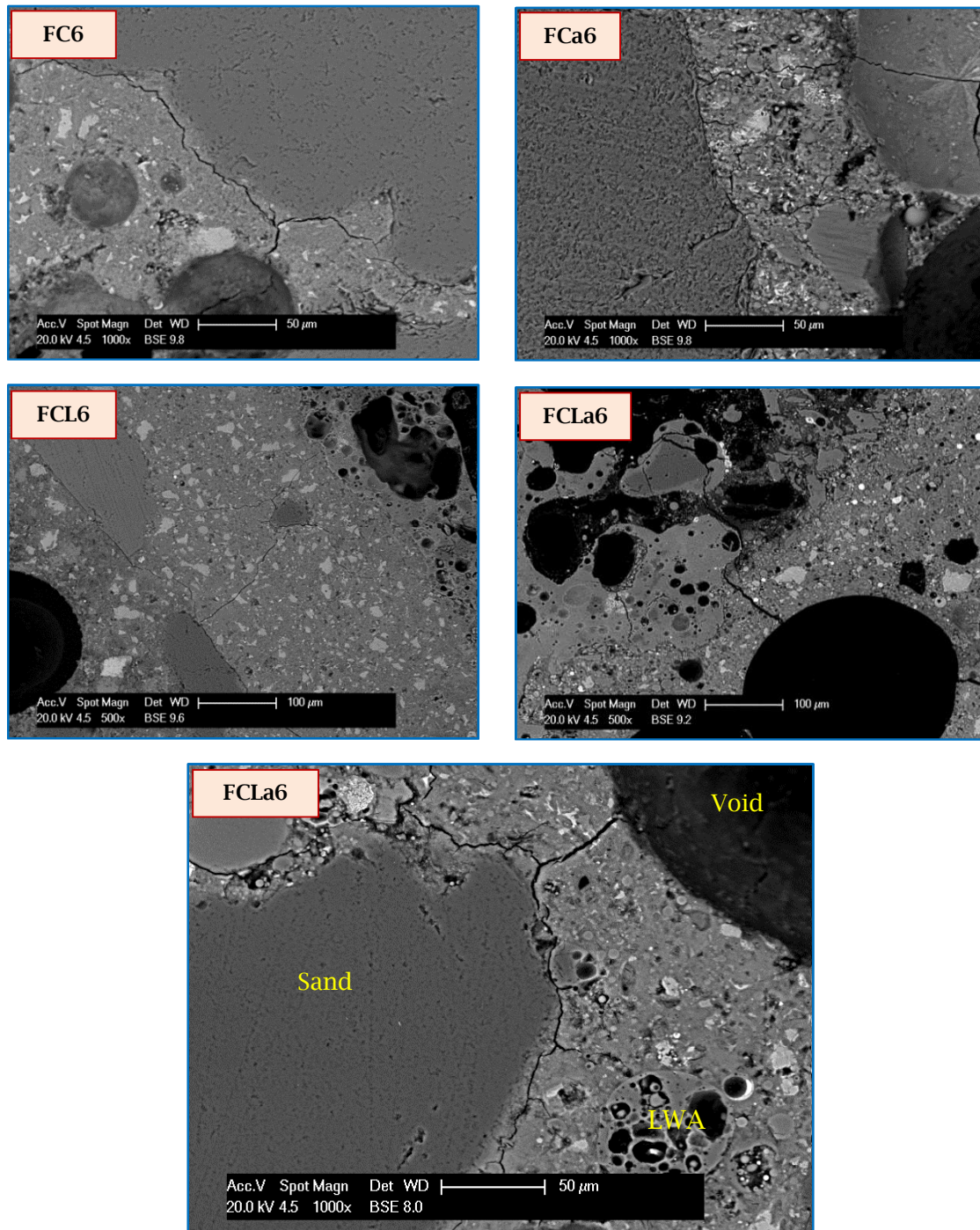
Figure 7-21 Microstructure images showing that there are no bond cracks around the LWA and voids

For *Inclination* of cracks, the lengths and angles of microcracks, **Figure 7-22**, were measured using a straight tool in the ImageJ software and grouped at 10-degree intervals from 0-90° as shown in **Figure 7-23**. From this figure, the strong tendency of cracks to form and propagate in the direction of uniaxial compressive

load is evident in the unfoamed mixes much more than in the foamed mixes, which is in agreement with what had been observed on normal concrete by Raju (1970). In fact, a fairly random orientation was noticed in all investigated foamed concrete mixes due to the presence of voids and LWA which led to inducing and dispersing of microcrack towards them. However, from **Figure 7-24**, in terms of FC mixes the inclination degree (θ_{crack}) of the median of the microcracks decreased with reduced added foam, i.e. in the FC9 mix compared to the FC6 and FC3 mixes. In addition, θ of the median of the microcracks reduces with additives for the same density; however, inclusion of LWA increases θ in mixes with additives compared to FCa6. The fact that the major proportion of microcracks was oriented in the direction of applied load in unfoamed mix is attributed to the absence of entrained air voids.
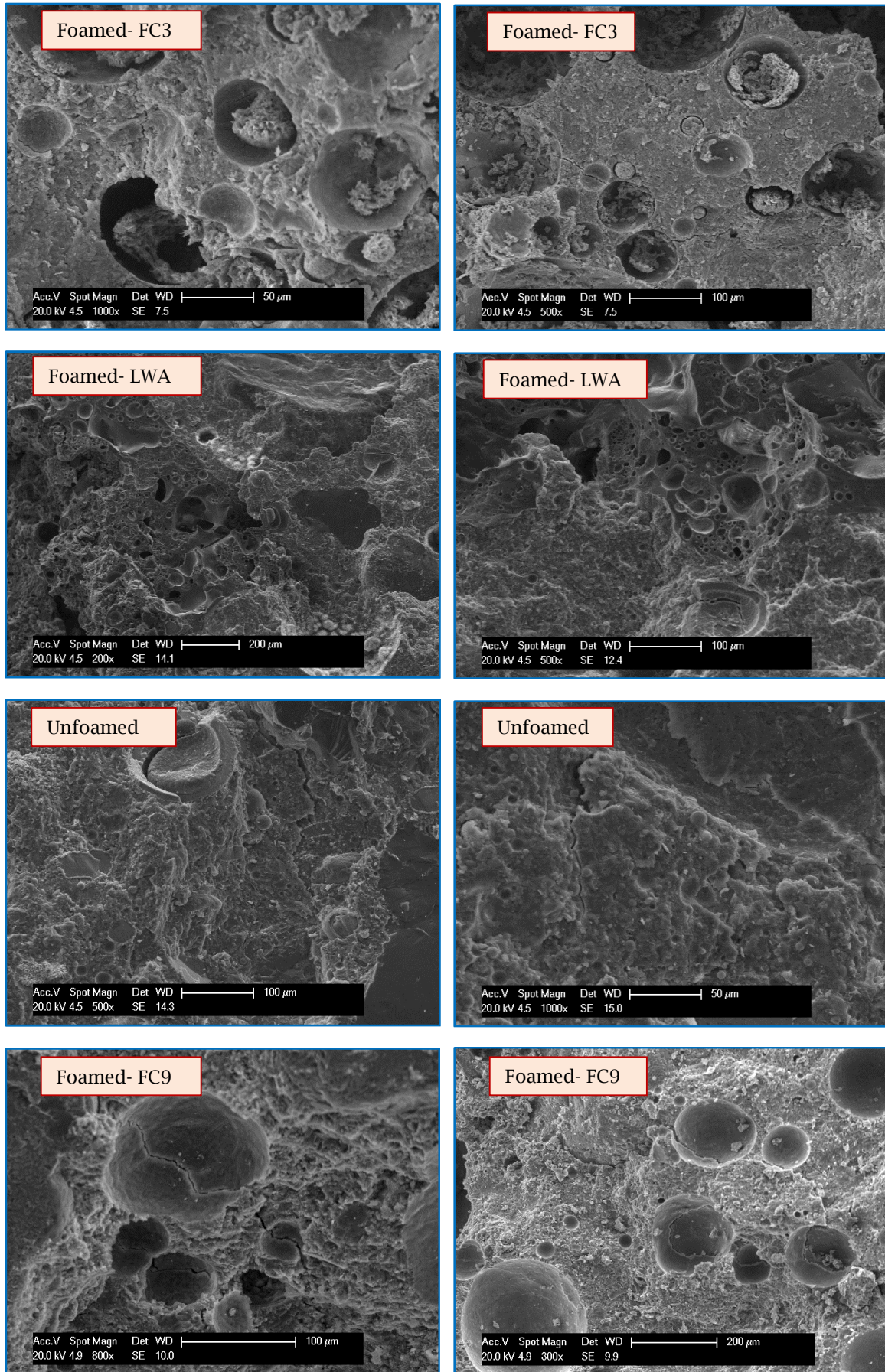
Figure 7-22 SEM images for investigation of microcracks orientation
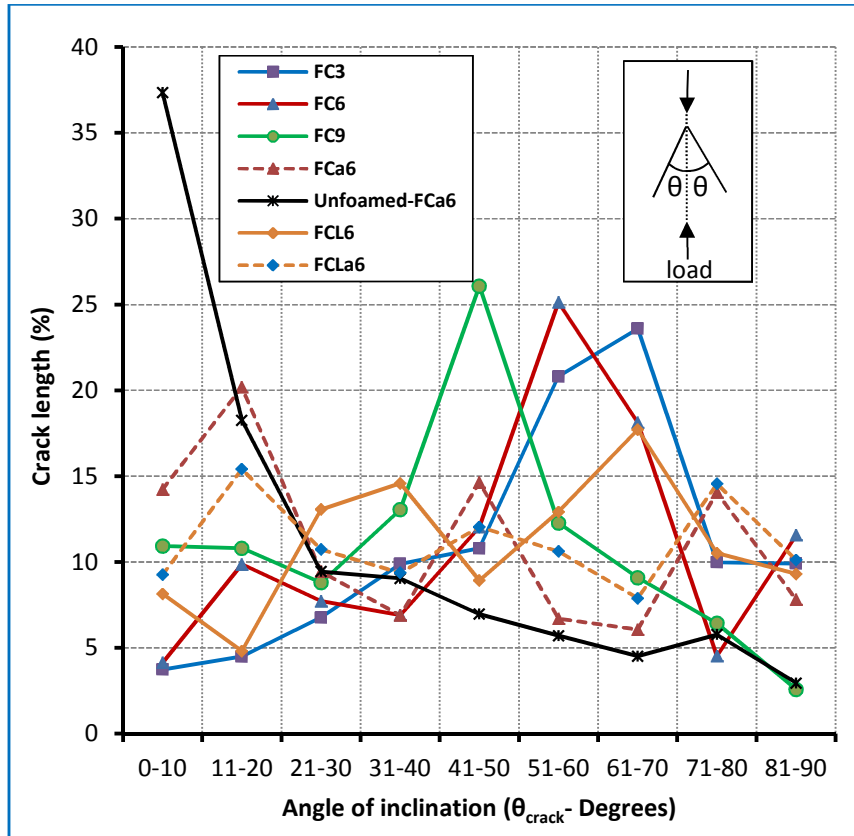
Figure 7-23 Distribution of microcracks orientation of selected mixes
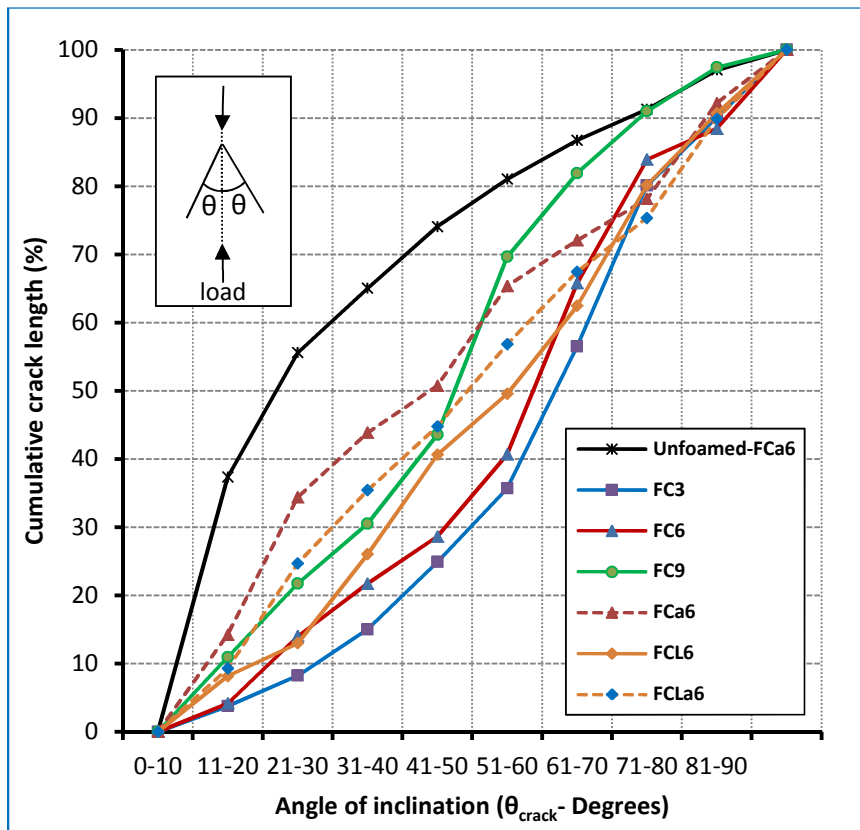
Figure 7-24 Cumulative distribution of microcracks orientation of selected mixes

Since brittle materials, such as concrete, have a lower resistance to tensile splitting, their failure under uniaxial compression is fundamentally a tension failure (Raju, 1970). To understand the various crack phenomena, a **qualitative** study of the nature of microcracks formed in investigated foamed concrete mixes was made and a brief summary of the typical nature of the microcracks observed is as follows:

- Bond cracks propagate at the fine aggregate (sand) interfaces and do not form at LWA or void interfaces, **Figure 7-21**.

- The microcracks through the entrained air voids were observed to have propagated in different directions (not only in the load direction) depending on the nature of features around them, **Figure 7-25a**.

- Regions with minimum thickness separating sand-void, LWA-void, void-void and LWA-LWA are the most probable locations for the microcracks, **Figure 7-25b, c**.

- Unlike the observation of Raju (1970) on microcracks in normal concrete, the matrix microcracks were in general wider than the bond cracks in all the investigated foamed concrete mixes.

- In addition to the void effect, because of the arresting, deflection and branching phenomena in the fine aggregate (sand), it has been observed that the microcracks formed in foamed concrete progress as combined (connected) rather than single continuous cracks, **Figure 7-25d, e**.

- Many microcracks were arrested in the LWA, **Figure 7-25f**. However, evidence was found of voids also arresting the microcracks, **Figure 7-26a, b**.

- From this investigation, it is difficult to conclude if the microcracks initiate first from the voids or from the ITZ between the fine aggregate (sand) and the cement paste. However, the width variation of microcracks might sometimes be a useful indication of the direction of their propagation, **Figure 7-26c**.
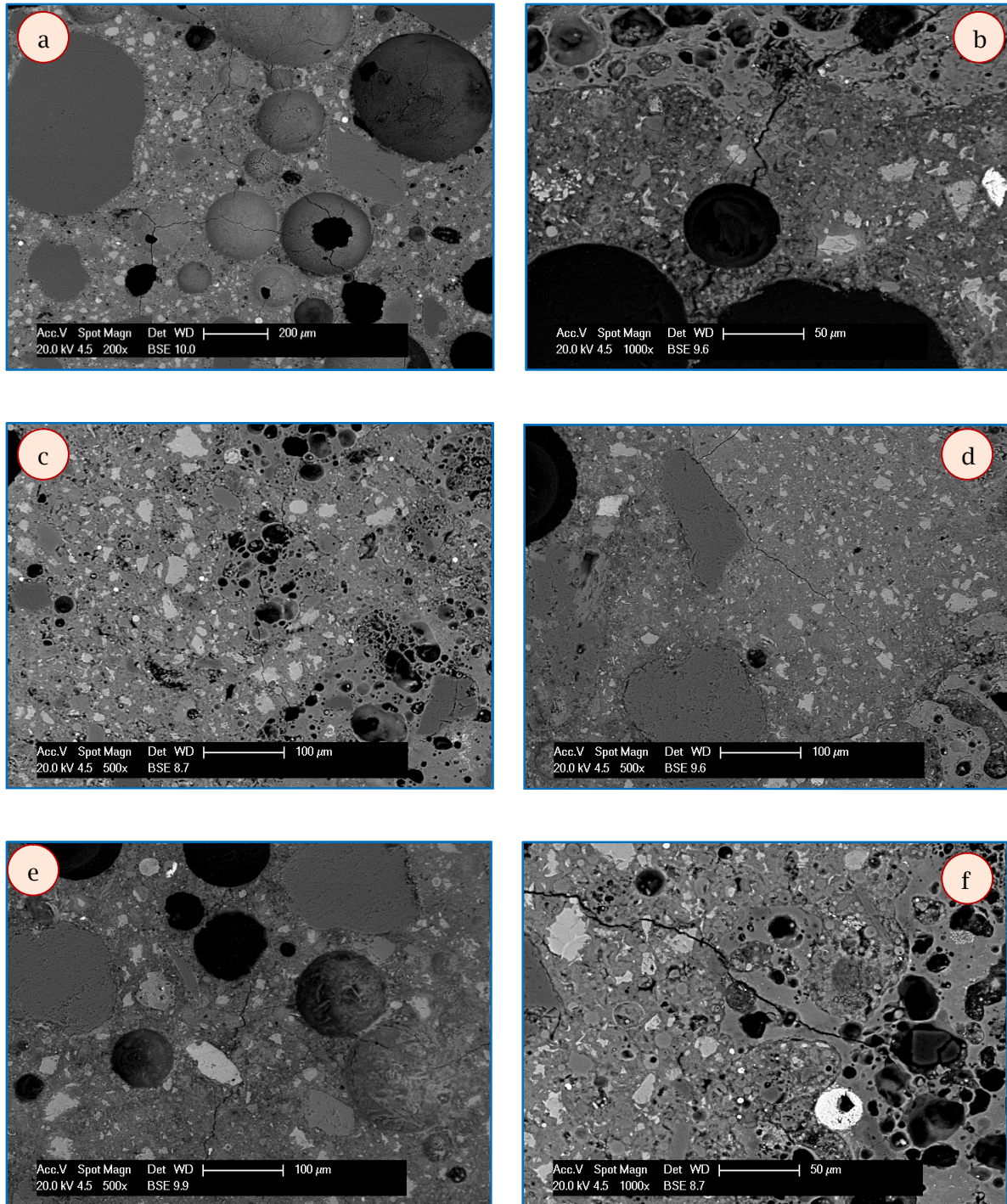
Figure 7-25 SEM images showing microcracks propagation
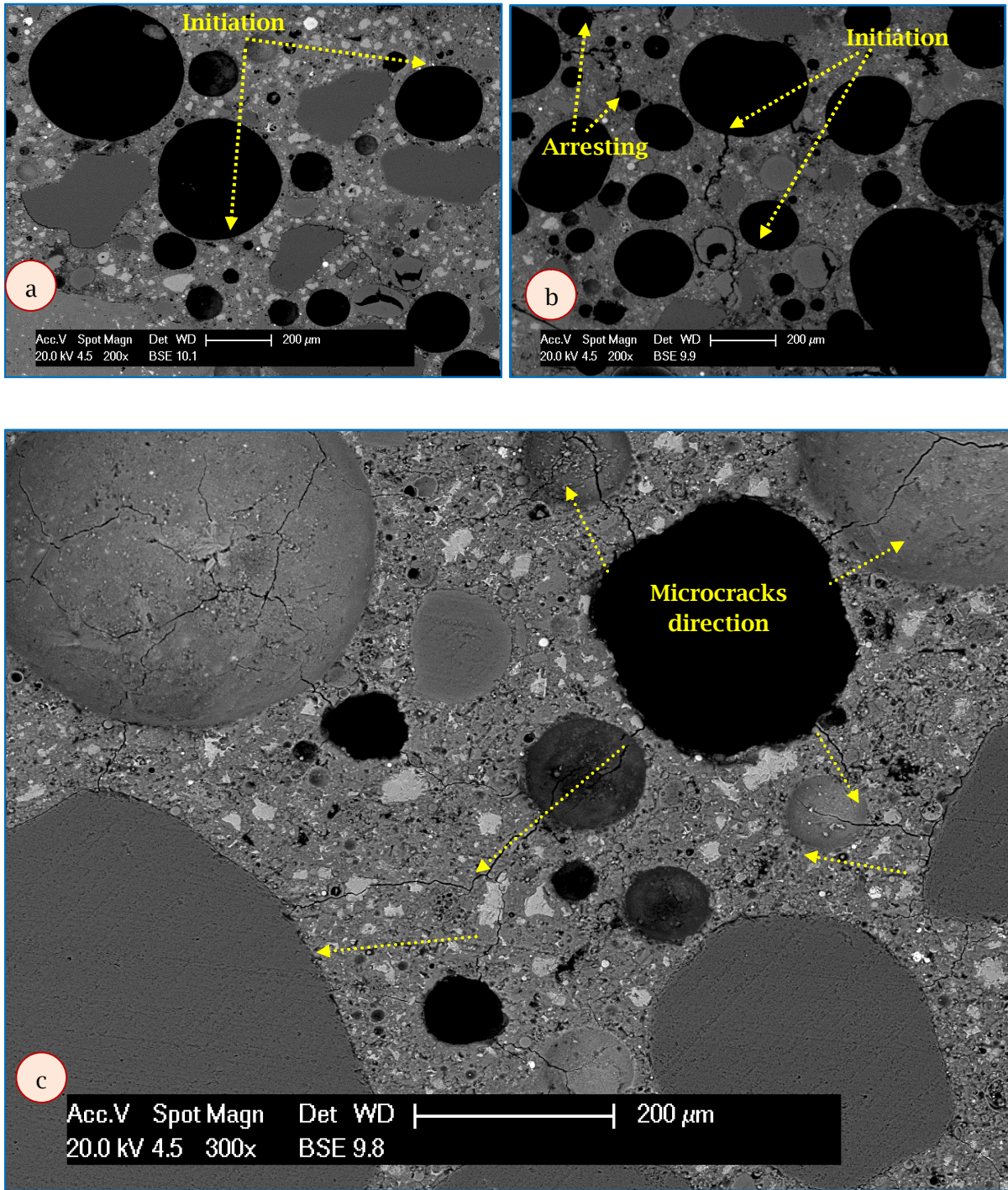
Figure 7-26 SEM images showing microcracks initiation and arresting

The finding that there were no bond cracks, at a micro level, around the LWA is supported by the observation of crack propagation at a macro level. It was observed that during compression loading on small specimens, **Figure 7-27**, the macrocrack propagated through the LWA particle in both FCL6 and FCLa6 mixes indicating that its ITZ is stronger than the LWA itself. In addition, a similar behaviour was noticed on disc specimens after applying a splitting tensile load, see **Figure 7-28**.
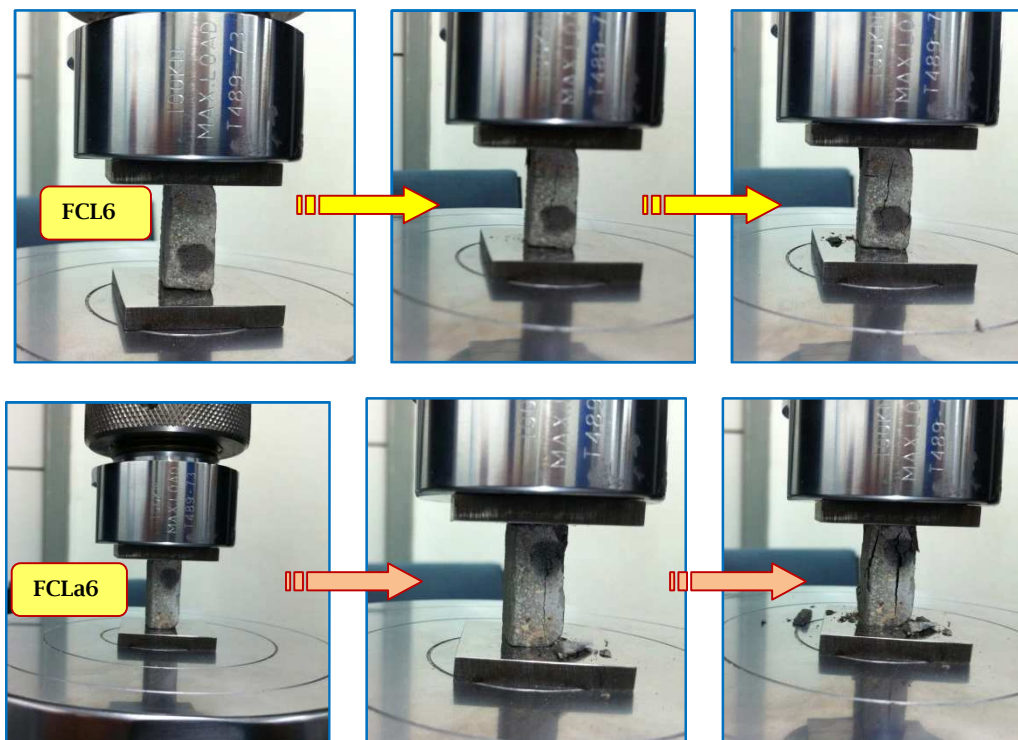
Figure 7-27 Macrocrack during compressive test
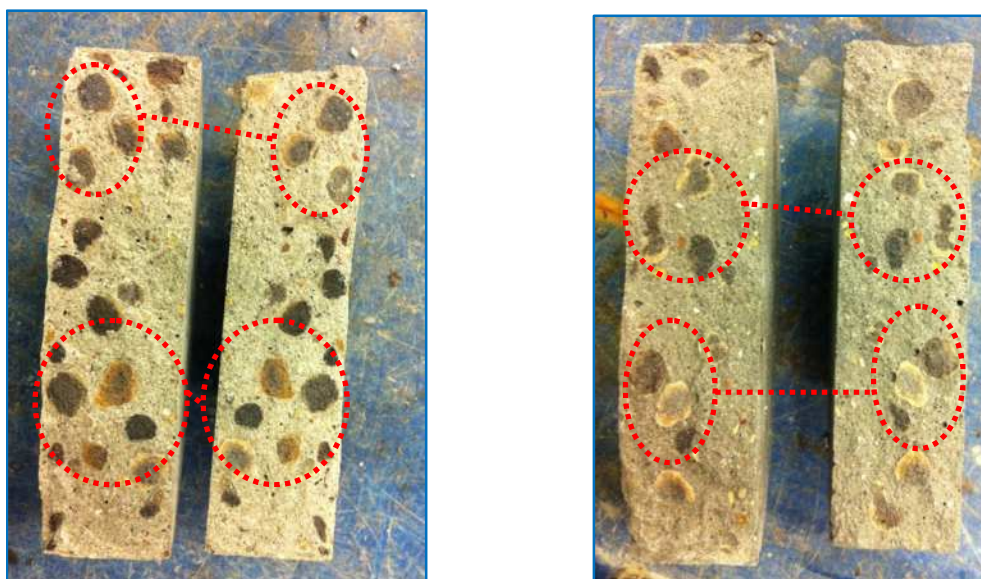
Figure 7-28 Macrocrack through LWA during splitting test

7.7 Summary

Because of the tendency to utilise a higher proportion of the strength of the concrete, knowledge of the basic nature and behaviour of cracks formed as response to external loads is required. Therefore, work to investigate the mechanical loading induced-damage at macro and micro levels of foamed concrete mixes produced with/without additives and/or LWA has been undertaken. To achieve this, DIC, video Gauge and SEM techniques were adopted.

At a macro level, based on the stress-strain curves obtained from the DIC data, the critical stresses, the onset of unstable propagation of cracks in the concrete matrix, were obtained. In addition, the types of crack propagation in foamed concrete specimens at three stages, which are microcrack growth stage (before peak), peak and the stage of branching and bridging of macrocracks (after peak), were investigated. Moreover, the influence of additives (microstructural changes) on the fracture properties of foamed concrete was estimated by means of fractal dimension of surface macrocracks. Finally, the brittleness of the investigated mixes

was examined from the elasticity, fracture and fractal points of view. It was found that the brittleness increases with additives while it reduces with inclusion of LWA.

At a micro level, the nature and distribution of cracks formed under compressive load were studied in order to understand the failure mechanism of the foamed concrete. For a quantitative analysis, the formed microcracks were analysed in terms of bond, matrix and aggregate distribution and orientation to the applied load as well as the crack density. To understand the various crack phenomena, a qualitative study of the nature (formation and propagation) of microcracks formed in the investigated foamed concrete mixes was made. It was found at this level that less damage occurred in mixes with LWA and the bond microcrack percentage increases with inclusion of additives. In addition, the major proportion of microcracks was oriented in the direction of applied load in unfoamed mix, while it was in random directions in foamed mixes depending on the nature of local microstructural features.

Chapter 8: Conclusions and Recommendations

8.1 Introduction

This project aimed to produce foamed concrete mixes which are suitable for semi-structural or structural purposes with good insulation and durability properties and to evaluate their damage behaviour. Since their performance in service can be assessed based on an understanding of the material behaviour, the fundamentals of how this material behaves and how to develop it to be capable of withstanding the mechanical, thermal and permeation loadings associated with changes in its microstructure resulting from inclusion of admixture, additives and lightweight aggregate (LWA) were investigated.

In order to satisfy the aims of this study, the objectives were divided into three main stages as follows:

  i)   Design and production of selected foamed concrete mixes,

  ii)   Micro and macro properties investigation,

  iii)   Behaviour evaluation.

From the findings of this study, an improvement in the strength properties of foamed concrete was achieved, by inclusion of the mineral admixtures and superplasticizer in combination, with slightly increased in thermal conductivity. In addition, adding additives helped in reducing the water absorption, sorptivity and permeability of foamed concrete by making its pore structure less connected. However, the brittleness was increased with inclusion of theses additives while it decreases with adding LWA. Therefore, the aim of this study was achieved but with a need to improve the ductility of modified foamed concrete mixes by adding, for example, fibres.

8.2 Main Conclusions

In this section, a general summary of the results obtained and documented in previous chapters is presented as follows:

❖ **Void characterisation**

Porosity:

➢ On the basis of the measured results, the most appropriate test to obtain a relatively accurate porosity for foamed concrete (conventional, with additives and with LWA) is the vacuum saturation method.

➢ It has been determined that the theoretical equation derived by Zheng (2004) can be used to predict the porosity of foamed concrete mixes reasonably well.

Void structure (distribution, shape and connectivity):

➢ By treating the foam with bitumen emulsion, a clear image of its structure was captured using an optical microscope. Using this technique, a significant difference was found between the size distribution of foam bubbles and those of air pores within foamed concrete mixes.

➢ For all mixes, higher foam volume (1300 kg/m^3) resulted in a greater degree of void merging, leading to large irregular voids which resulted in a wide distribution of void sizes (increased O_{50} and O_{90}) and lower strength.

➢ From circularity factor results, the evidence for bubble merging is higher with increased added foam volume (decreased density).

Additive Effects:

➢ It was found that the effect of additives, SF and FA, (both individually and in combination) was significant.

➢ Although both O_{50} and O_{90} increased with foam volume, they decreased significantly with additives in combination (FCa mixes) suggesting that the

inclusion of these additives helps in achieving more uniform distribution of air voids (less merging) than FC mixes.

➢ This is also evident from the circularity results since reducing void merging resulted in less irregularity in the shape of voids, pushing the circularity factors (F_{circ50} and F_{circ10}) toward 1.

➢ Superplasticizer has the most beneficial influence on voids when used alone and it further improves void structure (smaller and number voids) when used in combination with other additives.

➢ For a given density, although the additives in combination led to increased void numbers, both void size and connectivity were reduced by preventing their merging and this resulted in a narrow void size distribution.

➢ Using the additives individually slightly deceased $O_{50,}$ while O_{90} was significantly decreased implying that additives helped in reducing the merging of voids and so reduced the areas of the larger voids.

➢ The void connectivity reduces with increased density and with use of additives for the same density.

➢ The addition of LWA instead of part of the sand also helps in improving the air-void structure by making the void size distribution narrower compared to that of mix without LWA.

❖ **Mechanical properties**

➢ The mineral admixtures (SF and FA) and superplasticizer combination provides improvement in the strength properties of foamed concrete due to reduced void size and connectivity, by preventing their merging and producing a narrow void size distribution (decreased O_{50} and O_{90}).

➢ Compared to other studies on foamed concrete produced by using sand and/or fly ash as a filler material, the results from the mixes investigated in

this study showed higher strengths (for a given density), higher tensile to compressive strength ratios and higher moduli of elasticity.

➤ A reduction in air void size parameters (O_{50} and O_{90}) is clearly linked to an increase in strength for each density implying that the effect of additives (both individually and in combination) was significant. However, it is proved that changes to the hydrated microstructure also contribute to strength gain.

➤ The difference between values of unfoamed and foamed concrete with and without additives implies that not only the enhancement of cement paste microstructure but also improvements in the void structure of foamed concrete both contribute to strength gain.

➤ Adding LWA helped in increasing the strength and modulus of elasticity due to enhancing the ITZ between the cement paste and LWA (internal curing) and reducing the volume of added foam which is offset by the air pores in the LWA to gain similar density.

❖ **Thermal properties**

➤ Due to their making the cement paste denser and less porous, addition of additives and superplasticizer in combination led to slightly increased thermal conductivity in the dry state. However, owing to reduced water absorption, the thermal conductivity in the saturated state was slightly lower for FCa mixes than FC mixes.

➤ Compared to mixes with the same density but without lightweight aggregate, inclusion of LWA slightly increased the thermal conductivity.

➤ The specific heat decreases as the density increases (decrease of porosity) owing to enhanced inter-particle contact when the void ratio is minimised. However, for a given density, it is similar for mixes with additives (individual or in combination) compared to conventional mixes.

➢ For all mixes, there is an increase in the structural efficiency (compressive strength/thermal conductivity) with increase of density while, for the same density, this ratio increases with the presence of additives.

❖ **Permeation properties**

➢ For conventional foamed concrete mixes, although porosity increases with a reduction in density (due to an increase of the foam volume), the water absorption (% by volume) exhibits a reduction. Therefore, many of the artificial pores due to the added foam are not taking part in water absorption since their weaker suction compared to that of capillary pores.

➢ Adding additives (individually or in combination) helped in reducing the sorptivity of foamed concrete. However, inclusion of LWA resulted in increased sorptivity compared to the same density mixes, conventional or with additives in combination.

➢ For all investigated mixes, the sorptivity values of unfoamed mixes were higher than those of corresponding foamed concrete mixes and the sorptivity reduction (from unfoamed to foamed mixes) was greater for mixes without a superplastisizer than those with it.

➢ The predictive permeability equation derived by Katz and Thompson best fits the air permeability results determined in this study.

➢ The critical pore diameter (from the MIP test) and the pore volume >200nm are found to be closely related to the permeability of foamed concrete. Since they decrease with increased density and, for a given density, with additives, the permeability of foamed concrete reduces with increased density and inclusion of additives.

➢ Compared to the same density mixes but without LWA, inclusion of LWA resulted in increased air permeability.

❖ **Damage evaluation**

At macro level:

➢ From elasticity, fracture and fractal points of view, it was found that brittleness increases with additives while it reduces with inclusion of LWA.

➢ The fractal dimension deceases with increase in the amount of added foam and for a given density it increases with additives and adding LWA. In addition, it was found that there is a good correlation between the fractal dimensions and the fracture energies of the foamed concrete mixes investigated in this study.

➢ The percentage of critical stress increases with increased density (reduced added foam) and for a given density it increases with inclusion of additives in combination showing a tendency to a more brittle failure mechanism. In addition, adding LWA helped in decreasing the percentage of critical stress leading to more ductile behaviour compared to mixes with the same density but without LWA.

➢ In general, during a tension test, the stronger the concrete the larger the lateral deformation (crack width) until failure.

At micro level:

➢ Less damage occurred in mixes with LWA and the bond microcracks percentage increased with inclusion of additives. Moreover, bond cracks propagate at the fine aggregate (sand) interfaces and do not form at LWA or void interfaces. Matrix cracks formed the major percentage of the total length of cracks in all investigated foamed concrete mixes and this percentage reduced with inclusion of additives.

➢ The median of microcracks decreases with reduced added foam. In addition, for a given density, degree of orientation at median of microcracks reduces with additives.

> ➢ The major proportion of microcracks was oriented in the direction of applied load in an unfoamed mix, while it was in random directions in foamed mixes depending on the nature of microstructural features.

❖ **In general**
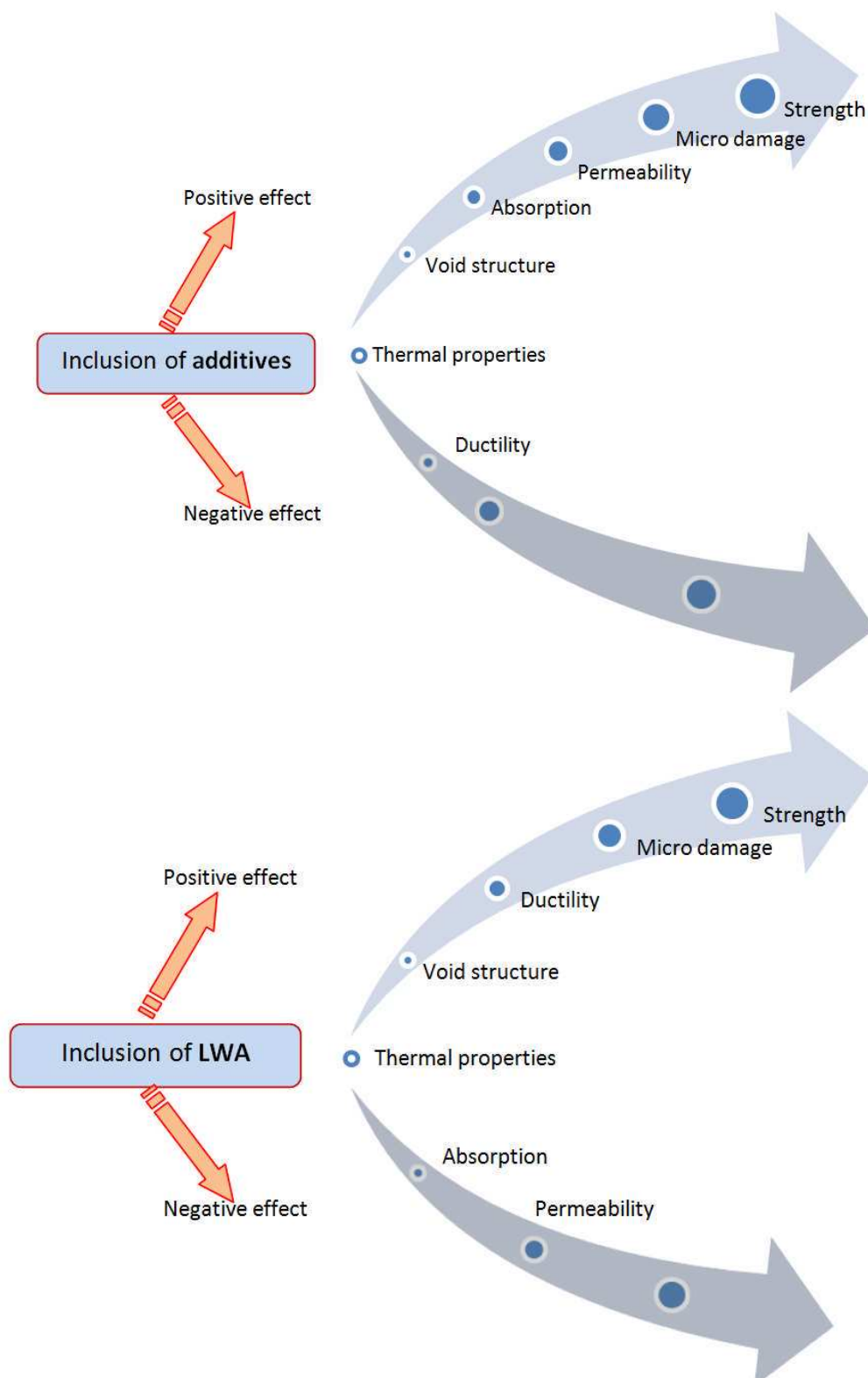
8.3 Recommendations for Future Research

❖ Although the findings of this study in terms of strength considerations are encouraging for the potential of using modified foamed concrete with additives in semi-structural and structural applications, there is still a need to investigate and evaluate the following points:

➢ The potential of using foamed concrete in reinforced structural elements such as beams, columns, slabs and reinforced walls needs to be experimentally examined and evaluated using, for example, a design code for reinforced Autoclaved Aerated Concrete which is recommended by the two RILEM Technical Committees, 51-ALC and 78-MCA, (Aroni, 1993).

➢ Evaluate use of foamed concrete as load bearing masonry by adopting a structural design of unreinforced foamed concrete block masonry in buildings using a design code for unreinforced Autoclaved Aerated Concrete recommended by the two RILEM Technical Committees, 51-ALC and 78-MCA, (Aroni, 1993) as well as British standards BS EN 1052-1 (1999) [Methods of test for masonry] and BS 5628-1 (2005) [Code of practice for the use of masonry- Part 1: Structural use of unreinforced masonry].

❖ Conduct a cost analysis study on the production process as well as a long term cost study of using this lightweight material in construction projects.

❖ Investigate the effect of additives on the carbonation and drying shrinkage of foamed concrete.

❖ Sound insulation, noise reduction and fire resistance need to be investigated.

❖ Investigate the effect of lightweight aggregate size and content on the properties of foamed concrete.

❖ To improve the ductility of modified foamed concrete with additives, the effect of inclusion of fibres needs to be investigated.

References

ABDUL HASSAN, N. 2012. *Microstructural Characterisation of Rubber Modified Asphalt Mixtures.* PhD Thesis, The University of Nottingham.

ACI-523.1R-92 1992. Guide for Cast-in-Place Low Density Concrete. American Concrete Institute.

ACI-523.2R-96 1997. Guide for Precast Cellular Concrete Floor, Roof, and Wall Units. American Concrete Institute.

ACI-523.3R-93 1993. Guide for Cellular Concretes Above 50 pcf, and for Aggregate Concretes Above 50 pcf with Compressive Strengths Less than 2500 psi. American Concrete Institute.

AGARWAL, S. 2006. Pozzolanic activity of various siliceous materials. *Cement and concrete research,* 36**,** 1735-1739.

AHMAD, S. H. & SHAH, S. P. 1985. Structural properties of high strength concrete and its implications for precast prestressed concrete. *PCI Journal,* 30**,** 92-119.

AKÇAOĞLU, T., TOKYAY, M. & ÇELIK, T. 2004. Effect of coarse aggregate size and matrix quality on ITZ and failure behavior of concrete under uniaxial compression. *Cement and Concrete Composites,* 26**,** 633-638.

AKÇAOĞLU, T., TOKYAY, M. & ÇELIK, T. 2005. Assessing the ITZ microcracking via scanning electron microscope and its effect on the failure behavior of concrete. *Cement and Concrete Research,* 35**,** 358-363.

AKÇAY, B. 2007. *Effects of lightweight aggregates on autogenous deformation and fracture of high performance concrete.* Ph D, Istanbul Technical University.

ALSHAMSI, A. M. & IMRAN, H. D. 2002. Development of a permeability apparatus for concrete and mortar. *Cement and concrete research,* 32**,** 923-929.

AMMOUCHE, A., RISS, J., BREYSSE, D. & MARCHAND, J. 2001. Image analysis for the automated study of microcracks in concrete. *Cement and Concrete Composites,* 23**,** 267-278.

AMPARANO, F. E., XI, Y. & ROH, Y.-S. 2000. Experimental study on the effect of aggregate content on fracture behavior of concrete. *Engineering Fracture Mechanics,* 67**,** 65-84.

ARONI, S. 1993. *Autoclaved aerated concrete: properties, testing, and design: RILEM recommended practice*, Taylor & Francis.

ASTM C144 1987. Standard Specification for Aggregate for Masonry Mortar. American Society for Testing and Materials.

ASTM C330 2003. Standard Specification for Lightweight Aggegate for Structural Concrete. American Society for Testing and Materials.

ASTM C457 1998. Standard test method for Microscopical Determination of Parameters of the Air-Void System in Hardened Concrete. American Society for Testing and Materials.

ASTM C495-99A 1999. Standard test method for compressive strength of lightweight insulating concrete American Society for Testing and Materials.

ASTM C796 1997. Standard test method for foaming agent for use in producing cellular concrete using preformed foam. American Society for Testing and Materials.

BABU, D. S. 2008. *mechanical and Deformational Properties, and Shrinkage Cracking Behaviour of Lightweight Concretes.* PhD, National University of Singapore.

BALENDRAN, R. V., ZHOU, F. P., NADEEM, A. & LEUNG, A. Y. T. 2002. Influence of steel fibres on strength and ductility of normal and lightweight high strength concrete. *Building and Environment,* 37**,** 1361-1367.

BOUVARD, D., CHAIX, J. M., DENDIEVEL, R., FAZEKAS, A., LÉTANG, J., PEIX, G. & QUENARD, D. 2007. Characterization and simulation of microstructure and properties of EPS lightweight concrete. *Cement and concrete research,* 37**,** 1666-1673.

BOUXSEIN, M. L., BOYD, S. K., CHRISTIANSEN, B. A., GULDBERG, R. E., JEPSEN, K. J. & MÜLLER, R. 2010. Guidelines for assessment of bone microstructure in rodents using micro–computed tomography. *Journal of Bone and Mineral Research,* 25**,** 1468-1486.

BRADY, K., WATTS, G., JONES, I. V. R. & TRANSPORT RESEARCH LAB., C. 2001a. Specification for foamed concrete. *Specification for foamed concrete,* 1**,** 1-65.

BRADY, K., WATTS, G. & JONES, M. 2001b. Specification for foamed concrete. *Highways Agency and TRL Application Guide AG,* 39.

BS 882 1992. Specification for aggregates from natural sources for concrete. *British Standards Institution, London*.

BS 1881-117 1983. Testing concrete- Part 117: Method for determination of tensile splitting strength. *British Standards Institution, London.*

BS 1881-121 1983. Testing concrete- Part 121: Method of derermination of static modulus of elasticity in compression. *British Standards Institution, London*.

BS 5628-1 2005. Code of practice for the use of masonry- Part 1: Structural use of unreinforced masonry. British Standards Institution, London.

BS 8110 1985. Structural use of concrete. Part 1: Code of practice for densign and construction. *British Standards Institution, London*.

BS EN 197-1 2011. Cement-Part 1: Composition, Specifications and Conformity Criteria for Common Cements. *British Standards Institution, London.*

BS EN 405-1 2005. Fly ash for concrete- Part 1: Defination, specifications and conformity criteria.

BS EN 480-11 2005. Admixtures for concrete, mortar and grout- Test methods- Part 11: Determination of air void characteristics in hardened concrete. British Standards Institution, London.

BS EN 1052-1 1999. Methods of test for masonry- Part 1: Dertermination of compressive strength. British Standards Institution, London.

BS EN 12390-3 2002. Testing hardened concrete—Compressive strength of test specimens. *British European Standards Specifications*.

BS EN 12390-5 2000. Testing hardend concrete- Part 5: Flexural strength of test specimens. *British Standards Institution, London*.

BS EN 13055-1 2002. Lightweight aggregates- part 1: Lightweight aggregates for concrete, mortar and grout

C-THERM TCI. 2014. *Thermal conductivity instruments: How it works* [Online]. C-Therm Technologies Ltd.Available:http://www.ctherm.com/products/tci_thermal_conductivity/how_the_tci_works/ [Accessed 1 Oct. 2014].

CADUFF, D. & VAN MIER, J. G. M. 2010. Analysis of compressive fracture of three different concretes by means of 3D-digital image correlation and vacuum impregnation. *Cement and Concrete Composites,* 32**,** 281-290.

CENGEL, Y. 2002. *Heat Transfer: A Practical Approach,* New York, McGraw-Hill Comapnies, Inc.

CHANG, T. P. & SHIEH, M. M. 1996. Fracture properties of lightweight concrete. *Cement and concrete research,* 26**,** 181-188.

CHARKALUK, E., BIGERELLE, M. & IOST, A. 1998. Fractals and fracture. *Engineering Fracture Mechanics,* 61**,** 119-139.

CHEESEMAN, C. R., MAKINDE, A. & BETHANIS, S. 2005. Properties of lightweight aggregate produced by rapid sintering of incinerator bottom ash. *Resources, Conservation and Recycling,* 43**,** 147-162.

CHEN, B. & LIU, J. 2008. Experimental application of mineral admixtures in lightweight concrete with high strength and workability. *Construction and Building Materials,* 22**,** 1108-1113.

CHIAIA, B., VAN MIER, J. G. M. & VERVUURT, A. 1998. Crack Growth Mechanisms in Four Different Concretes: Microscopic Observations and Fractal Analysis. *Cement and concrete research,* 28**,** 103-114.

CHOI, S. & SHAH, S. 1997. Measurement of deformations on concrete subjected to compression using image correlation. *Experimental Mechanics,* 37**,** 307-313.

CHRISTENSEN, B. J., MASON, T. O. & JENNINGS, H. M. 1996. Comparison of measured and calculated permeabilities for hardened cement pastes. *Cement and concrete research,* 26**,** 1325-1334.

CUI, L. & CAHYADI, J. H. 2001. Permeability and pore structure of OPC paste. *Cement and concrete research,* 31**,** 277-282.

DIAMOND, S. 2000. Mercury porosimetry: An inappropriate method for the measurement of pore size distributions in cement-based materials. *Cement and concrete research,* 30**,** 1517-1525.

DOMONE, P. & ILLSTON, J. 2010. Construction Materials : Their Nature and Behaviour, Fourth Edition. 4 ed. Hoboken: Taylor and Francis.

EL-DIEB, A. S. & HOOTON, R. D. 1994. Evaluation of the Katz-Thompson model for estimating the water permeability of cement-based materials from mercury intrusion porosimetry data. *Cement and concrete research,* 24**,** 443-455.

ELSHARIEF, A., COHEN, M. D. & OLEK, J. 2003. Influence of aggregate size, water cement ratio and age on the microstructure of the interfacial transition zone. *Cement and concrete research,* 33**,** 1837-1849.

ERDEM, S. 2012. *Impact Load-Induced microstructural Damage of Concrete Made With Unconventional aggregates.* PhD PhD, The University of Nottingham.

ESMAILY, H. & NURANIAN, H. 2012. Non-autoclaved high strength cellular concrete from alkali activated slag. *Construction and Building Materials,* 26**,** 200-206.

EXPANDED SHALE CLAY AND SLAT INSTITUTE. 2010. *Internal curing using expanded shale, clay and slate lightweight aggregate* [Online]. ESCSI, http://www.escsi.org/ContentPage.aspx?id=205. [Accessed 2013].

FÉDÉRATION INTERNATIONALE DE LA PRÉCONTRAINTE 1983. *FIP manual of lightweight aggregate concrete,* Glasgow, Surrey University Press.

FRIEDMAN, S. P. & SEATON, N. A. 1998. Critical path analysis of the relationship between permeability and electrical conductivity of three-dimensional pore networks. *Water Resources Research,* 34**,** 1703–1710.

GIACCIO, G., DE SENSALE, G. R. & ZERBINO, R. 2007. Failure mechanism of normal and high-strength concrete with rice-husk ash. *Cement and Concrete Composites,* 29**,** 566-574.

GOUAL, M., BALI, A., DE BARQUIN, F., DHEILLY, R. & QUENEUDEC, M. 2006. Isothermal moisture properties of Clayey Cellular Concretes elaborated from clayey waste, cement and aluminium powder. *Cement and concrete research,* 36**,** 1768-1776.

GUO, L.-P., SUN, W., ZHENG, K.-R., CHEN, H.-J. & LIU, B. 2007. Study on the flexural fatigue performance and fractal mechanism of concrete with high proportions of ground granulated blast-furnace slag. *Cement and concrete research,* 37**,** 242-250.

HALAMICKOVA, P., DETWILER, R. J., BENTZ, D. P. & GARBOCZI, E. J. 1995. Water permeability and chloride ion diffusion in portland cement mortars: Relationship to sand content and critical pore diameter. *Cement and concrete research,* 25**,** 790-802.

HAN, W. K. 2006. *Thermal Conductivity of Foamed Concrete.* MSc, National University of singapore.

HEMAVIBOOL, S. 2007. *The microstructure of synthetic aggregate produced from waste materials and its influence on the properties of concrete.* PhD Thesis University of Leeds.

HILTON LTD, P. A. 1994. Experimental Operating and Maintenance Manual, Thermal conductivity of Building and Insulating Materials Unit. Hampshire: P. A. Hilton Ltd.

HOLCOMB, M. 2012. *Is an asphalt shingle roof or concrete tile better, energy wise?* [Online]. Green Home Guide Available: http://greenhomeguide.com/askapro/question/is-an-asphalt-shingle-roof-or-concrete-tile-better-energy-wise [Accessed 25 Sep. 2014].

ISO 8301 1996. Thermal Insulation – Determination of Steady-State Thermal Resistance and Related Properties – Heat Flow Meter Apparatus. *International Organization for tandardization.* Genève, Switzerland.

JANSEN, D. C. & SHAH, S. P. 1997. Effect of length on compressive strain softening of concrete. *Journal of engineering mechanics,* 123**,** 25-35.

JITCHAIYAPHUM, K., SINSIRI, T. & CHINDAPRASIRT, P. 2011. Cellular Lightweight Concrete Containing Pozzolan Materials. *Procedia Engineering,* 14**,** 1157-1164.

JONES, M. & MCCARTHY, A. 2005. Preliminary views on the potential of foamed concrete as a structural material. *Magazine of concrete research,* 57**,** 21-31.

JONES, M. R. & MCCARTHY, A. 2006. Heat of hydration in foamed concrete: Effect of mix constituents and plastic density. *Cement and concrete research,* 36**,** 1032-1041.

JUST, A. & MIDDENDORF, B. 2009. Microstructure of high-strength foam concrete. *Materials Characterization,* 60**,** 741-748.

KATZ, A. & THOMPSON, A. 1986. Quantitative prediction of permeability in porous rock. *Physical review. B, Condensed matter,* 34**,** 8179-8181.

KAYALI, O. 2008. Fly ash lightweight aggregates in high performance concrete. *Construction and Building Materials,* 22**,** 2393-2399.

KEARSLEY, E. 1999. *The Effect of High Volume of Ungraded Fly Ash on the Properties of Foamed Concrete.* PhD, The University of Leeds.

KEARSLEY, E. & WAINWRIGHT, P. 2001a. The effect of high fly ash content on the compressive strength of foamed concrete. *Cement and concrete research,* 31**,** 105-112.

KEARSLEY, E. & WAINWRIGHT, P. 2001b. Porosity and permeability of foamed concrete. *Cement and concrete research,* 31**,** 805-812.

KEARSLEY, E. & WAINWRIGHT, P. 2002. The effect of porosity on the strength of foamed concrete. *Cement and concrete research,* 32**,** 233-239.

KEIKHAEI DEHDEZI, P. 2012. *Enhancing pavements for thermal applications.* University of Nottingham.

KHAN, R. 2010. *Quantification of microstructural damage in asphalt.* PhD, University of Nottingham.

KOSMATKA, S. H., PANARESE, W. C. & ASSOCIATION, P. C. 2002. *Design and control of concrete mixtures*, Portland Cement Association Skokie, IL.

KUMAR, S. & BARAI, S. V. 2011. *Concrete Fracture Models and Applications*, Springer Verlag.

LAWLER, J. S., KEANE, D. T. & SHAH, S. P. 2001. Measuring three-dimensional damage in concrete under compression. *ACI Materials Journal,* 98.

LECOMPTE, D., SMITS, A., BOSSUYT, S., SOL, H., VANTOMME, J., VAN HEMELRIJCK, D. & HABRAKEN, A. M. 2006. Quality assessment of speckle patterns for digital image correlation. *Optics and Lasers in Engineering,* 44**,** 1132-1145.

LI, H., JIAO, J. J. & LUK, M. 2004. A falling-pressure method for measuring air permeability of asphalt in laboratory. *Journal of Hydrology,* 286**,** 69-77.

LIAN, C., ZHUGE, Y. & BEECHAM, S. 2011. The relationship between porosity and strength for porous concrete. *Construction and Building Materials,* 25**,** 4294-4298.

LO, T. Y., CUI, H. Z., NADEEM, A. & LI, Z. G. 2006. The effects of air content on permeability of lightweight concrete. *Cement and concrete research,* 36**,** 1874-1878.

LOFGREN, I. 2005. *Fibre-reinforced concrete for industrial construction- a fracture mechanics approach to material testing and structural analysis.* PhD PhD, Chalmers University of Technology.

MACKIE, G. 1985. Recent uses of structural lightweight concrete. *Concrete Constr,* 30**,** 497-502.

MAIRE, E., COLOMBO, P., ADRIEN, J., BABOUT, L. & BIASETTO, L. 2007. Characterization of the morphology of cellular ceramics by 3D image processing of X-ray tomography. *Journal of the European Ceramic Society,* 27**,** 1973-1981.

MEHTA, P. K. & MONTEIRO, P. J. M. 2006. *Concrete: microstructure, properties and materials*, McGraw-Hill.

MINDESS, S., YOUNG, J. F. & DARWIN, D. 2003. *Concrete*, Pearson Education, Inc.

MONDAL, P., SHAH, S. P. & MARKS, L. 2007. A reliable technique to determine the local mechanical properties at the nanoscale for cementitious materials. *Cement and concrete research,* 37**,** 1440-1444.

NAJIM, K. B. & HALL, M. R. 2012. Mechanical and dynamic properties of self-compacting crumb rubber modified concrete. *Construction and Building Materials,* 27**,** 521-530.

NAMBIAR, E. & RAMAMURTHY, K. 2006. Influence of filler type on the properties of foam concrete. *Cement and Concrete Composites,* 28**,** 475-480.

NAMBIAR, E. & RAMAMURTHY, K. 2007a. Air-void characterisation of foam concrete. *Cement and concrete research,* 37**,** 221-230.

NAMBIAR, E. K. K. & RAMAMURTHY, K. 2007b. Sorption characteristics of foam concrete. *Cement and concrete research,* 37**,** 1341-1347.

NAMBIAR, E. K. K. & RAMAMURTHY, K. 2008. Fresh state characteristics of foam concrete. *Journal of materials in civil engineering,* 20**,** 111.

NAMBIAR, E. K. K. & RAMAMURTHY, K. 2009. Shrinkage Behavior of Foam Concrete. *Journal of materials in civil engineering,* 21**,** 631.

NARAYANAN, N. & RAMAMURTHY, K. 2000. Structure and properties of aerated concrete: a review. *Cement and Concrete Composites,* 22**,** 321-329.

NATH, P. & SARKER, P. 2011. Effect of Fly Ash on the Durability Properties of High Strength Concrete. *Procedia Engineering,* 14**,** 1149-1156.

NAWY, E. G. 2001. *Fundamentals of high-performance concrete*, Wiley.

NEMATI, K. M. 1997. Fracture analysis of concrete using scanning electron microscopy. *Scanning,* 19**,** 426-430.

NEMATI, K. M., MONTEIRO, P. J. M. & SCRIVENER, K. L. 1998. Analysis of compressive stress-induced cracks in concrete. *ACI Materials Journal,* 95**,** 617-630.

NEVILLE, A. M. 2011. *Properties of concrete,* London Pearson Education Limited.

NEWMAN, J. B. & CHOO, B. S. 2003. *Advanced concrete technology*, Butterworth-Heinemann.

NRMCA 2003. Concrete in practice- what, why and how? : National Ready Mixed Concrete Association (NRMCA).

ODGAARD, A. & GUNDERSEN, H. J. G. 1993. Quantification od Connectivity in Cancellous Bone, with Special Emphasis on 3-D Reconstructions. *Bone,* 14**,** 173-182.

OLUOKUN, F. 1991. Prediction of concrete tensile strength from its compressive strength: an evaluation of existing relations for normal weight concrete. *ACI Materials Journal,* 88.

ORCHARD, D. F. 1976. Concrete technology: Volume I, DF Orchard, John Wiley and Sons, New York and Toronto, 1973. *Cement and concrete research,* 6**,** 331.

OTHUMAN, M. A. & WANG, Y. C. 2011. Elevated-temperature thermal properties of lightweight foamed concrete. *Construction and Building Materials,* 25**,** 705-716.

PAN, Z., HIROMI, F. & WEE, T. 2007. Preparation of high performance foamed concrete from cement, sand and mineral admixtures. *Journal of Wuhan University of Technology--Materials Science Edition,* 22**,** 295-298.

RAJU, N. 1970. Microcracking in concrete under repeated compressive loads. *Building Science,* 5**,** 51-56.

RAMAMURTHY, K., KUNHANANDAN NAMBIAR, E. K. & INDU SIVA RANJANI, G. 2009. A classification of studies on properties of foam concrete. *Cement and Concrete Composites,* 31**,** 388-396.

RASHID, M., MANSUR, M. & PARAMASIVAM, P. 2002. Correlations between mechanical properties of high-strength concrete. *Journal of materials in civil engineering,* 14**,** 230-238.

REGAN, P. & ARASTEH, A. 1990. Lightweight aggregate foamed concrete. *Structural Engineer,* 68**,** 167-173.

RIDLER, T. & CALVARD, S. 1978. Picture thresholding using an iterative selection method. *IEEE transactions on Systems, Man and Cybernetics,* 8**,** 630-632.

RONEZ 2011. Price Guide July 2011. www.ronez.com.

ROSSELLÓ, C., ELICES, M. & GUINEA, G. V. 2006. Fracture of model concrete: 2. Fracture energy and characteristic length. *Cement and concrete research,* 36**,** 1345-1353.

RUIWEN, K. 2004. *Properties of high-strength foam concrete.* MSc. National University of Singapore.

SANCHEZ, F. & SOBOLEV, K. 2010. Nanotechnology in concrete – A review. *Construction and Building Materials,* 24**,** 2060-2071.

SANJUAN, M. & MUNOZ-MARTIALAY, R. 1996a. Modelling of the concrete air permeability evolution over time. *Materials Letters,* 27**,** 269-272.

SANJUÁN, M. & MUÑOZ-MARTIALAY, R. 1997. Variability of the concrete air permeability coefficient with time. *Building and Environment,* 32**,** 51-55.

SANJUAN, M. A. & MUNOZ-MARTIALAY, R. 1996b. Influence of the water/cement ratio on the air permeability of concrete. *Journal of Materials Science,* 31**,** 2829-2832.

SCHEFFLER, M. & COLOMBO, P. 2005. *Cellular ceramics: structure, manufacturing, properties and applications*, WILEY-VCH Verlag GmbH & Co. KGaA.

SCRIVENER, K., CRUMBIE, A. & LAUGESEN, P. 2004. The Interfacial Transition Zone (ITZ) Between Cement Paste and Aggregate in Concrete. *Interface Science,* 12**,** 411-421.

SHAH, S. & CHOI, S. 1999. Nondestructive techniques for studying fracture processes in concrete. *International journal of fracture,* 98**,** 351-359.

SHAH, S. P., SWARTZ, S. E. & OUYANG, C. 1995. *Fracture mechanics of concrete: applications of fracture mechanics to concrete, rock and other quasi-brittle materials*, Wiley-Interscience.

SHANNAG, M. J. 2011. Characteristics of lightweight concrete containing mineral admixtures. *Construction and Building Materials,* 25**,** 658-662.

SHI, Z. 2009. *Crack analysis in structural concrete: theory and applications*, Butterworth Heinemann.

SOMERTON, W. H. 1992. *Thermal properties and temperature-related behavior of rock/fluid systems*, Elsevier Science Limited.

SOROUSHIAN, P. & ELZAFRANEY, M. 2004. Damage effects on concrete performance and microstructure. *Cement and Concrete Composites,* 26**,** 853-859.

TANYILDIZI, H. 2008. Effect of temperature, carbon fibers, and silica fume on the mechanical properties of lightweight concretes. *New Carbon Materials,* 23**,** 339-344.

TANYILDIZI, H. & COSKUN, A. 2008. Performance of lightweight concrete with silica fume after high temperature. *Construction and Building Materials,* 22**,** 2124-2129.

TARASOV, A., KEARSLEY, E. P., KOLOMATSKIY, A. & MOSTERT, H. 2010. Heat evolution due to cement hydration in foamed concrete. *Magazine of concrete research,* 62**,** 895-906.

TIKALSKY, P. J., POSPISIL, J. & MACDONALD, W. 2004. A method for assessment of the freeze–thaw resistance of preformed foam cellular concrete. *Cement and concrete research,* 34**,** 889-893.

TOUTANJI, H. A. & EL-KORCHI, T. 1995. The influence of silica fume on the compressive strength of cement paste and mortar. *Cement and concrete research,* 25**,** 1591-1602.

WANG, Y. H., JIANG, J. H., WANINTRUDAL, C., DU, C., ZHOU, D., SMITH, L. M. & YANG, L. X. 2010. WHOLE FIELD SHEET-METAL TENSILE TEST USING DIGITAL IMAGE CORRELATION. *Experimental Techniques,* 34**,** 54-59.

WEIGLER, H. & KARL, S. 1980. Structural lightweight aggregate concrete with reduced density--lightweight aggregate foamed concrete. *International Journal of Cement Composites and Lightweight Concrete,* 2**,** 101-104.

WWW.DR-LUCA.COM 2009. Building materials industry LithoPore[TM] - Foamed concrete system. Dr Luca and Partner.

WWW.FOAMCONCRETE.CO.UK 2013. Advantages of using foam concrete. Foam Concrete Ltd.

WWW.PROVOTON.COM 2006. Foam concrete. PROVOTON.

YANG, C., CHO, S. & WANG, L. 2006. The relationship between pore structure and chloride diffusivity from ponding test in cement-based materials. *Materials chemistry and physics,* 100**,** 203-210.

YEN, L. B. 2007. *Study of water ingress into foamed concrete.* MSc, NATIONAL UNIVERSITY OF SINGAPORE.

YU, X. G., LUO, S. S., GAO, Y. N., WANG, H. F., LI, Y. X., WEI, Y. R. & WANG, X. J. 2011. Pore Structure and Microstructure of Foam Concrete. *Advanced Materials Research,* 177**,** 530-532.

ZHANG, D., LI, Z., ZHOU, J. & WU, K. 2004. Development of thermal energy storage concrete. *Cement and concrete research,* 34**,** 927-934.

ZHANG, M.-H. & GJØRV, O. E. 1990. Microstructure of the interfacial zone between lightweight aggregate and cement paste. *Cement and concrete research,* 20**,** 610-618.

ZHANG, Z. & ANSARI, F. 2006. Fracture mechanics of air-entrained concrete subjected to compression. *Engineering Fracture Mechanics,* 73**,** 1913-1924.

ZHENG, M. 2004. *Physical and mechanical performance of porous concrete for drainage base.* PhD, Chang'an University.

ZHOU, F. P. 1992. *Time-dependent Crack Growth and Fracture in Concrete.* PhD, Lund University.

Appendices

This list below describes the appendices to this thesis which were included in a compacted disc (CD).

Appendix	Description	File Type
Appendix 1	Mix design, cost estimation, spreadability, w/b ratios and dry/wet densities	Excel sheet
Appendix 2	Porosity and connectivity	Excel sheet and photos
Appendix 3	Void size distribution and shape factor	Excel sheet and photos
Appendix 4	Mechanical and thermal properties	Excel sheet and photos
Appendix 5	Water absorption and sorptivity	Excel sheet and photos
Appendix 6	Permeability	Excel sheet
Appendix 7	Macro and microcracks	Excel sheet and photos
Appendix 8	Published journal and conference papers	Pdf files